UNIVERSITA' DEGLI STUDI DI PARMA

DIPARTIMENTO DI CHIMICA GENERALE ED INORGANICA,
CHIMICA ANALITICA, CHIMICA FISICA

PHD THESIS IN CHEMICAL SCIENCES

Scorpionate Ligands and Surroundings.

Coordination Properties - Solution Studies

CYCLE XX

SCIENTIFIC-SECTOR CHIM/03

PhD candidate

Dr. Marcello Gennari

Tutors

Dr. Luciano Marchiò
Prof. Maurizio Lanfranchi

2005 – 2007

Contents

List of Abbreviations

mes	mesityl
ph	phenyl
PPh_3	triphenylphosphine
py	pyridine
pz	pyrazole
tu	thiourea
*	stereogenic center
#	distinguish two interconverting $[Zn(LOH)_2]^{2+}$ isomers (see Chapter 3)

1

General Introduction

In 1966 Trofimenko first reported the synthesis of a class of molecules that would become a precious ligand system in modern coordination chemistry: tris(pyrazol-1-yl)borate anions (Tp and analogs) [1,2]. He defined this discovery "a new and fertile field of remarkable scope". Like the pincer of a scorpion, these versatile tripodal ligands generally bind metal centers with nitrogen atoms from two pyrazole rings attached to the central boron atom; the third pyrazole attached to boron rotates forward like a scorpion's tail to "sting" the metal; hence the name of "scorpionates"[3-7] (Figure 1.1).

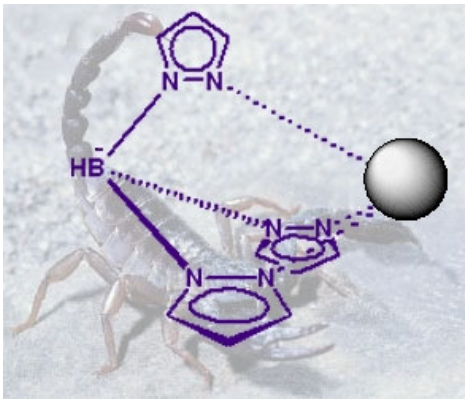

Figure 1.1 Illustration of the analogy between Tp, the first scorpionate ligand, and a scorpion.

As regards the coordination properties, we are dealing with ligands that, as a result of their trigonal nature, preferably link to metal ions by occupying a trigonal face of a coordination polyhedron (*fac* binding), as a tetrahedron or an octahedron, so that the T-shaped coordination mode (*mer* binding) is precluded (Figure 1.2).

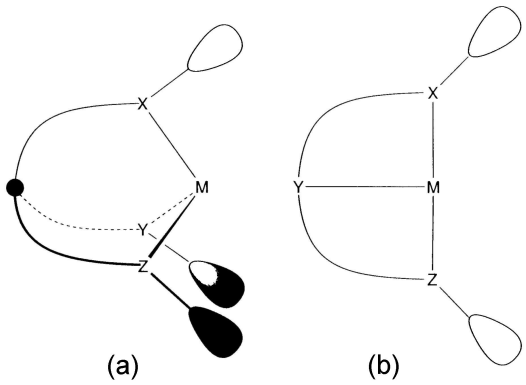

Figure 1.2 Comparison between (a) the *fac* coordination of a κ^3 tripodal ligand and (b) the *mer* binding of a κ^3 pincer ligand.[8]

In general, however, tris(pyrazolyl)borates include a wide set of coordination modes in addition to the typical κ^3-N,N',N''[9] (Scheme 1.1). They can behave also as tridentate κ^3-N,N',B-H donors[10] with a borohydride moiety linked to the metal, as bidentates κ^2-N,N'[11-13] or κ^2-N,B-H[14-16] and, more rarely, as κ^1 and "κ^0" (*i.e.* as uncoordinated counterion).[17,18] Higher hapticities (κ^6 and occasionally κ^4 and κ^5) are possible in case the substituents in 3-position of the pyrazole rings (Scheme 1.2) contain additional donor atoms.[19,20]

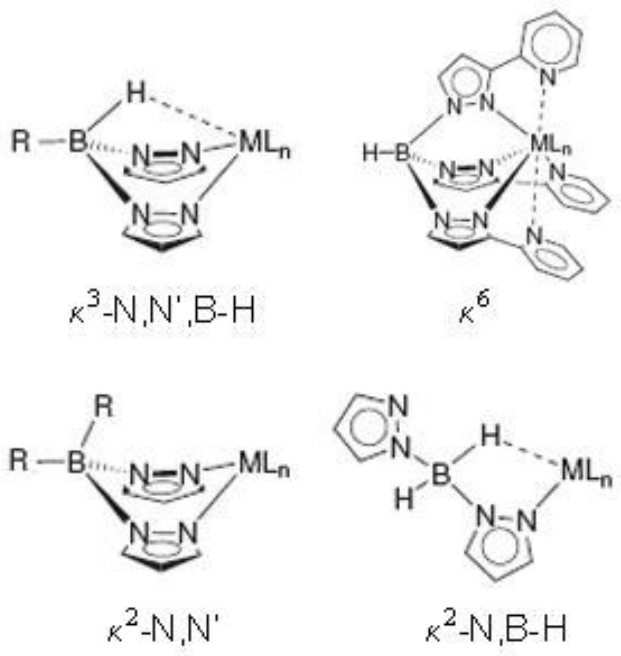

Scheme 1.1 More common coordination modes of Tps, alternative to κ^3-N,N',N''.

The coordination properties of Tp ligands (Tps) strictly depend on the steric and electronic effects of the substituents on pyrazoles, which are usually located on C3 and C5 of each heterocycle[21] (see Scheme 1.2).

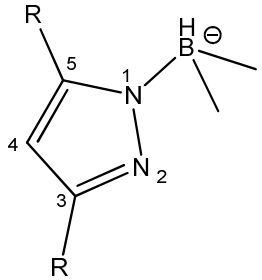

Scheme 1.2

In particular, the steric hindrance exerted on the metal center mainly depends on the substitution on C3 of each pyrazole and it was quantified by Trofimenko, who measured the *cone angle* (ϑ)[21] of different Tp^X ligands[22-24] (X indicates the C3 substituent). Clearly, larger cone angles favor the formation of $[Tp^XML]$ complexes over $[Tp^X{}_2M]$ ones (M = metal, L = co-ligand). It is worth of note that the steric bulk on C3 has the result of creating a hydrophobic pocket around the metal ion, which may affect its reactivity with other species (*e.g.* substrates, co-ligands).[25] As regards the electronic effects of the substituents, the electron-donation of the ligands to the metal is affected by them in analogy to what happen in organic chemistry for substituted hydrocarbons.[21]

The definition of scorpionates has been extended to tripodal ligand analogs to tris(pyrazolyl)borates with different donor groups and bridging atoms. Central atoms other than boron, such as carbon, silicon,[26,27] germanium and tin,[28] aluminium, gallium and indium,[29] phosphorus[30-32] and nitrogen[33,34], possibly affecting the total charge of the ligand, have been reported (Scheme 1.3), even though the most studied classes of scorpionates are the Trofimenko's B-centered tris(pyrazol-1-yl)borate derivatives and the C-centered poly(pyrazol-1-yl)alkane derivatives.[35-40] Their coordination properties with s,p-block elements[41] and transition metals have been reviewed.[42-45]

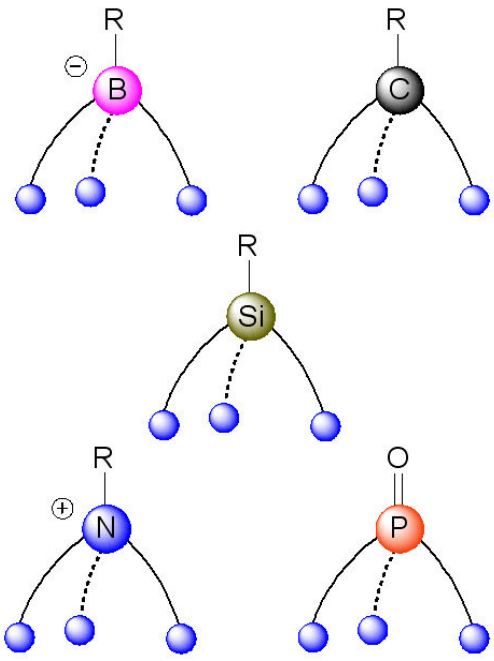

Scheme 1.3 Stylized examples of scorpionate ligands with different central atoms/groups.

In general, independently from the nature of the bridging atom, two families of scorpionate ligands may be distinguished, namely *homoscorpionates* and *heteroscorpionates*, according to the presence of one or more types of metal binding groups, respectively. We are dealing not only with different substituted pyrazoles[5,46], but also with other types of heterocycles (possibly with different donor atoms), such as methimazole,[47,48] indole,[49] indazole[50], pyridine,[34] triazole[51] and others, and even with acyclic donor groups.[52-54] As an example, three classes of B-centered tripods are reported in Scheme 1.4, the classical Tp^{R2} in comparison with the *soft* analogs Tm^{R} [48] and $Tr^{R,R1}$,[55] containing respectively methimazole and thioxo-triazole as donor 'arms'.

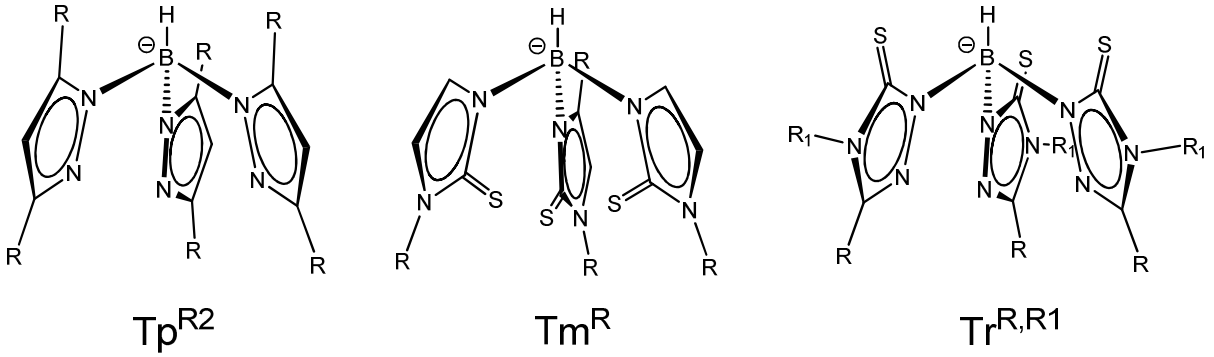

Scheme 1.4

As regards the synthesis of scorpionates, we focus on the two major classes, *i.e.* tris(pyrazol-1-yl)borate and poly(pyrazol-1-yl)methane derivatives. In particular, B-centered Tps and analogs can be prepared most easily by the neat reaction of a heterocycle (*e.g.* pyrazole) with a borohydride anion in a temperature-controlled solvent-free reaction, but even in presence of dry solvents as THF and toluene (Scheme 1.5).

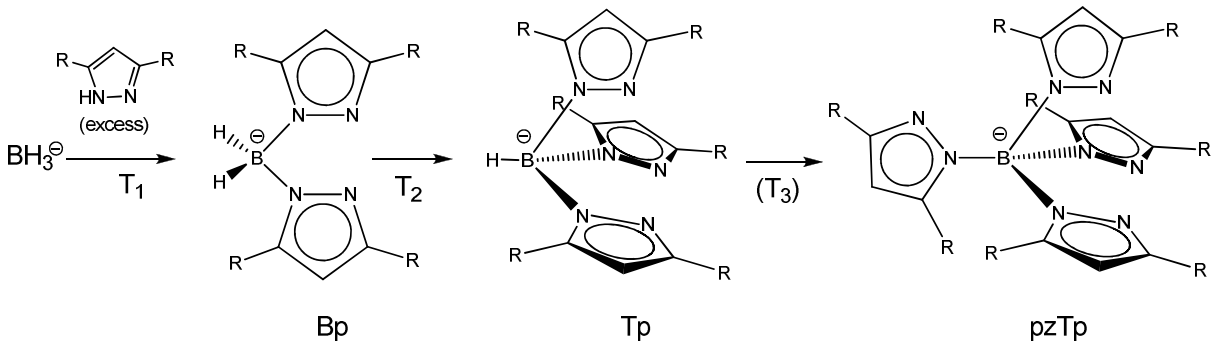

Scheme 1.5

Whereas the synthesis of B-centered homoscorpionates is quite plain, the preparation of the homologous heteroscorpionates (which implies the employment of a mixture of different heterocycles)[46,56] is not always successful, due to the scarce control achievable on the substitution grade on boron. Preparation of heteroleptic scorpionates is simpler in the case of carbon as central atom of the tripod, because of the greater variability of carbon chemistry with respect to boron one. Tris(pyrazol-1-yl)methane[35-38,57-62] and bis(pyrazol-1-yl)methane[39,40] derivatives are mainly prepared as shown in Scheme 1.6.

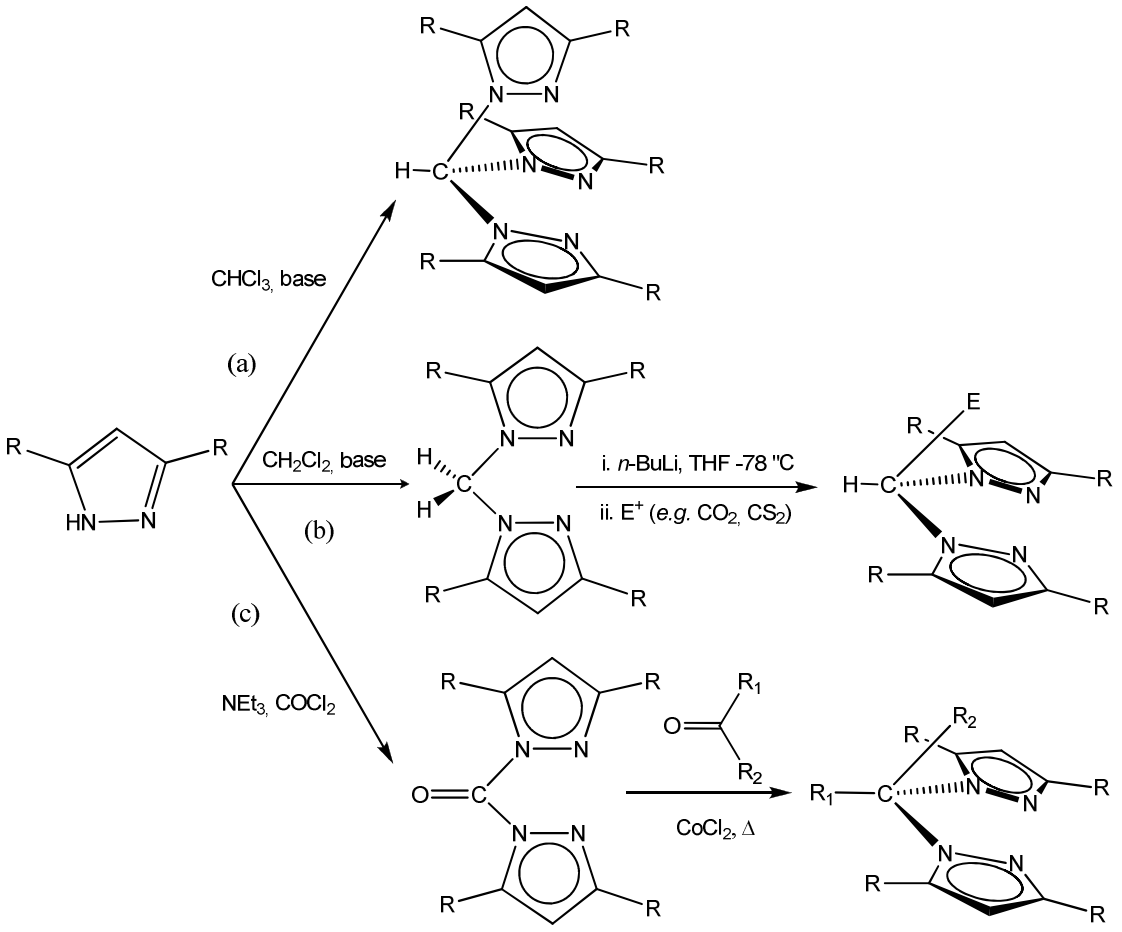

Scheme 1.6

The wide use of scorpionate ligands in coordination chemistry is due to their reliability and accountability as "spectator ligands",[9] which normally do not interfere with the reaction scenarios occurring at the metal centers. Because we are dealing with polydentate ligands, which possibly impose steric hindrance on the metal, their role is that of blocking certain sites and to leave a specific set of sites available for the "actor ligands", so that the desired chemistry can occur. Thus, scorpionates are inclined only to modulate and tune the electronic

and steric properties of the metal ion and of the co-ligands, without taking part to the reactivity of the complexes. Studies about the effects of the presence of scorpionates on the rate of co-ligand substitution in metal complexes are reported in literature.[63]

The most important applications of the metal-scorpionate complexes are based on the behaviour of these tripodal molecules as spectator ligands. More specifically, the main fields of application can be grouped in four categories: biomimetics, catalysis, material science and production of radiopharmaceuticals.

1) As regards biomimetics, many metal-scorpionate complexes behave as structural and/or functional models for active sites of metalloproteins or metalloenzymes. In fact, Tp and analogs (broadly speaking) would mimic the donor groups of the protein framework, which coordinate the metal ion as a spectator, only affecting its electronic and steric properties, and without directly taking part to the reactivity of the substrates. In particular, pyrazole groups, and more appropriately imidazole ones, model the nitrogen-donor hystidine residues of the protein, whereas more *soft* 'arms' (as methimazole) mimic the S-cysteine residues. Many works regard the modeling of active sites containing late transition-metals, such as zinc (*e.g.* Scheme 1.7),[8,64-68] copper[21,69-73] or iron,[74-76] even though the biomimetics of vanadium,[77] molybdenum,[78-80] tungsten[81,82] and manganese[83,84] has been also studied.

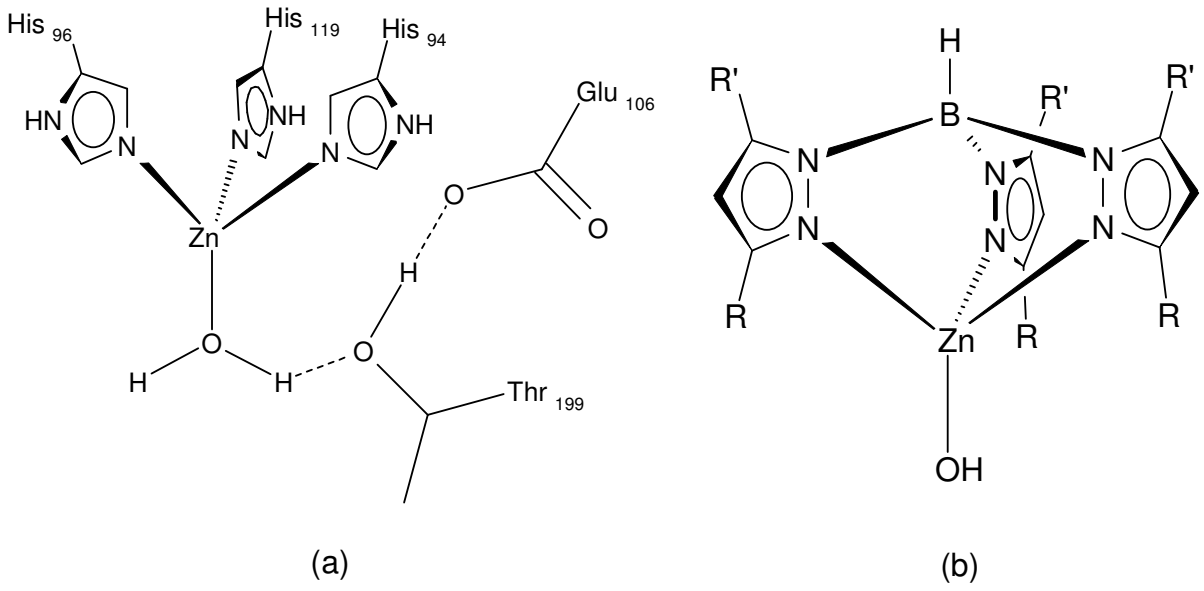

Scheme 1.7 Tp-zinc-hydroxide complexes (b) mimicking the active site of carbonic anhydrase (a).[85-88]

A peculiar case is represented by the structural and functional mimics of T1 sites of *blue copper proteins* by means of Tp-metal-thiolate complexes[89-92] (*e.g.* Scheme 1.8). Blue copper proteins are small copper proteins (10-20 kDa), which control electron transfer from donor to acceptor biomolecules in respiratory and photosynthetic processes of many bacteria and plants.[93,94] The unusual coordination of T1 centers, intermediate between trigonal planar and distorted tetrahedral, is characterized by strong bonds between the metal and three donor atoms on a plane (N-His, N-His, S-Cys) and by a weaker interaction with a fourth axial ligand (usually S-Met). Copper geometry and donor set favor a reversible and fast electron transfer of the Cu(II)/Cu(I) couple, associated with low reorganization energy in the redox process.[95]

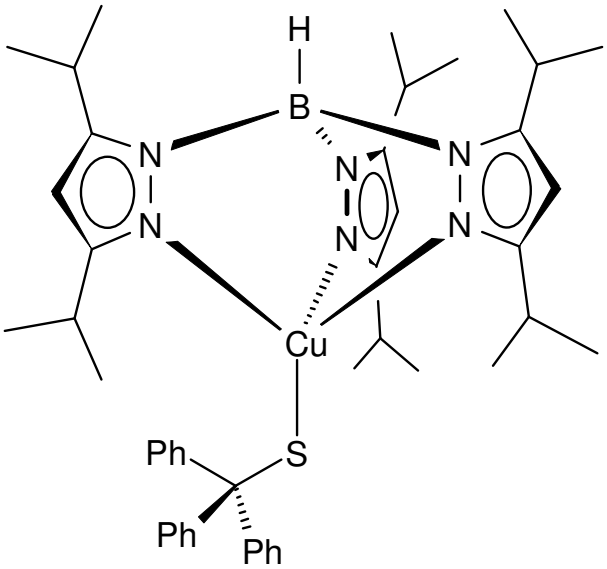

Scheme 1.8 A Tp-Cu(II)-thiolate model for T1 sites of blue copper proteins.[89]

2) Moving from enzymatic to chemical catalysis is natural; in fact, many metal-scorpionate complexes have found application also in relation to the latter aspect. The hydrotris(pyrazolyl)borate ligand is formally analogous to the cyclopentadienide (Cp^-) ligand, in that both are uninegative, six-electron donors, and even formally isolobal.[96] Hence, the use of Tp and derivatives in analogy to Cp as spectator ligands in organometallic catalysts, as 6-electron *hard* donors. Many scorpionate complexes, often containing late transition metal ions (such as Cu(I), Ag(I), Rh(I), Ir(I), Pt(II), Ru(II)) are active in the activation of aromatic and aliphatic CH bonds.[97-103] Catalytic formation of C-C,[104] C-O,[105] and C-N[106-108] bonds are reported (Cu(I) complexes). Usually, carbene or nitrene intermediates are involved in the catalytic mechanisms (*e.g.* Scheme 1.9). Early transition metal complexes (and especially

metals of group 4) are active as catalysts for olefine polymerization.[102,109-114] The recent characterization of the thermally stable gold complex [(Tp)Au(CH_2CH_2)] prefigures the use of Au-scorpionate complexes in catalysis.[115] Quasi-heterogeneous catalysts (which may be nanofiltered) were obtained by grafting dendrimers to scorpionate complexes of Rh.[116] Stereoselective catalysis in presence of chiral scorpionate systems was also studied.[104,117]

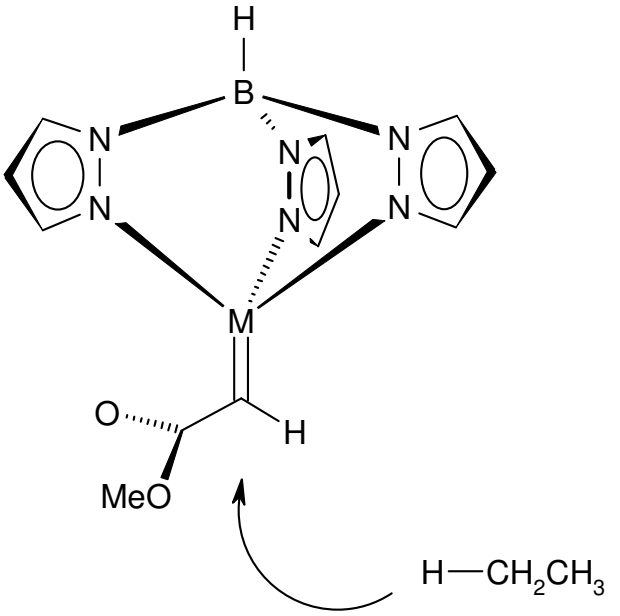

Scheme 1.9 An example of carbene-complex involved in the activation of C-H bonds (M = Cu, Ag).[101]

3) Regarding the applications in material science and crystal engineering, some metal-scorpionate complexes have polynuclear solid state structures, *i.e.* can be considered as coordination polymers, and in particular as metal-organic frameworks (MOFs).[118-120] We are dealing with materials with special electronic and magnetic properties,[121] or with application as non-linear optics media,[122] or as exchanging agents for small molecules (*e.g.* Figure 1.3),[123] possibly paramagnetic.[124] Other metal-scorpionate complexes give rise to supramolecular assemblies through weak interactions involving the ligands, instead through coordination bonds.[125-129]

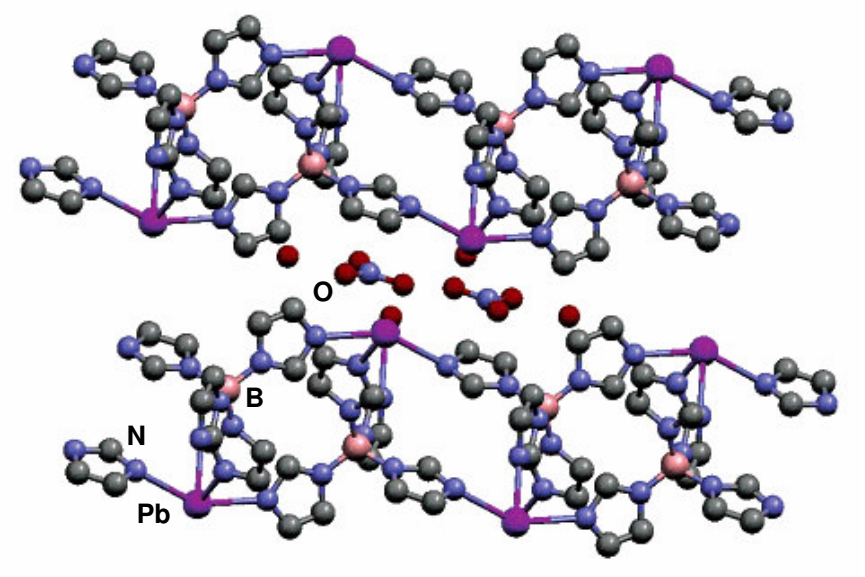

Figure 1.3 The compound $Pb(B(Im)_4)(NO_3)\cdot 1.35H_2O$ is a coordination polymer, which can readily undergo anion exchange in the solid state with retention of crystallinity.

4) Recently, some scorpionate-containing complexes of ^{99m}Tc and Re have found application respectively as radiopharmaceuticals or as models for these ones.[130-135] Clearly, water-solubility and water-stability are essential conditions for the applicability of these complexes in this field.[136] As an example, $[^{99m}Tc\{\kappa^3\text{-}HB(tim^{Me})_3\}(CO)_3]$ (Scheme 1.10) acts as radio-emitting target for particular receptors of the central nervous system.[137,138]

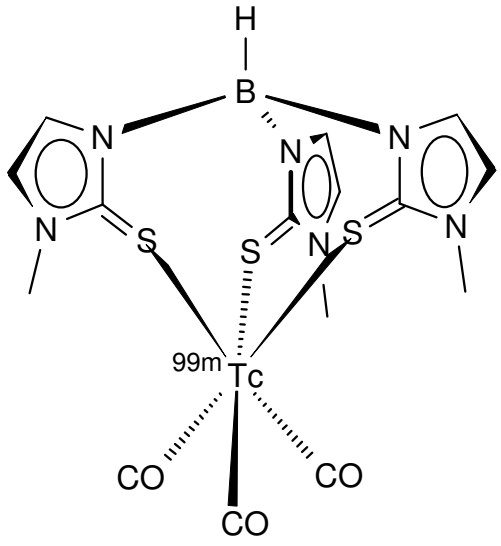

Scheme 1.10 The *fac*-$[^{99m}Tc\{\kappa^3\text{-}HB(tim^{Me})_3\}(CO)_3]$ acts as a radio-emitting target for the 5-HT1A receptor of CNS.[138]

Our work regards the synthesis and characterization of new metal-scorpionate complexes, with a focus on Cu(I) complexes with N/S-donor tripodal ligands. In particular, amongst the above-mentioned possible fields of application for these systems, we focused our efforts almost exclusively on the modeling of metal-sites of Cu-proteins (as the T1 reduced sites of blue copper proteins). We have been interested in evaluating the coordination modes of the employed ligand systems, the nuclearity of the resulting complexes and the geometries around the metal. We have placed a special emphasis on the often neglected solution properties of the complexes, together with the structural characterization at the crystalline state. We aimed at verifying if the employed scorpionates have the ability of imposing coordination geometry on the metal centers, or the electronic and steric requirements of the latter dominate the coordination, instead. In the former case we would be dealing with sufficiently preorganized ligands that induce an 'energized state' of the metal, defined as entatic state,[139] which may be conserved with no appreciable structural arrangements in the oxidized state, in analogy to what possibly happens in the T1 sites of blue copper proteins.[140-146]

Initially, we considered dinuclear Cu(I) complexes with anionic tripodal B-centered S_3 and S_2N donor ligands[147] and investigated their reactivity with monodentate co-ligands (Chapter 2). Analyzing the drawbacks of these systems (scarce tunability of the scorpionate arms and possible coordination of the borohydride to the metal) we pointed our attention towards neutral C-centered scorpionates. A new class of tripods based on a pyridine-pyrazole moiety was developed, the first of which is the N,N',O-donor LOH (Chapter 3), whose coordination capabilities were tested with late transition metal ions (Ni^{2+}, Cu^{2+}, Zn^{2+}). N/S-donor ligands of the same typology, namely N,N',S,S'-scorpionates (Chapters 5 and Section 6.1) and a N,N',S precursors (Chapter 4), were prepared and coordinated to Cu(I) Finally, we tested the binding capabilities of new N_2S,S'-donor bis(pyrazolyl)methane derivatives with Cu(I) (Section 6.2).

2

Cu(I) Dinuclear Complexes with B-Centered N/S-Scorpionates. Reactivity with σ-Donor Monodentate Ligands[148]

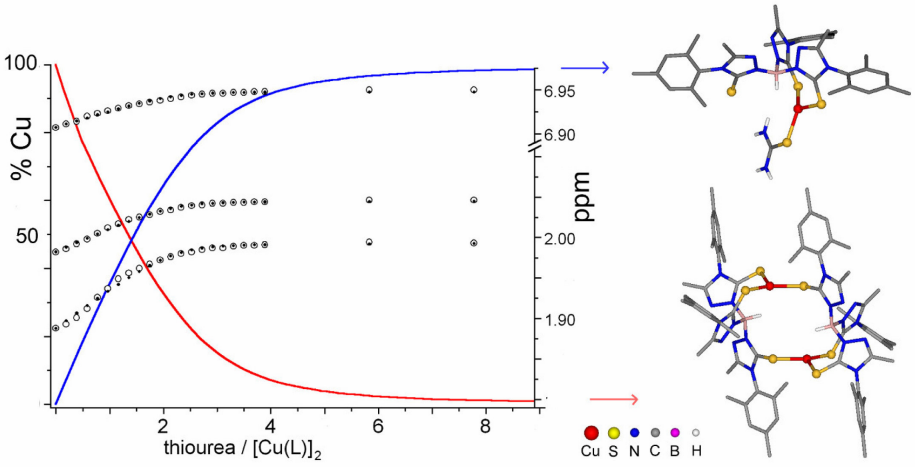

The complexes [(PPh$_3$)Cu(Tr^{Mes,Me})] (**1**), [(PPh$_3$)Cu(Tr$^{Me,o\text{-}Py}$)] (**2**) and [(PPh$_3$)Cu(Br^{Mes}pz$^{o\text{-}Py}$)] (**3**) {Tr^{Mes,Me} = hydrotris[1,4-dihydro-3-methyl-4-mesityl-5-thioxo-1,2,4-triazolyl]borate; Tr$^{Me,o\text{-}Py}$ = hydrotris[1,4-dihydro-4-methyl-3-(2-pyridyl)-5-thioxo-1,2,4-triazolyl]borate; Br^{Mes}pz$^{o\text{-}Py}$ = hydro[bis(thioxotriazolyl)-3-(2-pyridyl)pyrazolyl]borate} were synthesized by reaction of the dinuclear complexes [Cu(L)]$_2$ (L= Tr^{Mes,Me}, Tr$^{Me,o\text{-}Py}$, Br^{Mes}pz$^{o\text{-}Py}$) with PPh$_3$. As revealed by X-ray studies, **1** and **2** are mononuclear complexes with the metal in a slightly distorted tetrahedral geometry (S_3P coordination) bound by a κ^3-S_3 ligand and a PPh$_3$. No fluxionality in solution is evidenced by ^{1}H VT NMR (210-310 K, CDCl$_3$).The compound **3** was characterized only by ^{1}H VT NMR (320-200 K, CD$_2$Cl$_2$) and ^{1}H-^{1}H NOESY: an equilibrium between two species, **3a** and **3b**, was detected (coalescing temperature = ~260 K). DFT calculations suggest that **3a** and **3b** present S$_2$HP and S$_2$NP coordination to copper, respectively. The mononuclear complex [(tu)Cu(Tr^{Mes,Me})] (**4**) crystallized in presence of an excess of tu with respect to [Cu(Tr$^{Me,o\text{-}Py}$)]$_2$ (~6:1). The metal adopts a distorted tetrahedral geometry with an overall S_3H coordination determined by the ligand κ^3-S_2H bound (two C=S groups and a [B-H···Cu] interaction) and by a tu. The reactivity of the dinuclear complexes [Cu(L)]$_2$ with monodentate ligands (L' = PPh$_3$, tu and py) was investigated by means of ^{1}H NMR titrations, which allowed to determine the formation constants of the [(L')Cu(L)] adducts.

2.1 Introduction

In a previous study the coordination properties of three B-centered S/N-donor scorpionates with Cu(I) were investigated (Scheme 2.1), aiming at obtaining models for reduced T1 sites of *blue copper proteins.*[147]

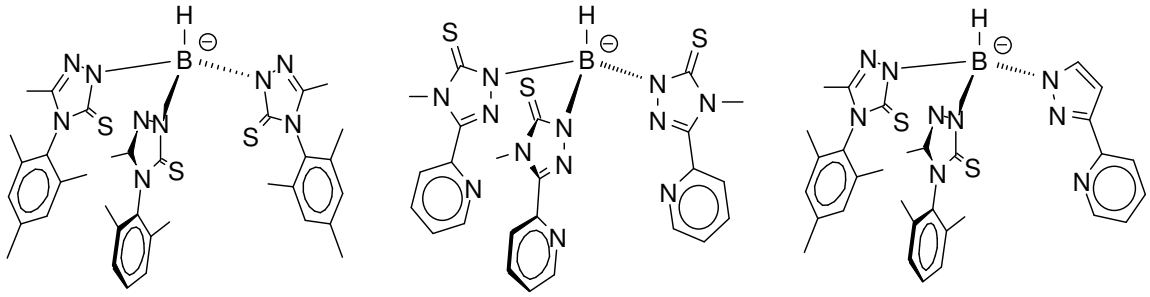

[Tr^{Mes,Me}]$^-$ **[Tr$^{Me,o\text{-}Py}$]$^-$** **[Br^{Mes}pz$^{o\text{-}Py}$]$^-$**

Scheme 2.1

The dinuclear complexes [Cu(L)]$_2$ (L = Tr^{Mes,Me}, Tr$^{Me,o\text{-}Py}$, Br^{Mes}pz$^{o\text{-}Py}$), exhibiting fluxional behavior in solution, are poor candidates for our purposes. This status is favored by the availability of various energetically accessible geometries for Cu(I) and its intrinsic lability.[149,150]

In the present chapter, to further investigate the properties of the dinuclear complexes, we followed their reactivity with monodentate ligands such as triphenylphosphine, thiourea, and pyridine, providing a varied donor set. The evaluation of the stability of the dinuclear complexes against σ-donor ligands is important for the interpretation of possible equilibria occurring in solution. In addition, the ternary adducts [(L')Cu(L)] (L' = PPh_3, tu, py) could have importance as catalytic precursors, wherein L' could be substituted by a substrate (*e.g.* to rise a carbene complex).[101,151] In a first step, some adducts were structurally characterized by X-ray diffraction or by 2D NMR techniques/DFT calculations: all these species are mononuclear. Subsequently, the speciation equilibria and the stability constants of the adducts were determined, when possible, by means of ^{1}H NMR titrations[152] of the Cu(I) dimers with the monodentate ligands.

2.2 Experimental

2.2.1 General procedures

All reagents and solvents were commercially available (Aldrich), except for $[Cu(L)]_2$ (L = $Tr^{Mes,Me}$, $Tr^{Me,o\text{-}Py}$, $Br^{Mes}pz^{o\text{-}Py}$), which were prepared as previously reported.[147] The solvents were stored under nitrogen on molecular sieves 4Å (1-2 mm) and degassed before use. The ^1H, ^{13}C and 2D NMR (homonuclear COSY and ^1H-^{13}C HSQC, useful for peak assignment, and homonuclear NOESY) spectra were recorded on a Bruker Avance 300 spectrometer using standard pulse sequences, whereas the ^{31}P NMR spectra were recorded on a Bruker AMX-400 spectrometer. Chemical shifts are reported in ppm referenced to residual solvent signals (^1H and ^{13}C), or to an external standard ($^{31}P^{45}$, 85% H_3PO_4). The 2D-NOESY experiments were recorded using a mixing time (τ_m) of 0.6 s for **1-3**. Variable temperature ^1H NMR experiments were recorded at 10 K intervals in the 210-310 K range ($CDCl_3$) for **1** and **2** and in the 210-300 K range (CD_2Cl_2) for **3** in controlled atmosphere valve NMR tubes. Mass spectra were acquired on a Micromass ZMD spectrometer. The mixtures were analyzed in negative and positive ionization modes by direct perfusion in ESI-Mass interface. Infrared spectra were recorded from 4000 to 400 cm^{-1} on a Perkin-Elmer FT-IR Nexus spectrometer (KBr pellets). Elemental analyses (C, H, N) were performed with a Carlo Erba EA 1108 automated analyzer.

*2.2.2 Synthesis of [(PPh_3)Cu($Tr^{Mes,Me}$)] (**1**)*

$[Cu(Tr^{Mes,Me})]_2$ (211 mg, 0.137 mmol) and PPh_3 (81 mg, 0.309 mmol) were mixed in $CHCl_3$ (6 ml). The solution was stirred for 1 h, hexane (~10 ml) was added until a minimum amount of precipitate formed. It was filtered off, and an exceess of hexane was added to the residual solution, causing the slow formation of colorless micro-crystals, which were filtered, washed with hexane, dried under vacuum and collected (**1**, 85 mg, 0.082 mmol, 30%). IR (cm^{-1}): 3050w, 2997w, 2968w, 2920w, 2858w, 2492w br, [ν(BH)], 1609w, 1580m, 1488m, 1419s, 1369s, 1325s, 1301s, 1275s, 1172w, 1153w. ^1H NMR (300 MHz, $CDCl_3$): δ 1.73 (s, 9H, CH_3 mes *ortho*), 2.03 (s, 18H, CH_3 mes *ortho*; CH_3 triazole), 2.38 (s, 9H, CH_3 *para*), 5.07 (br, 1H, BH), 6.98 (s, 3H, CH mes), 6.99 (s, 3H, CH mes), 7.06 (m, 6H, CH, PPh_3 *meta*), 7.21 (m, 9H, CH, PPh_3 *ortho* and *para*). ^{13}C NMR (75 MHz, $CDCl_3$): δ 11.17 (CH_3 mes *ortho* / CH_3 triazole), 18.14 (CH_3 mes *ortho* / CH_3 triazole), 18.62 (CH_3 mes *ortho*), 21.20 (CH_3 mes

para), 127.7 (d, J_{CCCP} = 8.8 Hz, CH PPh_3 *meta*), 128.6 (s, CH PPh_3 *para*), 129.24 (CH mes), 129.49 (CH mes), 130.06 (C quat.), 133.85 (d, J_{CCP} = 14.3 Hz, CH PPh_3 *ortho*), 134.48 (d, J_{CP} = 25.7 Hz, C quat. PPh_3), 136.17 (C quat.), 136.73 (C quat.), 139.17 (C quat.), 148.20 (C quat.), 167.66 (C=S). ^{31}P NMR (160 MHz, $CDCl_3$): δ 9.7 (s br). Anal. calcd for $C_{54}H_{58}N_9S_3BCuP$ (1134.62): C, 62.69; H, 5.65; N, 12.18. Found: C, 62.12; H, 5.21; N, 11.91%. Colorless crystals suitable for X-ray structure determination were obtained by slow evaporation from a $CHCl_3$/hexane solution of **1**, corresponding to $[Cu(Tr^{Mes,Me})]_2$ $4CHCl_3$ (**1a**).

*2.2.3 Synthesis of [(PPh$_3$)Cu(Tr$^{Me,o\text{-}Py}$)] (**2**)*

$[Cu(Tr^{Me,o\text{-}Py})]_2$ (81 mg, 0.062 mmol) and PPh_3 (34 mg, 0.130 mmol) were mixed in CH_2Cl_2 (10 ml). The solution was stirred for 1 h and concentrated under reduced pressure to about 5 ml. A pale yellow product was precipitated by the addition of hexane, filtered, washed with hexane, dried under vacuum and collected (**2**, 80 mg, 0.088 mmol, 71%). IR (cm^{-1}): 3050w, 2498w [ν(BH)], 1589m, 1478s, 1455m, 1434m, 1411s, 1341s, 1216m, 1084m. ^{1}H NMR (300 MHz, $CDCl_3$): δ 3.98 (s, 9H, CH_3), 5.15 (s br, 1H, BH), 7.31 (m, 12H, CH py (3H) and CH PPh_3 *meta* and *para* (9H)), 7.59 (m, 6H, CH PPh_3 *ortho*), 7.73 (t, J = 7.2 Hz, 3H, CH py), 8.15 (d, J = 7.8 Hz, 3H, CH py), 8.63 (d, J = 4.2 Hz, 3H, CH py). ^{13}C NMR (75 MHz, $CDCl_3$): δ 33.34 (CH_3 triazole), 124.07 (CH py), 128.28 (d, J_{CCCP} = 7.3 Hz, CH PPh_3 *meta*), 129.30 (CH PPh_3 *para*), 133.80 (d, J_{CCP} = 15.2 Hz, CH PPh_3 *ortho*), 136.61 (CH py), 147.24 (C quat.), 148.48 (CH py), 149.11 (C quat.), 169.95 (C=S). ^{31}P NMR (160 MHz, $CDCl_3$): δ 5.0 (s br). Anal. calcd for $C_{42}H_{37}N_{12}S_3BCuP$ (911.35): C, 55.35; H, 4.09; N, 18.44. Found: C, 54.77; H, 4.13; N, 17.97%. Colorless crystals were grown by slow evaporation from a DMF solution of **2**, corresponding to $[(PPh_3)Cu(Tr^{Me,o\text{-}Py})]\cdot DMF$ (**2a**).

*2.2.4 Synthesis of [(PPh$_3$)Cu(Br^{Mes,Me}pz$^{o\text{-}Py}$)] (**3**)*

PPh_3 (21 mg, 0.080 mmol) was added to a CH_2Cl_2 solution (5 ml) of $[Cu(Br^{Mes,Me}pz^{o\text{-}Py})]_2$ (50 mg, 0.036 mmol). After 30 min. of stirring, the volume was reduced to about 1 ml under reduced pressure. A bright yellow product was precipitated by the addition of an excess of hexane (~10 ml). The product was filtered, washed with hexane, dried under vacuum and collected (**3**, 24 mg, 0.025 mmol, 35%). IR (cm^{-1}): 3048w, 3004w, 2963w, 2919w, 2854w,

2471w br [ν(BH)], 1609w, 1592w, 1568w, 1488m, 1434s, 1414s, 1364m, 1325m, 1263s, 1199m, 1094s, 1017s. ^{1}H NMR (300 MHz, CD_2Cl_2): δ 1.97 (s, 12H, CH_3), 2.05 (s, 6H, CH_3), 2.38 (s, 6H, CH_3), 6.81 (br, 1H, CH py), 6.87 (d, J = 2.1 Hz, 1H, CH pyrazole), 7.05 (s, 2H, CH mes), 7.07 (s, 2H, CH mes), 7.32 (m, 16H, CH PPh_3 (15H) and CH py), 7.63 (br, 1H, CH py), 8.16 (br, 1H, CH py), 8.27 (br, 1H, CH py). ^{31}P NMR (160 MHz, $CDCl_3$): δ 2.4 (br). Anal. calcd for $C_{50}H_{50}N_9S_2BCuP$ (946.45): C, 63.45; H, 5.32; N, 13.32. Found: C, 63.12; H, 5.62; N, 13.23%.

2.2.5 Synthesis of [(tu)Cu($Tr^{Mes,Me}$)]·3CH_2Cl_2 ***(4)***

Colorless crystals of [(tu)Cu($Tr^{Mes,Me}$)] were obtained from a 1:1 hexane:CH_2Cl_2 solution of [Cu($Tr^{Mes,Me}$)]$_2$ (50 mg, 0.032 mmol) and tu (14 mg, 0.184 mmol). The crystals were filtered, dried under vacuum and collected (**4**, 20 mg, 0.023 mmol, 35%). IR (cm^{-1}): 3381m br, 3301m br, 3184m br, 3014m, 2959w, 2920w, 2855w, 2481w, 2410w, 1609s, 1576m, 1488m, 1406s, 1374s, 1326s, 1301s, 1274m, 1172m, 1144m, 1013m, 852w. ^{1}H NMR (300 MHz, 300 K, CD_2Cl_2): δ 1.954 (s, 18H, CH_3), 2.03 (s, 9H, CH_3), 2.32 (s, 9H, CH_3), 6.43 (s, br, 4H, NH_2), 6.97 (s, 6H, CH mes). ^{13}C NMR (75 MHz, CD_2Cl_2): δ 11.45 (CH_3), 18.00 (CH_3), 21.29 (CH_3), 129.64 (CH mes), 130.22 (C quat.), 136.53 (C quat.), 140.20 (C quat.), 148.96 (C quat.), 168.05 (C=S), 182.63 (C=S tu). Anal. calcd for $C_{37}H_{47}N_{11}S_4BCu$ (848.46): C, 52.38; H, 5.51; N, 17.91. Found: C, 52.42; H, 5.48; N, 18.22%.

2.2.6 X-ray crystallography

A summary of data collection and structure refinement for [(PPh_3)Cu($Tr^{Mes,Me}$)]·5$CHCl_3$ (**1a**), [(PPh_3)Cu($Tr^{Me,o\text{-}Py}$)]·DMF (**2a**) and [(tu)Cu($Tr^{Mes,Me}$)]·3CH_2Cl_2 (**4**) is reported in Table 2.1. Single crystal data was collected with a *Bruker AXS Smart 1000* area detector diffractometer (Mo Kα: λ = 0.71073 Å) for **1a** and **2a** and with an *Enraf Nonius CAD4* diffractometer (Cu Kα: λ = 1.54183 Å) equipped with an Oxford Cryosystems liquid nitrogen cryostream for **4** operating at 245 K. The crystal of **4** decomposed during the data collection with a 40% intensity loss of the reference reflection. An absorption correction was applied using the program SADABS[153] with transmission factors in the ranges 0.757-1.000 (**1a**) and 0.915-1.000 (**2a**) and using the method of Walker & Stuart[154] for **4** with min. and max. transmission

factors of 0.816 and 1.000. The structures were solved by direct methods (SIR97)[155] and refined with full-matrix least-squares (SHELXL-97),[156] using the Wingx software package.[157]

Table 2.1 Summary of X-ray crystallographic data for **1a**, **2a** and **4**.

	1a	**2a**	**4**
Empirical formula	$C_{58}H_{62}BCl_{12}CuN_9PS_3$	$C_{45}H_{38}BCuN_{13}OPS_3$	$C_{56}H_{106}B_2Cl_{12}Cu_2N_{22}S_8$
Formula weight	1512.07	978.38	1918.21
Colour, habit	Colourless, block	Colourless, block	Colourless, block
Crystal size, mm	0.35x0.30x0.15	0.35x0.25x0.18	0.45x0.20x0.10
Crystal system	Triclinic	Triclinic	Monoclinic
Space group	P-1	P-1	P21/c
a, Å	12.328(1)	10.573(1)	19.682(8)
b, Å	12.901(1)	13.571(1)	17.139(8)
c, Å	24.666(2)	38.381(2)	32.789(9)
α deg.	77.466(1)	106.265(2)	90
β deg.	79.834(1)	97.971(2)	97.26(2)
γ deg.	75.178(1)	104.757(2)	90
V, $Å^3$	3671.5(5)	2384.9(4)	10972(7)
Z	2	2	4
T, K	293	293	245
ρ(calc), Mg/m^3	1.368	1.362	1.161
μ, mm^{-1}	0.883	0.673	4.906
θ range, deg.	1.66 to 27.02	1.64 to 27.07	3.31 to 64.68
No.of rflcn/obsv F>4σ(F)	21770 / 7068	25981 / 4328	16374 / 5352
GooF	1.003	1.004	1.010
R1	0.0551	0.0465	0.0850
wR2	0.1123	0.0804	0.1655

$R1 = \Sigma||F_o|-|F_c||/\Sigma|F_o|$, $wR2 = [\Sigma[w(F_o^2-F_c^2)^2]/\Sigma[w(F_o^2)^2]]^{½}$, $w = 1/[\sigma^2(F_o^2) + (aP)^2 + bP]$, where $P = [\max(F_o^2,0) + 2F_c^2]/3$

Non-hydrogen atoms were refined anisotropically; for **1a** and **2a** the B-*H* hydrogen atoms were found and refined whereas the remaining hydrogen atoms were placed at their calculated positions. In **4** all the hydrogen atoms were placed at their calculated positions. In **1a**, three $CHCl_3$ molecules could be located from the difference Fourier map and two $CHCl_3$ solvent molecules were found disordered and were modeled with the SQUEEZE PLATON program.[158] The DMF molecule in **2a** was found disordered in two positions with site

occupancy factors of 0.57 and 0.43, respectively. In **4**, a CH_2Cl_2 solvent molecule was located from the difference Fourier map and two CH_2Cl_2 molecules were modeled with the SQUEEZE PLATON program. Molecular drawings were prepared using the Mercury 1.4.2 program.[159]

2.2.7 DFT calculations

All the calculations were performed with Gaussian 03 program suite.[160] Geometry optimizations were performed for the isomers of compounds **3** starting from geometries proposed on the basis of 1D and 2D NMR experiments. The two layers ONIOM technique[161-163] was employed. All the mesityl groups and the methyl groups on the triazoline rings were approximated to hydrogen atoms in the *model system*, and the gradient-corrected hybrid density functional B3LYP[164,165] and double-ζ basis set LANL2DZ with Hay and Wadt effective core potential (ECP)[166,167] were employed. A polarization d-function for the sulfur and phosphorous atoms were also added in the basis set. For the *real system*, Hartree-Fock with the LANL2MB basis set with Hay and Wadt ECP were used, the details of the partitioning scheme are given in the Appendix 1, Fig. A1. Single point energy calculations were performed for all compounds using the B3LYP density functional and the LANL2DZ basis set for copper and the 6-31G(d) basis set for the C, H, N, B, S and P atoms. The energies of the various compounds do not include thermal or entropy corrections.

2.2.8 NMR titrations

Dilution ^{1}H NMR experiments on $[Cu(L)]_2$, complexes were performed in the 10^{-2}-10^{-4} M copper concentration range (C_{Cu}). Samples of $[Cu(L)]_2$ (500 μL, $C_{Cu} = 10^{-3}$ M) were titrated with 0.1 M solutions of PPh_3 in $CDCl_3$. The $[Cu(L)]_2$/tu systems were studied by titrating a 800 μL sample of $[Cu(L)]_2$ ($C_{Cu} = 10^{-3}$ M) with a 0.1 M solution of tu (300K, fast-exchange regime). 25 spectra were collected up to a tu:$[Cu(Tr^{Mes,Me})]_2$ molar ratio of 10 in $CDCl_3$:MeOD 1:1 and 12 spectra up to a tu:$[Cu(Br^{Mes}pz^{o\text{-}Py})]_2$ ratio of 12.4 in CD_2Cl_2:MeOD 1:1. The solubility properties of $[Cu(Tr^{Me,o\text{-}Py})]_2$ and tu did not allow us to perform the NMR titration in this case. All sets of chemical shifts were treated simultaneously with the HypNMR 2004 program to compute the stability constants.[168] For L = $Tr^{Mes,Me}$ the chemical shifts of the mesityl *o*-CH_3 (~1.9 ppm), the triazolyl CH_3 (~2.0 ppm) and the mesityl CH

(~6.9 ppm) protons were computed, whereas in the case of L = $Br^{Mes}pz^{o\text{-}Py}$ the data fitting was performed on the chemical shifts of the mesityl-*o*-CH_3, the triazolyl-CH_3 and the mesityl-CH protons. The $[Cu(L)]_2$/py systems were studied by titrating a 500 μL sample of $[Cu(L)]_2$ (C_{Cu} = $6 \cdot 10^{-3}$ M) with a 0.1 M solution of py in $CDCl_3$ (300K, slow-exchange regime). 20 spectra were collected in the py:$[Cu(Tr^{Mes,Me})]_2$ range up to 40 ($CDCl_3$), 13 spectra were collected in the py:$[Cu(Tr^{Me,o\text{-}Py})]_2$ range up to 64 ($CDCl_3$) and 10 spectra were collected in the py:$[Cu(Br^{Mes}pz^{o\text{-}Py})]_2$ range up to 40 (CD_2Cl_2). The titrations of $[Cu(Tr^{Me,o\text{-}Py})]_2$ and $[Cu(Br^{Mes}pz^{o\text{-}Py})]_2$ with py were performed under nitrogen because of the air-sensitive products. All solutions were prepared by weight and used within 24 hours. The distribution diagrams were calculated and plotted by the program HySS 2000.[169]

2.3 Results and Discussion

In order to explore their stability/reactivity, the dinuclear complexes $[Cu(L)]_2$ (L = $Tr^{Mes,Me}$, $Tr^{Me,o\text{-}Py}$ or $Br^{Mes,Me}pz^{o\text{-}Py}$) were reacted with the σ-donor ligands PPh_3, tu and py. All the reactions were monitored through ^1H NMR titrations to evaluate the formation constants of the ternary complexes [(L')Cu(L)]. As the reactions with PPh_3 are quantitative, the $[(PPh_3)Cu(L)]$ adducts were isolated in stoichiometric conditions (Scheme 2.2).

$$[Cu(L)]_2 + 2\ PPh_3 \xrightarrow{CHCl_3\ /\ CH_2Cl_2} 2\ [Ph_3PCu(L)]$$

Scheme 2.2

The compounds can also be obtained by the one-pot reaction between $[Cu(CH_3CN)_4]BF_4$,[170] LiL, and PPh_3. The products are colorless (**1**) or pale yellow (**2**-**3**) air-stable solids. The stability constants (*K*) of the complexes [(tu)Cu(L)] and [(py)Cu(L)] are much lower (in some cases too low to be determined). Due to the latter, we cannot isolate the complexes from a 1:2 mixture of $[Cu(L)]_2$ and tu or py. However, colorless crystals of $[(tu)Cu(Tr^{Mes,Me})]$ were obtained from an hexane:CH_2Cl_2 solution of $[Cu(Tr^{Mes,Me})]_2$ and tu in 1:6 ratio.

2.3.1 Molecular structures

Essentially, the solid state structures of the phosphinic complexes **1a** and **2a** (Fig. 2.1-2.2) present an equivalent type of copper coordination. Selected bond lengths and angles are reported in Tables 2.2 and 2.3.

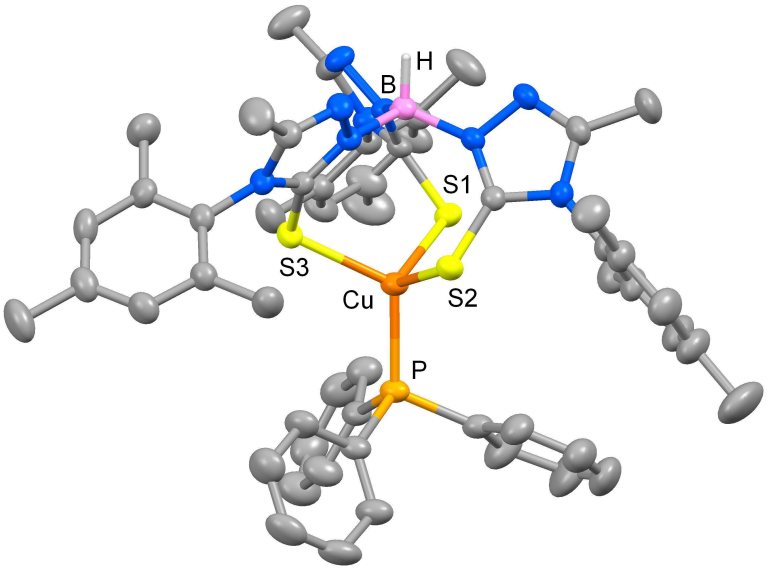

Figure 2.1 Molecular drawing of **1a** at the 30% thermal ellipsoids probability level. Hydrogen atoms, except the B-*H*, have been removed for clarity.

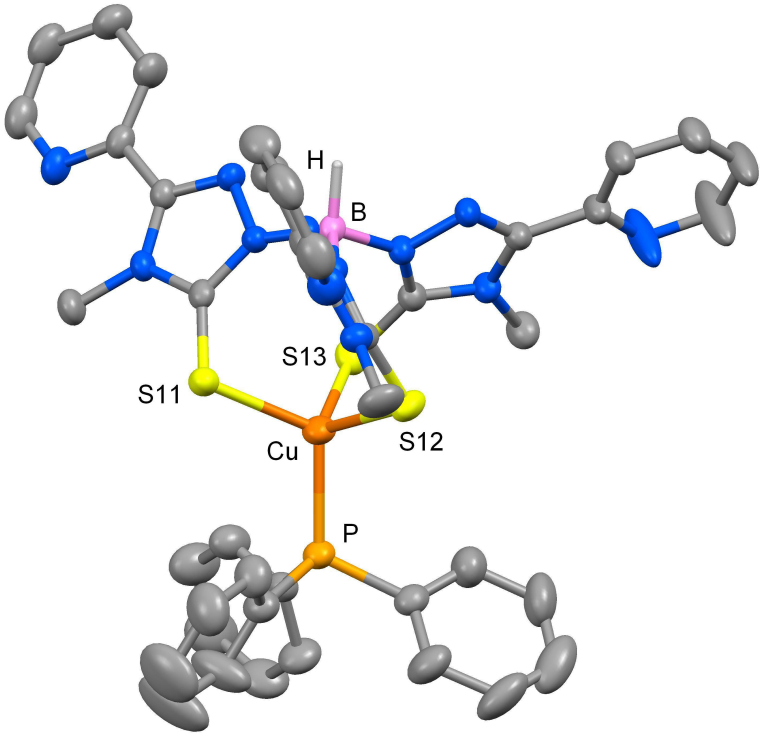

Figure 2.2 Molecular drawing of **2a** at the 30% thermal ellipsoids probability level. Hydrogen atoms, except the B-*H*, have been removed for clarity.

Table 2.2 Selected bond lengths (Å) and angles (°) for **1a**.

Cu-S(1)	2.379(5)	S(1)-Cu-S(2)	107.03(4)
Cu-S(2)	2.383(1)	S(1)-Cu-S(3)	105.77(3)
Cu-S(3)	2.372(1)	S(2)-Cu-S(3)	102.39(4)
Cu-P	2.243(1)	S(1)-Cu-P	112.48(4)
B-H	1.04(3)	S(2)-Cu-P	111.53(4)
		S(3)-Cu-P	116.75(4)

The metal exhibits a tetrahedral geometry, bound by a tridentate ligand (κ^3-S_3) and by a terminal PPh_3 with an overall S_3P coordination. Both complexes present non-crystallographic C_3 symmetry. The Cu-P bond lengths [2.243(1) Å, **1a**; 2.220(1) Å, **2a**] and the Cu-S ones [2.372(1)-2.385(1) Å, **1a**; 2.343(2)-2.363(1) Å, **2a**] are in accordance with the Cu-S and Cu-P separations reported for the [(PR_3)Cu(Tm))] (R = *m*-tolyl, *p*-tolyl) compounds.[171] **1a** and **2a** exhibit the same coordinative environment, despite the ligands $Tr^{Mes,Me}$ and $Tr^{Me,o\text{-}Py}$ present different substituents on the triazoline rings. The S-Cu-S bond angles in **1a** [102.39(4)-107.03(4)°] are significantly smaller than the S-Cu-P bond angles [111.53(4)-116.75(4)°], whereas **2a** presents a more regular tetrahedral geometry [S-Cu-S = 105.22(4)-108.58(4)°; S-Cu-P = 107.65(4)-114.59(4)°]. The former may be the result of the pronounced steric hindrance determined by the mesityl groups of $Tr^{Mes,Me}$, which would limit the approach of the tripod to the $[Cu(PPh_3)]^+$ fragment.

Table 2.3 Selected bond lengths (Å) and angles (°) for **2a**.

Cu-S(11)	2.352(1)	S(11)-Cu-S(12)	105.22(4)
Cu-S(12)	2.363(1)	S(11)-Cu-S(13)	106.73(4)
Cu-S(13)	2.343(1)	S(12)-Cu-S(13)	108.58(4)
Cu-P	2.220(1)	S(11)-Cu-P	114.59(4)
B-H	1.14(2)	S(12)-Cu-P	107.65(4)
		S(13)-Cu-P	113.62(4)

In solution of chlorinated solvents the compounds **1** and **2** essentially preserve the solid state structures. In fact, in the ^1H and ^{13}C NMR spectra only a set of signals was detected for the three donor groups of the tripodal ligands, in accordance with the pseudo-C_3 symmetry exhibited by the complexes in the solid state. Any fluxional behavior was excluded by means of variable temperature NMR experiments performed in the 220-305 K temperature range (only a slight derive of the chemical shifts was observed). The NOESY spectra (not reported)

show cross-peaks between the *ortho* and *meta* CH of PPh_3 and the CH_3-mesityl groups (**1**), or the triazoline methyl groups (**2**), thus confirming the proximity between PPh_3 and the tripodal fragment. Moreover, the nitrogen atoms of the pyridine rings of **2** are oriented towards the triazoline methyl groups, as evidenced by the cross peak between the N-*ortho* proton of py and the CH_3 of triazoline.

Despite all attempts to crystallize the phosphinic compound **3**, we could not obtain suitable crystals for an X-ray structure analysis. However, some structural information comes from NMR data and quantum mechanical calculations. Compound **3** exhibits a fluxional behavior in CD_2Cl_2 solution, as resulted from variable temperature NMR experiments (220-300 K, Figure 2.3).

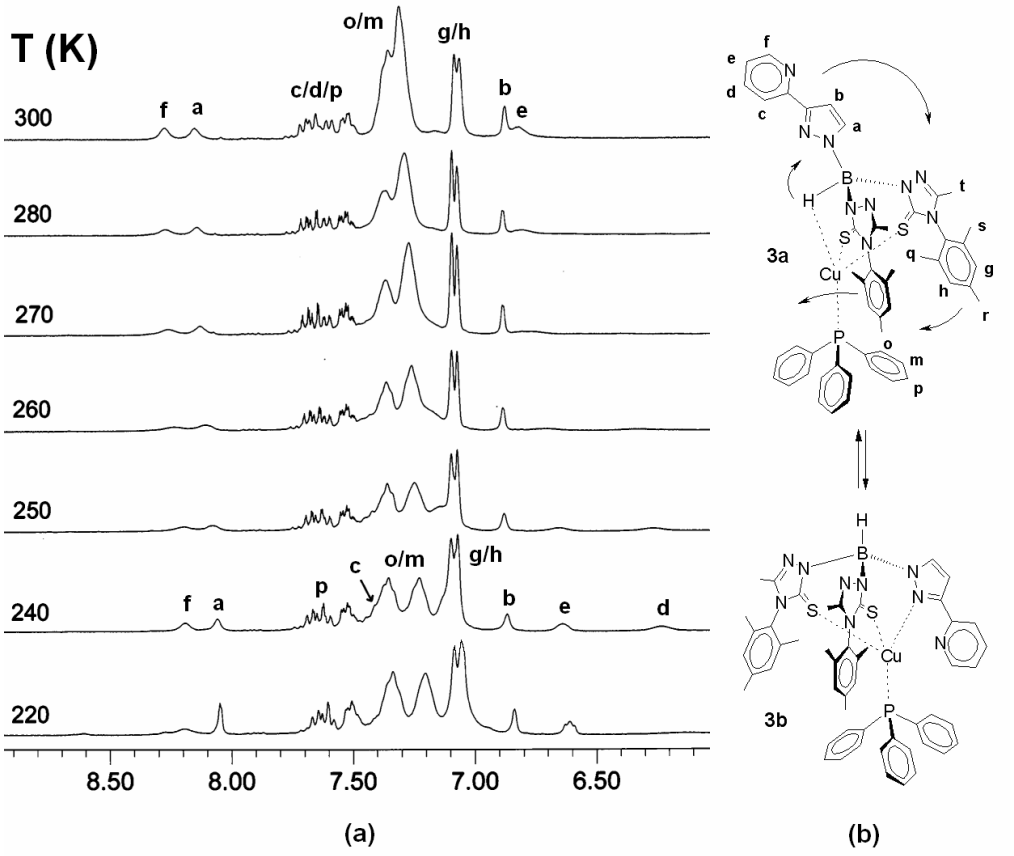

Figure 2.3 (a)Temperature dependence of the ^{1}H NMR spectrum (aromatic region) of **3** in CD_2Cl_2 and (b) interpretation as an equilibrium between the isomers **3a** and **3b**.

A major species evident at 240 K is in equilibrium with a second species present in a small concentration, whose signals are broad or covered by the major species peaks. The NOESY spectrum recorded in CD_2Cl_2 at 300 K (above the coalescence temperature) presents a

positive cross peak indicative of the fluxional behavior of the complex, which involves the **a** proton and another proton of a second species exhibiting a very broad signal at approximately 8.50 ppm (Appendix 1, Figure A2). Unfortunately, the remaining positive cross peaks arising from the dynamic process could not be detected.

Quantum calculations were employed to propose reasonable structures of **3** and to explain its fluxional behavior in solution. The conformations and the relative energies of three possible isomers of **3** (**3a**-**c**) are reported in Figure 2.4 and their relevant geometric parameters are listed in Appendix 1, Table A1.

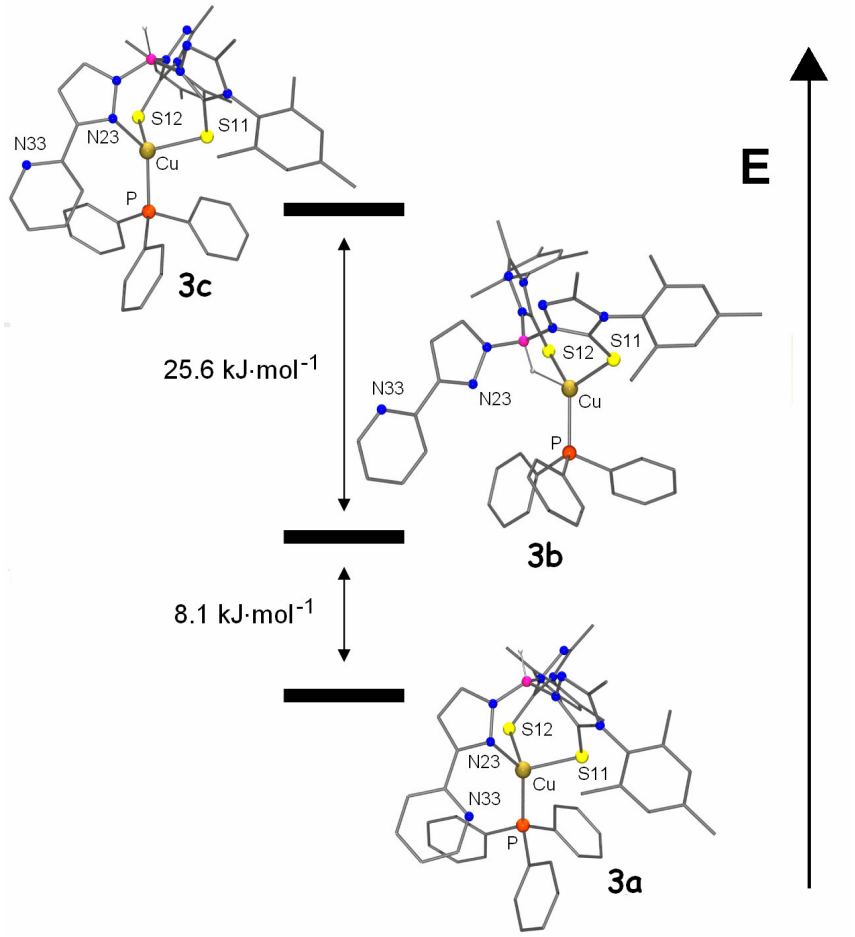

Figure 2.4 Calculated energy diagram for the **3a-c** isomers. Optimized geometries were obtained at the ONIOM b3lyp/lanl2dz-HF/lanl2mb level. Single point energy calculations were performed with the b3lyp density functional and with the lanl2dz (Cu) and 6-31G(d) (other atoms) basis set.

The geometry optimizations were performed by using initial geometries proposed on the basis of the NOESY spectrum (CD_2Cl_2, 240 K), which suggests the coordination of PPh_3 to copper in the major species (as attested by negative cross-peaks between the *ortho* mesityl CH_3

groups of $Br^{Mes,Me}pz^{o\text{-}Py}$ and the *ortho* and *meta* PPh_3 protons, Figure 2.5). In the **3a**-**c** isomers the metal is always tetrahedral, whereas the scorpionate ligand presents different conformations and donor sets (S_2H for **3a** and S_2N for **3b**-**c**). The energy difference between **3a**, which results the most stable species, and **3b** is of 8.3 $kJ \cdot mol^{-1}$, being in agreement with an equilibrium between the two species, which would be consistent with the NMR evidences (see Figure 2.3 a). This energy difference also justifies the fact that **3b** is essentially undetected by the NMR experiments.

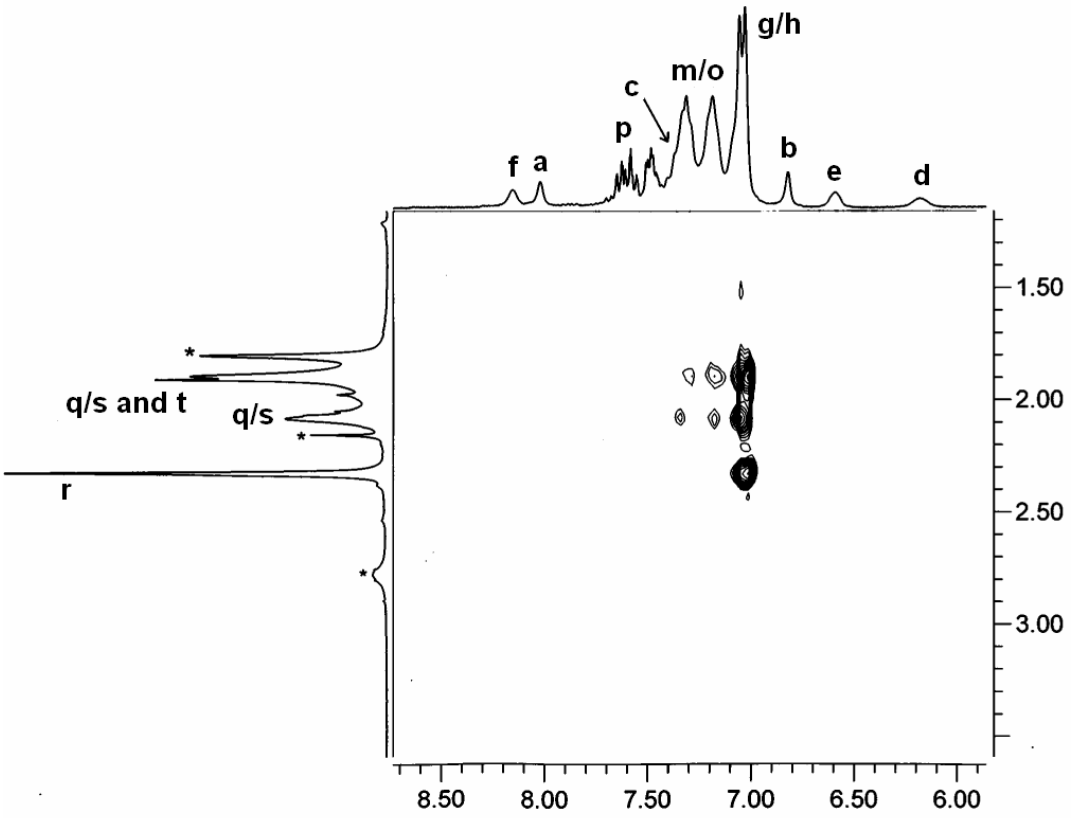

Figure 2.5 Aromatic-methylic region of the ^1H-^1H NOESY NMR spectrum of **3** at 240 K in CD_2Cl_2. Solid lines denote negative cross-peaks (* = water and impurities). See Figure 2.3 for the attribution.

The structural reorganization for the **3a** ⇌ **3b** process involves the inversion of the ligand conformation since in **3a** the hydride is bound to the metal (1.915 Å), whereas in **3b** it points outward and the pirazole nitrogen atom enters the metal coordination (see Figure 2.3 b). In **3b**, the pyridinyl nitrogen N33 is directed toward Cu, but it is located at a non interacting distance (3.320 Å). The destabilization of the hypothetical **3c** isomer, absent in solution, with respect to **3b** (25.6 $kJ \cdot mol^{-1}$) is due to the pyridine conformation, which presents a C-H group that interferes with the metal and the C-H_{ortho} of PPh_3. Finally, in solution of CD_2Cl_2 an

equilibrium between a major species presenting a *S_2HP* coordination to copper (**3a**) and a minor one (**3b**, *S_2NP* coordination) can be supposed for the phosphinic complex **3**.

As regards the tu complexes, we have information only for the compound [(tu)Cu($Tr^{Mes,Me}$)] (**4**), which crystallized from a solution of [Cu($Tr^{Mes,Me}$)]$_2$ in presence of an excess of tu. The X-ray structure of **4** is reported in Figure 2.6 and selected bond distances and angles in Table 2.4.

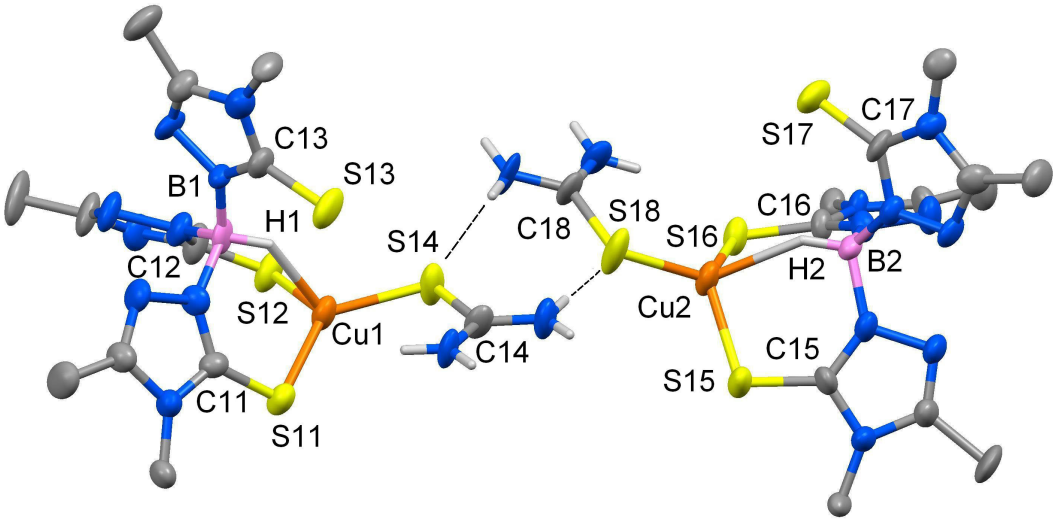

Figure 2.6 Molecular drawing of **4** at the 30% thermal ellipsoids probability level. Hydrogen atoms, except those of the B-H and of the NH_2 groups, have been removed for clarity.

Two independent molecules are present in the unit cell, exhibiting the same structure. The metal is bound to the tridentate ligand (κ^3-*S_2H*) and to tu in a tetrahedral *$S_2S'H$* coordination environment. One of the three thioxo groups of the ligand is not bound to copper. The ligand adopts the same conformation as observed for the dinuclear parent compound [Cu($Tr^{Mes,Me}$)]$_2$, with the B-H moiety pointing toward the metal. The B-H hydrogens could not be located from the difference Fourier map, so that they were placed in their calculated positions. The interacting Cu-H(B) distances of 2.108 (Cu(1)-H(1)) and of 2.152 Å (Cu(2)-H(2)) are in agreement with 3-center-2-electron [B-H···Cu] interactions for both independent molecules[172] and they are comparable with the Cu-H(B) distances found in the dinuclear complexes [Cu($Tr^{Mes,Me}$)]$_2$, [Cu($Tr^{Me,o\text{-}Py}$)]$_2$ and [Cu($Tr^{Et,Me}$)]$_2$ (1.94(4)-2.29(3) Å range).[147,173] Accordingly, the metal sites exhibit a significant deviation from the plane defined by the three sulfur atoms (sum of angles at copper: 356.0(5) for Cu(1) and 355.2(5)° for Cu(2)) and the distortion from planarity (0.262(1) Å for Cu(1) and 0.286(2) Å for Cu(2)) is directed toward

the B-H group. From the analysis of the distances, it appears that tu interacts more strongly with copper with respect to the triazoline thioxo groups of the ligand. In fact, the Cu-S_{tu} distances are shorter (2.221(3)-2.223(3) Å) than the Cu-S_{ligand} bond lengths (2.260(3)-2.288(3) Å) and, at the same time, the C=S_{tu} distances (1.748(8)-1.759(8) Å) are significantly longer than the C=S_{ligand} ones (1.680(8)-1.722(8) Å).

Table 2.4 Selected geometric parameters (Å) for **4.**

Cu(1)-S(11)	2.264(3)	C(11)-S(11)	1.707(9)
Cu(1)-S(12)	2.281(2)	C(12)-S(12)	1.698(9)
Cu(1)-S(14)	2.221(3)	C(13)-S(13)	1.682(8)
Cu(1)-B(1)	2.91(1)	C(14)-S(14)	1.748(8)
Cu(2)-S(15)	2.288(3)	C(15)-S(15)	1.715(8)
Cu(2)-S(16)	2.260(3)	C(16)-S(16)	1.722(8)
Cu(2)-S(18)	2.223(3)	C(17)-S(17)	1.680(8)
Cu(2)-B(2)	2.93(1)	C(18)-S(18)	1.759(8)

All of the tu hydrogens are involved in an extensive net of hydrogen bonds (*H.B.*) that determine the formation of layers in the *ab* plane (Figure 2.7).

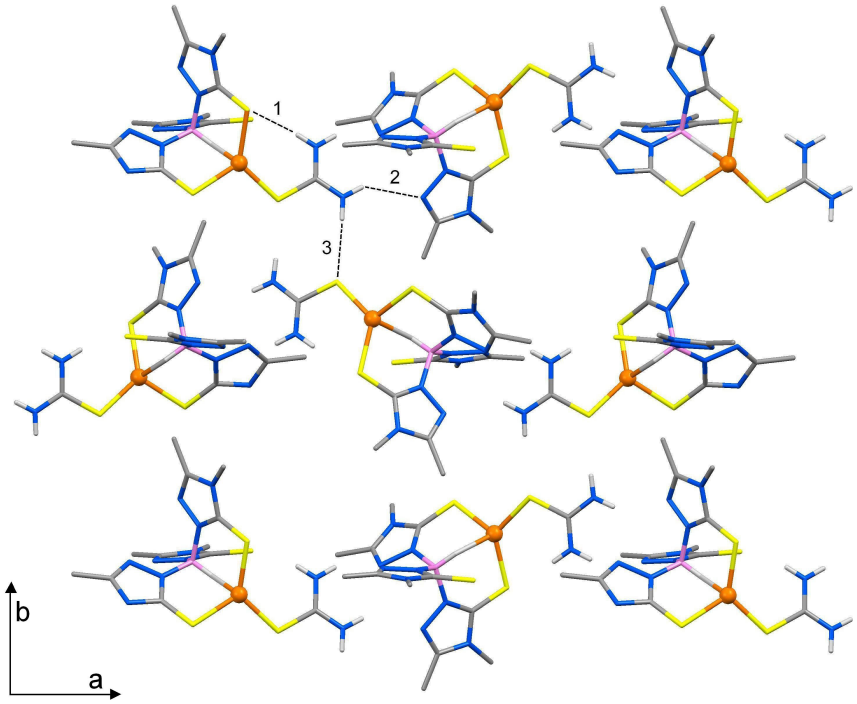

Figure 2.7 Crystal packing of **4** in the *ab* plane. Three types of hydrogen bonds are present. The mesityl groups and the hydrogen atoms (except the B-*H* and NH_2) have been removed for clarity.

The *H.B.*s can be classified in three types according to the *H.B.* acceptor: 1) *intramolecular NH···S* (triazoline thioxo group as acceptor); 2) *intermolecular NH···N* (triazoline nitrogen atoms as acceptors); 3) *intermolecular NH···S* ($C{=}St_u$ as acceptor). The mesityl groups of $Tr^{Mes,Me}$ are pointing above and below these layers, determining the packing along the *c* crystallographic axis through hydrophobic interaction.

2.3.2 Solution equilibria

The dinuclear complexes $[Cu(L)]_2$ (L = $Tr^{Mes,Me}$, $Tr^{Me,o\text{-}Py}$, $Br^{Mes}pz^{o\text{-}Py}$) were titrated with PPh_3, tu and py in order to gain insights concerning their stability/reactivity with respect to monodentate σ donor ligands and to determine the formation constants (*K*) of the respective ternary complexes. The reactions with PPh_3 are quantitative, suggesting that the *K* for the reactions $[Cu(L)]_2 + 2PPh_3 \rightarrow 2[(PPh_3)Cu(L)]$ are quite high. Under these experimental conditions, it is not possible to determine their values since the titrations go to completeness when the $[Cu(L)]_2$:PPh_3 ratio is 1:2. As regards the compound **3**, the explanation of its fluxional behavior in solution through a conformational rearrangement (**3a** ⇌ **3b**) and not through a PPh_3 dissociative mechanism, was ensured by performing the titration of $[Cu(Br^{Mes}pz^{o\text{-}Py})]_2$ with PPh_3 up to a ratio of 1:10.

More interesting are the titrations of $[Cu(L)]_2$ (L = $Tr^{Mes,Me}$, $Br^{Mes}pz^{o\text{-}Py}$) with tu, since the reaction completion is reached at higher tu:$[Cu(L)]_2$ ratios in both the cases. We are dealing with fast exchange equilibria (with respect to NMR time scale) above approximately 290 K, whereas the systems exhibit slow exchange features at lower temperature, with distinguishable signals of the [(tu)Cu(L)] adducts and of the dinuclear complexes. Unfortunately an accurate determination of the coalescence temperature is difficult as a consequence of the overlap of the $[Cu(L)]_2$ and [(tu)Cu(L)] peaks, so that no information could be obtained concerning the activation parameters. We studied the tu/$[Cu(L)]_2$ systems in fast exchange regime, by following the chemical shift variation as a function of tu concentration (Figure A3 of Appendix 1 for the titration of $[Cu(Tr^{Mes,Me})]_2$) using the curve fitting procedure.[152]

Supposing that the equilibria reported in Scheme 2.3 are reasonable, *i.e.* the formation of a ternary adduct following the dissociation of the corresponding dinuclear complex into monomers, the stability constant of the $[Cu(L)]_2 + 2tu \rightleftharpoons 2[(tu)Cu(L)]$ process ($\log K$) can be calculated only knowing the dimerization constant ($\log\beta_{DIM}$).

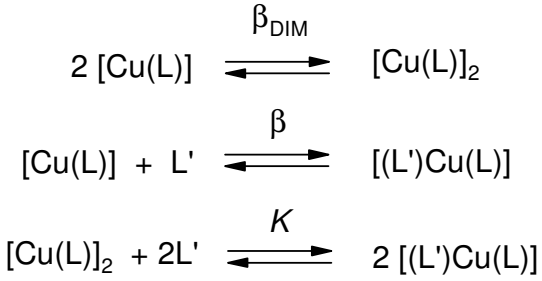

Scheme 2.3

In this way, log*K* can be obtained from the relation:

$$\log K = 2\log\beta - \log\beta_{DIM}$$

where logβ is the formation constant of the ternary adduct from [Cu(L)] monomers, as derived from the fitting of the NMR data. However, it can be easily demonstrated that if logβ_{DIM} is high enough (*i.e.* [Cu(L)] is negligible), log*K* becomes independent from it. Dilution studies on the $[Cu(Tr^{Mes,Me})]_2$ and $[Cu(Br^{Mes}pz^{o\text{-}Py})]_2$ complexes in CD_3OD:CD_3Cl 1:1 showed no dissociation of the dimers in the 10^{-2}-10^{-4} M concentration range, so that logβ_{DIM} is expected to be quite high. Assuming that a 5% dissociation of the dimeric complex may occur, but that it cannot be detected at the experimental copper concentration of 10^{-3} M (*i.e.* $5\cdot10^{-5}$ M of [Cu(L)]), logβ_{DIM} would be > 5.3. In this approximation (logβ_{DIM} = 5.3), log*K* values for the $[Cu(L)]_2 + 2tu \rightleftharpoons 2[(tu)Cu(L)]$ equilibria resulted 4.3(2) and 2.1(2), respectively for L = $Tr^{Mes,Me}$ and $Br^{Mes}pz^{o\text{-}Py}$. The distribution diagram of the $[Cu(Tr^{Mes,Me})]_2$/tu system is reported in Figure 2.8. The data fitting was performed also by using higher logβ_{DIM}, leading to the same log*K* values. Thus, the stability of [(tu)Cu(L)] with respect to the $[Cu(Tr^{Mes,Me})]_2$ dimer is 2.2 order of magnitude higher than in the case of $[Cu(Br^{Mes}pz^{o\text{-}Py})]_2$. Being log*K* independent from the dimerization constant β_{DIM} this difference reflects directly the tendency of tu to react preferentially with $[Cu(Tr^{Mes,Me})]_2$ over $[Cu(Br^{Mes}pz^{o\text{-}Py})]_2$.

We attempted to evaluate the dependence of the log*K* on the temperature according to the Van't Hoff analysis, in order to obtain information on ΔH° and ΔS°. Unfortunately, both in the slow exchange and in the fast exchange regimes, the observed log*K* variations in function of the temperature are well within the experimental error, thus providing no direct insights into the thermodynamic parameters for the reactions. However, if the formation constant does not vary appreciably with the temperature, it can be concluded that ΔH° has to be small. This

is in agreement with the equivalence of the Cu coordination environment in $[Cu(Tr^{Mes,Me})]_2$ and in the $[(tu)Cu(Tr^{Mes,Me})]$ adduct, whose X-ray geometries are reported. In fact, in both compounds three C=S groups and a BH hydride are linked to the metal center.

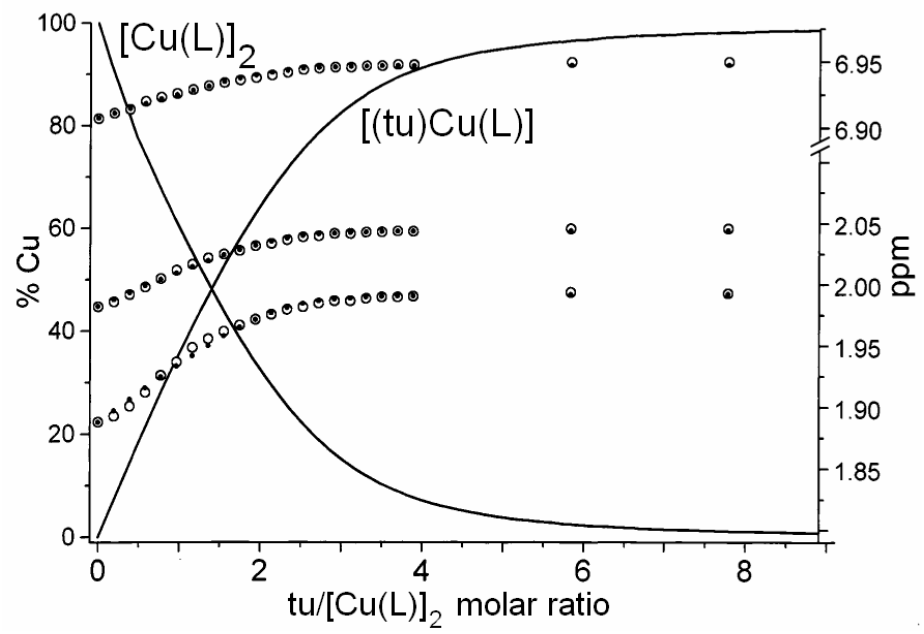

Figure 2.8 Distribution diagram corresponding to the ^{1}H NMR titration of $[Cu(Tr^{Mes,Me})]_2$ with tu in CD_3OD:$CDCl_3$ 1:1 at 300 K. Three different chemical shifts are reported (○ = observed, • = calculated).

Attempts to determine the log*K* for the competitive reaction $[(tu)Cu(L)] + PPh_3 \rightleftharpoons [(PPh_3)Cu(L)] + tu$ were unsuccessful. Even in presence of an excess of a competitor such as tu (10:1 with respect to $[Cu(L)]_2$) the reaction goes to completeness with 2 equivalents of PPh_3. With the limit of 5% of free dimer present in solution after the addition of 2 equivalents of PPh_3, we could determine that the log*K* for the reaction $[Cu(L)]_2 + 2PPh_3 \rightleftharpoons 2[(PPh_3)Cu(L)]$ should be > 8.2 and > 7.2 respectively for L = $Tr^{Mes,Me}$ and $Br^{Mes}pz^{o\text{-}Py}$ (simulations performed with $C_{dimer} = 5 \cdot 10^{-3}$ M, C_{tu} $25 \cdot 10^{-3}$ M). This values mean that PPh_3 reacts at least four orders of magnitude more favorably than tu with the studied dimers.

According to the ^{1}H NMR titrations, the only dimer that reacted with py was $[Cu(Tr^{Mes,Me})]_2$ whereas for $[Cu(Tr^{Me,o\text{-}Py})]_2$ and $[Cu(Br^{Mes}pz^{o\text{-}Py})]_2$ a py excess of 40-or 64-fold, respectively, did not give any product. The analysis of the $[Cu(Tr^{Mes,Me})]_2$/py system was performed at 300 K under slow exchange conditions (220-340 K), evaluating the ratio between the integrals of the parent dimer and the py adduct (Figure A4 and fitting equation derivation in Appendix 1).

This procedure was hindered by the overlap of signals of $[Cu(Tr^{Mes,Me})]_2$ and $[(py)Cu(Tr^{Mes,Me})]$, which were deconvoluted. A log*K* of 1.6(1) was obtained, much lower than that of the corresponding tu-adduct. Moreover, the $[(py)Cu(Tr^{Mes,Me})]$:$[Cu(Tr^{Mes,Me})]_2$ ratio was noticeably temperature-dependent, ensuring the possibility of extracting thermodynamic parameters from the $[Cu(Tr^{Mes,Me})]_2$/py titration carried out at different temperatures (260-305 K). The Van't Hoff analysis provides a $\Delta H°$ of -53(3) $kJ \cdot mol^{-1}$ and a $\Delta S°$ of -140(20) $J \cdot mol^{-1}\ K^{-1}$ (Figure 2.9).

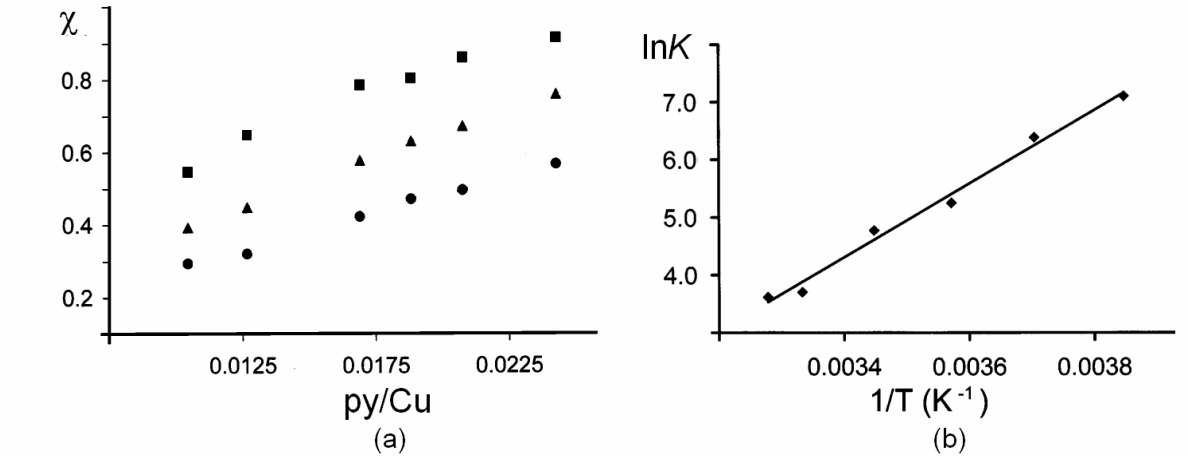

Figure 2.9 (a) Saturation plots reporting the molar fraction χ = (mol [(py)Cu(L)]) / (mol [(py)Cu(L)] + mol $[Cu(L)]_2$) with L = $Tr^{Mes,Me}$ *vs.* py/Cu molar ratio in $CDCl_3$ at three representative temperatures. ■ = 270 K, ▲ = 290 K, ● = 305 K. (b) Van't Hoff plot: lnK = -(ΔH°/R)/T + ΔS°/R, R = 8.3145 J $mol^{-1}\ K^{-1}$, T = 260-305 K, experimental values (♦) and least-squares fit (—).

The exothermic character of the reaction can be explained by considering the different donor set of Cu(I) in the product and in the reagent. A tentative assignment of the $[(py)Cu(Tr^{Mes,Me})]$ molecular structure leads to the hypothesis of tetrahedral S_3N coordination of copper, rather than S_2NH, in analogy to the PPh_3 adducts. In fact, a $S_3H \rightarrow S_3N$ change in the coordination sphere (Scheme 2.4) of each metal center of the dimer would be consistent with the negative experimental ΔH°, suggesting a greater donor ability of N-py with respect to B-H. Finally, to explain why log*K* is much lower for py addition than for tu one, the entropic factor becomes decisive, in so far ΔH (negative in the former case and close to zero in the latter) would favor the tu-complex.

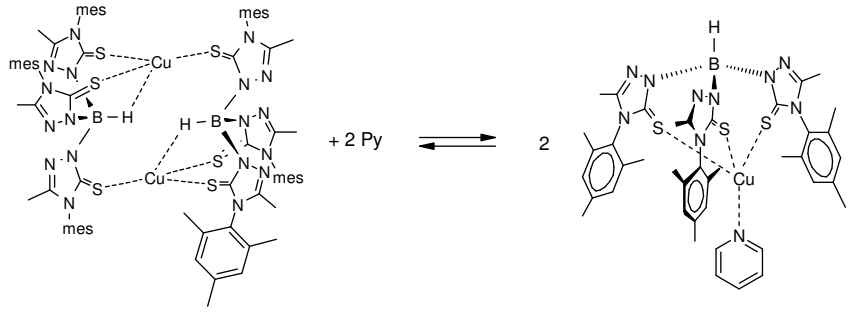

Scheme 2.4

2.4 Conclusions

The reactivity of the dinuclear complexes $[Cu(L)]_2$ (L = $Tr^{Mes,Me}$, $Tr^{Me,o\text{-}Py}$, $Br^{Mes}pz^{o\text{-}Py}$) with the monodentate ligands PPh_3, tu and py (L') was investigated. A summary of the formation constants (*K)* of the [(L')Cu(L)] adducts, determined by means of ^1H NMR titrations, is shown in Table 2.5.

Table 2.5 Summary of the log*K* for the $[Cu(L)]_2 + 2L' \rightleftharpoons 2[(L')Cu(L)]$ equilibria (300 K).

	PPh_3	tu	py
$[Cu(Tr^{Mes,Me})]_2$	>8.2[a] (300)	4.3(2)[a] (300)	1.6(1) (300)[c]
$[Cu(Tr^{Me,o\text{-}Py})]_2$	n.d.	n.d.	-[d]
$[Cu(Br^{Mes}pz^{o\text{-}Py})]_2$	>7.2[b] (300)	2.1(2)[b] (300)	-[d]

a = $CDCl_3$:MeOD 1:1; b = CD_2Cl_2:MeOD 1:1; c = $CDCl_3$; d = too low; n.d. = not determined.

Assuming that the effect of the solvent on the stability constants is minimal, the dimers $[Cu(Tr^{Mes,Me})]_2$ and $[Cu(Br^{Mes,Me}pz^{o\text{-}Py})]_2$ show a precise trend: $K([(PPh_3)Cu(L)])$ >> $K([(tu)Cu(L)])$ > $K([(py)Cu(L)])$. $[Cu(Tr^{Me,o\text{-}Py})]_2$ reacts quantitatively with PPh_3 but no appreciable reaction occurs even with a large excess of py (the reaction with tu could not be studied due to solubility drawbacks).

The products $[(PPh_3)Cu(Tr^{Mes,Me})]$ and $[(PPh_3)Cu(Tr^{Me,o\text{-}Py})]$ show a tetrahedral Cu(I) environment (κ^3-S_3 ligand plus a PPh_3) both at the solid state and in solution. Only solution data and DFT calculations are available for $[(PPh_3)Cu(Br^{Mes}pz^{o\text{-}Py})]$: an equilibrium between two mononuclear isomers, with κ^3-S_2H and κ^3-S_2N coordination of the tripodal ligand on

copper, was assumed. The B-H involvement into the metal coordination, noticed in the more stable *S_2HP* isomer (as in the parent compound $[Cu(Br^{Mes}pz^{o\text{-}Py})]_2$), is not surprising, as for analogous boron-centered scorpionates several examples are known.[174-177] The reactions of $[Cu(L)]_2$ with PPh_3 are about quantitative, so that only minimum values of log*K* can be (indirectly) determined. In the case of tu adducts the equilibrium constants are lower and can be determined by means of NMR titrations. The minimal *K* dependence on temperature implies a small ΔH° of reaction (as well as a positive ΔS°), which is presumably related to the equivalence of the copper donor set in the parent compound and in the corresponding adduct. This is evidenced by the X-ray structure of $[(tu)Cu(Tr^{Mes,Me})]$, which presents three C=S groups coordinated to copper and a Cu···H-B interaction, as in $[Cu(Tr^{Mes,Me})]_2$. The smaller values of *K* for the py complexes (*K* is high enough to be detectable only when L = $Tr^{Mes,Me}$), which prevented to isolate any adduct at the solid state, is due to entropic reasons (ΔH° = -53(3) $kJ{\cdot}mol^{-1}$, ΔS° = -140(20) $J{\cdot}mol^{-1}\ K^{-1}$).

3

A First Example of a New Class of C-Centered Scorpionate Ligands. Solution Studies on M^{2+} Complexes (M = Ni, Cu, Zn)[178]

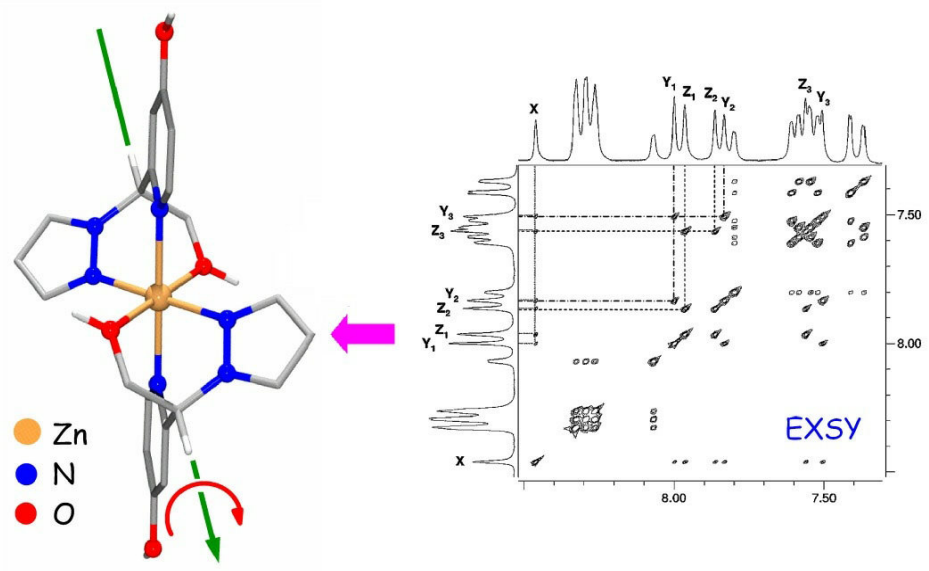

The neutral N,N',O heteroscorpionate ligand 1-(4-Methoxy-3,5-dimethyl-pyridin-2-yl)-2-methyl-1-pyrazol-1-yl-propan-2-ol (LOH) was prepared in two high yield steps. The complexes $[M(LOH)_2][MCl_4]$ (M = Cu and Zn) and $[M(LOH)_2]Cl_2$ (M = Ni and Cu) were prepared and characterized by X-ray crystallography. The speciation in solution of the M^{2+}/LOH systems was investigated by means of spectrophotometric/^{1}H NMR titrations, determining the global formation constants β_1 and β_2 for the $[M(LOH)]^{2+}$ and $[M(LOH)_2]^{2+}$ species (MeOH:H_2O 95:5). The Zn^{2+}/LOH system was studied by quantitative ^{1}H-^{1}H EXSY spectroscopy (300 K, mixing time = 0.2-0.8 s), which allows the description of the equilibria occurring between five octahedral $[Zn(LOH)_2]^{2+}$ structural isomers and the tetrahedral [Zn(LOH)Cl]Cl species. Exchange constants k^{ex}_{ij} and associated rate constants k_{ij} suggest that two types of interconversion occur: octahedral-octahedral (faster) and octahedral-tetrahedral (slower). DFT calculations (b3lyp/6-311+G(d)) were employed to evaluate the relative stability of the $[Zn(LOH)_2]^{2+}$ isomers, which are comparable for the five complexes with a maximum energy difference of 6.3 kJ/mol.

3.1 Introduction

The N,N,O-donor heteroscorpionate ligands have found application in biomimetics, as synthetic models of the 2-Hys-1-carboxylate triad, which is present in various metalloproteins and metalloenzymes (mainly containing Zn and Fe, but also Mn, Ni and Cu),[66,76,80,179-186] in catalysis (Ti, Zr, Ru, Mo and Al complexes)[109,110,112,113,187,188] and, more recently, as models for radiopharmaceuticals (Re complexes).[134,135] As far as the topology of the ligands is concerned, N,N,O-heteroscorpionates can be grouped in three categories: (a) C-centered pyrazole-based, such as the bis(pyrazol-1-yl)-acetates,[76,182,183,189-192] bis(pyrazoly1-yl)-ethoxydes,[193,194] bis(pyrazolyl)-phenolates[66,195-198] and tris(pyrazol-1-yl)methane sulfonates[199-202] (Scheme 3.1 a); (b) B-centered bis(pyrazol-1-yl)borato derivatives (HCO_2)Bp and (MeO)Bp,[179,180] (Scheme 3.1 b); (c) C-centered imidazole-based bis(imidazol-2-yl)propionates[186] and bis(imidazol-2-yl)nitromethane[170] (Scheme 3.1 c).

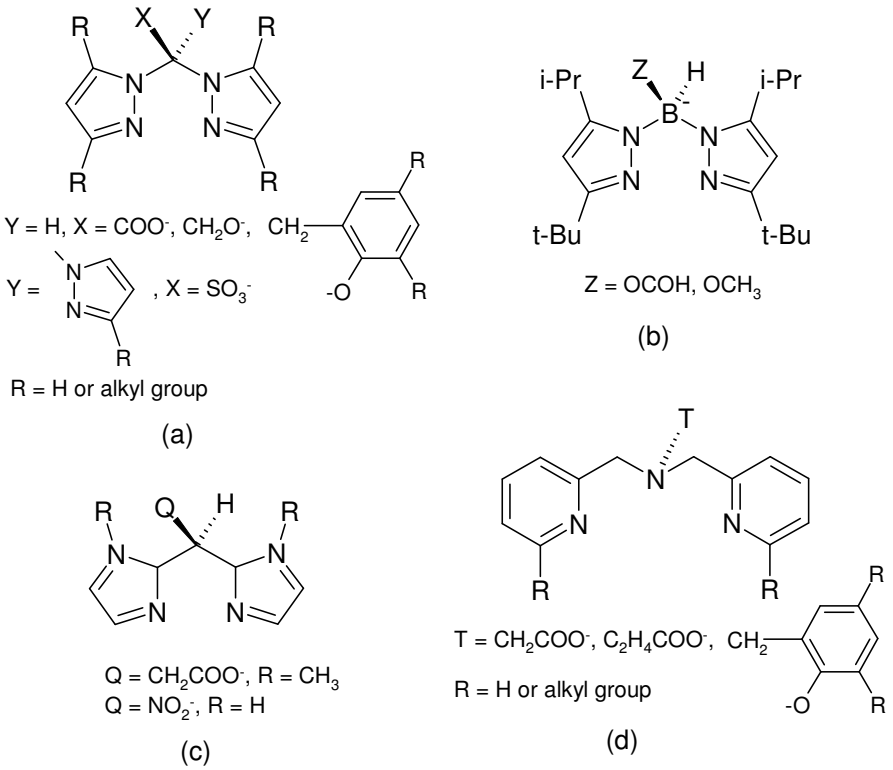

Scheme 3.1

An additional class is represented by N-centric tripodal ligands in which the bridging nitrogen atom is able to coordinate together with the N,N,O donor set so that these ligands can be considered as N_3O tetradentate[33,203] (Scheme 3.1 d).

Some N,N,O-scorpionates are chiral. The asymmetry is usually introduced (a) by employing three different donor groups connected to the central atom[184,204] or (b) by using an enantiopure heterocycle (*e.g.* camphorpyrazole or menthylpyrazole) as a precursor to yield a Hc^*_2AX ligand (Hc^* = enantiopure heterocycle, A = bridging atom, X = O-donor group), Scheme 3.2.[205,206] It is worth of note that only the latter method yields a homochiral ligand without complex enatiomeric/diasteroisomeric separations.

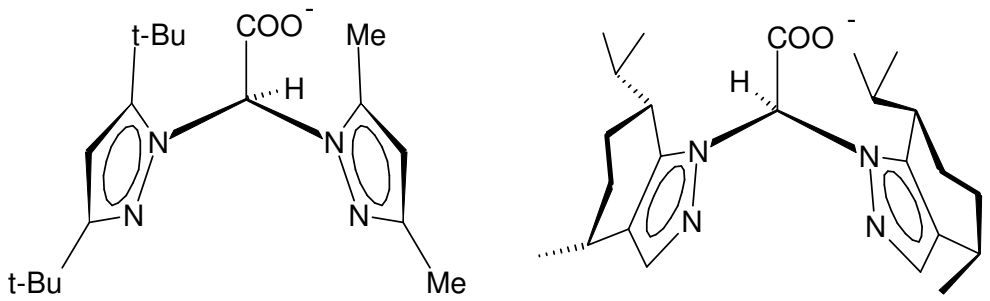

Scheme 3.2

This work reports the synthesis of a new pyrazolyl-pyridine based N,N'O tripodal ligand (LOH, Scheme 3.3), which represents the first example of a new class of heteroscorpionate N,N',E donor ligands (E = additional donor group).

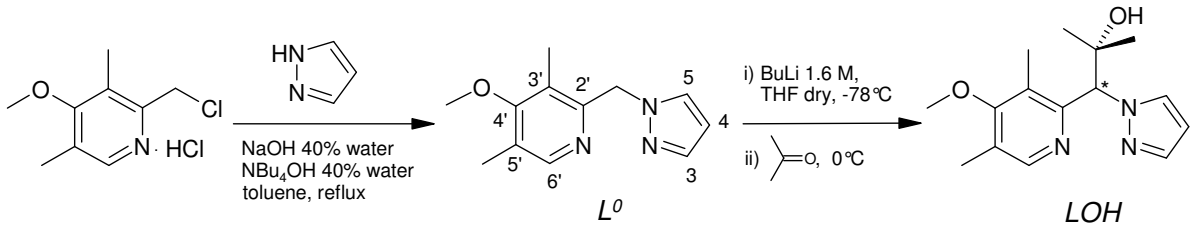

Scheme 3.3

LOH can be prepared in two high-yield steps even though the reaction is not stereoselective. This synthetic pathway first generates a prochiral N,N' bidentate ligand, which can be opportunely functionalized on the methylene bridge by applying the procedures developed for the derivatisation of the bis(pyrazolyl)methanes.[40]

The coordination properties of LOH were explored by reacting it with MCl_2 salts (M = Ni, Cu and Zn) in 1:1 and 1:2 M:LOH ratios. The crystal structures of the $[M(LOH)_2]Cl_2$ (M = Cu and Ni) and $[M(LOH)_2][MCl_4]$ (M = Cu and Zn) complexes show that the ligand behaves always as κ^3-N,N'O ,coordinating. The speciation of the M^{2+}/LOH systems in methanol:water

(95:5) was investigated by UV-Visible (Ni^{2+} and Cu^{2+}) and by ^{1}H-NMR (Zn^{2+}) titrations. A detailed structural description of the Zn^{2+}/LOH system in solution was performed by means of ESI-Mass spectrometry, ^{1}H-^{1}H EXSY NMR spectroscopy and DFT calculations.

3.2 Experimental

3.2.1 General procedures

All the reagents and solvents, except for THF (distilled from sodium benzophenone), were used as purchased from Aldrich. Synthesis of LOH was performed under N_2 atmosphere using standard Schlenk techniques. The NMR spectra (^{1}H, ^{13}C and 2D) were recorded on a Bruker Avance 300 spectrometer. 2D experiments (^{1}H-^{1}H NOESY/EXSY and not reported ^{1}H-^{1}H COSY, ^{1}H-^{13}C HSQC) were recorded using standard Bruker pulse sequences. Chemical shifts are reported in ppm referenced to residual solvent protons ($CDCl_3$, CD_3OD and CD_3OD:D_2O 95:5[207]). Visible spectra were recorded on a Perkin–Elmer Lambda 25 spectrophotometer (range 200–1100 nm) using matched cells of 1 cm pathlength. Mass spectra were obtained with a Micromass ZMD spectrometer. The mixtures were analyzed in positive ionization mode by direct perfusion in ESI-Mass interface. Infrared spectra were recorded from 4000 to 700 cm^{-1} on a Perkin-Elmer FT-IR Nexus spectrometer equipped with a Thermo-Nicolet microscope. Elemental analyses (C, H, N) were performed with a Carlo Erba EA 1108 automated analyzer.

3.2.2 Synthesis of 4-Methoxy-3,5-dimethyl-2-pyrazol-1-yl-methyl-pyridine (L^0)

2-Chloroethyl-4-methoxy-3,5-dimethylpyridine hydrochloride (5.00 g, 22.51 mmol) and pyrazole (1.80 g, 26.44 mmol) were mixed in toluene (150 ml). After adding aqueous NaOH (40% in water, 50 ml) and 30 drops of *n*-tetrabutylammonium hydroxide (40% in water) the mixture was refluxed 4 h with stirring. The organic phase was separated from the aqueous one, washed with water (20 ml), dried with anhydrous Na_2SO_4 and filtered. The solvent was removed under vacuum and a colorless microcrystalline powder was collected (L^0, 4.56 g, 93%). IR (cm^{-1}): 3121w, 2966w, 2927w, 1585m, 1569m, 1510s, 1470s, 1438s, 1390s, 1255m, 1089s, 993s, 964s, 874m, 864m, 747vs. ^{1}H NMR (300 MHz, $CDCl_3$): δ 2.25 (s, 6H, C*H*$_3$),

3.74 (s, 3H, C*H*$_3$O), 5.44 (s, 2H, C*H*$_2$), 6.24 (t, J = 2.1 Hz, 1H, C-C*H*-C pz), 7.43 (d, J = 2.1 Hz, 1H, C-C*H*-N pz), 7.50 (d, J = 1.4 Hz, 1H, C-C*H*-N pz), 8.23 (s, 1H, C*H* py). ^{13}C NMR (75 MHz, $CDCl_3$): δ 11.09 (CH_3), 13.55 (CH_3), 56.24 (CH_3O), 60.13 (CH_2), 106.00 (C-*C*H-C pz), 126.09 (C quat), 126.44 (C quat), 129.42 (C-*C*H-N pz), 139.30 (C-*C*H-N pz), 149.68 (CH py), 164.55 (C quat, *C*-OCH_3). Anal. calcd for $C_{12}H_{15}N_3O$ (217.27): C, 66.34; H, 6.96; N, 19.34. Found: C, 66.41; H, 7.01; N, 19.18%.

3.2.3 Synthesis of 1-(4-Methoxy-3,5-dimethyl-pyridin-2-yl)-2-methyl-1-pyrazol-1-yl-propan-2-ol (LOH)

To a THF solution (100 ml) of L^0 (4.56 g, 20.99 mmol) cooled at -78 °C, *n*-BuLi in hexane (1.6 M, 15 ml, 24 mmol) was slowly added. The resulting red solution was stirred for 0.5 h at -78 °C, and then acetone (1.8 ml, 24.51 mmol) was added. The solution was allowed to warm to room temperature, becoming slowly colorless. After 1 h, EtOH 95% (50 ml) were added and the solution was stirred for 2 h. The cloudy mixture was dried under vacuum and the solid was extracted with diethyl ether (50 ml). The organic phase was washed with water (3 x 20 ml), dried with anhydrous Na_2SO_4 and filtered. The solvent was removed under vacuum, and a colorless microcrystalline powder was isolated (LOH, 5.03 g, 87%). Colorless crystals suitable for X-ray diffraction were obtained by stratification of hexane on an ethereal solution of the product. IR (cm^{-1}): 3289m br, 3149w, 2988w, 2975m, 2945w, 1586m, 1567m, 1470s, 1416s, 1396s, 1261s, 1146m, 1086s, 1078s, 1048s, 996s, 801s, 761vs. ^{1}H NMR (300 MHz, CD_3OD): δ 1.02 (s, 3H, C*H*$_3$), 1.29 (s, 3H, C*H*$_3$), 2.24 (s, 3H, C*H*$_3$ py), 2.32 (s, 3H, C*H*$_3$ py), 3.79 (s, 3H, C*H*$_3$O), 5.61 (s, 1H, C*H**), 6.29 (t, J = 2.1 Hz, 1H, C-C*H*-C pz), 7.50 (d, J = 1.8 Hz; 1H, C-C*H*-N pz), 7.70 (d, J = 2.4 Hz, 1H, C-C*H*-N pz), 8.34 (s, 1H, CH py). ^{13}C NMR (75 MHz, CD_3OD): δ 11.75 (CH_3 py), 14.28 (CH_3 py), 27.99 (CH_3), 29.47 (CH_3), 56.76 (C quat), 61.57 (CH_3O), 68.48 (CH*), 76.19 (C-*C*H-C pz), 107.63 (C-*C*H-C pz), 129.36 (C quat), 129.60 (C quat), 131.86 (C-*C*H-N pz), 139.77 (C-*C*H-N pz), 149.97 (CH py), 157.89 (C quat), 167.44 (C quat). Anal. calcd for $C_{15}H_{21}N_3O_2$ (275.35): C, 65.43; H, 7.69; N, 15.26. Found: C, 65.52; H, 7.60; N, 15.24%.

*3.2.4 Synthesis of $[Ni(LOH)_2][NiCl_4]$ (**1**)*

A solution of LOH (100 mg, 0.36 mmol) in methanol (3 ml) was added drop-wise to a methanolic solution (2 ml) of $NiCl_2 \cdot 6H_2O$ (87 mg, 0.37 mmol). The resulting solution was stirred for 15 min. By adding an excess of diethyl ether, a green gluey precipitate slowly formed. The solvent was removed by suction and the solid was dissolved in CH_2Cl_2 (5 ml). The mixture was micro-filtered and dried under vacuum, yielding a green-light blue powder (**1**, 102 mg, 0.13 mmol, 72%). IR (cm^{-1}): 3250s br, 3103s br, 2979s, 2866s, 1594m, 1574m, 1470s, 1408s, 1380s, 1294m, 1260s, 1154m, 1115w, 1098w, 1076s, 994m, 845m, 813s, 769s br. ESI-MS (cone 70 V, CH_3OH, *m/z*, I%): 304.4, 100 $[Ni(LOH)_2]^{2+}$; 368.3, 10 $[Ni(LOH)Cl]^+$; 607.6, 8 $[Ni(LOH)(LO)]^+$. Anal. calcd for $C_{30}H_{42}N_6O_4Ni_2Cl_4$ (809.88): C, 44.49; H, 5.23; N,10.38. Found: C, 44.53; H, 5.18; N, 10.33%.

*3.2.5 Synthesis of $[Ni(LOH)_2]Cl_2$ (**2**)*

A solution of LOH (100 mg, 0.36 mmol) in methanol (3 ml) was added drop-wise to a methanolic solution (2 ml) of $NiCl_2 \cdot 6H_2O$ (43 mg, 0.18 mmol). The resulting violet solution was stirred for 15 min. The product was precipitated with an excess of diethyl ether, filtered and dried under vacuum, yielding a light violet microcrystalline powder (**2**, 60 mg, 0.09 mmol, 49%). Crystals suitable for X-ray diffraction were obtained by diffusion of diethyl ether in a methanolic solution of the product, corresponding to $[Ni(LOH)_2]Cl_2 \cdot 3CH_3OH$ (**2a**). IR (cm^{-1}): 3423s, 3381s, 3100s, 2974vs, 2885s, 2777s, 1677w, 1598m, 1574m, 1407s, 1295m, 1216m, 1194w, 1157m, 1082s br, 993 s, 925w, 908w, 886w, 844m, 812s, 778s br. Anal. calcd for $C_{30}H_{42}N_6O_4NiCl_2$ (680.29): C, 52.97; H, 6.22; N, 12.35. Found: C, 52.89; H, 6.30; N, 12.27%.

*3.2.6 Synthesis of $[Cu(LOH)_2][CuCl_4]$ (**3**)*

A solution of LOH (100 mg, 0.36 mmol) in methanol (3 ml) was added drop-wise to a methanolic solution (2 ml) of $CuCl_2 \cdot 2H_2O$ (65 mg, 0.38 mmol). The resulting dark green solution was stirred for 15 min. Dark green crystals of the product (**3**, 80 mg, 0.10 mmol, 54%), suitable for X-ray diffraction, were obtained by diffusion of diethyl ether in the methanolic solution, corresponding to $[Cu(LOH)_2][CuCl_4] \cdot 2CH_3OH$ (**3a**). IR (cm^{-1}): 3257s br, 3098s, 2973s, 1596s, 1572m, 1472s br, 1409s, 1294s, 1264vs, 1159s, 1078vs, 989s, 920w,

811s, 773s. ESI-MS (cone 70 V, CH_3OH, *m/z*, I%): 306.8, 25 $[Cu(LOH)_2]^{2+}$; 338.4, 10 $[Cu(LO)]^+$; 370.4, 20 $[Cu(LOH)(CH_3OH)]^+$; 612.5, 2 $[Cu(LOH)(LO)]^+$. Anal. calcd for $C_{30}H_{42}N_6O_4Cu_2Cl_4$ (819.59): C, 43.96; H, 5.16; N, 10.25. Found: C, 44.05; H, 5.21; N, 10.15%.

*3.2.7 Synthesis of $[Cu(LOH)_2]Cl_2$ (**4**)*

A solution of LOH (100 mg, 0.36 mmol) in methanol (3 ml) was added drop-wise to a methanolic solution (2 ml) of $CuCl_2{\cdot}2H_2O$ (31 mg, 0.18 mmol). The resulting bright blue solution was stirred for 15 min. Blue crystals of the product (**4**, 87 mg, 0.13 mmol, 70%), suitable for X-ray diffraction, were obtained by diffusion of diethyl ether in the methanolic solution, corresponding to $[Cu(LOH)_2]Cl_2{\cdot}2H_2O$ (**4a**). IR (cm^{-1}): 3476s, 3406s, 3104s br, 2977m, 2739w, 2527w, 1624w, 1595m, 1407s, 1380s, 1296m, 1260vs, 1188w, 1156s, 1076vs, 993s, 846m, 812s, 766vs. Anal. calcd for $C_{30}H_{42}N_6O_4CuCl_2$ (685.14): C, 52.59; H, 6.18; N, 12.27. Found: C, 52.63; H, 6.22; N, 12.19%.

*3.2.8 Synthesis of $[Zn(LOH)_2][ZnCl_4]$ (**5**)*

A solution of LOH (100 mg, 0.36 mmol) in methanol (3 ml) was added drop-wise to a methanolic solution (2 ml) of $ZnCl_2$ (50 mg, 0.37 mmol). The resulting colorless solution was stirred for 15 min. The product was precipitated with an excess of diethyl ether, filtered and dried under vacuum, yielding a colorless microcrystalline powder (**5**, 128 mg, 0.31 mmol, 86%). Crystals suitable for X-ray diffraction were obtained by diffusion of diethyl ether in an acetonitrile solution of the product, corresponding to $[Zn(LOH)_2][ZnCl_4]{\cdot}2CH_3CN$ (**5a**). IR (cm^{-1}): ~3430br, ~3230br, 3103s, 2936s, 2974s, 1593m, 1570m, 1512w, 1406s, 1289m, 1187w, 1150m, 1073s br, 990m, 954w, 922w, 809m, 769m. ^{1}H-NMR spectrum (300 MHz, CD_3OD:D_2O 95:5): see discussion for Zn^{2+}:LOH 1:1 ratio. ESI-MS (cone 25 V, CH_3OH, *m/z*, I%): 307.3, 100 $[Zn(LOH)_2]^{2+}$; 374.0, 10 $[Zn(LOH)Cl]^+$; 613.2, 20 $[Zn(LOH)(LO)]^+$. Anal. calcd for $C_{30}H_{42}N_6O_4ZnCl_2$ (823.28): C, 43.77; H, 5.14; N, 10.21. Found: C, 43.70; H, 5.20; N, 10.29%.

3.2.9 X-ray crystallography

A summary of data collection and structure refinement for the ligand LOH and for the compounds $[Ni(LOH)_2]Cl_2 \cdot 3CH_3OH$ (**2a**), $[Cu(LOH)_2][CuCl_4] \cdot 2CH_3OH$ (**3a**), $[Cu(LOH)_2]Cl_2 \cdot 2H_2O$ (**4a**) and $[Zn(LOH)_2][ZnCl_4] \cdot 2CH_3CN$ (**5a**) is reported in Table 3.1.

Table 3.1 Summary of X-ray crystallographic data for LOH, **2a**, **3a**, **4a** and **5a**.

	LOH	**2a**	**3a**	**4a**	**5a**
Empirical formula	$C_{15}H_{21}N_3O_2$	$C_{33}H_{54}Cl_2N_6NiO_7$	$C_{32}H_{48}Cl_4Cu_2N_6O_6$	$C_{30}H_{46}Cl_2CuN_6O_6$	$C_{34}H_{48}Cl_4N_8O_4Zn$
Formula weight	275.35	776.43	881.64	721.17	905.34
Colour, habit	Colorless, block	Violet, block	Green, block	Blu, plate	Colorless, block
Crystal size, mm	0.45x0.45x0.35	0.55x0.50x0.50	0.50x0.45x0.30	0.45x0.25x0.10	0.25x0.20x0.17
Crystal system	Triclinic	Monoclinic	Monoclinic	Orthorhombic	Monoclinic
Space group	*P*-1	$P2_1/n$	*C*2/c	*P*bca	*C*2/c
a, Å	8.515(1)	11.3780(1)	25.631(2)	14.037(8)	26.383(3)
b, Å	10.540(2)	15.3700(1)	8.455(1)	18.297(6)	9.016(2)
c, Å	10.582(2)	11.4960(1)	21.883(2)	13.928(8)	22.609(2)
αdeg.	63.298(2)	90	90	90	90
β, deg.	86.374(2)	102.49(1)	121.860(2)	90	125.33(2)
γdeg.	69.046(2)	90	90	90	90
V, Å^3	786.9(2)	1962.8(3)	4027.8(7)	3577(3)	4387.5(12)
Z	2	2	4	4	4
T, K	293(2)	293(2)	293(2)	293(2)	293(2)
ρ(calc), Mg/m^3	1.162	1.314	1.454	1.339	1.371
μ, mm^{-1}	0.079	0.681	1.369	0.808	1.380
θ range, deg.	2.17 to 27.99	2.25 to 27.96	1.87 to 27.98	3.03 to 27.01	1.89 to 27.02
No.of rflcn/obsv	8456 / 3418	20820 / 4345	21494 / 4578	4459 / 3902	23449 / 4764
GooF	1.010	1.008	1.010	1.004	0.861
*R*1	0.0429	0.0372	0.0345	0.0419	0.0424
*wR*2	0.1297	0.0920	0.0857	0.0650	0.0431

$R1 = \Sigma||F_o|-|F_c||/\Sigma|F_o|$, $wR2 = [\Sigma[w(F_o^2-F_c^2)^2]/\Sigma[w(F_o^2)^2]]^{1/2}$, $w = 1/[\sigma^2(F_o^2) + (aP)^2 + bP]$, where $P = [\max(F_o^2,0) + 2F_c^2]/3$

Single crystal data was collected with a *Bruker AXS Smart 1000* area detector diffractometer (Mo Kα: λ = 0.71073 Å, LOH, **2a**, **3a** and **5a**) and with a *Philips PW 1100* diffractometer (Mo Kα: λ = 0.71073 Å, **4a**). Cell parameters were refined from the observed setting angles

and detector positions of selected strong reflections for LOH, **2a**, **3a** and **5a**. Intensities were integrated from several series of exposures frames covering the sphere of reciprocal space.[208] For **4a** the cell constants were obtained by a least-square refinement of the setting angles of 24 randomly distributed and carefully centered reflections. An absorption correction was applied using the program SADABS[153] with transmission factors in the ranges 0.830-1.000 (LOH), 0.715-1.000 (**2a**), 0.794-1.000 (**3a**) and 0.752-1.000 (**5a**) and using the method of Walker & Stuart[154] for **4a** with min. and max. transmission factors of 0.886 and 1.000. The structures were solved by direct methods (SIR97[155]) and refined on F^2 with full-matrix least squares (SHELXL-97[156]), using the Wingx software package.[157] Non hydrogen atoms were refined anisotropically for all compounds. The hydrogen atom of the hydroxyl group was found and refined for all compounds, whereas the remaining hydrogen atoms of the ligands were placed at their calculated positions. One of the three solvent molecules of crystallization (CH_3OH) in **2a** was found disordered in two positions with a site occupancy factor of 0.5 for each molecule. For **3a**, the independent crystallization solvent molecule was found disordered in three positions, each with a site occupancy factor of 0.33. Molecular drawings were prepared using the Mercury 1.4.2 program.[159]

3.2.10 DFT calculations

All the calculations were performed with Gaussian 03 software.[160] Assuming that the ligand LOH is a racemic mixture of the R and S enantiomers, five possible octahedral $[Zn(LOH)_2]^{2+}$ complexes can be obtained: three RR/SS enantiomeric pairs, the RS/SR non centro-symmetric pair and the RS centro-symmetric complex (see discussion). For the optimization of the molecular geometry of the five $[Zn(LOH)_2]^{2+}$ model complexes, in which the methyl groups were replaced by hydrogen atoms, the gradient-corrected hybrid density functional B3LYP[164,165] and the 6-31+G basis set were used. Single point energy calculations were performed using the B3LYP density functional and the 6-311+G(d) basis set. The energies of the various compounds do not include thermal or entropy corrections.

3.2.11 Spectrophotometric and NMR titrations

Complexation of M^{2+} ions (M = Ni, Cu, Zn) with the ligand LOH was studied in a methanol:water 95:5 mixture at T = 25 °C by spectrophotometric titrations in the visible range (400–900 nm). Ni^{2+} and Cu^{2+} stock solutions (C_{Ni} = 0.207 M; C_{Cu} = 0.035 M) were prepared

by weight from their chloride salts and contained NMe_4Cl as an ionic medium (C_{NMe4Cl} = 0.46 M). Metal ions and ligand stock solutions (prepared by weight) were used immediately. Speciation of the Ni^{2+} or Cu^{2+}/LOH systems was studied by collecting visible spectra of batch samples containing a fixed metal ion concentration with increasing concentrations of ligand up to 1:2.71 (Ni^{2+}/LOH) and 1:2.26 (Cu^{2+}/LOH) ratios. Speciation of the Zn^{2+}/LOH system was investigated by collecting ^1H NMR spectra (26) of a 0.009 M ligand sample titrated with aliquots of a 0.05 M $ZnCl_2$ solution (up to a 7.4:1 Zn^{2+}:LOH ratio). Visible spectrophotometric data were treated by means of the SPECFIT32 program,[209,210] which allowed determination of both the complexation log β values and the molar absorbancies of the complex species. For the Zn^{2+}/LOH system, the equilibria between LOH, $[Zn(LOH)Cl]^+$ and $[Zn(LOH)_2]^{2+}$ occur in the slow-exchange NMR condition, with the inconvenience of signal overlap between various species. Nevertheless, the observed intensity at a certain chemical shift can be expressed by the sum of the integrals appearing at that chemical shift value if all the contributions derive from the same type of protons. This is expressed by:

$$I_\delta^{\,*} = \sum_{species,\delta} I_L^{0\,*}\, \chi_\delta^{species} \cdot n \cdot m = \sum_{species,\delta} \frac{I_L^{0\,*}}{C_L} \cdot n \cdot m \cdot C_\delta^{species} \qquad (3.1)$$

where: $I_\delta^{\,*}$ = observed integral at chemical shift δ, $I^0{}_L^{\,*}$ = ligand one-proton integral at the initial condition, χ_δ = molar fraction of the species (LOH, $[M(LOH)Cl]^+$ or $[M(LOH)_2]^{2+}$) with protons absorbing at chemical shift δ, n = number of protons of the functional groups at chemical shift δ of each species, m = number of ligands in the absorbent species, C_L = total ligand concentration. $I_\delta^{\,*}$ and $I^0{}_L^{\,*}$ were normalized for the internal standard integral (TMS). The right side of Equation 3.1 closely resembles the Lambert-Beer equation for an optical pathlength of 1 cm and $\varepsilon = (n \cdot m \cdot I^0{}_L^{\,*}/C_L)$. On this ground, least square regression calculation procedures, employed to treat spectrophotometric data, can be applied to the treatment of slow-exchange NMR data. In this work, SPECFIT32 program was used for the calculations. The application of this *pseudo* Lambert-Beer equation to obtain global formation constants (β) simply consists of the introduction of the $n \cdot m \cdot I^0{}_L^{\,*}/C_L$ values (*pseudo* ε) for each of the signals taken into account in the calculations, together with the $I_\delta^{\,*}$ (*pseudo* adsorbance). Species which does not possess protons absorbing at a given chemical shift δ are treated with $n \cdot m \cdot I^0{}_L^{\,*}/C_L = 0$.

3.2.12 EXSY spectroscopy

^{1}H-^{1}H EXSY spectra of **5** were recorded in CD_3OD at 300 K using a conventional phase sensitive NOESY pulse sequence employing different mixing times (τ_m), 0.2, 0.4, 0.6 and 0.8 s. The method of Perrin was applied to calculate the exchange rate constants:[211] $\mathbf{R} = \ln\mathbf{A}/\tau_m$, where **R** is the relaxation matrix, which contains exchange constants k^{ex}_{ij} (*i* = starting species/proton, *j* = derived species/proton) as diagonal elements and **A** is a matrix whose elements are $I_{ij}(\tau_m)/M^0_j$ (I_{ij} = volumes of the 2D peaks, M^0_j = volumes of the diagonal peaks at $\tau_m = 0$). The final k^{ex}_{ij} elements are reported as the mean value of the experimental $k^{ex}_{ij}(\tau_m)$ obtained at different mixing times.[212] Rate constants k_{ij} and semi-reaction rates r_{ij} were calculated from k^{ex}_{ij} by considering a first order mechanism for the interconversion of the $[Zn(LOH)_2]^{2+}$ isomers, and a second order one for the exchange between $[Zn(LOH)Cl]^+$ and the octahedral $[Zn(LOH)_2]^{2+}$ species (see Appendix 2). Equilibrium concentrations were derived from the integration of the diagonal peaks volumes at $\tau_m = 0$ and from the analytical concentration of Zn in the solution (C_{Zn} = 0.015 M). Uncertainties of k_{ij} and of r_{ij} were calculated by propagation and neglecting concentration errors.

3.3 Results and Discussion

The two-steps synthesis of LOH is described in Scheme 3.3. The first reaction between the electrophilic chloromethyl-dimethylpyridine derivative and pyrazole, performed in biphasic solvent (toluene/water) *via* phase transfer catalysis (*n*-Bu_4NOH), is analogous to a procedure reported in the literature.[213] The second step involves insertion of an electrophile on the generated carbanion in agreement with the method developed for the synthesis of bis(pyrazolyl)methane derivatives.[40] The use of acetone as an electrophile provides the N,N',O heteroscorpionate ligand LOH in good yield. The selective deprotonation of the methylene bridge without competition from other acidic groups, such as the C5 proton on pyrazole,[214,215] is favoured by the benzylic-like character of the coniugated base. Moreover, the methyl substituents on pyridine allow electrophile insertion exclusively on the bridging carbon and not on the 3 and 5 positions of the pyridine ring. This synthetic pathway has a more general application concerning the preparation of mixed N,N',X (X = heteroatom) scorpionates. In fact, variously substituted pyrazoles can be in principle employed without the drawbacks of pyrazole deprotonation on the C5 position. However, it has to be noted that when a mono-substituted pyrazole is employed, two structural isomers can be obtained depending on which pyrazole nitrogen atom is eventually attached to the bridging methylene group, Scheme 3.4.

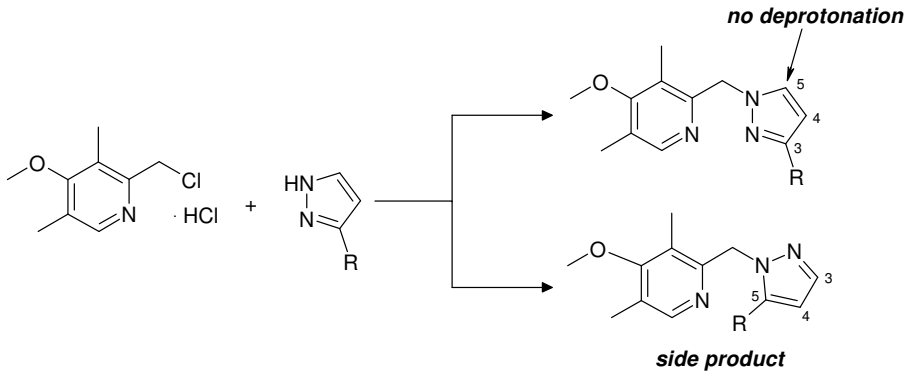

Scheme 3.4

Nevertheless, this inconvenience has minimum consequences since the reaction usually favors the isomer which is unsubstituted on the C5-pyrazole position (see Chapter 4). Furthermore, the stability of the pyrazole-pyridine conjugate base (with respect to the bispyrazolyl one) allows it to react with electrophiles that exhibit weak acidic character such as acetone. LOH is chiral due to the asymmetry of the bridging carbon, even though the synthetic route is not

stereoselective. On the other hand, the introduction of a stereogenic center on analogous bis(pyrazolyl)methane derivatives requires the use of two differently substituted pyrazoles, a procedure that can generate at least three possible products in a first step (two symmetric compounds and the prochiral molecule) with subsequent low yields and purification/separation inconveniences.[204] It is worth considering that the acidic nature of the bridging CH of LOH may limit the use of the ligand in its R or S enantiopure forms, in the presence of mild basic conditions.

The donor ability of the neutral LOH ligand versus 3d late transition metal ions was investigated by reacting LOH with MCl_2 salts (M = Ni, Cu and Zn) in both 1:1 and 2:1 M:LOH ratios that exclusively gave $[M(LOH)_2]^{2+}$ cationic complexes. For Ni^{2+} and Cu^{2+}, the M:LOH stoichiometric ratio determined the type of counterions, which was Cl^- or $[MCl_4]^{2-}$ for M:LOH of 1:2 and 1:1, respectively, whereas only the Zn-complex $[Zn(OH)_2][ZnCl_4]$ was isolated, regardless of stoichiometric conditions.

We attempted to explore the coordination properties of the deprotonated ligand LO^- with Zn^{2+} in 1:1 ratio in order to obtain a [Zn(LO)Cl] neutral complex analogous to bis(pyrazolyl)-alkoxides.[80,193,194] The Li(LO) alkoxide was prepared by deprotonating the alcoholic function of LOH using *n*-BuLi in THF. The reaction with anhydrous $ZnCl_2$ did not give the desired [Zn(LO)Cl] complex since decomposition of LOH occurred, presumably in a metal catalyzed pathway, which generated the carbanionic ligand precursor $(L^0)^-$ and acetone, followed by protonation of $(L^0)^-$ by adventitious moisture. In fact, the $[Zn(L^0)Cl_2]$ complex was isolated from this reaction (not reported structure).

3.3.1 Solid state structures

The molecular structures of the ligand LOH and of the complexes $[Cu(LOH)_2][CuCl_4]\cdot 2CH_3OH$ (**3a**) are reported in Figure 3.1-3.2, whereas the molecular geometries (Ortep drawings[216]) of $[Cu(LOH)_2]Cl_2\cdot 2H_2O$ (**4a**), $[Ni(LOH)_2]Cl_2\cdot 3CH_3OH$ (**2a**), and $[Zn(LOH)_2][ZnCl_4]\cdot 2CH_3CN$ (**5a**) are reported in Appendix 2 (Figures A5, A6, A7). Selected geometric parameters are listed in Table 3.2. The main difference between the free and coordinated LOH resides in the different orientation of the pyrazole and pyridine groups with respect to the central C atom, since in the free ligand they point in opposite directions in order to minimize the N lone pairs repulsion. In addition, in the free ligand, the hydroxyl group acts as hydrogen bond donor with the pyridine nitrogen atom (d[O(12)-N(13)] = 2.741(2) Å).

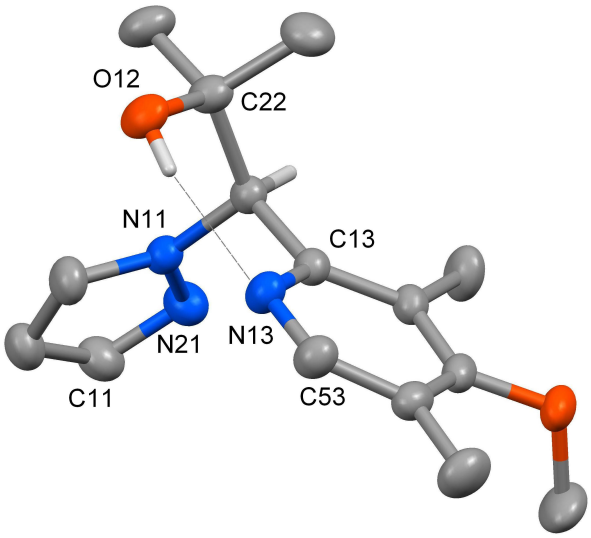

Figure 3.1 Molecular drawing of the ligand LOH at the 30% thermal ellipsoids probability level. Hydrogen atoms (except for hydroxylic and methinic ones) and the CH_3OH solvent molecules were omitted for clarity. Selected bond distances (Å): O(12)-C(22) = 1.425(2), N(13)-C(53) = 1.337(2), N(13)-C(13) = 1.339(2), N(21)-C(11) = 1.326(2), N(21)-N(11) = 1.354(2).

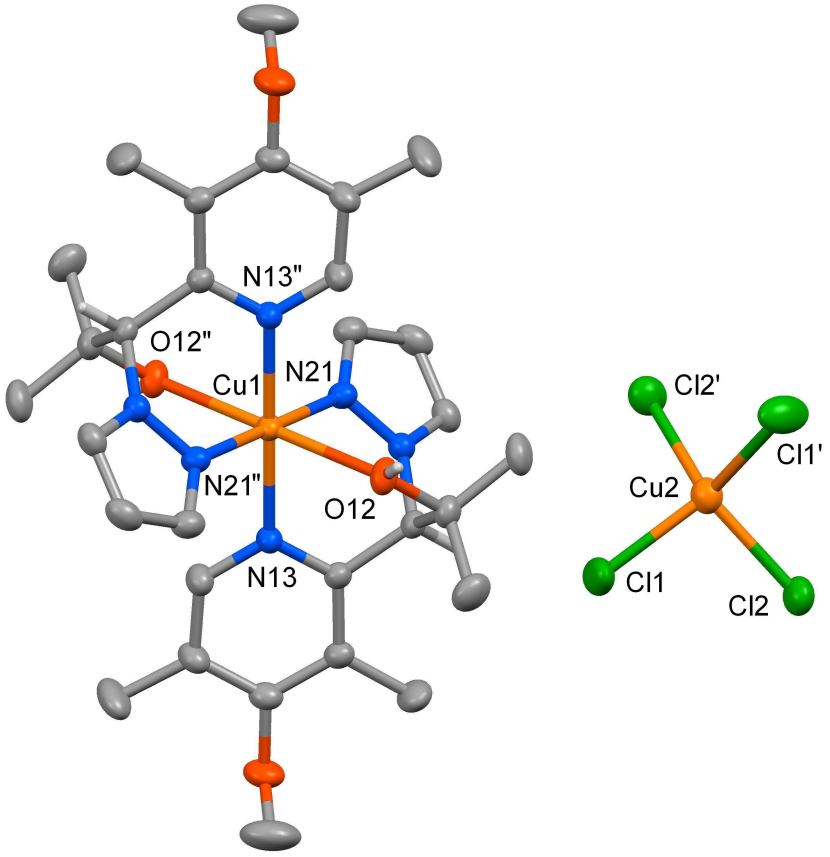

Figure 3.2 Molecular drawing of $[Cu(LOH)_2][CuCl_4]\cdot 2MeOH$ (**3a**) at the 30% thermal ellipsoids probability level. Hydrogen atoms (except for hydroxylic and methinic ones) and the CH_3OH solvent molecules were omitted for clarity. ‘ = -x; y; ½-z; ‘’ = ½-x; ½-y; -z.

In **3a** and **4a** the metal lies on a crystallographic inversion center and the complexes present a distorted octahedral geometry with the equatorial plane defined by the nitrogen atoms of two pyrazole and two pyridine groups from two N,N',O chelate ligands. The apical positions are occupied by two hydroxyl groups and the Cu-O bond lengths are ~ 0.3 Å greater than the Cu-N one (d[Cu-O(12)] is 2.331(2) Å for **3a** and 2.298(2) Å for **4a**), as a consequence of the tetragonal distortion typical of the Cu^{2+} ion. The $[CuCl_4]^{2-}$ counter-anion of **3a** adopts a geometry intermediate between the square planar and the tetrahedral one. The tetrahedron is flattened along the Cl(1)-Cu(1)-Cl(1)' (141.30(6)°) and Cl(2)-Cu(1)-Cl(2)' (140.53(5)°, ' = -x; y; 1/2-z) angles bisector. The chlorine anions of **4a** are exchanging hydrogen bonds with two crystallization water molecules. In addition, the hydroxyl groups of **3a** and **4a** behave as hydrogen bond donors with the Cl(2) chlorine anion (d[O(12)-Cl(2)'''] = 3.216(2) Å, ''' = 1-x; y-1; 1/2-z) and with the Cl(1) chlorine anion (d[O(12)-Cl(1)''''] = 3.063(3) Å, '''' = 1/2+x; 1/2-y; -z), respectively.

Table 3.2 Selected bond lengths (Å) for **2a**, **3a**, **4a** and **5a**.

2a		**3a**		**4a**		**5a**	
Ni-N(21)	2.051(2)	Cu(1)-N(21)	1.989(2)	Cu-N(21)	1.973(2)	Zn(1)-N(21)	2.098(3)
Ni-N(13)	2.056(2)	Cu(1)-N(13)	2.027(2)	Cu-N(13)	2.033(2)	Zn(1)-N(13)	2.131(2)
Ni-O(12)	2.092(2)	Cu(1)-O(12)	2.331(2)	Cu-O(12)	2.298(2)	Zn(1)-O(12)	2.134(2)
		Cu(2)-Cl(1)	2.242(1)			Zn(2)-Cl(1)	2.227(1)
		Cu(2)-Cl(2)	2.264(1)			Zn(2)-Cl(2)	2.282(1)

The molecular structures of the Zn^{2+} and Ni^{2+} complexes are in agreement with the structure reported for compound **3a** and **4a**, respectively. The metal, in both complexes, lies on an inversion center and it is in a regular octahedral geometry with M-(donor atom) bond distances that essentially reflect the differences between the ionic radii of the two metals (range distances: Ni^{2+}-donor = 2.051(2)-2.092(2) Å, Zn^{2+}-donor = 2.098(3)-2.134(2) Å), Table 2. The $[ZnCl_4]^{2-}$ counterion of **5a** exhibits a regular tetrahedral geometry with the Cl-Zn-Cl angles in the range 105.70(5)-116.10(5)°.

3.3.2 Solution studies

Speciation of the three M^{2+}/LOH systems (M = Ni, Cu, Zn) was evaluated in a methanol:water 95:5 solution by titration methods (Figures 3.3 and 3.4).

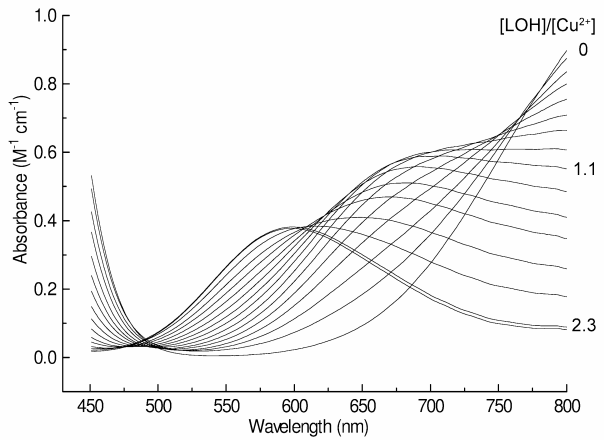

Figure 3.3 Visibile spectra of $CuCl_2 \cdot 2H_2O$ titrated with LOH (Cu^{2+}:LOH = 1:0-2.26, C_{Cu} = 0.018 M).

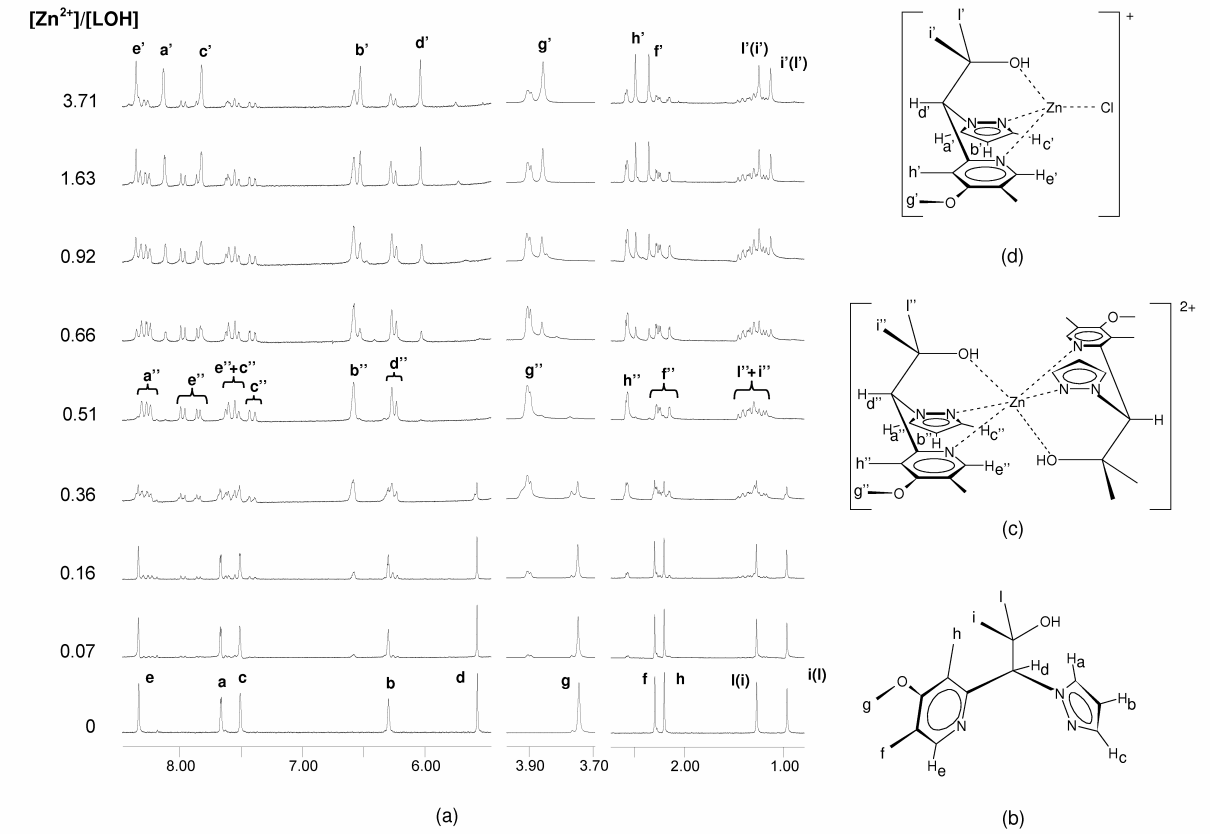

Figure 3.4 ^{1}H NMR titration of the Zn^{2+}/LOH system (a). The assignment of the different NMR signals for each Zn^{2+}/LOH species is reported in (b), (c) and (d) (for LOH, $[Zn(LOH)Cl]^+$ and $[Zn(LOH)_2]^{2+}$ respectively).

The choice of the solvent depends on the solubility properties of both the MCl_2 salts and the ligand. For all of the M^{2+}/LOH systems, three-species equilibria were obtained (Scheme 3.5) and the distribution diagrams are reported in Figure 3.5.

$$M^{2+} + LOH \overset{\beta_1}{\rightleftharpoons} [M(LOH)]^{2+}$$

$$M^{2+} + 2LOH \overset{\beta_2}{\rightleftharpoons} [M(LOH)_2]^{2+}$$

Scheme 3.5

The global formation constants (β) of $[M(LOH)]^{2+}$ and $[M(LOH)_2]^{2+}$ are in agreement with the Irving-Williams series ($Ni^{2+}<Cu^{2+}>Zn^{2+}$), Table 3.3.[217,218] The greater stability constants of the Zn^{2+} complexes with respect to the Ni^{2+} ones could be due to the presence of the OH group, which increases the *hard* character of the ligand.

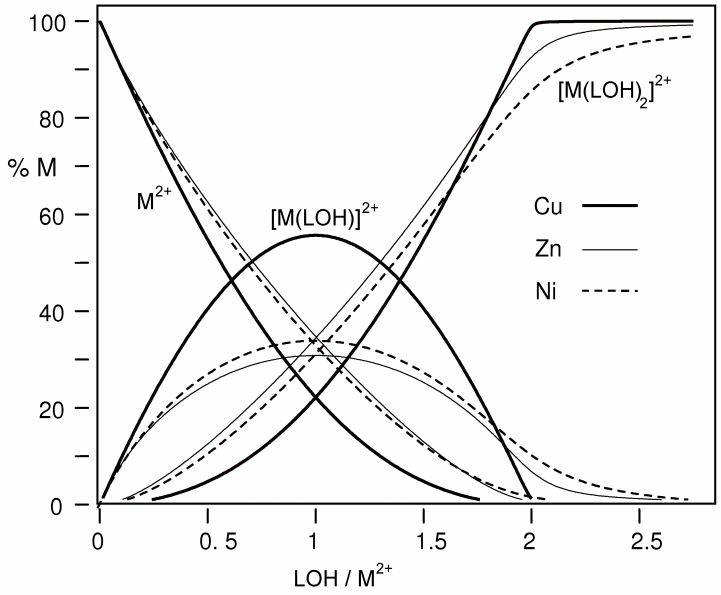

Figure 3.5 Distribution diagrams of the different M^{2+}/LOH systems (M = Ni, Cu, Zn).

Table 3.3 Logarithms of the global formation constants of $[M(LOH)]^{2+}$ (β_1) and $[M(LOH)_2]^{2+}$ (β_2).

	Ni^{2+}	Cu^{2+}	Zn^{2+}
$log\ \beta_1$	2.7(4)	6.4(4)	3.8(1)
$log\beta_2$	5.3(5)	12.0(5)	7.7(2)
$\sigma^{[a]}$	0.02	0.01	0.56

$\sigma^{[a]} = [\Sigma(A_i^o-A_i^c)^2/(n-m)]^{1/2}$ = sample standard deviation; A_i^o = experimental absorbance or intensity; n = number of observations, m = number of parameters refined.

The metal coordination of the $[M(LOH)]^{2+}$ species is most probably completed by chlorine ions or solvent molecules whereas it is easy to describe the $[M(LOH)_2]^{2+}$ complexes as octahedral analogous with the X-ray structures. ESI-Mass spectra recorded from a methanolic solution of **1**, **3** and **5** (M:LOH = 1:1), revealed the occurrence of the $[M(LOH)_2]^{2+}$ complex together with the $[M(LOH)Cl]^{+}$ (Ni^{2+} and Zn^{2+}) and $[Cu(LOH)(CH_3OH)]^{+}$ species. In addition, in the ESI-Mass spectrum obtained from a solution of **5** containing a large excess of Zn^{2+} (10:1 over LOH), only the peak of $[Zn(LOH)Cl]^{+}$ is present (Figure A8 of Appendix 2). This would provide evidence for the chlorine and solvent coordination to the $[M(LOH)]^{2+}$ moiety, but it also supports the molecular structures reported in Figure 3.4, with the $[Zn(LOH)Cl]^{+}$ complex exhibiting a tetrahedral structure bound by the N,N',O ligand and by an apical chlorine ion. The $[M(LOH)_2]^{2+}$ (M = Cu and Zn) complexes crystallized also in 1:1 stoichiometric conditions; a reason for this comes from the analysis of the distribution diagrams, wherefrom results evident that the global concentration of $[MCl_4]^{2-}$ and $[M(LOH)_2]^{2+}$ is greater or comparable to the $[M(LOH)]^{2+}$ one for a 1:1 M^{2+}:LOH ratio. Moreover, $[Zn(LOH)_2][ZnCl_4]$ is precipitated also from a solution containing a 1:2 Zn^{2+}:LOH ratio. This probably occurs as a consequence of favourable packing forces between the tetrahedral $[ZnCl_4]^{2-}$ and the octahedral $[Zn(LOH)_2]^{2+}$.

The ^1H NMR spectra of LOH titrated with $ZnCl_2$ in CD_3OD:D_2O 95:5 and the peak-assignments of LOH, $[Zn(LOH)Cl]^{+}$ and $[Zn(LOH)_2]^{2+}$are reported in Figure 3.4. Various sets of signals appear in the ^1H NMR spectrum in the presence of the maximum concentration of $[Zn(LOH)_2]^{2+}$, whereas only a set of signals appears when increasing the Zn^{2+} concentration (up to ~4 fold with respect to LOH). This is in agreement with the ESI-Mass findings, suggesting that the $[Zn(LOH)Cl]^{+}$ complex becomes preponderant when increasing the Zn^{2+} concentration. It is helpful to resort to 2D NMR techniques for the elucidation of the equilibria occurring between the various solution species. The ^1H-^1H NOESY/EXSY spectrum of **5** registered at 300 K (τ_m = 0.6 s, not reported), along with the negative cross-peaks deriving from cross-relaxation (NOE), shows a set of positive cross-peaks (same diagonal sign) disappearing at 250 K (τ_m = 0.6 s), which are due to chemical exchange between different species in solution. In order to quantitatively analyze the chemical exchange processes, a series of more resolved EXSY spectra were registered in the 7.25-8.55 ppm range and at various τ_m (0.2, 0.4, 0.6, 0.8 s) that focused on the set of seven well-separated pyridyl protons (Figure 3.6).

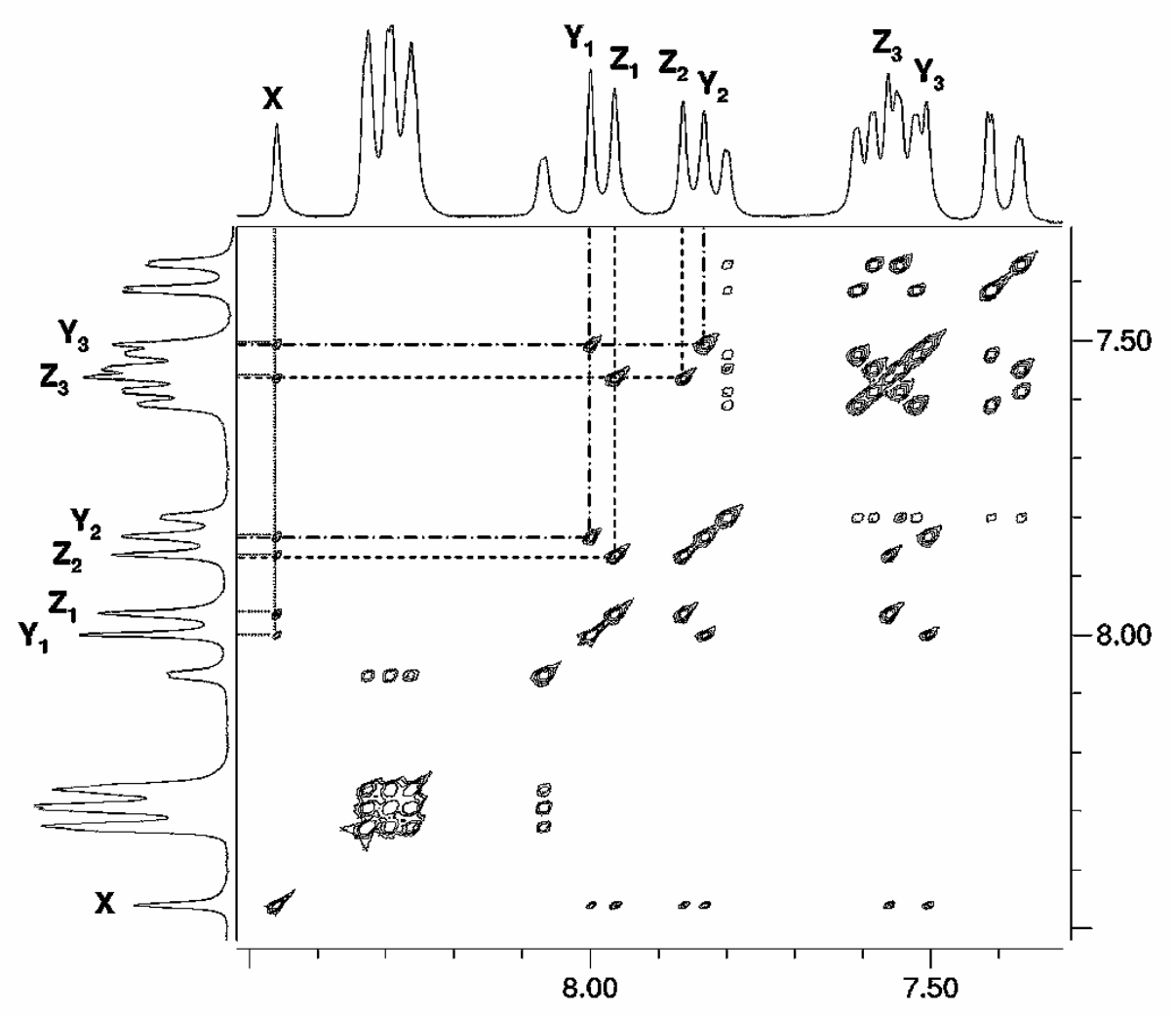

Figure 3.6 ^{1}H-^{1}H EXSY spectrum of **5** in CD_3OD registered at 300 K in the 7.25-8.55 ppm range (mixing time = 0.8 s). The pyridyl protons of $[Zn(LOH)Cl]^+$ (X) and of the $[Zn(LOH)_2]^{2+}$ isomers ($Y_{1\text{-}3}$ and $Z_{1\text{-}3}$) are evidenced. Exchange between X and the two groups of $Y_{1\text{-}3}$ and $Z_{1\text{-}3}$ protons (····); exchange within the two groups of $Y_{1\text{-}3}$ and $Z_{1\text{-}3}$ protons (— ▪ — and ----).

According to the NMR titration, the X proton belongs to the $[Zn(LOH)Cl]^+$ tetrahedral species (1A, Figure 3.7), while the other six (Y_1, Y_2, Y_3 and Z_1, Z_2, Z_3 protons) belong to the $[Zn(LOH)_2]^{2+}$ structural isomers (2A-E). The two groups of protons $Y_{1\text{-}3}$ and $Z_{1\text{-}3}$ exchange with X, but there is no evidence of $Y_{1\text{-}3} \rightleftharpoons Z_{1\text{-}3}$ interconversion, *i.e.* Y_1, Y_2, Y_3 exchange with each other but not with $Z_{1\text{-}3}$. This implies that $[Zn(LOH)Cl]^+$ is in equilibrium with two distinct sets of octahedral $[Zn(LOH)_2]^{2+}$ isomers (2A-C and 2D-E).

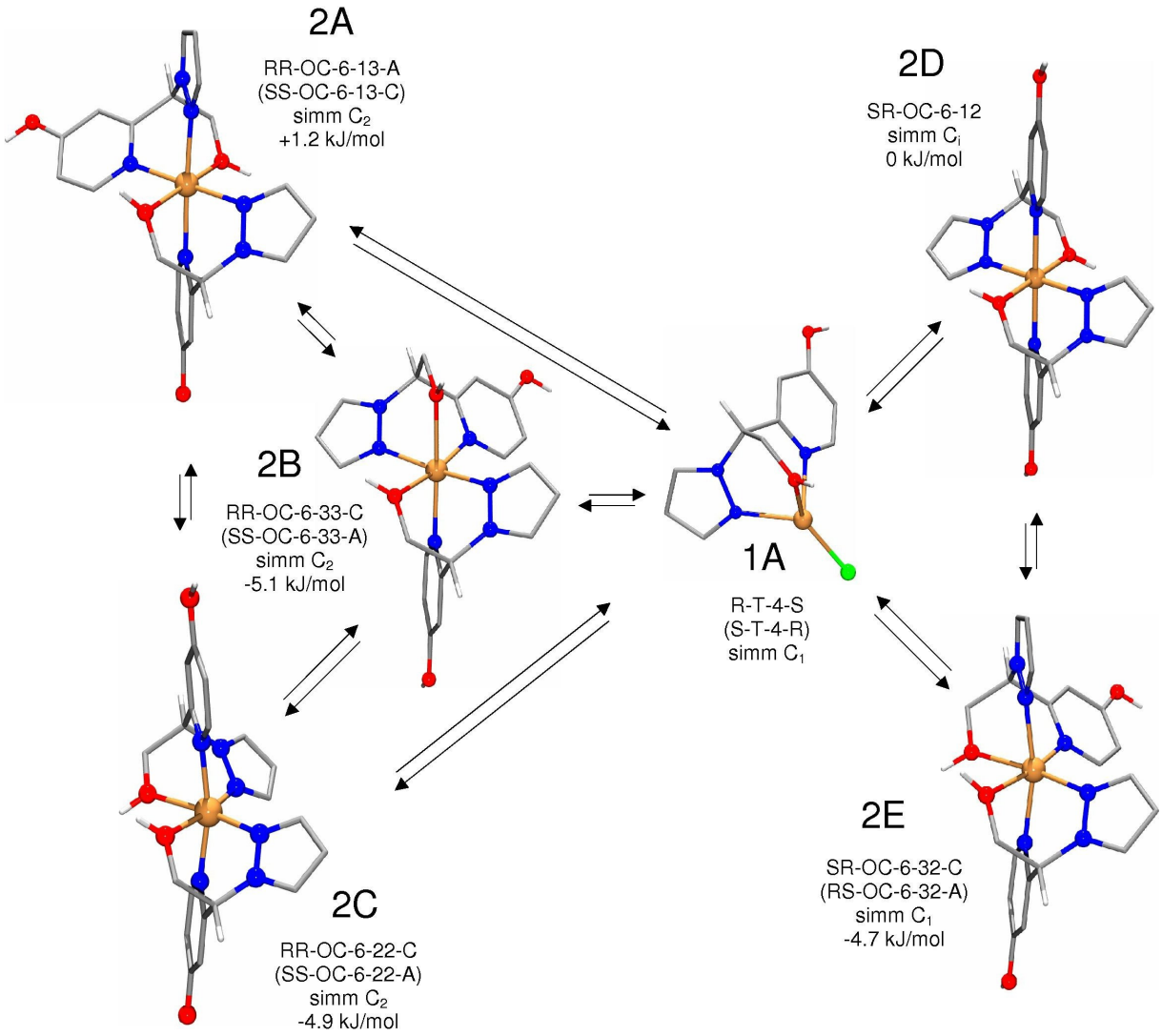

Figure 3.7 DFT optimized model complexes of the $[Zn(LOH)_2]^{2+}$ (2A-E) and $[Zn(LOH)Cl]^{+}$ (1A) species together with the equilibrium scheme proposed for the Zn^{2+}/LOH system in methanol:water 95:5. The centro-symmetric isomer (2D) is taken as reference for the energy level of the isomers. The complete nomenclature for each isomer is reported with, in parenthesis, the energetically equivalent enantiomers.

To explain such a complexity, it has to be borne in mind that five octahedral isomers can be generated when using a racemic mixture of LOH, as a consequence of the ligand and metal chirality (see Figure 3.7): three C_2-symmetric RR/SS isomers in enantiomeric pair (2A, 2B, and 2C), a centrosymmetric RS isomer (2D, as found in the solid state structure) and finally an RS asymmetric isomer (2E). According to their symmetry, 2A-D have to display a single set of signal, whereas 2E has to display two sets of signals. This would correspond to the six exchanging signals found in the EXSY at 300 K. A DFT optimization of five $[Zn(LOH)_2]^{2+}$

model complexes was performed and the relative energies were calculated by taking as a reference the centrosymmetric isomer 2D. The various molecular arrangements are too close in energy to provide information of a structural preference. In fact, the maximum energy difference of 6.3 kJ/mol (between 2A and 2B) is within the accuracy of the DFT calculation method[219,220] and would confirm that all the five species can be present in solution in approximately equimolar ratio, in agreement with the NMR spectrum.

By means of quantitative EXSY analysis, the values of the exchange rate constants k^{ex}_{ij} (*i* = starting species/proton, *j* = derived species/proton) between the different pyridyl protons (X, Y_{1-3} and Z_{1-3}) were obtained (Table 3.4).

Table 3.4 Relaxation matrix containing the exchange constants k^{ex}_{ij} (i = column, j = row, s^{-1}) between the different Zn^{2+}/LOH species in CD_3OD (1A, 2A-E, see Figure X7). The corresponding X, Y_{1-3} and Z_{1-3} exchanging-sites (NMR signals) are reported in the same order of the EXSY spectrum (see Figure 3.6).

	X	**Y_1**	**Z_1**	**Z_2**	**Y_2**	**Z_3**	**Y_3**
X		0.03(1	0.07(1	0.05(1	0.05(2	0.06(1	0.07(2)
Y_1	0.06(2)		-	-	0.48(4	-	0.14(7)
Z_1	0.13(3)	-		1.8(1)	-	1.7(2)	-
Z_2	0.09(2)	-	1.4(1)		-	0.12(9	-
Y_2	0.12(3)	0.45(2	-	-		-	2.7(3)
Z_3	0.12(2)	-	1.3(2)	0.11(8	-		-
Y_3	0.15(5)	0.13(6	-	-	2.6(3)	-	

Since k^{ex}_{ij} are of pseudo-first order, they can be compared, thus making speculations about the mechanisms of interconversion between various isomers, possible. It is evident that eight (underlined in Table 4) $[Zn(LOH)_2]^{2+} \rightarrow ([Zn(LOH)_2]^{2+})^{\#}$ interconversions (k^{ex}_{ij}: 2.7(3)-0.45(2) s^{-1}) are faster than the $[Zn(LOH)Cl]^{+} \rightarrow [Zn(LOH)_2]^{2+}$ (0.06(2)-0.15(5) s^{-1}) and $[Zn(LOH)_2]^{2+} \rightarrow [Zn(LOH)Cl]^{+}$ (0.03(1)-0.07(2) s^{-1}) semi reactions by approximately an order of magnitude. This would exclude the "dissociative/associative" pathway for the interconversion of the octahedral species, $[Zn(LOH)_2][ZnCl_4] \rightarrow 2[Zn(LOH)Cl]^{+} + 2Cl^{-} \rightarrow [Zn(LOH)_2]^{\#}[ZnCl_4]$, in favor of a rotational mechanism that would involve a ligand C_3 rotation around the C_{chiral}-Zn-C_{chiral} axis, with the transition state exhibiting a trigonal pyramidal geometry (Scheme 3.6).

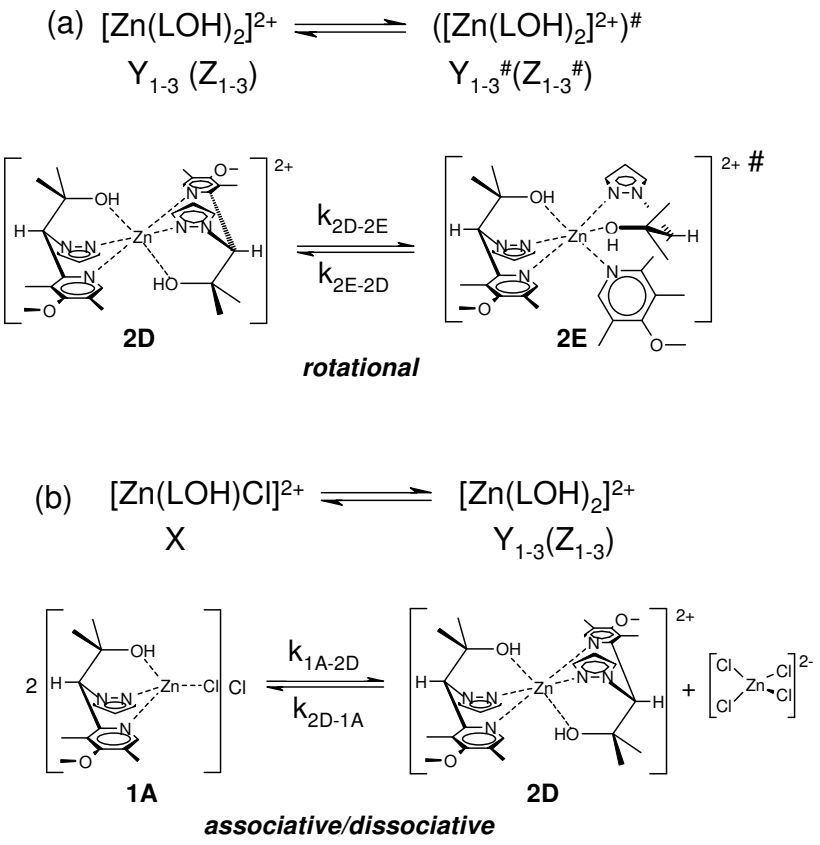

Scheme 3.6 First order (a) and second order (b) reaction pathways proposed for the interconversion of the different Zn^{2+}/LOH species. X and $Y_{1-3}(Z_{1-3})$ correspond to $[Zn(LOH)Cl]^+$ and $[Zn(LOH)_2]^{2+}$ pyridyl protons, respectively. Selected examples are reported.

The other four interconversions $[Zn(LOH)_2]^{2+} \rightarrow ([Zn(LOH)_2]^{2+})^{\#}$ are slower (k^{ex}_{ij}: 0.11(8)-0.14(7) s^{-1}) and their k^{ex}_{ij} are comparable with those of the $[Zn(LOH)Cl]^+ \rightarrow [Zn(LOH)_2]^{2+}$ and $[Zn(LOH)_2]^{2+} \rightarrow [Zn(LOH)Cl]^+$ processes, making it difficult to discriminate between dissociative/associative or rotational mechanisms. This would signify that if the isomerization proceeds through a rotational mechanism, it would involve a considerably hindered trigonal prismatic transition state.

3.4 Conclusions

The heteroscorpionate ligand 1-(4-Methoxy-3,5-dimethyl-pyridin-2-yl)-2-methyl-1-pyrazol-1-yl-propan-2-ol (LOH) was synthesised in two high yield steps. Its versatile and easy two-step preparation could be exploited for the synthesis of chiral N,N',X(,Y) tripodal donor ligands (*e.g.* X = O, S; Y = additional donor group as substituent on the pyrazole ring). The synthesis and coordination properties of N,N',S and N,N',S,S' ligands prepared according to this procedure will be analyzed in the next chapters.

LOH exhibits κ^3-N,N',O coordination towards late transition divalent ions (M = Ni, Cu and Zn) as evidenced by the X-ray structures of the complexes. Spectrophotometric (Cu^{2+} and Ni^{2+}) and ^{1}H NMR (Zn^{2+}) titrations provided further insights on the solution speciation and on the complexation constants, which are in accordance with the Irving-Williams series. Interestingly, in the solid state only octahedral centrosymmetric $[M(LOH)_2]^{2+}$ complexes were isolated also for 1:1 M^{2+}:LOH ratio, whereas in solution there are also evidences of 1:1 species. In the case of Zn^{2+}, ^{1}H-^{1}H EXSY spectroscopy revealed the occurrence of equilibria between different $[Zn(LOH)_2]^{2+}$ octahedral isomers and the $[Zn(LOH)Cl]^+$ tetrahedral species. Quantitative EXSY allowed the determination of the rate constants of the different semi-reactions and to propose two main interconversion pathways: a) rotational mechanism, which involves the octahedral species interconversion (faster) and b) dissociative/associative mechanism, which involves the octahedral-tetrahedral interconversion (slower). It is reasonable to assume that the presence of exchanging isomeric octahedral complexes in solution can be extended to the Ni^{2+} and Cu^{2+} systems even though we do not have direct evidence for it.

4

A N,N',S-Scorpionate Precursor. Ternary Cu(I) Complexes. Biomimetics of Cu-Thioneins[221]

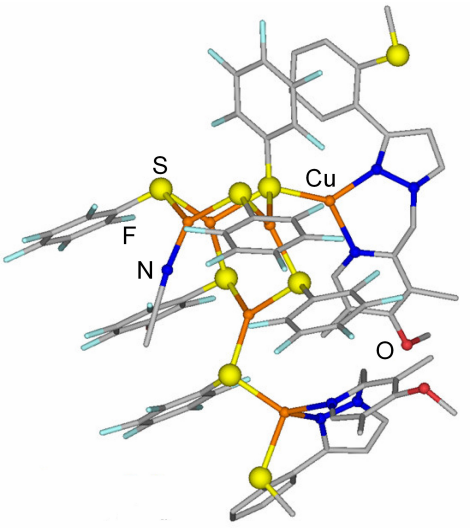

The N,N',S-donor ligand L^1, based on the pyrazole-pyridine moiety, and the Cu(I) complexes $[Cu_2(L^1)_2(CH_3CN)][Cu(L^1)(CH_3CN)](BF_4)_3$ (**1**), $[Cu(L^1)(PPh_3)]BF_4$ (**2**) and $[Cu_6(L^1)_2(C_6F_5S)_6]$ (**3**) were prepared and characterized by X-ray crystallography. The unit cell of **1** consists of co-crystallized mononuclear and dinuclear entities wherein all of the copper atoms exhibit distorted tetrahedral coordination. **2** is monomeric, with a κ^3-N,N',S ligand and PPh_3 giving tetrahedral coordination, and fluxional in $CDCl_3$ solution due to the boat inversion of the six-membered N,N' chelate ring ($\Delta H^{\#}$ = +43.6(3) kJ mol^{-1}, $\Delta S^{\#}$ = -16(1) J mol^{-1} K^{-1}). Crystallization of **3** in CH_3CN leads to a polynuclear structure: $[Cu_6(L^1)_2(C_6F_5S)_6(CH_3CN)]$ (**3a**). The core of **3a** partially resembles a $\{Cu_4S_6\}$ adamantane-like moiety, the only difference being a Cu-$NCCH_3$ interaction that leads to the opening of the cluster by disrupting a Cu-Cu interaction. Part of this assembly is found in the yeast metallothionein copper(I)-cysteinate core whose crystal structure has recently been reported. Two additional $[Cu(L^1)]^+$ peripheral moieties interact with the cluster by means of bridging thiolates. ESI-Mass, conductivity and $^1H/^{19}F$-PGSE NMR experiments suggest the dissociation of **3a** in acetonitrile: **3a** + $CH_3CN \rightleftharpoons [Cu_4(C_6F_5S)_6]^{2-} + 2[Cu(L^1)(CH_3CN)]^+$. The stability of the cluster with respect to the hypothetical mononuclear species, $[Cu(L^1)(C_6F_5S)]$, is confirmed by DFT calculations (B3LYP).

4.1 Introduction

The bioinorganic relevance of copper is evidenced through its involvement in many crucial biological functions.[222] These can be classified as follows: (a) dioxygen activation (tyrosinase[223,224]); (b) dioxygen transport (hemocyanin[225]); (c) electron transfer (blue copper proteins[226-229]); and (d) copper delivery, storage and detoxification (thioneins[230]). The metal coordination is fundamental in the definition of the functional properties of these copper-proteins.[231,232]

We are interested in preparing new Cu complexes with nitrogen-sulfur donor ligands suitable as mimics of copper sites in biological systems. In particular, the easy synthesis of a variously substituted pyrazole-pyridine platform (see Chapter 3) prompted us to investigate the coordination ability of new ligands belonging to this class with opportune pyrazole substituents. It is noteworthy that, due to the easy deprotonation of the bridging methylene group and further functionalization, these ligands can be considered as parent compounds for the synthesis of new scorpionates, which should produce a more pre-organized coordination environment.

In this work we have used a thioether-substituted pyrazole, 3-(2-(methylthio)phenyl)-pyrazole, as a precursor, thus producing a new N,N',S-donor ligand (L^1, Scheme 4.1).

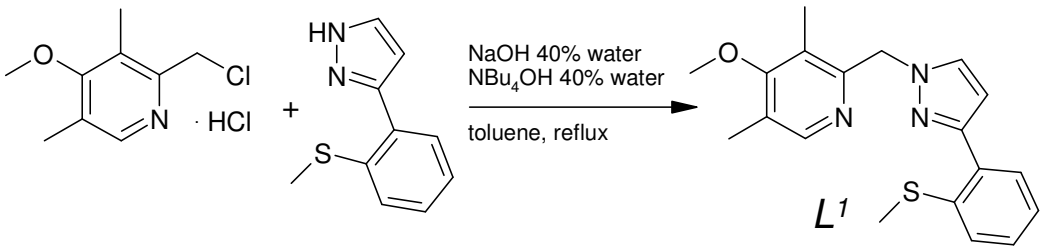

Scheme 4.1

Here we describe the coordination properties of L^1 with copper(I). To complete the coordination at the metal, PPh_3 and $C_6F_5S^-$ were also employed as coligands. The crystal structures of $[Cu_2(L^1)_2(CH_3CN)][Cu(L^1)(CH_3CN)](BF_4)_3$ (**1**), $[Cu(L^1)(PPh_3)]BF_4$ (**2**), and $[Cu_6(L^1)_2(C_6F_5S)_6(CH_3CN)]$ (**3a**) are reported and they point to a certain coordination flexibility of L^1, which appears not to be able to impose a definite geometry at the metal. After using PPh_3, which led to the isolation of **2** as a mononuclear complex, we employed the $C_6F_5S^-$ thiolate ligand to mimic the $^-$S-Cys fragment of proteins. In the present case, the

ternary ensemble Cu(I)/L^1/$C_6F_5S^-$ affords the polynuclear structure **3**, which can be rationalized in terms of the general property of the thiolates to form M-S-M bridges,[233-236] and by the lack of specific steric hindrance on the ligand L^1. This copper-sulfur structural arrangement can be found in metallothionein models[237] and it bears similarities with the copper(I)-thiolate core of the yeast copper thionein, whose crystal structure has recently been reported.[238] We also wished to evaluate the stability of the cluster structure of **3** in solution. For this purpose, ^1H and ^{19}F PGSE (Pulsed Gradient Spin Echo) NMR spectroscopy was employed,[239] affording a hydrodynamic radius (r_H) and the corresponding volume (V_H), which are consistent with the multinuclear solid state structure, even though some degree of dissociation of **3** into the $[Cu_4(C_6F_5S)_6]^{2-}$ and $[Cu(L^1)(CH_3CN)]^+$ ions can be envisaged. This hypothesis was also supported by conductivity measurements and ESI-Mass spectrometry.

4.2 Experimental

4.2.1 General procedures

All reagents and solvents were commercially available, except for 3-(2-(methylthio)phenyl)-1H-pyrazole[56] and $[Cu(CH_3CN)_4]BF_4$,[170] which were prepared as previously reported. Dichloromethane and acetonitrile were dried over CaH_2 and distilled before use. The syntheses of the complexes were performed in inert gas (N_2) using Schlenk techniques.

4.2.2 Synthesis of 4-methoxy-3,5-dimethyl-2-((3-(2-(methylthio)phenyl)-1H-pyrazol-1-yl)methyl)pyridine (L^1)

2-Chloromethyl-4-methoxy-3,5-dimethylpyridine hydrochloride (5.84 g, 26.29 mmol) and 3-(2-(methylthio)phenyl)-1H-pyrazole (5.00 g, 26.28 mmol) were mixed in toluene (150 ml). After adding a 40% NaOH water solution (50 ml) and a 40% NBu_4OH water solution (30 drops), the mixture was refluxed for 3 h. The organic phase was separated, washed with water (30 ml), and dried with Na_2SO_4. The solvents were removed under vacuum. Purification of the product by flash chromatography using ethyl acetate as the eluent produced a yellow oil, which was washed and triturated with hexane and finally dried under vacuum, yielding a light orange microcrystalline powder (L^1, 5.35 g, 15.77 mmol, 60%). Colorless crystals suitable for

X-ray diffraction were obtained by layering hexane over a dichloromethane solution of the product, corresponding to L^1. IR (cm^{-1}): 3146w, 3122m, 3059w, 3047w, 2999m, 2957m, 2943m, 2918m, 1586m, 1569m, 1480m, 1450s, 1437m, 1401m, 1332m, 1255s, 1213m, 1086m, 1050m, 999m, 867w br, 753vs. ^{1}H NMR (300 MHz, $CDCl_3$): δ 2.28 (s, 3H, CH_3 py *o*-CH), 2.33 (s, 3H, CH_3 py *p*-CH), 2.43 (s, 3H, CH_3S), 3.77 (s, 3H, CH_3O), 5.51 (s, 2H, CH_2), 6.60 (d, J = 2.2 Hz, 1H, CH pz(ph)), 7.18 (dt, J = 7.0, 1.9 Hz, 1H, CH ph), 7.29 (m, 2H, CH ph), 7.45 (d, J = 2.2 Hz, 1H, CH pz(CH_2)), 7.56 (d, J = 7.4 Hz, 1H, CH ph), 8.26 (s, 1H, CH py). ^{13}C NMR (75 MHz, $CDCl_3$): δ 10.7 (CH_3 py *p*-CH), 13.0 (CH_3 py *o*-CH), 15.7 (CH_3S), 56.1 (CH_2), 59.5 (CH_3O), 106.2 (CH pz(ph)), 124.1 (CH ph), 124.9 (CH ph), 125.9 (C quat. py), 125.9 (C quat py), 127.7 (CH ph), 129.2 (CH pz(CH_2R)), 129.3 (CH ph), 132.1 (C quat ph), 137.0 (C quat ph), 149.0 (CH py), 149.6 (C quat), 153.4 (C quat), 164.0 (C quat CH_3O). ESI-MS (p.i., cone 50 V, MeOH, m/z, I%): 340.5, 100, $[LH]^+$. Anal. calcd for $C_{19}H_{21}N_3OS$ (339.46): C, 67.23; H, 6.23; N, 12.38. Found: C, 67.14; H, 6.30; N, 12.44%.

*4.2.3 Synthesis of $[Cu_2(L^1)_2(CH_3CN)][Cu(L^1)(CH_3CN)](BF_4)_3$ (**1**)*

A solution of $[Cu(CH_3CN)_4]BF_4$ (264 mg, 0.84 mmol) in dichloromethane (20 ml) was added to a solution of L^1 (272 mg, 0.80 mmol) in dichloromethane (20 ml) at room temperature while stirring. After 1 h, the solution was concentrated to ~5 ml under vacuum; a white product was precipitated with hexane (25 ml), and filtered and dried under vacuum, yielding a colorless powder (**1**, 250 mg, 0.16 mmol, 62%). Colorless crystals suitable for X-ray diffraction were obtained by evaporation from an acetonitrile:water solution of the product. IR (cm^{-1}): 3138m, 3016w, 2946w, 1591m, 1521w, 1494m, 1473s, 1434s, 1411m, 1366m, 1298m, 1256s, ~1050vs br, 761s. ^{1}H NMR (300 MHz, CD_2Cl_2): δ 2.22 (s br, 6H, CH_3 py), 2.48 (s, 3H, CH_3S), 3.82 (s br, 3H, CH_3O), 5.29 (s br, 2H, CH_2), 6.43 (s br, 1H, CH pz(ph)), 7.45 (s br, 4H, CH(ph)), 7.87 (s br, 1H, CH pz(CH_2), 8.20 (s br, 1H, CH py). ^{13}C NMR (75 MHz, CD_2Cl_2): δ 2.80, 11.40, 13.29, 20.89, 51.90, 60.41, 106.40, 127.55, 128.28, 129.37, 129.70, 130.28, 131.02, 131.75, 132.16, 132.60, 148.85, 151.08, 165.64. Anal. calcd for $C_{61}H_{69}B_3F_{12}N_{11}O_3S_3Cu_3$ (1551.54): C, 47.22; H, 4.48; N, 9.93. Found: C, 47.02; H, 4.35; N, 9.49%.

*4.2.4 Synthesis of [Cu(L^1)(PPh_3)]BF_4 (**2**)*

A solution of [Cu(CH_3CN)$_4$]BF_4 (195 mg, 0.62 mmol) in acetonitrile (5 ml) was added to a solution of L^1 (206 mg, 0.61 mmol) and PPh_3 (155 mg, 0.59 mmol) in acetonitrile (20 ml) at room temperature while stirring. After 1 hour, the solution was dried under a vacuum, producing a colorless solid, which was recrystallized in dichloromethane:hexane, yielding a white powder (**2**, 400 mg, 0.53 mmol, 90%). Colorless crystals suitable for X-ray diffraction were obtained by layering hexane over a THF solution of the product. IR (cm^{-1}): 3139w, 3054w, 3005w, 1591m, 1569m, 1475m, 1433s, 1256m, 1061vs br, 755s br, 695s. ^{1}H NMR (300 MHz, $CDCl_3$): δ 1.78 (s, 3H, CH_3S), 2.20 (s, 3H, CH_3 py *o*-CH), 2.57 (s, 3H, CH_3 py *p*-CH), 3.82 (s, 3H, CH_3O), 5.49 (s br, 2H, CH_2), 6.52 (s, 1H, CH pz(ph)), 7.15-7.30 (m, 17H, CH ph), 7.46 (t, J = 6.9 Hz, 1H, CH ph), 7.58 (d, J = 7.2 Hz, 1H, CH ph), 7.99 (s, 1H, CH py), 8.25 (s, 1H, CH pz(CH_2)). ESI-MS (p.i., cone 29 V, MeOH, m/z, I%): 402.2, 100, [Cu(L)]$^+$; 664.2, 70, [Cu(L)PPh_3]$^+$. Anal. calcd for $C_{37}H_{36}BF_4N_3OPSCu$ (752.09): C, 59.09; H, 4.82; N, 5.59. Found: C, 59.17; H, 4.90; N, 5.51%.

*4.2.5 Synthesis of [Cu_6(L^1)$_2$(C_6F_5S)$_6$] (**3**)*

L^1 (720 mg, 2.12 mmol) was added to a suspension of CuCl (630 mg, 6.36 mmol) in acetonitrile (20 ml), and produced an orange solution. After few minutes, C_6F_5SH (0.85 ml, d = 1.5 g/ml, 6.37 mmol) and NH_4OH 15.71 M (0.41 ml, 6.44 mmol) were added, with consequent formation of a precipitate. After 30 min, water (10 ml) was added and the white solid was filtered and dried under vacuum, yielding a bright yellow powder (**3**, 1.68 g, 0.74 mmol, 70 %). IR (cm^{-1}): ~2920w, 1636w, 1626w, 1508vs, 1473vs, 1373w, 1357w, 1294w, 1260w, 1138w, 1082vs, 1009w, 968vs, 850vs, 761w. Anal. calcd for $C_{74}H_{42}F_{30}N_6O_2S_8Cu_6$ (2254.92): C, 39.42; H, 1.88; N, 3.73. Found: C, 39.51; H, 1.79; N, 3.65%. Colorless crystals suitable for X-ray diffraction were obtained by cooling to 8°C an acetonitrile/water solution of **3**, corresponding to *[Cu_6(L)$_2$(C_6F_5S)$_6$$CH_3CN$]* (**3a**). The solution characterization of **3** was performed in acetonitrile (see Results and discussion section). ^{1}H NMR (300 MHz, CD_3CN): δ 2.12 (s, 3H, CH_3), 2.20 (s, 3H, CH_3), 2.42 (s, 3H, CH_3S), 3.78 (s, 3H, CH_3O), 5.50 (s, 2H, CH_2), 6.50 (d, J = 2.2 Hz, 1H, CH pz(ph)), 7.30 (m, 3H, CH ph), 7.42 (m, 1H, CH ph), 7.83 (d, J = 2.2 Hz, 1H, CH pz(CH_2)), 8.16 (s, 1H, CH py). ^{13}C NMR (75 MHz, CD_3CN): δ 11.7, 13.4, 18.2, 53.0, 107.0, 128.0, 129.8, 130.1, 131.3, 132.8, 136.3 (m), 139.6 (m), 145.4 (m),

148.5 (m), 151.3. ^{19}F NMR (564 MHz, CD_3CN): δ-200.7 (d, J = 28 Hz, 2F), -233.0 (t, J = 25 Hz, 1F), -233.8 (t, J = 23 Hz, 2F). ESI-MS (n.i., cone -41 V, CH_3CN, m/z, I%): 461.0, 100, $[Cu(C_6F_5S)_2)]^-$; 724.8, 25, $[Cu_2(C_6F_5S)_3)]^-$; 986.6, 30, $[Cu_3(C_6F_5S)_4)]^-$; 1248.7, 12, $[Cu_4(C_6F_5S)_5)]^-$; 1512.5, 8, $[Cu_5(C_6F_5S)_6)]^-$. ESI-MS (p.i., cone 85 V, CH_3CN, m/z, I%): 387.3, 100; 402.3, 40, $[Cu(L)]^+$.

4.2.6 Physical Techniques

^{1}H, ^{13}C and 2D NMR spectra were recorded on a Bruker Avance 300 spectrometer using standard Bruker pulse sequences. Chemical shifts are reported in ppm referenced to residual solvent protons ($CDCl_3CD_2Cl_2$, CD_3CN). ^{1}H and ^{19}F PGSE NMR measurements were performed in a solution of **3** (10^{-3} M) in CD_3CN using a standard stimulated echo (STE) sequence on a Varian Inova spectrometer (600 MHz) at 300 K and without spinning. An external reference (trifluorotoluene, -63.72 ppm) was used for the ^{19}F chemical shift calibration. Tetrakismethylsilylsilane (TMSS, hydrodynamic radius $r_H \sim r_{vdW} = 4.28$ Å) was used as an internal standard. The hydrodynamic radius (r_H) and volume ($V_H = 4/3 \cdot \pi \cdot r_H^3$) were obtained as described in the literature[239,240] (see also Section 5.2.8, accounting that $(\gamma(^1H)/\gamma(^{19}F))^2 = 1.13$). The van der Waals volumes (V_{vdW}) and the solvent-excluded volumes (V_{soft})[241] were computed on **3a** and on the mononuclear unit of **1** starting from the X-ray coordinates using the software package DS Viewer Pro 5.0.[242]

Mass spectra were obtained with a Micromass ZMD spectrometer. The mixtures were analyzed in the positive and negative ionization modes by direct perfusion in ESI-Mass interface. Infrared spectra were recorded from 4000 to 700 cm^{-1} on a Perkin-Elmer FT-IR Nexus spectrometer equipped with a Thermo-Nicolet microscope. Elemental analyses (C, H, N) were performed with a Carlo Erba EA 1108 automated analyzer. The luminescence spectrum of **3** (yellow powder) was recorded on a Horiba Jobin Yvon SPEX FluoroMax 4 Spectrofluorometer, using a UG11 band-pass filter on the excitation slit and a long-pass filter GG475 on the emission slit. Conductivity measurements were performed on a Crison microCM 2202 conductometer operating at 25° C.

4.2.7 X-ray crystallography

A summary of data collection and structure refinement for L^1, **1, 2** and **3a** is reported in Table 4.1. The Ortep drawing[216] of L^1 is reported in Appendix 3 (Figure A9).

Table 4.1 Summary of X-ray crystallographic data for L^1, **1**, **2**, and **3a**.

	L^1	**1**	**2**	**3a**
Empirical formula	$C_{38}H_{42}N_2S_2$	$C_{61}H_{69}B_3Cu_3F_{12}N_{11}O_3S_3$	$C_{37}H_{36}B_4CuF_4N_3OPS$	$C_{76}H_{45}Cu_6F_{30}N_7O_2S_8$
Formula weight	678.90	1551.50	752.07	2295.91
Colour, habit	Colorless, block	Colorless, block	Colorless, block	Colorless, plate
Crystal size, mm	0.45x0.20x0.15	0.18x0.10x0.08	0.38x0.30x0.10	0.35x0.15x0.10
Crystal system	Monoclinic	Monoclinic	Triclinic	Triclinic
Space group	$P2_1/c$	$P2_1$	P-1	P-1
a, Å	16.984(3)	12.430(9)	10.431(1)	15.502(2)
b, Å	7.628(1)	20.105(9)	12.378(1)	16.672(2)
c, Å	28.302(5)	14.665(8)	15.213(2)	18.535(2)
αdeg.	90	90	78.13(1)	106.93(1)
β, deg.	98.15(1)	107.10(3)	78.95(1)	100.92(1)
γdeg.	90	90	70.41(1)	93.45(1)
V, Å^3	3630(1)	3503(4)	1794.8(3)	4465.7(9)
Z	4	2	2	2
T, K	293(2)	293(2)	293(2)	293(2)
ρ(calc), Mg/m^3	1.242	1.471	1.392	1.707
μ, mm^{-1}	0.188	1.075	1.766	1.701
θ range, deg.	1.45 to 27.04	1.45 to 24.00	1.77 to 27.97	1.35 to 25.00
No.of rflcn/obsv	38065 / 4095	10942 / 4747	19539 / 4898	42725 / 3759
GooF	1.006	0.892	1.009	0.979
Flack parameter	-	0.04(1)	-	-
$R1$	0.0409	0.0587	0.0357	0.0780
$wR2$	0.0841	0.0675	0.0683	0.0843

$R1 = \Sigma||F_O|-|F_C||/\Sigma|F_O|$, $wR2 = [\Sigma[w(F_O^2-F_C^2)^2]/\Sigma[w(F_O^2)^2]]^{½}$, $w = 1/[\sigma^2(F_O^2) + (aP)^2 + bP]$, where $P = [\max(F_O^2,0) + 2F_C^2]/3$

Single crystal data were collected with a Bruker Smart 1000 area detector diffractometer (Mo Kα; λ = 0.71073 Å). Cell parameters were refined from the observed setting angles and detector positions of selected strong reflections. Intensities were integrated from several series of exposure frames covering the sphere of reciprocal space.[208] No crystal decay was observed. Absorption corrections using the program SADABS[153] was applied for L^1, **2** and **3a**, which resulted in transmission factors ranging from 0.720-1.000 (L), 0.653-1.000 (**2**) and 0.834-1.000 (**3a**), whereas the program XABS2[243] was used for **1** (max. and min. absorption correction coefficients of 1.000-0.497). For **1**, the space group ($P2_1$) was chosen on the basis

of the systematic extinction and intensity statistics, the absolute configuration has been confirmed at the 3σ level of the Flack parameter (0.04(1)).[244] The structures were solved by direct methods (SIR97)[155] and refined with full-matrix least-squares (SHELXL-97),[156] using the Wingx software package.[157] Non-hydrogen atoms were refined anisotropically for L^1 and **2**. The BF_4^- anions in **1** were severely disordered and were refined isotropically. The carbon atoms in **3** were also refined isotropically due to the poor quality of the crystal and the limited number of observed reflection available. The hydrogen atoms were placed at their calculated positions. Molecular drawings were prepared using the Mercury 1.4.2 program.[159]

4.2.8 DFT calculations

Theoretical calculations were carried out using the Gaussian 03 program suite.[160] Geometry optimization of the mononuclear model compound [Cu(L')(C_6H_5S)] was performed starting from a pseudo-tetrahedral copper coordination as found in **2**, by substituting PPh_3 with $C_6H_5S^-$ and by substituting the -CH_3 and -OCH_3 groups of the pyridine ring of L^1 with hydrogen atoms, thus giving the model ligand L'. The CH_3CN molecule and the isolated model ligand L' were also optimized. The complex $[Cu(L')(CH_3CN)]^+$ was optimized starting from the X-ray coordinates of the mononuclear species of **1**. The polynuclear model complexes $[Cu_6(L')_2(C_6H_5S)_6]$ and $[Cu_4(C_6H_5S)_6]^{2-}$ were optimized starting from the $[Cu_4(C_6F_5S)_6]^{2-}$ adamantane-like core as found in various copper(I)-thiolate clusters,[236] whereas $[Cu_4(C_6H_5S)_6(CH_3CN)]^{2-}$ was optimized starting from the X-ray geometry of **3a** by removing the peripheral $[Cu(L^1)]^+$ moieties. The gradient-corrected hybrid density functional B3LYP[164,165] and the lanl2dz basis set with Hay and Wadt effective core potential (ECP) were employed.[166,167] Vibrational frequencies were calculated at the same level of theory to ensure that the stationary points were true minima, and for the calculation of zero-point energies. Thermal corrections and free energy of reaction were calculated at 300 K. In order to take into account the effect of the solvent on the energy of reactions involving ionic dissociation, the solvation energies (ΔG^{solv}) were estimated using the polarizable continuum model (PCM)[245-249] at the B3LYP/lanl2dz level. ΔG^{solv} represents the energy required to bring a molecule of solute from the gas phase to a polarizable dielectric media. This requires the opening of a cavity in the solvent where the solute can be fitted (ΔG^{cav}), giving rise to solvent-solute electrostatic interactions (ΔG^{eletr}), to van der Waals solvent-solute contributions (ΔG^{disp}), and to some steric repulsion (ΔG^{rep}), so that $\Delta G^{solv} = \Delta G^{cav} + \Delta G^{rep} + \Delta G^{disp} +$

ΔG^{electr}.[250] Single-point energy calculations at the PCM level were performed on the gas-phase structures without further optimization, assuming that the stationary points in the gas phase are also stationary points in solution. We therefore approximated the ΔG^{solv} as the difference between the free energy in solution (G^{solv}) and the gas-phase total energy (E) without zero-point or thermal correction. Inside the cavity that hosts the solute, the dielectric constant is the same as in vacuum, whereas outside it takes the value of the solvent (acetonitrile, ε = 36.6). Finally, the free energy of reaction in solution ($\Delta G^{solution}$) was computed as the sum of the gas-phase free energy (ΔG_{300}) and the solvation free energy $\Delta G^{solution} = \Delta G_{300} + \Delta\Delta G^{solv}$ (where $\Delta\Delta G^{solv} = \Delta G_P{}^{solv} - \Delta G_R{}^{solv}$), according to the thermodynamic cycle reported in Scheme 4.2.

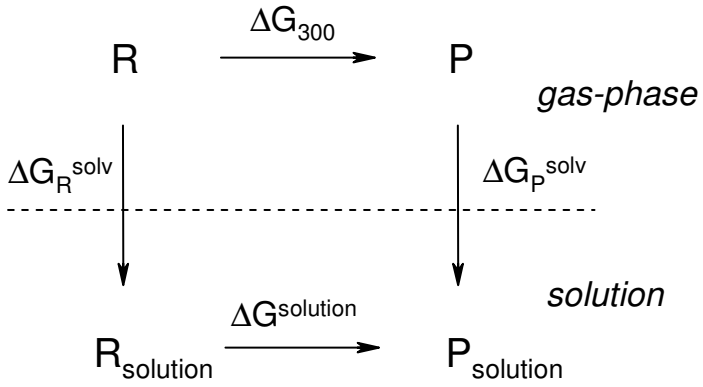

Scheme 4.2 Thermodynamic cycle for the calculation of the reactions free energies in solution, $\Delta G^{solution} = \Delta G_{300} + \Delta\Delta G^{solv}$ (where $\Delta\Delta G^{solv} = \Delta G_P{}^{solv} - \Delta G_R{}^{solv}$).

4.3 Results and Discussion

*4.3.1 Solid state structure of $[Cu_2(L^1)_2(CH_3CN)][Cu(L^1)(CH_3CN)](BF_4)_3$ (**1**)*

At first, the coordination capabilities of the N,N',S-donor ligand L^1 versus Cu(I) were tested through reaction with $[Cu(CH_3CN)_4]BF_4$ in acetonitrile in a 1:1 ratio to yield compound **1**. As can be seen in Figure 4.1, a mononuclear and a dinuclear complex co-crystallize in the unit cell.

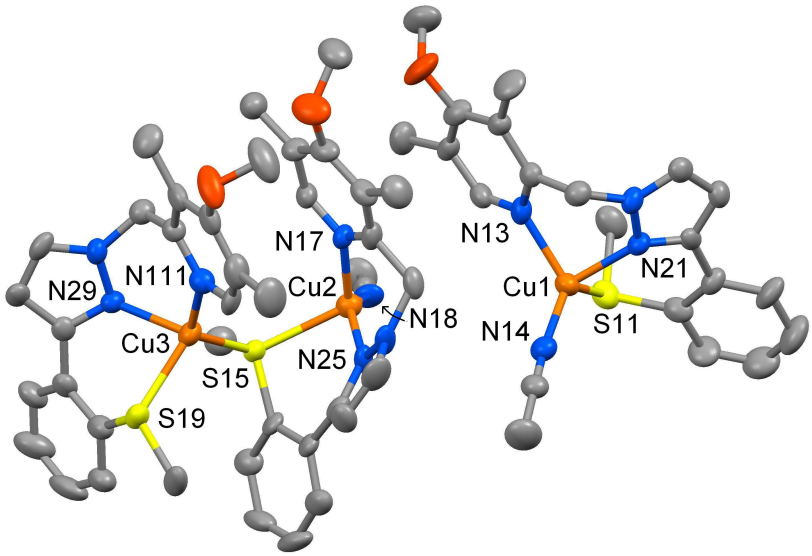

Figure 4.1 Molecular drawing of **1** at the 30% thermal ellipsoids probability level. A mononuclear and a dinuclear unit are present in the unit cell. The hydrogen atoms and the BF_4^- counterions have been omitted for clarity.

The former is comprised by a copper(I) center, Cu(1), bound by a κ^3-N,N',S chelate ligand and a CH_3CN molecule. The metal geometry is distorted tetrahedral since the coordination angles range from 122.1(3) to 89.6(3)°. The dinuclear unit exhibits two metal centers in different coordination environments. In particular, Cu(2) is bound by an acetonitrile molecule and by a N,N'S chelate ligand, which in turn bridges to the Cu(3) atom with the thioether sulfur atom S(15). The coordination of Cu(3) is completed by another N,N'S chelate ligand. Interestingly, the bond distances (Table 4.2) within the sulfur bridge are not equivalent since Cu(3)-S(15) (2.230(3) Å) is significantly shorter than Cu(2)-S(15) (2.462(3) Å). This is related to the different geometry of the Cu(2) and Cu(3) atoms since the latter exhibits a more

regular tetrahedral geometry, which is distorted as a consequence of the constraints imposed by the chelate ligand. Conversely, Cu(2) is in a tetrahedral geometry severely distorted towards the trigonal one (equatorial atoms: N(17), N(25), N(18)) due to the long Cu(2)-S(15) interaction . The nearly trigonal geometry of Cu(2) is supported by the sum of the equatorial angle values, 353.1(3)°, which is close to the theoretical value of 360°, and by the fact that Cu(2) is only 0.282(1) Å out of the equatorial plane and is directed towards the apical sulfur S(15). The three metal atoms are stereogenic centers and they all exhibit an *S* configuration. Interestingly, this leads to a spontaneous resolution at the solid state since **1** crystallizes in the chiral space group $P2_1$. Each of the three BF_4^- counterions are disordered in two positions that roughly define a spherical structural site occupation. In light of these results, it can be concluded that the nuclearity of **1** cannot be defined *a priori*, due to the flexibility and the lack of appropriate sterical hindrance of L^1.

Table 4.2 Selected bond lengths (Å) for **1**, **2**, and **3a**.

	1		
Cu(1)-S(11)	2.304(3)	Cu(2)-N(17)	2.044(7)
Cu(1)-N(21)	2.033(7)	Cu(2)-N(18)	1.890(8)
Cu(1)-N(13)	2.054(8)	Cu(3)-S(15)	2.230(3)
Cu(1)-N(14)	1.919(9)	Cu(3)-S(19)	2.390(3)
Cu(2)-S(15)	2.462(3)	Cu(3)-N(29)	2.016(6)
Cu(2)-N(25)	1.988(7)	Cu(3)-N(111)	2.062(7)
	2		
Cu-S(11)	2.4482(7)	Cu-N(13)	2.092(2)
Cu-P(14)	2.1957(7)	Cu-N(21)	2.014(2)
	3a		
Cu(1)-N(21)	1.937(8)	Cu(4)-S(19)	2.214(3)
Cu(1)-N(13)	2.072(7)	Cu(5)-S(18)	2.234(4)
Cu(1)-S(17)	2.156(3)	Cu(5)-S(19)	2.259(3)
Cu(2)-N(16)	2.028(8)	Cu(5)-N(1)	1.88(1)
Cu(2)-N(24)	2.03(1)	Cu(6)-S(17)	2.297(3)
Cu(2)-S(14)	2.399(4)	Cu(6)-S(18)	2.341(3)
Cu(2)-S(111)	2.254(3)	Cu(6)-S(112)	2.244(3)
Cu(3)-S(110)	2.261(3)	Cu(4)-Cu(5)	2.768(2)
Cu(3)-S(111)	2.223(3)	Cu(5)-Cu(6)	2.814(2)
Cu(3)-S(112)	2.244(3)	Cu(4)-Cu(6)	2.842(2)
Cu(4)-S(110)	2.241(3)	Cu(3)-Cu(4)	3.489(2)
Cu(4)-S(17)	2.330(3)	Cu(3)-Cu(6)	3.396(2)

*4.3.2 Solid state structure and solution properties of [Cu(L^1)(PPh_3)]BF_4 (**2**)*

The hypothesis that an ancillary σ-donor ligand such as PPh_3 would complement the coordination properties of L^1 to yield a mononuclear species has led to the synthesis and isolation of **2**. The copper coordination is achieved through the N(21), N(13) and S(11) atoms of L^1 and by PPh_3 (Figure 4.2).

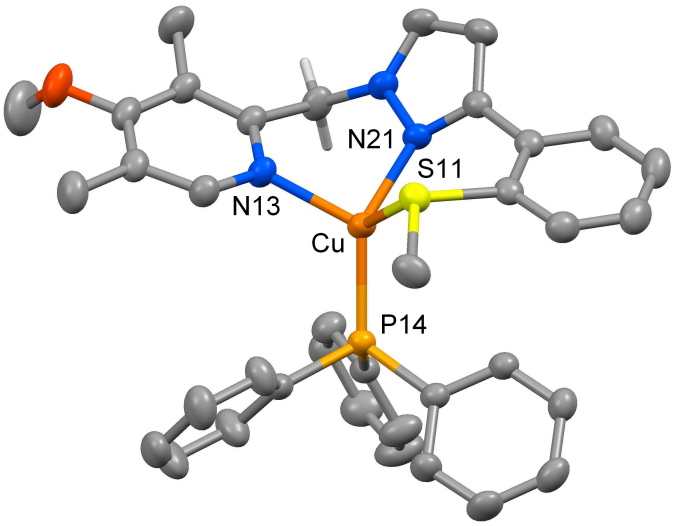

Figure 4.2 Molecular drawing of the cationic unit of **2** at the 30% thermal ellipsoids probability level. The hydrogen atoms (except for the methylenic ones) and the BF_4^- counterion have been omitted for clarity.

The metal geometry is intermediate between trigonal-pyramidal and tetrahedral: the trigonal plane can be defined by P(14), N(21) and N(13) with S(11) in the apical position (Cu-S(11) = 2.4482(7) Å). This geometry is supported by the following criteria: i) the sum of equatorial angles is 344.23(5)° (*cfr.* 328.5° for a tetrahedral geometry and 360° for trigonal planar geometry), and ii) the metal lies out of the trigonal plane by ~ 0.46 Å in the direction of S(11). The BF_4^- counterion is statically disordered in three positions that occupy a structural spherical site.

Complex **2** presents a fluxional behaviour in solution, as shown by the ^{1}H VT NMR spectrum in $CDCl_3$, Figure 4.3. The bridging methylene of the ligand gives a broad signal at 270 K, which splits into two sharp doublets by lowering the temperature to 210 K, while the other peaks exhibit only a chemical shift temperature dependence. This behaviour is justified with the diastereotopic nature of the methylene group at low temperatures, which can be explained in two ways: (a) the presence of the stereogenic Cu(I) center, and (b) the boat conformation of

the N,N' chelate six-membered ring around the metal center. The kinetic parameters of the exchange process were determined from the complete lineshape analysis[251,252] to be: $\Delta H^{\#}$ = +43.6(3) kJ·mol^{-1}, $\Delta S^{\#}$ = -16(1) J mol^{-1} K^{-1}. These values suggest a non-dissociative rearrangement, which is most likely the inversion of the boat, as shown by some examples reported in the literature.[42,215,253] This implies a fast inversion (on the NMR time-scale) around the Cu center, which probably involves the stretching or rupture of the labile Cu(I)-S-thioether bond.

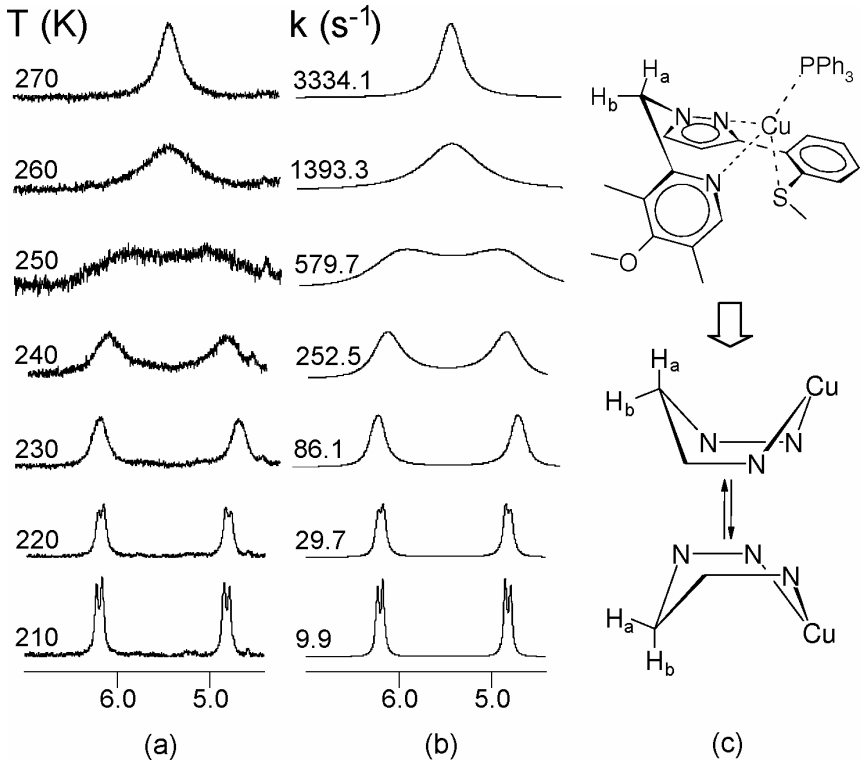

Figure 4.3 Experimental (a) and simulated (b) ^{1}H NMR spectrum of **2** in the region of the H_a and H_b diasterotopic protons. A description of the boat inversion process is reported in (c).

*4.3.3 Solid state structure, solution properties, DFT calculations for [Cu$_6$(L^1)$_2$(C$_6$F$_5$S)$_6$] (**3**)*

By using the monodentate sulfur donor ligand $C_6F_5S^-$ as a coligand in place of PPh_3, additional complications became evident. The idea of obtaining a neutral copper(I) complex exhibiting an approximately tetrahedral structure with a N,N',S,S' donor set is difficult to fulfill, mainly because of the absence of steric hindrance on both L^1 and on the thiolate group, which enables the thiolate to bridge metal centers. In the first stage, the 1:1:1 Cu:$C_6F_5S^-$: L^1 stoichiometric ratio was employed for the synthesis, but this led nonetheless to the isolation

and X-ray characterization of a 3:3:1 hexanuclear complex (**3a**). We therefore optimized the synthesis in 3:3:1 conditions to give **3**, which crystallized as **3a** by incorporating an acetonitrile molecule. An exemplified molecular drawing, depicting the coordination environment of the six copper atoms, is reported in Figure 4.4. The structure consists of six metal atoms, six thiolate groups and two L^1 ligands arranged in a cluster-like fashion. Cu(1) and Cu(2) are the only atoms that are bound to L^1, and they are located in the peripheral part of a $[Cu_4(C_6F_5S)_6]^{2-}$ copper-thiolate cluster. The four metals of the core adopt a trigonal geometry determined by bridging thiolate groups, and in the case of Cu(5), also by an acetonitrile molecule (crystallization solvent).

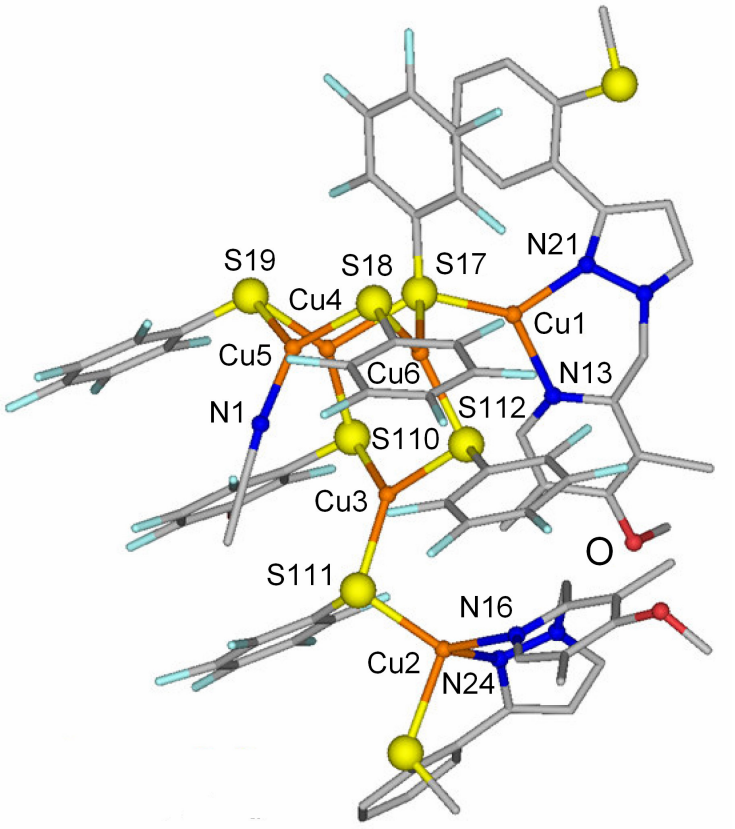

Figure 4.4 Molecular structure of the copper(I)-SC_6F_5 cluster crystallized from an acetonitrile:water solution (**3a**). The hydrogen atoms have been omitted for clarity.

The structure of the copper-thiolate cluster is likely derived from a closed $[Cu_4(C_6F_5S)_6]^{2-}$ adamantane-like structure,[234,236,254] by disruption of S-Cu-S links and subsequent insertion of CH_3CN, now bound to Cu(5) to give an 'open' structure. The negative charge (2-) of the open $[Cu_4(C_6F_5S)_6(CH_3CN)]^{2-}$ cluster is compensated by two $[Cu(L^1)]^+$ peripheral moieties, which are bound to the former by means of thiolate groups. As a consequence of the open structure, three Cu-Cu interactions are shorter, ~ 2.8 Å (between Cu(4), Cu(5) and Cu(6)) and two are

longer, ~ 3.4 Å (Cu(3)-Cu(4) and Cu(3)-Cu(6)). Interestingly, part of this structure reproduces that present in the core of the yeast copper metallothionein (Cu-MT),[238] a protein rich in cysteine residues that can bind up to eight copper(I) ions, six of which are in a trigonal geometry whereas two are in a digonal arrangement. It has been proposed that these two labile peripheral metals confer to the protein the ability to regulate copper homeostasis and they are also involved in the delivery of copper to apo-copper chaperones. Figure 4.5 reports, for comparison, the atom connectivity of the Cu-MT core and that found in **3a**. Even though the Cu-MT cluster is more complex and it hosts more metal ions, some similarities with **3a** are evident. It is interesting to note that the Cu-MT core may be imagined as a superposition of open $\{Cu_4S_6\}$ clusters.

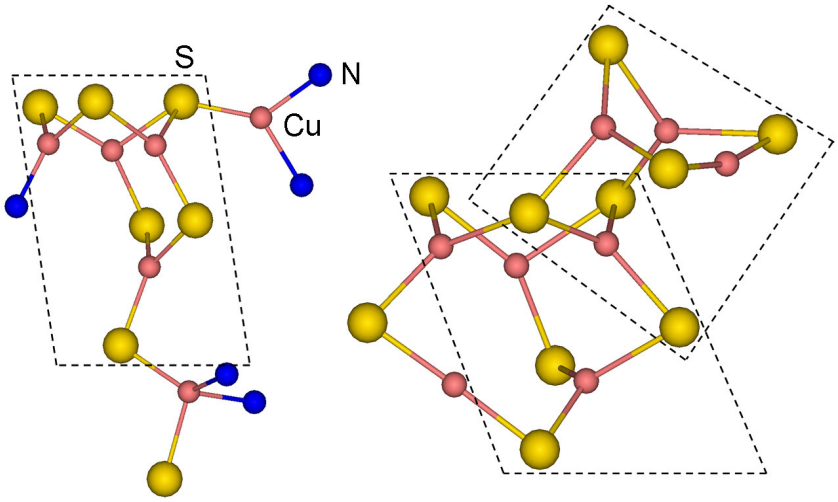

Figure 4.5 Copper-donor atom connectivity in **3a** (left), and in the yeast copper metallothionein (right). Structural analogies are highlighted in the dashed boxes.

When acetonitrile, which is present in the structure of **3a** (colorless crystals), is removed under vacuum, the deep yellow product **3** forms. This process is reversible: by adding few drops of acetonitrile, the product turns white. The complex **3** is luminescent in the solid state, emitting at 680 nm (excitation: 300 nm, 300 K, Figure 4.6), whereas in acetonitrile solution there is no evidence of emitting properties. This can be readily explained by a direct solvent-cluster interaction, also supported by the solid state structure **3a**, that results in luminescence quenching. The large stoke shift (380 nm) is typical of multinuclear copper compounds.[255] On the basis of these observations, and also according to known Cu(I) adamantane-like structures reported in the literature,[233,236] a closed adamantane-like structure (Scheme 4.3), derived from

the X-ray structure by elimination of the coordinated acetonitrile and by the closure of S(111) on Cu(5), may be proposed for the yellow solid **3**.

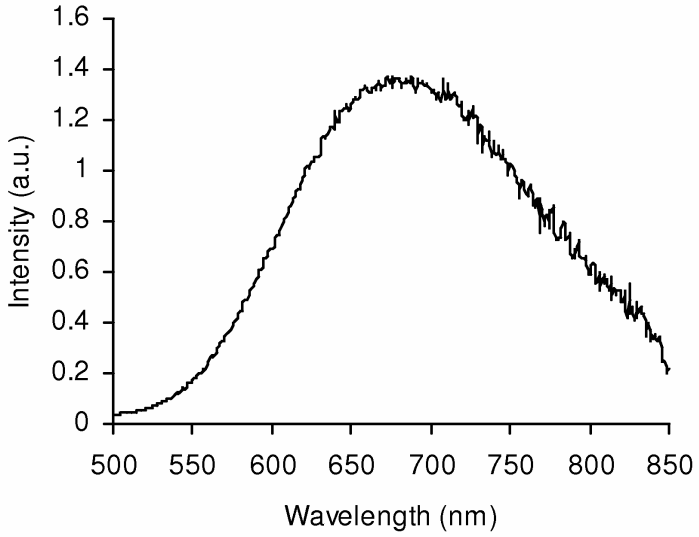

Figure 4.6 Emission spectrum of **3** (yellow powder) at 300 K (excitation wavelength of 300 nm).

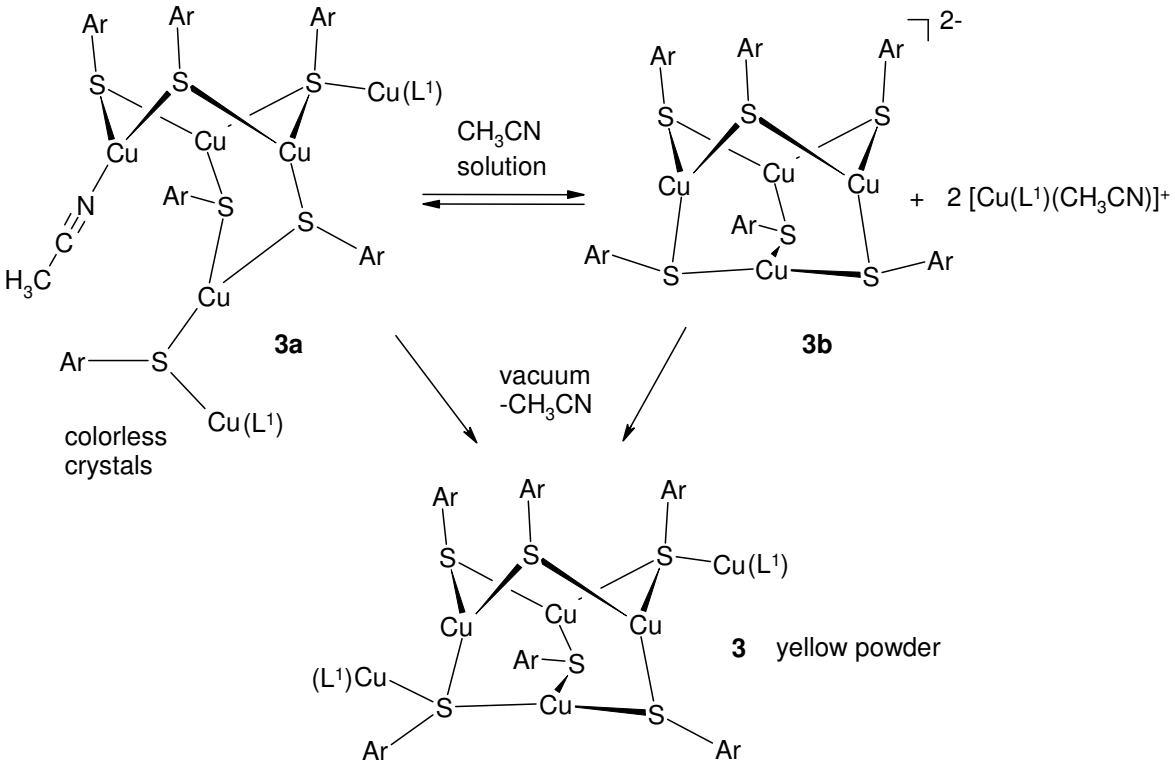

Scheme 4.3

Acetonitrile is the only common organic medium in which **3** is quite soluble, so that the solution characterization of **3** was performed in this solvent. The presence of a Cu(I)-thiolate cluster in solution is confirmed by the ESI-Mass spectrometry and by ^{19}F PGSE NMR experiments. In particular, the mass spectrum in negative ionization mode reveals the presence of monoanionic $[Cu_n(C_6F_5S)_{n+1}]^-$ (n = 1-5) fragments of the cluster, whereas in positive ionization mode, only the $[Cu(L^1)]^+$ fragment is present. This could arise during the ESI-Mass ionization process or be present in solution according to a ionic dissociation equilibrium: **3a** + $CH_3CN \rightleftharpoons [Cu_4(C_6F_5S)_6]^{2-}$ (**3b**) + 2$[Cu(L^1)(CH_3CN)]^+$ (see Scheme 4.3). The latter hypothesis is in agreement with conductivity measurements performed on a 10^{-3} M solution of **3**, which afford a molar conductivity value of 131(1) Ω^{-1} cm^2 mol^{-1}, slightly less than the range reported for 1:2 electrolytes in acetonitrile (145-336 Ω^{-1} cm^2 mol^{-1}).[256] This would give credit to the hypothesis of the ionic dissociation of **3a** in solution.

^{1}H and ^{19}F PGSE NMR experiments were performed in order to obtain the hydrodynamic radius (r_H) and volume (V_H) of **3**. The measurements based on ^{19}F afford a r_H of 6.8(1) Å and a V_H of 1300(60) Å^3, while the ^{1}H PGSE values point to significantly smaller dimensions (r_H = 5.2(1) Å and V_H = 600(30) Å^3). This discrepancy can be explained by considering the aforementioned dissociation equilibrium: the ^{19}F nucleus, in fact, is present only in the exhanging **3a** and **3b** clusters (large), while protons are shared by **3a** (large) and $[Cu(L^1)(CH_3CN)]^+$ (small). Hence, the V_H value derived from ^{1}H PGSE ($V_H(^1H)$) would corresponds to the weighted average between the volumes of **3a** and $[Cu(L^1)(CH_3CN)]^+$, and should result significantly smaller than $V_H(^{19}F)$. In addition, a comparison between the experimental $V_H(^1H)$ with the van der Waals volumes (V_{vdW}) of **3a** (1228 Å^3) and $[Cu(L^1)(CH_3CN)]^+$ (327 Å^3), would suggest only a partial ionic dissociation of **3a**, since $V_H(^1H)$ is intermediate between the above-mentioned values. On the other hand, by considering the solvent-excluded volume (V_{soft}) as an estimate of the hydrodynamic volume of the respective species (2039 Å^3 for **3a** and 605 Å^3 for $[Cu(L^1)(CH_3CN)]^+$) we would infer a nearly complete ionic dissociation, as $V_H(^1H)$ becomes comparable to the V_{soft} of $[Cu(L^1)(CH_3CN)]^+$. Since V_{vdW} represent the lower limit of V_H[257] and assuming that V_{soft} represents the upper V_H limit, the dissociation of **3a** is partial or complete according to which theoretical volume, V_{vdW} or V_{soft}, is taken as reference. However, a complete ionic dissociation appears quite plausible, as attested by the following evidences: (1) as stated above, the molar conductivity is close to that reported for completely dissociated 1:2 electrolytes in acetonitrile; (2) no peaks of a $[Cu_n(L^1)(C_6F_5S)_{n+1}]^-$ species appear in the ESI-

Mass spectrum; (3) both the ^{1}H and ^{19}F NMR spectra exhibit only a set of signals, and it would be consistent with the presence of a more symmetrical **3b** species (if compared to **3a**) and $[Cu(L^{1})(CH_3CN)]^{+}$. If this is not the case, a fast-exchange equilibrium with **3a** should be invoked.

To further support the hypothesis that a Cu(I)-thiolate cluster structure is energetically favored over a mononuclear complex, DFT calculations were performed to compute the free energy of the gas phase reaction, $6[Cu(L')(C_6H_5S)] \rightarrow [Cu_6(L')_2(C_6H_5S)_6] + 4L'$, as well as to evaluate the stability of the hexanuclear cluster in acetonitrile solution (Tables 4.3 and Figure 4.7).

Table 4.3 Computed thermodynamic properties for gas-phase (ΔE, ΔE_{300}, ΔG_{300})[a] and solution ($\Delta G^{solution}$)[b] reactions (a)-(c) reported in Figure 4.7 (kJ mol^{-1}, B3LYP/lanl2dz).

reaction	ΔE	ΔE_{300}	ΔG_{300}	$\Delta G^{solution}$
(a)	-125.6	-114.0	-58.6	-
(b)	668.1	682.5	634.7	-101.8
(c)	-40.4	-23.5	2.3	28.8

a, calculated as $\Delta G_{300} = \Sigma G_{Product} - \Sigma G_{Reactant}$; b, calculated according to the thermodynamic cycle reported in Scheme 4.2, $\Delta G^{solution} = \Delta G_{300} + \Delta\Delta G^{solv}$.

The $C_6H_5S^{-}$ thiolate was employed instead of the less electron-donating $C_6F_5S^{-}$ to save computational resources, so some caution is required when inferring properties of the real system by using these models. As an example, the comparison between the $[Cu(L')(C_6H_5S)]$ and $[Cu(L')(C_6F_5S)]$ optimized models reveals that in the former case the copper geometry is trigonal planar with the thioether sulfur not coordinated, whereas in the latter the metal geometry is tetrahedral with the thioether bound to copper and a longer Cu-SC_6F_5 bond distance (Figure A10 of Appendix 3).

The *in vacuo* free energy (ΔG_{300}) of cluster-formation from the mononuclear entities (Figure 4.7 a) is -58.6 kJ mol^{-1}, supporting the stability of the aggregate. This is in agreement with previous DFT calculations performed on cyclic copper(I)-thiolate assemblies showing that oligomerization is energetically favored.[258] The $[Cu_4(C_6H_5S)_6]^{2-}$ inner core of the $[Cu_6(L')_2(C_6H_5S)_6]$ optimized structure presents three copper atoms in trigonal planar arrangements and one copper atom in a distorted digonal geometry. The two outer trigonal copper centers are bound by two κ^2-N,N' ligands, and they are linked to the $[Cu_4(C_6H_5S)_6]^{2-}$

unit by bridging thiolates. We propose that this structure may model that adopted by **3** when acetonitrile is removed under vacuum (see Scheme 4.3).

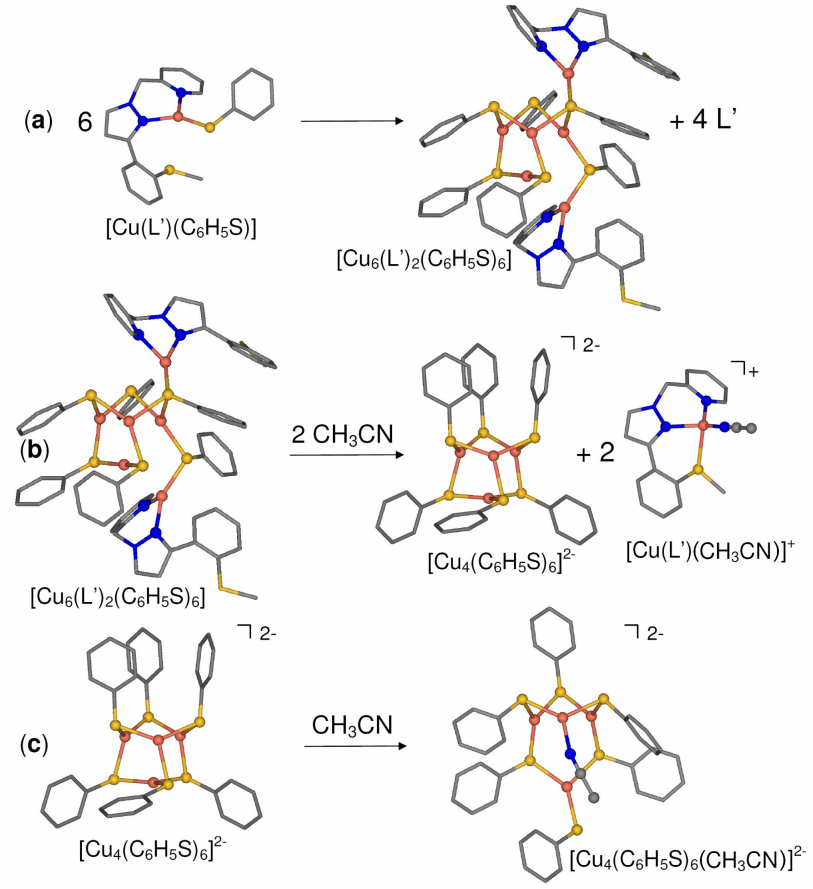

Figure 4.7 Optimized molecular structures for the Cu(I)/L'/$C_6H_5S^-$ system (B3LYP/lanl2dz). (a) Oligomerization reaction 6[Cu(L')(C_6H_5S)] → [Cu_6(L')$_2$(C_6H_5S)$_6$] + 4L', (b) ionic dissociation of the [Cu_6(L')$_2$(C_6H_5S)$_6$] cluster and (c) acetonitrile interaction with the [Cu_4(C_6H_5S)$_6$]$^{2-}$ cluster.

Since there is experimental evidence that the two peripheral [Cu(L^1)]$^+$ moieties of **3** may be subject to dissociation from the [Cu_4(C_6H_5S)$_6$]$^{2-}$ cluster in acetonitrile solution, we computed the energetics of this reaction to substantiate this hypothesis (Figure 4.7 b). The computed ΔE and ΔG_{300} of the ionic dissociation reaction are positive in the gas-phase (668.1 kJ mol^{-1} and 634.7 kJ mol^{-1}, respectively), pointing to a considerable stabilization of the neutral [Cu_6(L')$_2$(C_6H_5S)$_6$] assembly. However, if we take into account the effect of the solvent, and in particular the stabilization that derives from a polar solvent such as acetonitrile on the ionic products of the reaction, it appears that the reaction is exergonic ($\Delta G^{solution}$ = -101.8 kJ mol^{-1}), making the dissociation even more favored in the presence of a large excess of solvent.

The reaction reported in Figure 4.7 c describes the 'opening' of the closed $[Cu_4(C_6H_5S)_6]^{2-}$ cluster by acetonitrile. The gas phase reaction is exothermic (ΔE = -40.4 kJ mol^{-1}) but endergonic (ΔG_{300} = +2.3 kJ mol^{-1}) since it is entropically disfavoured. Moreover, the reaction is even more endergonic in CH_3CN solution ($\Delta G^{solution}$ = +28.8 kJ mol^{-1}), suggesting the greater stability of the closed $[Cu_4(C_6H_5S)_6]^{2-}$ cluster with respect to the open form. This is in agreement with the proposed **3b** structure, which is supported also by the absence of CH_3CN in all of the ESI-Mass fragments, and by the reported crystallization of $[(C_6H_5)_4P]_2[Cu_4(SC_6H_5)_6]$ from acetonitrile, in which the cluster is in the closed form.[233]

4.4 Conclusions

The coordination capabilities of the N,N',S ligand 4-methoxy-3,5-dimethyl-2-((3-(2-(methylthio)phenyl)-1H-pyrazol-1-yl)methyl)pyridine (L^1) were evaluated with Cu(I). Since the ligand possesses a weakly coordinating thioether group, ancillary monodentate ligands were employed (PPh_3 and $C_6F_5S^-$) to complete the copper coordination requirements. However, as evidenced by the X-ray structures, the nuclearity of the complexes can not be easily controlled, and only the ternary complex $[Cu(L^1)(PPh_3)]BF_4$ (**1**) is mononuclear, whereas the L^1/Cu(I) binary mixture in acetonitrile produces two co-crystallized entities: a monomeric $[Cu(L^1)(CH_3CN)]^+$ and a dinuclear $[Cu_2(L^1)_2(CH_3CN)]^{2+}$complex. In addition, the ternary Cu(I)/L^1/$C_6F_5S^-$ system gives rise to the isolation of a polynuclear compound, $[Cu_6(L^1)_2(C_6F_5S)_6(CH_3CN)]$ (**3a**), which bears similarities to an open adamantane-like $\{Cu_4S_6\}$ cluster. Part of this Cu-thiolate framework is found in the structure of the yeast metallothionein core, which exhibits eight Cu(I) metals bound by cysteinate residues. The propensity of the thiolate ligands to bridge metal centers is probably the driving force that led to the isolation of a multinuclear structure. Moreover, DFT calculations show how the hexanuclear unit is favored, in the gas phase, over a hypothetical mononuclear complex. Thus, in order to better control the nuclearity of Cu(I) centers, especially in presence of thiolates, it would be necessary to employ a more pre-organized ligand.[259] This could be obtained by functionalization of the prochiral methylene group of L^1 with proper donor moieties to yield tetradentate N,N',S,S' heteroscorpionates, which may alone satisfy the electronic and steric requirement of Cu(I) without additional monodentate co-ligands (see Chapter 5).

5

Cu(I) Complexes with C-Centered N,N',S,S'-Scorpionates. Evidence for Dimer-Monomer Equilibria[260]

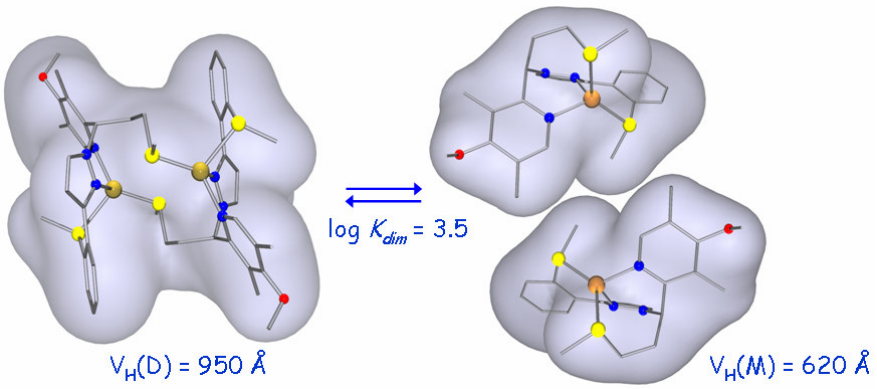

The heteroscorpionate N,N',S,S' donor ligands L^a and L^b, based on the pyrazole-pyridine moiety, were prepared. The Cu(I) complexes $[Cu(L^a)]_2(BF_4)_2$ ($\mathbf{a_2}(BF_4)_2$) and $[Cu(L^b)]_2(BF_4)_2$ ($\mathbf{b_2}(BF_4)_2$) were synthesised and characterized by X-ray crystallography. Both exhibit a dinuclear structure, presenting each Cu(I) center in a distorted N,N',S,S' tetrahedral environment. On the basis of NMR and ESI-Mass data, the presence of a mononuclear complex in equilibrium with the dimer was hypothesized for both complexes. The dimerization constants of the processes, $2\mathbf{a}^+ \rightleftharpoons \mathbf{a_2}^{2+}$ and $2\mathbf{b}^+ \rightleftharpoons \mathbf{b_2}^{2+}$, were obtained by ^{1}H NMR dilution experiments (fast-exchange regime) in CD_3CN: $\log K(\mathbf{a_2}^{2+}) = 3.55(6)$ and $\log K(\mathbf{b_2}^{2+}) = 3.23(5)$ at 300 K. Thermodynamic parameters were determined by a van't Hoff analysis (280 - 310 K temperature range): $\Delta H^0(\mathbf{a_2}^{2+}) = -12(1)$ kJ·mol^{-1}, $\Delta H^0(\mathbf{b_2}^{2+}) = -10(1)$ kJ·mol^{-1}, $\Delta S^0(\mathbf{a_2}^{2+}) = +27(4)$ kJ·mol^{-1}, and $\Delta S^0(\mathbf{b_2}^{2+}) = +28(4)$ kJ·mol^{-1}. Pulsed Gradient Spin Echo (PGSE) NMR experiments provided the weighted-average hydrodynamic volume (V_H) of the species present in CD_3CN solution at different copper concentrations (C_{Cu}). Nonlinear interpolation of V_H as function of C_{Cu} for a dimer-monomer equilibrium led to the hydrodynamic volumes of both monomers (V_H^0(M)) and dimers (V_H^0(D)): $V_H^0(\mathbf{a}^+) = 620(40)$ Å^3, $V_H^0(\mathbf{b}^+) = 550(10)$ Å^3, $V_H^0(\mathbf{a_2}^{2+}) = 950(20)$ Å^3, and $V_H^0(\mathbf{b_2}^{2+}) = 900(10)$ Å^3. Cyclic voltammetry experiments performed in CH_3CN and CH_2Cl_2 showed a quasireversible to irreversible behavior of the Cu(I)/Cu(II) redox couple for both complexes.

5.1 Introduction

We are currently exploring the coordination properties of polydentate ligands derived from the pyrazole-pyridine moiety (see Chapter 3 and 4). Due to the facile derivatization of this platform, we aim at designing preorganized N/S donor ligands based on it. The underlying idea is to obtain Cu(I) mononuclear complexes exhibiting a tetrahedral geometry of the metal center. The usefulness of this reside in the possible exploitation of low molecular weight complexes as functional models of Type 1 cupredoxins (electron transfer copper proteins).[90,92,261-266] Some of these models have recently been studied as electron-transfer mediators[267] in dye-sensitized solar cells.[268]

Thus, we present the coordination properties of two C-centered tetradentate N,N',S,S' donor ligands (L^a and L^b in Scheme 5.1) with Cu(I). L^a and L^b are based on an N,N'S-donor substituted pyrazole-pyridine platform with an alkyl-thioether group as the fourth coordination site.

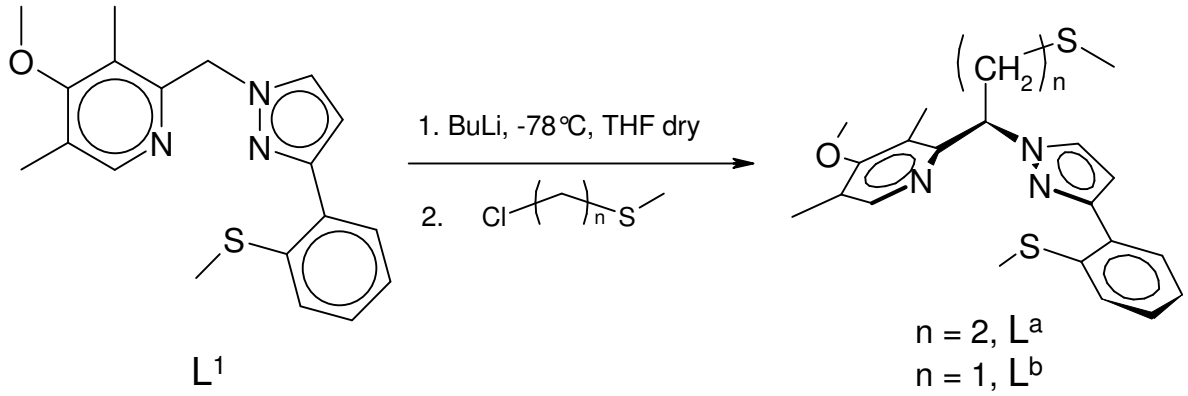

Scheme 5.1

Unfortunately, the major drawback with respect to the control of the nuclearity of the complexes presented in this work, is related to the flexible nature of the alkyl-thioether moiety of the ligands, which leads to the isolation of dinuclear species at the solid state, with the thioether-sulfur bridging a second metal center, $[Cu(L^a)]_2(BF_4)_2$ (**a₂**$(BF_4)_2$) and $[Cu(L^b)]_2(BF_4)_2$ (**b₂**$(BF_4)_2$). It is worth noting that this molecular arrangement is also retained when diminishing the length of the thioether group from $-CH_2-CH_2SCH_3$ in L^a to $-CH_2-SCH_3$ in L^b. However, from dilution ^1H NMR titrations and Pulsed Gradient Spin Echo (PGSE) NMR experiments performed in CD_3CN, we found evidence of the equilibrium involving the

$\mathbf{a_2}^{2+}$ and $\mathbf{b_2}^{2+}$ dimers and the corresponding mononuclear entities, $[Cu(L^a)]^+$ ($\mathbf{a}^+$) and $[Cu(L^b)]^+$ ($\mathbf{b}^+$): $\mathbf{a_2}^{2+} \rightleftharpoons \mathbf{2a}^+$ and $\mathbf{b_2}^{2+} \rightleftharpoons \mathbf{2b}^+$. ESI Mass spectrometry in CH_3CN would confirm this hypothesis. From a functional point of view, the electrochemical properties of the complexes were investigated by cyclic voltammetry in CH_3CN (wherein the dimerization constants were also determined) and CH_2Cl_2. A quasireversible to irreversible behavior of the Cu(I)/Cu(II) redox couple was found in all of the experimental conditions (*e.g.* solvent, concentration), attesting to a sizeable reorganization energy during the heterogeneous electron transfer.

5.2 Experimental

5.2.1 General procedures

All reagents and solvents were commercially available (Aldrich), except for 4-methoxy-3,5-dimethyl-2-((3-(2-(methylthio)phenyl)-1H-pyrazol-1-yl)methyl)pyridine (L^1, see Chapter 4) and $[Cu(CH_3CN)_4]BF_4$,[170] which were prepared as previously reported. THF and dichloromethane were distilled over Na/benzophenone and CaH_2, respectively. All syntheses were performed in inert gas (N_2) using Schlenk techniques. ^1H and ^{13}C NMR spectra were recorded on a Bruker Avance 300 spectrometer using standard Bruker pulse sequences. Chemical shifts are reported in ppm referenced to residual solvent protons ($CDCl_3$ CD_3CN). Mass spectra were obtained with a Micromass ZMD spectrometer. The mixtures were analyzed in positive ionization mode by direct perfusion in the ESI-Mass interface. Infrared spectra were recorded from 4000 to 700 cm^{-1} on a Perkin-Elmer FT-IR Nexus spectrometer equipped with a Thermo-Nicolet microscope. Elemental analyses (C, H, N) were performed with a Carlo Erba EA 1108 automated analyzer.

5.2.2 Synthesis of 4-methoxy-3,5-dimethyl-2-(3-(methylthio)-1-(3-(2-(methylthio)phenyl)-1H-pyrazol-1-yl)propyl)pyridine (L^a)

A solution of 4-methoxy-3,5-dimethyl-2-((3-(2-(methylthio)phenyl)-1H-pyrazol-1-yl)methyl)pyridine (L^1, 2.15 g, 6.33 mmol) in THF (80 ml) was cooled to -78 °C, and then *n*-BuLi (4.15 ml, 1.6 M in hexane, 6.64 mmol) was slowly added. After stirring the red solution at -78 °C for 45 min, 97% 2-chloroethyl methyl sulfide (0.68 ml, d = 1.11 g/ml, 6.62 mmol)

was added and the resulting solution was allowed to warm to room temperature with stirring. After 1 h, the clear yellow solution was dried under a vacuum and the residual solid was extracted in diethyl ether:water (80 ml:30 ml). The organic phase was washed with brine and dried with Na_2SO_4. The solvents were removed under vacuum, giving a yellow oil that was purified by silica column chromatography (hexane:ethyl acetate 75:25), yielding a colorless oil (L^a, 1.53 g, 3.70 mmol, 58%). IR (cm^{-1}): 3054w, 2917s, 2852w, 1587m, 1563s, 1472s, 1451s, 1436s, 1395s, 1337m, 1260s, 1048s, 999s, 754vs. ^{1}H NMR (300 MHz, $CDCl_3$): δ 2.11 (s, 3H, C*H*$_3$SR), 2.26 (s, 3H, C*H*$_3$ py *o*-CH), 2.35 (s, 3H, C*H*$_3$ py *p*-CH), 2.42 (s, 3H, C*H*$_3$SAr), 2.44-2.60 (m, 2H, C*H*$_2$(SCH$_3$)), 2.65-2.72 (m, 2H, C*H*$_2$(CH*)), 3.74 (s, 3H, C*H*$_3$O), 6.00 (m, 1H, C*H**), 6.57 (d, J = 2.1 Hz, 1H, C*H* pz(ph)), 7.17 (dt, 1H, J = 7.0, 2.0 Hz, C*H* ph), 7.28 (m, 2H, C*H* ph), 7.55 (m, 2H, C*H* pz(CH*) + C*H* ph), 8.30 (s, 1H, C*H* py). ^{13}C NMR (75 MHz, $CDCl_3$): δ 10.6 (*C*H$_3$ py *p*-CH), 13.2 (*C*H$_3$ py *o*-CH), 15.3 (*C*H$_3$SR), 15.4 (*C*H$_3$SAr), 30.7 (*C*H$_2$(SCH$_3$)), 33.8 (*C*H$_2$(CH*)), 59.9 (*C*H$_3$O), 61.8 (*C*H*), 106.5 (*C*H pz(ph)), 124.4 (*C*H ph), 125.3 (*C*H ph), 127.7 (*C*H ph), 127.9 (*C*H ph), 129.6 (*C*H pz(CH*)), 149.1 (*C*H py). ESI-MS (p.i., 50 V, CH_3OH, m/z, I%): 414.6, 100, $[L^aH]^+$. Anal. calcd for $C_{22}H_{27}N_3OS_2$ (413.60): C, 63.89; H, 6.58; N, 10.16. Found: C, 63.73; H, 6.85; N, 10.29%.

5.2.3 Synthesis of 4-methoxy-3,5-dimethyl-2-(2-(methylthio)-1-(3-(2-(methylthio)phenyl)-1H-pyrazol-1-yl)ethyl)pyridine (L^b)

The same procedure used to prepare L^a was applied by using the same quantities of reagents/solvent and 95% chloromethyl methyl sulfide (0.58 ml, d = 1.17 g/ml, 6.67 mmol) instead of 2-chloroethyl methyl sulfide. A colorless oil was obtained (L^b, 1.52 g, 3.80 mmol, 60%). IR (cm^{-1}): 2918m, 2850w, 1587w, 1563m, 1471s, 1454s, 1432s, 1395m, 1257m br, 1211m, 1036w, 999w, 750m. ^{1}H NMR (300 MHz, $CDCl_3$): δ 2.02 (s, 3H, C*H*$_3$SR), 2.25 (s, 3H, C*H*$_3$ py *o*-CH), 2.30 (s, 3H, C*H*$_3$ py *p*-CH), 2.38 (s, 3H, C*H*$_3$SAr), 3.33 (dd, J = 13.3, 5.9 Hz, 1H, *H*CH(CH*)), 3.65 (dd, J = 13.3, 8.9 Hz, 1H, *H'*CH(CH*)), 3.72 (s, 3H, C*H*$_3$O), 5.95 (dd, J = 8.8, 6.0 Hz, 1H, C*H**), 6.53 (d, J = 2.4 Hz, 1H, C*H* pz(ph)), 7.14 (dt, J = 7.0, 1.9 Hz, 1H, C*H* ph), 7.15 (m, 2H, C*H* ph), 7.51 (m, 2H, C*H* pz(CH*) + C*H* ph), 8.28 (s, 1H, C*H* py). ^{13}C NMR (75 MHz, $CDCl_3$): δ 10.8 (*C*H$_3$ py *p*-CH), 13.3 (*C*H$_3$ py *o*-CH), 16.1 (*C*H$_3$SR), 16.3 (*C*H$_3$SAr), 38.2 (*C*H$_2$), 60.0 (*C*H$_3$O), 62.9 (*C*H*), 106.6 (*C*H pz(ph)), 124.5 (*C*H ph), 125.3 (*C*H ph), 126.1 (*C* quat), 126.5 (*C* quat), 128.0 (*C*H ph), 129.7 (*C*H ph), 132.6 (*C* quat), 137.4 (*C* quat), 149.1 (*C*H pz(CH*)), 149.6 (*C* quat), 154.7 (*C* quat), 164.1 (*C* quat). ESI-MS (p.i.,

50 V, CH_3OH, m/z, I%): 400.6, 100, $[L^bH]^+$. Anal. calcd for $C_{21}H_{25}N_3OS_2$ (399.57): C, 63.12; H, 6.31; N, 10.52. Found: C, 63.31; H, 6.15; N, 10.33%.

5.2.4 Synthesis of $[Cu(L^a)]_2(BF_4)_2$ ($\mathbf{a_2}(BF_4)_2$)

A solution of $[Cu(CH_3CN)_4]BF_4$ (132 mg, 0.42 mmol) in dichloromethane (10 ml) was added to a solution of L^a (157 mg, 0.38 mmol) in dichloromethane (10 ml) at room temperature with stirring. After 1 h, the solution was concentrated to ~5 ml under a vacuum; hexane was added (25 ml) and a colorless oil formed, which was triturated, filtered and dried under a vacuum. A white powder was collected ($\mathbf{a_2}(BF_4)_2$, 147 mg, 0.13 mmol, 70%). Colorless crystals suitable for X-ray diffraction were obtained by stratification of hexane over a dichloromethane solution of the product, corresponding to $[Cu(L^a)]_2(BF_4)_2{\cdot}2CH_2Cl_2$ ($\mathbf{a_2}(BF_4)_2{\cdot}2CH_2Cl_2$). IR ($cm^{-1}$): 3125m, 2922m, 1591m, 1565m, 1476s, 1430s, 1366m, 1304m, 1264s, 1220w, ~1060 vs br, 762s. ^{1}H NMR (300 MHz, CD_3CN): δ 2.07 (s, 3H, C*H*$_3$SR), 2.24 (s, 3H C*H*$_3$ py *p*-CH), 2.26 (s, 3H, C*H*$_3$ py *o*-CH), 2.34 (m, 3H, C*H*$_2$(SCH_3) + *H*CH(CH*)), 2.43 (s, 3H, C*H*$_3$SAr), 2.87 (m, 1H, *H'*CH(CH*)), 3.80 (s, 3H, C*H*$_3$O), 6.04 (dd, J = 9.9, 4.6 Hz, 1H, C*H**), 6.57 (d, J = 2.4 Hz, 1H, C*H* pz(ph)), 7.42 (m, 2H, C*H* ph), 7.54 (m, 2H, C*H* ph), 7.89 (d, J = 2.4 Hz, 1H, C*H* pz(CH*)), 8.31 (s, 1H, C*H* py). ESI-MS (p.i., 45 V, CH_3CN, m/z, I%): 476.2, 100, $[Cu(L^a)]^+$.. ESI-MS (p.i., 39 V, CH_3OH, m/z, I%): 476.2, 100, $[Cu(L^a)]^+$.. Anal. calcd for $B_2C_{44}Cu_2F_8H_{54}N_6O_2S_4$ (1127.90): C, 46.85; H, 4.82; N, 7.45. Found: C, 47.24; H, 4.96; N, 7.18%.

5.2.5 Synthesis of $[Cu(L^b)]_2(BF_4)_2$ ($\mathbf{b_2}(BF_4)_2$)

The same procedure used to prepare $\mathbf{a_2}(BF_4)_2$ was applied by using L^b (160 mg, 0.40 mmol) instead of L^a and a different quantity of $[Cu(CH_3CN)_4]BF_4$ (139 mg, 0.44 mmol). A white powder was collected ($\mathbf{b_2}(BF_4)_2$, 170 mg, 0.15 mmol, 77%). Colorless crystals suitable for X-ray diffraction were obtained by cooling an acetonitrile:water solution of the product to 8 °C. IR (cm^{-1}): 3137 w, 3001 w, 2930 m, 1589 w, 1568 w, 1470 m, 1427 m, 1351 w, 1254 m, ~1035 m br, 762 m. ^{1}H NMR (300 MHz, CD_3CN): δ 2.16 (s, 3H, C*H*$_3$SR), 2.29 (s, 3H, C*H*$_3$ py o-CH), 2.30 (s, 3H, C*H*$_3$ py p-CH), 2.47 (s, 3H, C*H*$_3$SAr), 3.35 (dd, J = 14.5, 5.5 Hz, 1H, *H*CH(CH*)), 3.54 (dd, J = 14.4, 8.1 Hz, 1H, *H'*CH(CH*)), 3.84 (s, 3H, C*H*$_3$O), 6.01 (dd, J = 8.9, 5.9 Hz, 1H, C*H**), 6.64 (d, J = 2.4 Hz, 1H, C*H* pz(ph)), 7.46 (m, 2H, C*H* ph), 7.58 (m, 2H, C*H* ph), 7.98 (d, J = 2.4 Hz, 1H, C*H* pz(CH*)), 8.33 (s, 1H, C*H* py). ESI-MS (p.i., 54 V,

CH_3CN, m/z, I%): 462.2, 100, $[Cu(L^b)]^+$. ESI-MS (p.i., 30 V, CH_2Cl_2, m/z, I%): 462.2, 100, $[Cu(L^b)]^+$.Anal. calcd for $B_2C_{42}Cu_2F_8H_{50}N_6O_2S_4$ (1099.85): C, 45.86; H, 4.58; N, 7.64. Found: C, 45.61; H, 4.75; N, 7.80%.

5.2.6 X-ray crystallography

A summary of data collection and structure refinement for $\mathbf{a_2}(BF_4)_2{\cdot}2CH_2Cl_2$ and $\mathbf{b_2}(BF_4)_2$ is reported in Table 5.1.

Table 5.1. Summary of X-ray crystallographic data for $\mathbf{a_2}(BF_4)_2$ and $\mathbf{b_2}(BF_4)_2$.

	$\mathbf{a_2}(BF_4)_2{\cdot}2CH_2Cl_2$	$\mathbf{b_2}(BF_4)_2$
Empirical formula	$C_{46}H_{58}B_2Cl_4Cu_2F_8N_6O_2S_4$	$C_{42}H_{50}B_2Cu_2F_8N_6O_2S_4$
Formula weight	1297.72	1099.82
Colour, habit	Colorless, block	Colorless, block
Crystal size, mm	0.45x0.35x0.23	0.25x0.20x0.15
Crystal system	Triclinic	Monoclinic
Space group	*P*-1	$P2_1/c$
a, Å	10.548(1)	11.899(6)
b, Å	12.138(1)	21.022(7)
c, Å	12.780(1)	19.541(2)
α deg.	111.20(1)	90
β deg.	101.16(1)	91.14(2)
γ deg.	101.29(2)	90
V, Å^3	1432.1(2)	4887(3)
Z	1	4
T, K	293(2)	293(2)
ρ(calc), Mg/m^3	1.505	1.495
μ, mm^{-1}	1.143	1.114
θ range, deg.	1.79 to 28.07	1.71 to 26.00
No.of rflcn/obsv	16171 / 3779	9588 / 4067
GooF	1.037	0.996
*R*1	0.0426	0.0597
*wR*2	0.0910	0.0816

$R1 = \Sigma||F_O|-|F_C||/\Sigma|F_O|$, $wR2 = [\Sigma[w(F_O^2-F_C^2)^2]/\Sigma[w(F_O^2)^2]]^{1/2}$, $w = 1/[\sigma^2(F_O^2) + (aP)^2 + bP]$, where $P = [\max(F_O^2,0) + 2F_C^2]/3$

Single crystal data were collected with a Bruker Smart 1000 area detector diffractometer (Mo Kα; λ = 0.71073 Å). Cell parameters were refined from the observed setting angles and detector positions of selected strong reflections. Intensities were integrated from several series of exposure frames that covered the sphere of reciprocal space.[208] No crystal decay was observed. An absorption correction was applied for $\mathbf{a_2}(BF_4)_2 \cdot 2CH_2Cl_2$ and $\mathbf{b_2}(BF_4)_2$ using the program SADABS[153], with minimum and maximum transmission factors of 0.703-1.000 for $\mathbf{a_2}(BF_4)_2 \cdot 2CH_2Cl_2$ and 0.763-1.000 for $\mathbf{b_2}(BF_4)_2$. The structures were solved by direct methods (SIR97)[155] and refined with full-matrix least-squares (SHELXL-97),[156] using the Wingx software package.[157] Non-hydrogen atoms were refined anisotropically and the hydrogen atoms were placed at their calculated positions. In $\mathbf{a_2}(BF_4)_2 \cdot 2CH_2Cl_2$ the independent BF_4^- is disordered in two positions with site occupancy factors of ~0.4 and ~0.6, respectively, whereas in $\mathbf{b_2}(BF_4)_2$, one of the two independent BF_4^- molecules is disordered in three positions with site occupancy factors of 0.33 for each image. Molecular drawings were prepared using the Mercury 1.4.2 program.[159]

5.2.7 NMR titrations

Dilution ^1H NMR titrations for $\mathbf{a_2}(BF_4)_2$ and $\mathbf{b_2}(BF_4)_2$ were performed at 280, 290, 300 and 310 K in CD_3CN. Eleven spectra were registered in the copper concentration (C_{Cu}) range 0.1-0.00014 M for each temperature. TMS was used as the internal standard and a line broadening factor of 0.5 was applied. The variation of the chemical shifts with dilution was used to determine the equilibrium constants of the dimerization processes. The refinement of the data was initially performed with the HypNMR 2006 program,[168] yielding stoichiometric constants (K). Since the ionic strength varies over the course of the dilution an empirical correction for ionic strength variation was applied (Davies' equation),[269] yielding stability constants extrapolated at zero ionic strength (K^0) (Appendix 4). The program SPSS 15.0[270] was used to perform the van't Hoff analysis, which afforded the thermodynamic parameters for the dimerization equilibrium (ΔH^0 and ΔS^0). The distribution diagrams were calculated and plotted by the program HySS 2006.[169]

5.2.8 PGSE Experiments

^{1}H PGSE NMR measurements were performed for $\mathbf{a_2}(BF_4)_2$ and $\mathbf{b_2}(BF_4)_2$ solutions in CD_3CN (ε = 37.5 at 21 °C) at different C_{Cu} (10^{-1}-10^{-4} M range), using a standard stimulated echo (STE) sequence on a Bruker Avance 300 spectrometer at 300 K without spinning. The most intense signals were investigated. The dependence of the resonance intensity (I) on the gradient strength (g) is described by the following equation:

$$I = I_0 \cdot e^{-D\cdot\gamma^2\cdot g^2\cdot\delta^2\cdot(\Delta-\delta/3)}$$

where I = observed intensity (attenuated signal intensity), I_0 = reference intensity (unattenuated signal intensity), D = diffusion coefficient, γ = nucleus gyromagnetic ratio, g = gradient strength, δ = gradient duration, and Δ = diffusion delay. The parameters $\delta$and Δ were kept constant during the experiments, whereas g was varied from 2 to 95% in 16 steps. Different values of δ(1-2 ms), Δ (50-100 ms) and number of scans (depending on concentration) were used for different samples. All spectra were acquired using 16K points and processed with a line broadening of 1.0 Hz. PGSE data were treated by applying a procedure reported in the literature,[239,271] taking advantage of an internal standard (tetrakismethylsilylsilane, TMSS; r_H^{TMSS} (hydrodynamic radius) ~ r_{vdW}^{TMSS} (van der Waals radius) = 4.28 Å).[272] A nonlinear regression on *I* and g^2 data was performed with the SPSS 15.0 software in order to obtain the coefficients $m = D\cdot\gamma^2\cdot\delta^2\cdot(\Delta-\delta/3)$ for both the sample and the corresponding internal standard signals (m^{sample} and m^{TMSS}, respectively). The following expression (based on the Stokes-Einstein equation) was applied and numerically resolved to get the hydrodynamic radius of each sample (r_H^{sample}):

$$\frac{c^{TMSS}\cdot r_H^{TMSS}}{c^{sample}\cdot r_H^{sample}} = \frac{m^{sample}}{m^{TMSS}}$$

The coefficients c^{sample} and c^{TMSS} can be estimated from the semiempirical equation:[273]

$$c^x = \frac{6}{(1+0.695\cdot\frac{r^{solv}}{r_H^x})^{2.234}}$$

where x = sample or TMSS, and r^{solv} ~ van der Waals radius of the solvent (2.33 Å for CD_3CN). Hydrodynamic volumes were calculated from the respective radii: $V_H = 4/3 \cdot \pi \cdot (r_H)$. Uncertainties were obtained by error propagation on *m*.

The van der Waals volumes (V_{vdW})[274] and the Connolly volumes ($V_{Connolly}$)[241] were computed for both the X-ray ($\mathbf{a_2}^{2+}$ and $\mathbf{b_2}^{2+}$) and DFT optimized structures ($\mathbf{a}^{+}$ and $\mathbf{b}^{+}$) using the software package DS Viewer Pro 5.0. The X-ray volume ($V_{X\text{-}ray}$) was calculated by dividing the crystallographic unit cell volume by the number of molecular entities contained in the unit cell and by subtracting the $V_{Connolly}$ of counterions and solvent.

5.2.9 DFT calculations

DFT calculations were carried out with the Gaussian 03 program.[160] The mononuclear models $[Cu(L^a)]^+$ ($\mathbf{a}^{+}$) and $[Cu(L^b)]^+$ ($\mathbf{b}^{+}$) were optimized starting from hypothetical tetrahedral Cu(I) complexes in which the ligands are N,N',S,S' coordinated. The B3LYP[164,165] density functional and the lanl2dz basis set with Hay and Wadt effective core potential (ECP) were employed.[166,167] Vibrational frequencies were calculated at the same theoretical level in order to ensure that the stationary points were true minima. As described in the PGSE section, the optimized geometries were used to determine the theoretical volumes, V_{vdW} and $V_{Connolly}$, which were compared with the hydrodynamic volumes extrapolated from PGSE NMR experiments.

5.2.10 Electrochemistry

Cyclic voltammetry (CV) was performed in a three-electrode cell with a Pt disk as the working electrode, a Pt rod as the counter-electrode, and a 3 M Ag/AgCl/KCl (E^0 = +194 mV, T = 25 °C) as the reference electrode, by using a computerized electrochemical workstation consisting of an Autolab PGSTSAT 20 potentiostat (Ecochemie, Utrecht, The Netherlands) controlled by GPES 4.9 software. Cyclic voltammograms were recorded at different scan rates (20, 50, 100, 200, 500 $mV \cdot s^{-1}$) on freshly prepared solutions of $\mathbf{a_2}(BF_4)_2$ and $\mathbf{b_2}(BF_4)_2$ in CH_2Cl_2 and CH_3CN at two different concentrations (0.01 and 0.001 M). All the samples contained 0.1 M supporting electrolyte (tetra-*n*-butylammonium hexafluorophosphate, NBu_4PF_6).

5.3 Results and Discussion

The synthesis of L^a and L^b is described in Scheme 5.1. The reaction between 2-Chloromethyl-4-methoxy-3,5-dimethylpyridine and 3-(2-(methylthio)phenyl)-1H-pyrazole affords the N,N',S donor ligand, L^1, which can be functionalized on the methylene bridge with opportune electrophiles after deprotonation with *n*-butyllithium, in analogy to the preparation of bis(pyrazolyl)-scorpionates.[40] The use of 2-chloroalkyl methyl sulfides provides good yields of the N,N',S,S' heteroscorpionate ligands L^a and L^b. In order to obtain a more symmetric donor ligand, we first attempted the reaction between 3,5-alkyl-substituted bis(pyrazolyl)methanes (previously deprotonated with *n*-BuLi) and 2-chloromethyl methyl sulfide, but we recovered the parent bis(pyrazolyl)methanes instead of the desired product (Scheme 5.2).

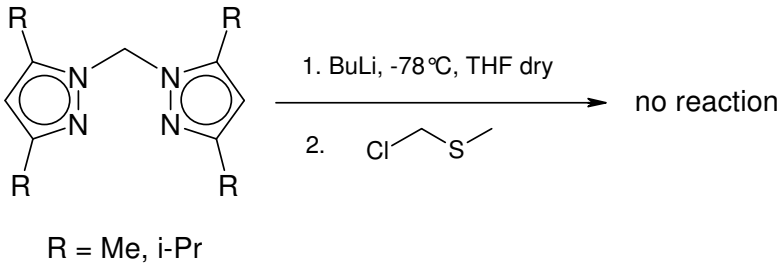

Scheme 5.2

With respect to this, in the synthesis of L^a and L^b the presence of the pyridyl group confers a greater stability to the benzylic carbanion, therefore allowing for the attack of weak acid electrophiles. L^a and L^b are chiral ligands due to the asymmetry of the central carbon atom, but we employed the racemic mixture for the preparation of the copper complexes. As far as the coordination capabilities of the ligands are concerned, the two thioether moieties and the pyrazole-pyridine assembly could provide the N_2S_2 coordination mode required by Cu(I) in a hypothetical mononuclear complex. Nevertheless, when reacting L^a with $[Cu(CH_3CN)_4]BF_4$, the dinuclear complex $\mathbf{a_2}(BF_4)_2$ was obtained, probably because of the extreme flexibility of the alkyl thioether arm of L^a. To reduce the degrees of freedom of this fourth donor group, we reduced the length of the alkyl chain from $-CH_2-CH_2SCH_3$ to $-CH_2-SCH_3$ (in L^b), but with no substantial changes in the coordination properties of the ligand or in the geometry of the resulting complex. In fact, from a Cu(I) coordination perspective, $\mathbf{b_2}(BF_4)_2$ is identical to $\mathbf{a_2}(BF_4)_2$**.** The two complexes are soluble in acetonitrile, nitromethane, and dichloromethane, and slightly soluble in acetone.

If dichloromethane solutions of $\mathbf{a_2}(BF_4)_2$ and $\mathbf{b_2}(BF_4)_2$ are exposed to air, after some time they turn green as a consequence of copper(I) oxidation; in the case of $\mathbf{b_2}(BF_4)_2$, green crystals of the oxidized product $[Cu(L^b)Cl_2]$ were isolated. On the other hand, the complex $[Cu(L^a)_2(H_2O)](OTf)_2$ (OTf^- = triflate) was prepared by reacting $Cu(OTf)_2$ and L^a in 1:1 molar ratio in methanol. These complexes may be taken as models for the coordination capabilities of the ligands with Cu(II) (see below).

5.3.1 Solid-state structures

Relevant geometric parameters of $\mathbf{a_2}(BF_4)_2$ and $\mathbf{b_2}(BF_4)_2$ are listed in Table 5.2. Both compounds exhibit a dinuclear structure, presenting an almost equivalent metal coordination geometry (Figures 5.1 and 5.2).

Table 5.2 Selected bond lengths (Å) and angles (°) for $\mathbf{a_2}(BF_4)_2 \cdot 2CH_2Cl_2$ and $\mathbf{b_2}(BF_4)_2$.

	$\mathbf{a_2}(BF_4)_2 \cdot 2CH_2Cl_2$		
Cu-S(11)	2.452(1)	Cu-N(13)	2.040(2)
Cu-S(12)'	2.201(1)	Cu-N(21)	2.001(2)
N(21)-Cu-N(13)	92.27(9)	S(12)'-Cu-S(11)	109.82(3)
N(21)-Cu-S(12)'	128.14(7)	N(13)-Cu-S(12)'	123.17(7)
N(21)-Cu-S(11)	87.81(7)	N(13)-Cu-S(11)	109.74(7)
	$\mathbf{b_2}(BF_4)_2$		
Cu(1)-S(11)	2.335(2)	Cu(2)-S(12)	2.239(2)
Cu(1)-S(15)	2.246(2)	Cu(2)-S(14)	2.302(2)
Cu(1)-N(21)	2.044(4)	Cu(2)-N(24)	2.034(4)
Cu(1)-N(13)	2.076(4)	Cu(2)-N(16)	2.071(4)
N(21)-Cu(1)-N(13)	90.1(2)	N(24)-Cu(2)-N(16)	90.9(2)
N(21)-Cu(1)-S(15)	124.0(1)	N(24)-Cu(2)-S(12)	123.8(1)
N(13)-Cu(1)-S(15)	117.3(1)	N(16)-Cu(2)-S(12)	118.6(1)
N(21)-Cu(1)-S(11)	85.6(1)	N(24)-Cu(2)-S(14)	93.7(1)
N(13)-Cu(1)-S(11)	113.5(1)	N(16)-Cu(2)-S(14)	114.5(1)
S(15)-Cu(1)-S(11)	119.35(6)	S(12)-Cu(2)-S(14)	111.89(6)

' = -x+1,-y,-z+1

Each Cu(I) is located in a distorted tetrahedral environment, bound by two nitrogen atoms and by the aryl-thioether sulfur atom of a ligand, with the fourth coordination site deriving from the alkyl-thioether sulfur atom of the second ligand. The Cu-N bond distances are nearly equivalent for both compounds (2.040(2)-2.001(2) Å in $\mathbf{a_2}(BF_4)_2$ and 2.076(4)-2.034(4)-Å in $\mathbf{b_2}(BF_4)_2$). The bridging alkyl-thioether group gives rise to Cu-S bond distances that are significantly shorter (with differences that vary from ~0.10 and ~0.25 Å) than those derived from the aryl thioether. The reason for this may reside in the better donor ability of the alkyl- with respect to the aryl-thioether, but it could also be a consequence of the major stereochemical constraints of the aryl-thioether, which results in a non-ideal overlap of the sulfur's coordinating lone pair with copper(I). $\mathbf{a_2}(BF_4)_2$ is centrosymmetric, with the two ligands presenting the stereogenic carbon in the R and S configurations, respectively.

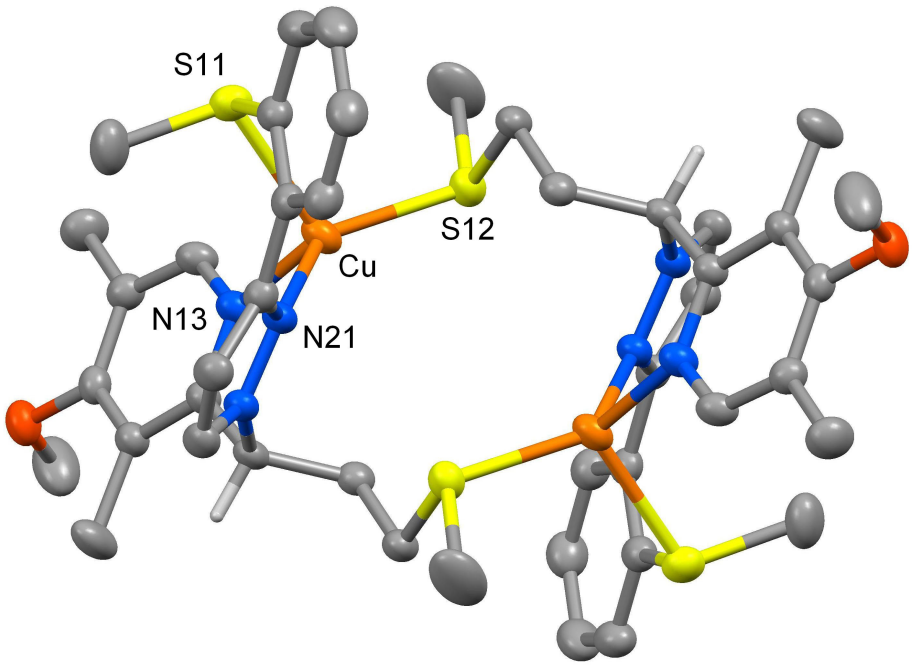

Figure 5.1 Molecular drawing of $\mathbf{a_2}(BF_4)_2\ 2CH_2Cl_2$ at the 30% thermal ellipsoids probability level. The BF_4^- counterions, the hydrogen atoms (except for the methinic ones) and the crystallization solvent molecules are omitted for clarity. ' = 1-x; -y; 1-z.

In $\mathbf{b_2}(BF_4)_2$, the ligands exhibit equivalent configurations for the central carbon, so that the complex is asymmetric; however, since the space group is centrosymmetric ($P2_1/c$) both RR and SS enantiomers are present in the unit cell. In addition, the metals are also stereogenic centers, and in $\mathbf{a_2}(BF_4)_2$ they exhibit opposite chirality (due to the center of symmetry),

whereas in $\mathbf{b_2}(BF_4)_2$ they adopt the same configuration. In summary, the overall chirality of $\mathbf{a_2}(BF_4)_2$ can be represented as $(RS)_C(RS)_{Cu}$, whereas that of $\mathbf{b_2}(BF_4)_2$ can be represented as $(RR)_C(RR)_{Cu}/(SS)_C(SS)_{Cu}$. The large distance between the two copper centers (4.972(1) Å in $\mathbf{a_2}(BF_4)_2$ and 5.212(2) Å $\mathbf{b_2}(BF_4)_2$) rules out any metal-metal interaction.

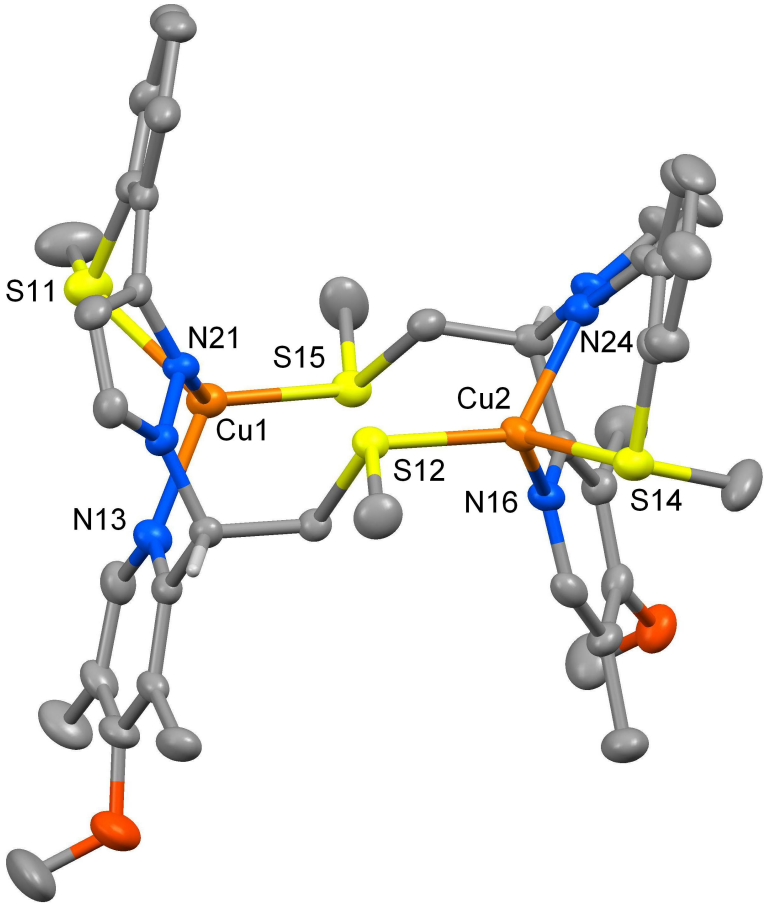

Figure 5.2 Molecular drawing of $\mathbf{b_2}(BF_4)_2$ at the 30% thermal ellipsoids probability level. The BF_4^- counterions and the hydrogen atoms (except for the methinic ones) are omitted for clarity.

The crystal structures of the Cu(II) complexes $[Cu(L^b)Cl_2]$ and $[Cu(L^a)_2(H_2O)](OTf)_2$ are reported in the Appendix 4 (Figures A11 and A12). In both structures, the metal exhibits a trigonal bipyramidal geometry. In $[Cu(L^b)Cl_2]$, the metal is bound to a k^3-N,N',S ligand and to two chloride ions. The apical positions are occupied by the aryl-thioether sulfur and by the pyridine nitrogen, whereas the pyrazole nitrogen atom and two chloride ions are in the equatorial plane. The alkyl-thioether sulfur does not take part in the metal coordination. In $[Cu(L^a)_2(H_2O)](OTf)_2$, the metal is bound by two κ^2-N,N' ligands, with both thioether groups not coordinated. The pyridine nitrogen atoms are in apical positions, whereas the pyrazole nitrogen atom and a water molecule occupy the equatorial positions.

5.3.2 Solution studies

To better comprehend the solution behavior of the complexes, we performed dilution ^{1}H NMR titrations for $\mathbf{a_2}(BF_4)_2$ and $\mathbf{b_2}(BF_4)_2$ in CD_3CN. In both cases, by varying the analytical copper concentration (C_{Cu}), we observed a drift in the chemical shift of various protons. In Figure 5.3 and in Figure A13 of Appendix 4, the NMR stacking plots of $\mathbf{b_2}(BF_4)_2$ and $\mathbf{a_2}(BF_4)_2$ are reported.

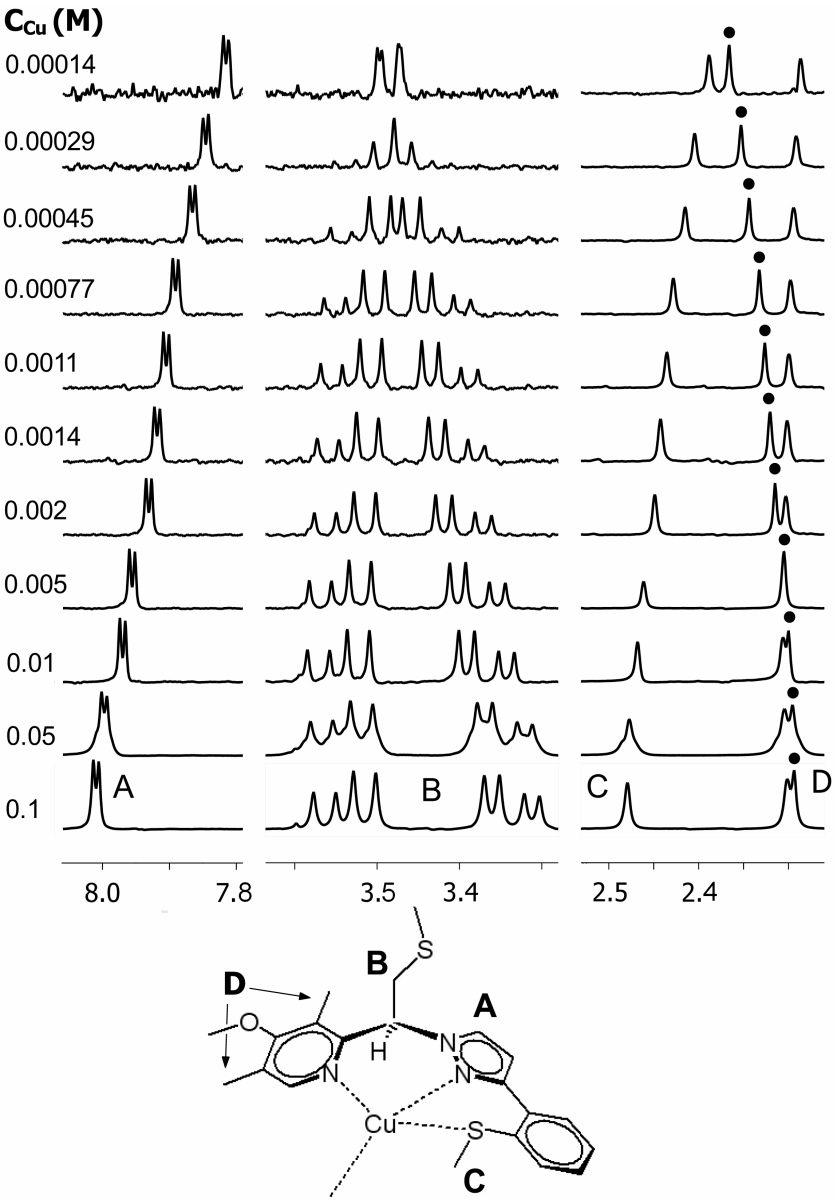

Figure 5.3 Stacking plot of ^{1}H NMR spectra of $\mathbf{b_2}(BF_4)_2$ in CD_3CN at different copper concentrations (C_{Cu}). The drifts of the A, C and D chemical shifts were used to derive the $\log K^0$ for the $2\mathbf{b}^+ \rightleftharpoons \mathbf{b_2}^{2+}$ equilibrium.

In addition, the diastereotopic methylene protons of $\mathbf{b_2}(BF_4)_2$ (peak B in Figure 5.3), constituting an ABX spin system, exhibit two doublets of doublets in concentrated solution, whereas in dilute solutions (C_{Cu} ~ 10^{-4} M), they give rise to a pseudo-doublet. This phenomenon can be explained with the gradual appearance, over the course of dilution, of a fast-exchanging species that is less "aggregated" than the complex predominant at high C_{Cu} (presumably the dinuclear complex), and whose methylene protons have closer chemical shifts, so that a pseudo-doublet appears for second-order effects. This is in accordance with the presence of a fast monomer-dimer equilibrium, which would also explain the variation of the chemical shifts of the other protons. In order to exclude the possibility that this behavior is related to the aggregation of cations and anions in solution (ion pairing),[275] BF_4^- was substituted with BPh_4^-, providing the complex $\mathbf{b_2}(BPh_4)_2$.[276] The trend of the NMR spectra at three different C_{Cu} (Figure A14 of Appendix 4) is analogous to that of $\mathbf{b_2}(BF_4)_2$ and would rule out the ion pairing hypothesis. These conclusions can be extended to $\mathbf{a_2}(BF_4)_2$. Moreover, in other solvents (CD_3NO_2, $(CD_3)_2CO$ and CD_2Cl_2) the complexes present spectral characteristics similar to the ones previously described, even though the spectra are much less resolved (data not reported). The equilibrium constants of the association processes, $2\mathbf{a}^+ \rightleftharpoons \mathbf{a_2}^{2+}$ and $2\mathbf{b}^+ \rightleftharpoons \mathbf{b_2}^{2+}$, were determined in CD_3CN at different temperatures (280 - 310 K, Table 5.3).

Table 5.3 Logarithms of the zero ionic strength equilibrium constants ($\log K^0$) for the dimerization processes $2\mathbf{a}^+ \rightleftharpoons \mathbf{a_2}^{2+}$ and $2\mathbf{b}^+ \rightleftharpoons \mathbf{b_2}^{2+}$ in the 280-310 K temperature range.

T (K)	$\log K^0(\mathbf{a_2}^{2+})$	$\log K^0(\mathbf{b_2}^{2+})$
280	3.70(10)	3.36(6)
290	3.65(7)	3.27(5)
300	3.55(6)	3.23(5)
310	3.48(5)	3.17(4)

As an example, the distribution diagram of $\mathbf{b_2}^{2+}$ at 300 K is reported in Figure 5.4, together with the variation in selected observed and calculated chemical shifts as a function of C_{Cu}; in a 10^{-4} M solution, the monomer/dimer ratio is ~9/1, whereas in a 10^{-1} M solution, this ratio is nearly reversed.

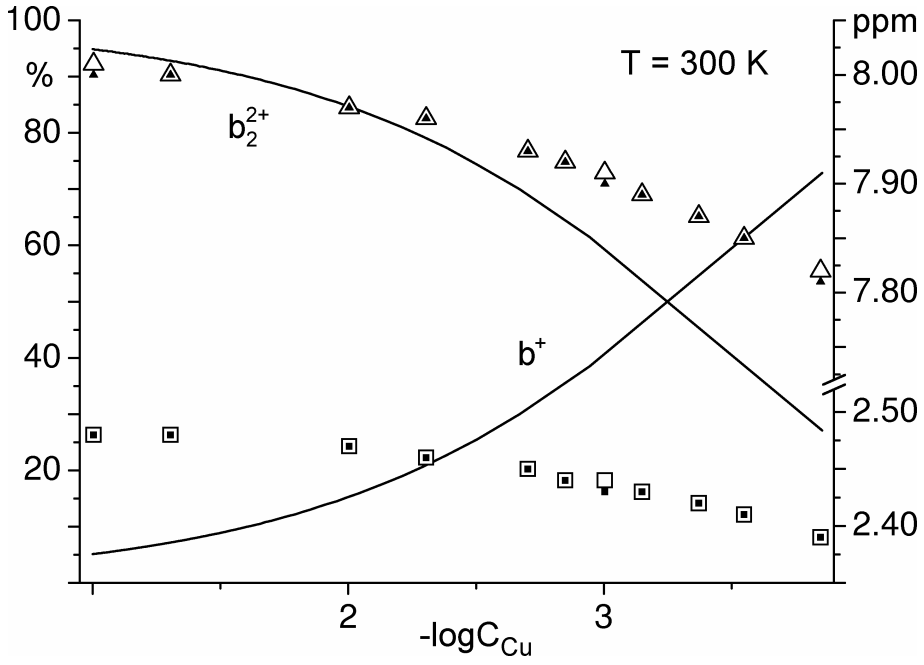

Figure 5.4. Distribution diagram corresponding to the dilution ^{1}H NMR titration of $\mathbf{b_2}(BF_4)_2$ in CD_3CN at 300 K (C_{Cu} = copper concentration). The observed and calculated chemical shifts for peaks A (Δ, ▲) and C (□, ■) of Figure 5.3 are reported.

By means of a van't Hoff analysis, the thermodynamic parameters of the dimerization processes were determined; the ΔH^0 show that both reactions are slightly exothermic ($\Delta H^0(\mathbf{a_2}^{2+})$ = -12(1) kJ·mol^{-1}, $\Delta H^0(\mathbf{b_2}^{2+})$ = -10(1) kJ·mol^{-1}), while the ΔS^0 are surprisingly positive ($\Delta S^0(\mathbf{a_2}^{2+})$ = +27(4) kJ·mol^{-1}, $\Delta S^0(\mathbf{b_2}^{2+})$ = +28(4) kJ·mol^{-1}). The small ΔH^0 values can be justified by considering that there is no net bond formation or rupture in these monomer/dimer equilibria, since two Cu(I)-S(thioether) dissociations are compensated for by two Cu(I)-S(thioether) formations. Furthermore, the hypothesis that acetonitrile would complete the coordination of copper in the monomer in place of a thioether group of L^a or L^b can be excluded by taking into account the energetics of the model reaction, $[Cu(MeCN)_2]^+$ + 2 Me_2S = $[Cu(Me_2S)_2]^+$ + 2 MeCN (+30.1 kJ·mol^{-1}),[277] from which it is evident that the substitution of acetonitrile bound at Cu(I) with a thioether is an unfavorable process. In the present case, given the exothermic nature of the dimerization, we can assume that no CH_3CN molecules are liberated in the reaction; hence, the ligands would behave as κ^4-N,N',S,S' tetradentate in the monomers. The entropy values deserve some comments, even though it has to be borne in mind that the determination of ΔS^0 through a van't Hoff analysis is affected by an intrinsic limited accuracy. In the present case, the positive ΔS^0 of dimerization can be

justified with a better overall solvation of the monomers with respect to the dinuclear entities, resulting in the release of solvent molecules during the association.[278-281]

To propose a molecular geometry for the mononuclear complexes, $\mathbf{a}^+$ and $\mathbf{b}^+$, DFT calculations were performed and the optimized structures are reported in Figure 5.5.

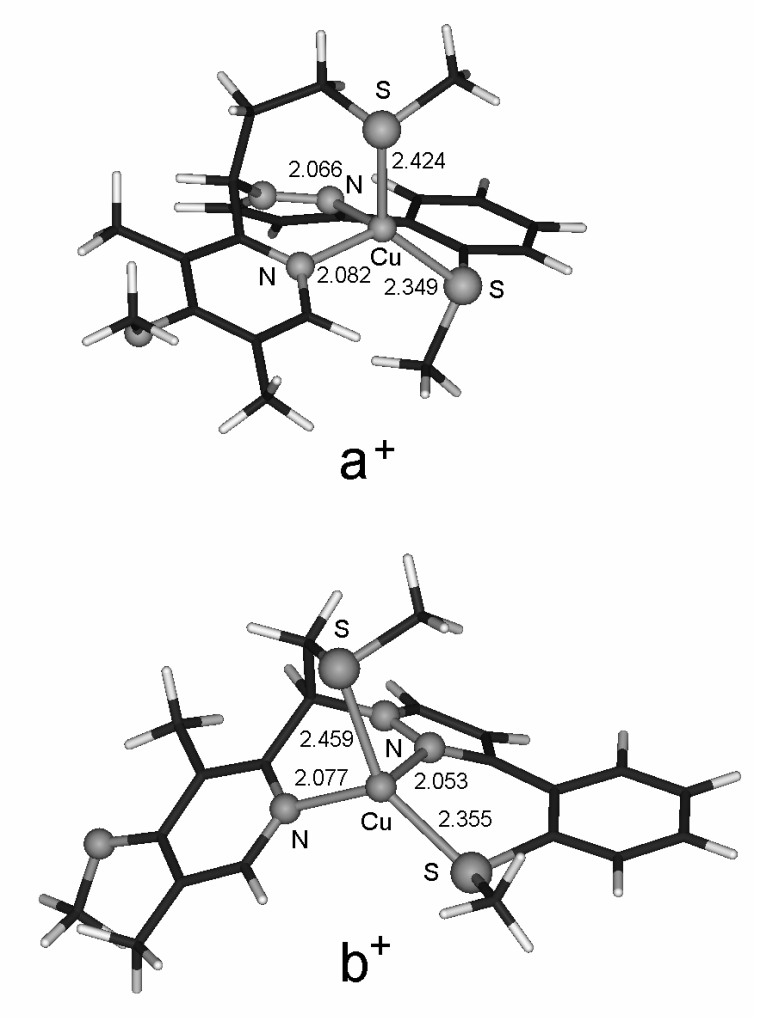

Figure 5.5 DFT-optimized geometries (B3LYP/lanl2dz) of the mononuclear species $\mathbf{a}^+$ and $\mathbf{b}^+$.

It appears that both L^a and L^b can accommodate Cu(I), even if in a considerably distorted tetrahedral, almost bisphenoidal, environment. In particular, the S-Cu-S angle in $\mathbf{a}^+$ and $\mathbf{b}^+$ is significantly greater than in $\mathbf{a_2}^{2+}$ and $\mathbf{b_2}^{2+}$ (Figure 5.6). In the monomers, the most relevant structural consequence that is derived from the different length of the alkyl-thioether arm is in a more pronounced coordination strain at the metal in $\mathbf{b}^+$ with respect to $\mathbf{a}^+$, with a consequent increase in the S-Cu-S angle by ~10°. This is also associated with a slight increase of the Cu-S_{alkyl} bond length by ~0.04 Å.

From the analysis of the log K^0 values, it appears that $\mathbf{a}^+$ exhibits a slightly greater propensity to dimerize if compared to $\mathbf{b}^+$; conversely, $\mathbf{b_2}^{2+}$ is more easily dissociated into monomers with respect to $\mathbf{a_2}^{2+}$. This can be tentatively explained by a close inspection of Figures 5.5 and 5.6, where the Cu(I) geometry of the dinuclear and mononuclear species (as derived by X-ray analysis and DFT calculations, respectively) are compared. In fact, in the mononuclear complex, the alkyl-thioether in L^a gives rise to two 7-member chelate rings and a 6-member one, whereas in L^b, it generates three 6-member chelate rings, and thus a more stable mononuclear complex.

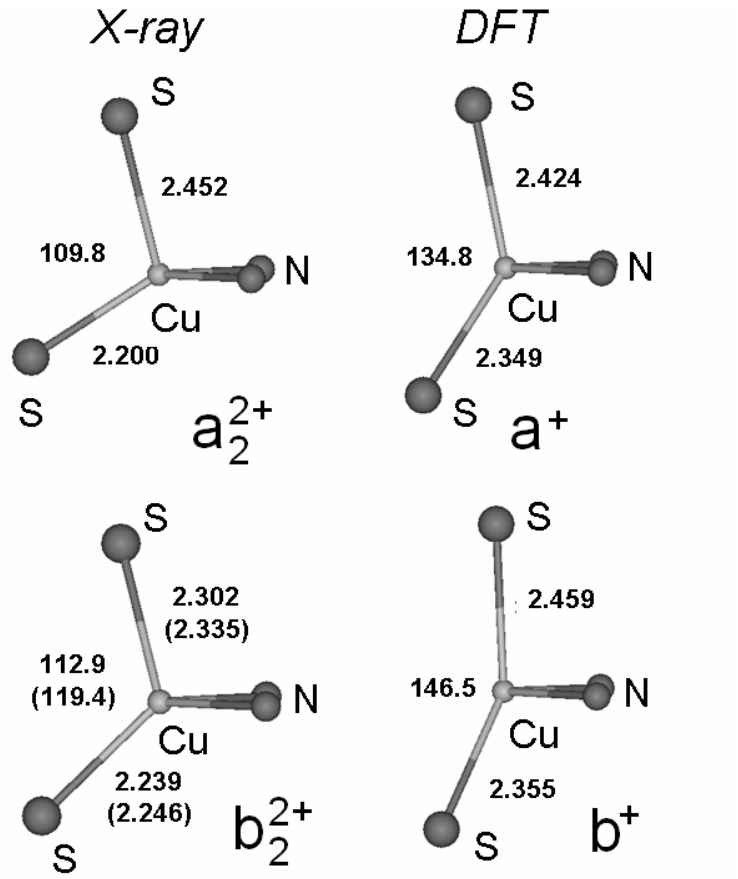

Figure 5.6. Comparison between the Cu(I) experimental geometries (X-ray) of the dinuclear complexes $\mathbf{a_2}^{2+}$ and $\mathbf{b_2}^{2+}$ with the respective DFT-optimized mononuclear species $\mathbf{a}^+$ and $\mathbf{b}^+$. The double values in $\mathbf{b_2}^{2+}$ reflect the two different metal geometries as found in the crystal structure.

As far as the kinetics of the dimerization process are concerned, the fast-exchange regime is in agreement with the lability of the Cu(I)-S(thioether) bonds and with the low viscosity of acetonitrile ($3.69 \cdot 10^{-4}$ Pa·s at 298 K). A variable-temperature NMR experiment was performed on a 0.00045 M sample of $\mathbf{b_2}(BF_4)_2$ in CD_3CN (wherein the dimer and the monomer are about

at equimolar ratio) in the 300 - 230 K range. On decreasing the temperature, an enlargement of the signals can be noted; this is particularly evident for the methylene protons (Figure 5.7). However, the kinetic parameters could not be determined through a complete lineshape analysis because of the slight broadening of all the peaks and the inability to estimate the chemical shifts of the single species below the temperature of coalescence.

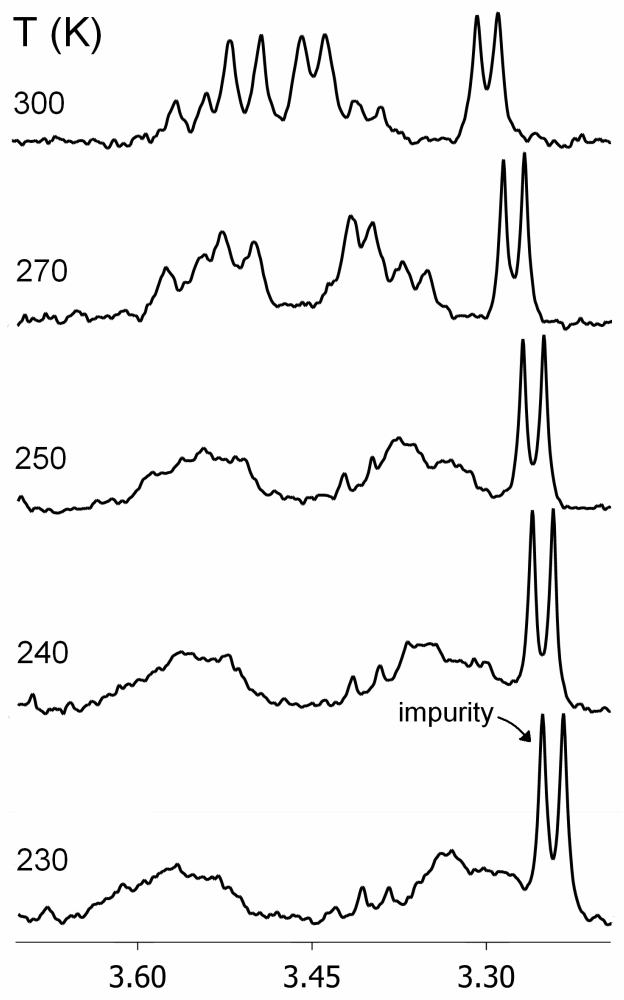

Figure 5.7 Variable temperature ^{1}H NMR of a $\mathbf{b_2}(BF_4)_2$ solution (C_{Cu} = 0.00045 M) in CD_3CN. B protons are shown (see Figure 5.3).

To further confirm the dissociation of the dimers in solution and to determine the hydrodynamic volumes of both the monomers ($\mathbf{a}^+$, $\mathbf{b}^+$) and the dimers ($\mathbf{a_2}^{2+}$, $\mathbf{b_2}^{2+}$), ^{1}H PGSE NMR experiments were performed on solutions of $\mathbf{a_2}(BF_4)_2$ and $\mathbf{b_2}(BF_4)_2$ at different C_{Cu} in CD_3CN (Table 5.4), and the data were interpolated for ideal monomer-dimer equilibria.

Table 5.4 Experimental hydrodynamic volumes (V_H) for $\mathbf{a_2}(BF_4)_2$ and $\mathbf{b_2}(BF_4)_2$ in CD_3CN at different copper concentrations (C_{Cu}) at 300 K.

C_{Cu} (M)	$V_H(\mathbf{a_2}(BF_4)_2)$ (Å^3)	$V_H(\mathbf{b_2}(BF_4)_2)$ (Å^3)
0.0001	700(20)	590(20)
0.001	780(20)	700(20)
0.01	860(30)	820(20)
0.1	950(30)	860(30)

The high permittivity of acetonitrile allows the exclusion of ionic aggregation of all the cationic complexes with BF_4^- anions,[240,257] which would not, however, affect the experimental hydrodynamic volumes due to the small encumbrance of BF_4^- (V_{vdW} = ~40 Å). For an ideal monomer-dimer equilibrium, the following equation can be derived (Appendix 4):

$$V_H = \frac{(V_H^0(D) - 2V_H^0(M))(\sqrt{8K^0C_{Cu}+1} - 4K^0C_{Cu}V_H^0(D) - V_H^0(D) + 2V_H^0(M)}{\sqrt{8K^0C_{Cu}+1} + 4K^0C_{Cu} - 1} \quad (5.1)$$

where V_H is the experimental hydrodynamic volume, $V^0_H(D)$ is the hydrodynamic volume of the dimer, $V^0_H(M)$ is that of the monomer and K^0 is the corrected dimerization constant (obtained from ^{1}H NMR titrations). The fitting with the experimental data is shown in Figure 5.8, whereas the hydrodynamic values of the individual species are reported in Table 5.5.

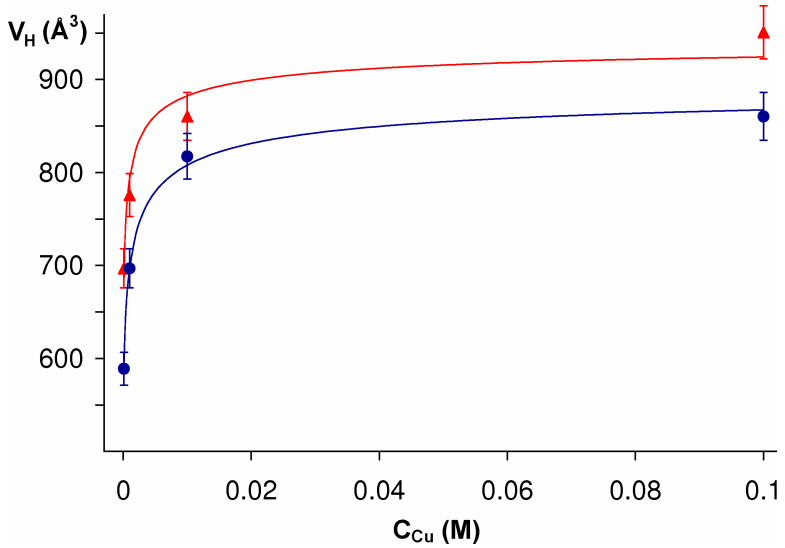

Figure 5.8 Experimental hydrodynamic volumes (V_H) of $\mathbf{a_2}(BF_4)_2$ (▲) and $\mathbf{b_2}(BF_4)_2$ (●) in CD_3CN plotted as function of C_{Cu} at 300 K. The fitting curves (see Equation 5.1) are reported.

Table 5.5. Hydrodynamic volumes ($V°_H$) of the dimeric ($\mathbf{a_2}^{2+}$ and $\mathbf{b_2}^{2+}$) and of the monomeric ($\mathbf{a}^+$ and $\mathbf{b}^+$) species in CD_3CN, together with the van der Waals (V_{vdW}), Connolly ($V_{Connolly}$) and X-ray ($V_{X\text{-}ray}$) volumes.

	$V°_H$ (Å^3)	V_{vdW}	$V_{Connolly}$	$V_{X\text{-}ray}$
$\mathbf{a_2}^{2+}$	950(20)	702	1339	1092
$\mathbf{a}^+$	620(40)	373	642	-
$\mathbf{b_2}^{2+}$	900(10)	669	1280	1061
$\mathbf{b}^+$	550(10)	357	612	-

For both complexes, $V^0_H(D)$ have values that lie between V_{vdW} and $V_{X\text{-}ray}$.[271] This latter volume is comparable to the solvent-excluded volume ($V_{Connolly}$) that is computed by taking into account the cavities and inlets of the solute, which are not accessible by the solvent (so that $V_{Connolly} > V_{vdW}$). As far as the monomers are concerned, in this case, $V^0_H(M)$ is also intermediate between V_{vdW} and $V_{Connolly}$. This is in agreement with previous results, which show that V_{vdW} and $V_{X\text{-}ray}/V_{Connolly}$ are the lower and upper limits of the real hydrodynamic volume.[271]

An additional proof of the predominance of the monomeric species in diluted solution comes from the ESI-Mass spectra (10^{-6} M solutions of $\mathbf{a_2}(BF_4)_2$ in CH_3CN and CH_3OH, and $\mathbf{b_2}(BF_4)_2$ in CH_3CN and CH_2Cl_2), which show only the presence of monomers ($[L^{a/b}Cu]^+$ for both complexes), and without solvent molecules bound to copper.

5.3.3 Electrochemistry

The cyclic voltammograms of the 0.01 and 0.001 M solutions of $\mathbf{a_2}(BF_4)_2$ in CH_2Cl_2 and CH_3CN are reported in Figures 5.9 and 5.10 (those of the analogous solutions of $\mathbf{b_2}(BF_4)_2$ are not reported).

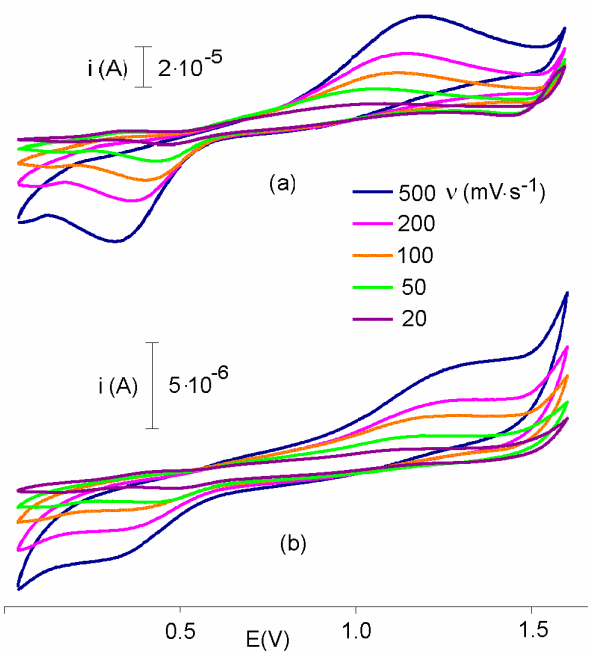

Figure 5.9 Cyclic voltammograms of $\mathbf{a_2}(BF_4)_2$ in CH_3CN at different scan rates (ν = 20 - 500 $mV \cdot s^{-1}$, third scans). (a) C_{Cu} = 0.01 M, (b) C_{Cu} = 0.001 M. Supporting electrolyte: NBu_4PF_6 0.1 M. Reference electrode: Ag/AgCl/KCl 3 M.

The voltammetric parameters of both the complexes are reported in Tables 5.6 and 5.7. CV experiments were also performed on 10^{-4} M solutions, but the voltammograms are not reported because the peaks are hardly detectable. In a first stage, the potential range employed allowed us to identify two redox systems for each sample: Cu(0)/Cu(I) and Cu(I)/Cu(II) couples. The former, in the Cu(0) → Cu(I) process, was characterized by high peak current and a narrow shape typical of Cu(0) deposition on the electrode surface ("anodic stripping").[282] The Cu(0) → Cu(I) oxidation generates a Cu(I) species that may be different from the initial Cu(I) complex. To avoid such an electrochemical process, the lower limit of the potential window was set at higher values; hence, the reported voltammograms depict only the Cu(I)/Cu(II) redox system.

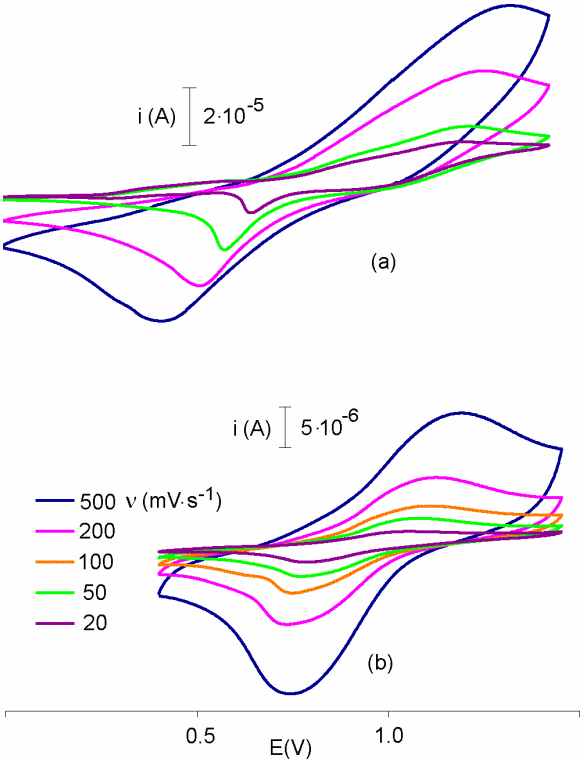

Figure 5.10 Cyclic voltammograms of $\mathbf{a_2}(BF_4)_2$ in CH_2Cl_2 at different scan rates (ν = 20 - 500 $mV \cdot s^{-1}$, third scans). (a) C_{Cu} = 0.01 M, (b) C_{Cu} = 0.001 M. Supporting electrolyte: NBu_4PF_6 0.1 M. Reference electrode: Ag/AgCl/KCl 3 M.

The complexes show quasireversible to irreversible redox behavior of the Cu(I)/Cu(II) couple in all of the experimental conditions (e.g., solvent, concentration); in fact, the separation between the forward (anodic, E_{pa}) and the reverse (cathodic, E_{pc}) peaks always increase with the scan rate (ν). Nevertheless, the ΔE_p values (E_{pa}-E_{pc}) are considerably large, implying a high reorganization energy involved in the electron transfer.[283] This is tentatively justified with the flexibility of the ligands, and in particular that of their alkyl-thioether "arm". This allows the electrogenerated Cu(II) to organize the coordination sphere according to its electronic and steric preferences; *i.e.* to adopt five or six coordinations, as supported by the crystal structures of Cu(II) with L^a and L^b (see Figures A11 and A12 of Appendix 4). The analysis of these Cu(II) complexes supports the hypothesis that the thioether groups may not be bound to Cu(II), so that the coordination/decoordination may contribute to the non-reversible behavior of the complexes. Moreover, the voltammetric behavior of the Cu(I) systems is complicated by the dimerization equilibrium preceding the redox event, which reasonably involves two electroactive species (monomer and dimer). It is worth noting that in the dimers, the two metal centers are electrochemically independent due to the large distance

between them (~5 Å). Bearing in mind that the Cu(I) coordination sphere is equivalent in the dimer and in the monomer (N,N',S,S'), comparable values of formal redox potential ($E^{0'}$) can be assumed for both species. Consistent with this, in changing C_{Cu} (*i.e.* varying the dimer:monomer ratio), minimal shifts in the anodic (E_{PA}) and cathodic (E_{PC}) potentials can be detected for equivalent scan rates (ν). The only significant variation of ΔE_p with C_{Cu} is seen for $\mathbf{a_2}(BF_4)_2$ in CH_2Cl_2; in fact, at ν = 200 $mV \cdot s^{-1}$, a difference of ΔE_p of 324 mV between the 0.01 M and the 0.001 M samples is detected.

Table 5.6 Summary of CV parameters for $\mathbf{a_2}(BF_4)_2$ in CH_2Cl_2 and CH_3CN at C_{Cu} 0.01 M and 0.001 M.

conc. (M) / solv.	ν	E_{pa}	E_{pc}	ΔE_p	i_{pa}/i_{pc}
0.01 / CH_2Cl_2	20	1.16	0.637	0.523	0.40
	50	1.157	0.569	0.588	0.46
	200	1.179	0.508	0.671	0.54
	500	1.223	0.42	0.803	0.45
0.001 / CH_2Cl_2	20	1.02	0.793	0.227	0.58
	50	1.057	0.781	0.276	0.66
	100	1.076	0.754	0.322	0.61
	200	1.096	0.749	0.347	0.65
	500	1.154	0.759	0.395	0.55
0.01 / CH_3CN	50	1.024	0.445	0.579	0.98
	100	1.087	0.421	0.666	1.02
	200	1.114	0.384	0.73	1.07
	500	1.161	0.343	0.818	1.00
0.001 / CH_3CN	20	1.124	0.492	0.632	0.66
	50	1.185	0.457	0.728	0.72
	100	1.175	0.411	0.764	1.53
	200	1.214	0.389	0.825	1.10
	500	1.244	0.348	0.896	0.98

ν = Scan Rate, E_{pa} = Anodic Peak Potential, E_{pc} = Cathodic Peak Potential, $\Delta E_p = E_{pa}-E_{pc}$, i_{pa} = Anodic Current, i_{pc} = Cathodic Current.

Table 5.7 Summary of CV parameters for $\mathbf{b_2}(BF_4)_2$ in CH_2Cl_2 and CH_3CN, at C_{Cu} 0.01, 0.001 M.

conc. (M) / solv.	ν	E_{pa}	E_{pc}	ΔE_p	i_{pa}/i_{pc}
0.01 / CH_2Cl_2	50	1.201	0.505	0.696	0.85
	100	1.245	0.447	0.798	0.85
	200	1.272	0.408	0.864	0.84
	500	1.377	0.332	1.045	0.86
0.001 / CH_2Cl_2	50	1.108	0.527	0.581	0.82
	100	1.111	0.503	0.608	0.81
	200	1.133	0.469	0.664	0.80
	500	1.243	0.4	0.843	0.82
0.01 / CH_3CN	20	0.981	0.376	0.605	0.68
	50	1.174	0.293	0.881	0.73
	100	1.138	0.285	0.853	0.71
	200	1.199	0.244	0.955	0.72
	500	1.265	0.2	1.065	0.73
0.001 / CH_3CN	50	1.108	0.398	0.71	0.75
	100	1.174	0.339	0.835	0.76
	200	1.211	0.327	0.884	0.77
	500	1.235	0.286	0.949	0.76

ν = Scan Rate, E_{pa} = Anodic Peak Potential, E_{pc} = Cathodic Peak Potential, i_{pa} = Anodic Current and i_{pc} = Cathodic Current.

5.4 Conclusions

The scorpionate N,N',S,S'-donor ligands L^a and L^b were synthesised. The Cu(I) complexes $[Cu(L^a)]_2](BF_4)_2$ ($\mathbf{a_2}(BF_4)_2$) and $[Cu(L^b)]_2](BF_4)_2$ ($\mathbf{b_2}(BF_4)_2$) are dinuclear at the solid state, with each copper center exhibiting a distorted tetrahedral N,N',S,S' coordination environment. However, the crystal structures of the complexes do not completely reflect the solution properties. In fact, in acetonitrile, there is evidence of mononuclear species in equilibrium with the dimers. In particular, the aggregation processes were quantitatively analyzed by means of ^{1}H NMR dilution titrations, which allowed the determination of the thermodynamic parameters of the dimerization reactions: $2\mathbf{a}^+ \rightleftharpoons \mathbf{a_2}^{2+}$ and $2\mathbf{b}^+ \rightleftharpoons \mathbf{b_2}^{2+}$. The equilibrium constant (K^0) was measured in the 280-310 K range, yielding a negative ΔH^0 and, surprisingly, a positive ΔS^0. The latter suggests that dimerization may be entropy-driven due to a better solvation in the monomers with respect to the dimers, resulting in the release of solvent molecules in the association. Furthermore, ^{1}H PGSE NMR experiments performed at different C_{Cu} provided a weighted-average hydrodynamic volume (V_H) of the exchanging species. The combination of ^{1}H NMR titration with ^{1}H PGSE NMR data (log K^0 and V_H, respectively), allowed us to determine the hydrodynamic volumes of the individual species (V_H^0(M) and V_H^0(D)). The applied procedure is analogous to one that was recently reported and that combines PGSE and conductimetric data.[284] As cyclic voltammetry attests, the complexes $\mathbf{a_2}(BF_4)_2$ and $\mathbf{b_2}(BF_4)_2$ show a quasireversible to irreversible behavior of the Cu(I)/Cu(II) redox couple (CH_3CN and CH_2Cl_2), with quite high ΔEp values (in the 0.2-0.9 V range for $\mathbf{a_2}(BF_4)_2$, and 0.6-1.1 V range for $\mathbf{b_2}(BF_4)_2$). Presumably, this is due to the flexibility of the ligands, especially the alkyl-thioether groups, which confer to the complexes a considerable conformational freedom, implying a high reorganization energy involved in the electron transfer.

6

More Cu(I) Complexes with C-Centered N/S-Scorpionate Ligands

6.1 A Luminescent Cu(I) Coordination Polymer: $[Cu(L^*)(PPh_3)]BF_4$ (L^* = N,N',S-Scorpionate Ligand)

Coordination polymers, and in particular metal-organic frameworks (MOFs), have attracted much attention in recent years due to their peculiar properties and structural diversity.[285] The fields of application of these compounds encompass catalysis, gas absorption, and nonlinear optics.[118,286] In addition, MOFs exhibiting luminescence properties are particularly interesting due to their possible employment in the construction of light-emitting devices or solar light-harvesting systems.[287,288]

In this report we present the X-ray structure and solid state fluorescence properties of a ternary complex of Cu(I) with a new N,N',S-scorpionate ligand and triphenylphosphine. The behaviour of the complex in solution was investigated by means of NMR techniques. The synthesis of the pyrazole-pyridine based ligand is reported in Scheme 6.1.

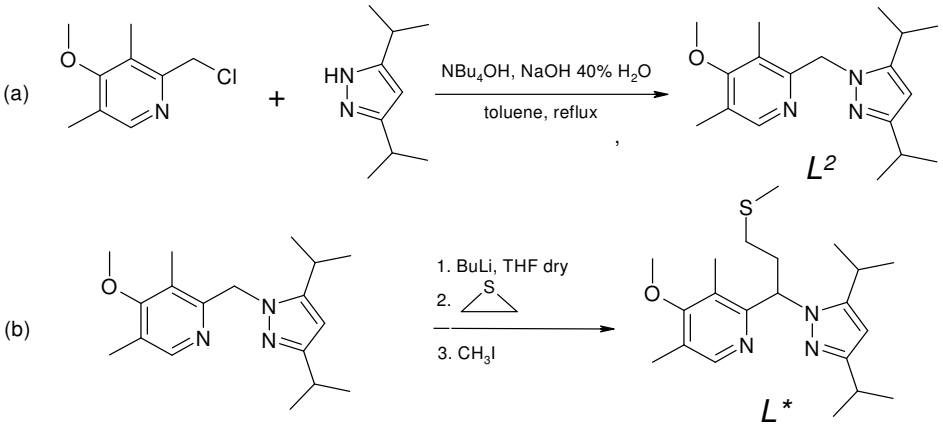

Scheme 6.1

The precursor L^2 could be easily prepared in a water/toluene biphasic mixture, employing NBu_4OH as phase transfer catalyst, step (a). The N,N',S tridentate ligand L* was prepared by deprotonation of the methylene bridge of L^2 with *n*-BuLi, by subsequent reaction with ethylene sulfide, and finally by conversion (*in situ)* of the generated thiolate into a thioether group by addition of methyl iodide, step (b). L* is chiral, and since the synthesis is not stereoselective, both enantiomers are produced and used for complexation. The thioether group of L* can in principle confer to the ligand the ability to occupy a face of a coordination polyhedron, as is the case with other N_2S scorpionate ligands (see General Introduction). However, in the present case, the flexibility of the thioether group prevents the possibility to

achieve κ^3-N_2S coordination on Cu(I) (see Chapter 5). This became evident when testing the coordination properties of L* with Cu(I), and using as a supporting ligand triphenylphosphine. As revealed by the X-ray structural analysis, $[Cu(L^*)(PPh_3)]BF_4$ exhibits a polymeric structure in the solid state. The coordination of copper is distorted trigonal planar (Figure 6.1), attained through the N,N chelate ligand and the phosphorus atom of PPh_3.

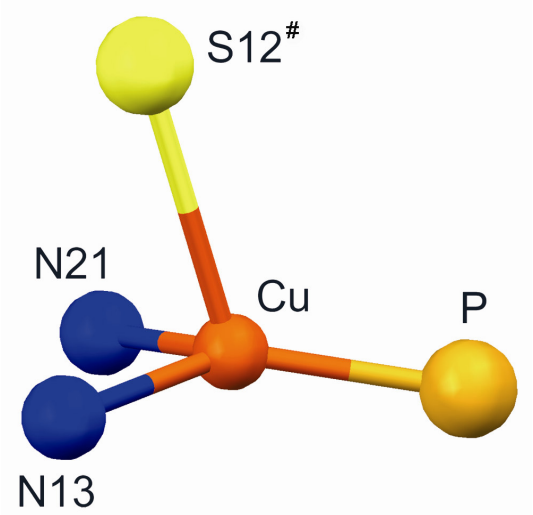

Figure 6.1 Cu(I) coordination sphere of $[Cu(L^*)(PPh_3)]BF_4$. Selected bond distances (Å) and angles (º): Cu-N(21) = 1.976(3), Cu-N(13) = 2.057(3), Cu-P = 2.184(1), Cu-S(12)$^{\#}$ = 2.917(1), N(21)-Cu-N(13) = 94.5(1), N(21)-Cu-P = 124.0(1), N(13)-Cu-P = 135.5(1), N(13)-Cu-S(12)$^{\#}$ = 79.7(1), N(21)-Cu-S(12)$^{\#}$ = 94.4(1), P-Cu-S(12)$^{\#}$ = 114.6(1). Symmetry code: $^{\#}$ = ½-x, ½+y, ½-z.

The Cu-N(21) bond distance (1.976(3) Å) is significantly shorter than the Cu-N(13) one (2.057(3) Å), suggesting the greater donor ability of the pyrazole ring with respect to the pyridine one. The N(21)-Cu-N(13) bite angle is of 94.5(1)º whereas the N-Cu-P angles are considerably greater than 120º. A very long contact with the S-thioether group from a second ligand (Cu-S(12)$^{\#}$ = 2.917(1) Å, $^{\#}$ = ½-x, ½+y, ½-z.) is responsible of the distortion from the ideal trigonal planar geometry. In agreement with this, the metal lies out of the plane defined by the N(21), N(13) and P atoms of 0.28 Å and is directed towards the sulfur atom. This long interaction is responsible for the generation of a chain, roughly aligned with the *b* crystallographic axis (Figure 6.2). It is worth noting that a single chain is homochiral (all the ligands and metals maintain the same configuration), but chains with opposite configurations are present in the structure, according to the fact that the compound crystallizes in a

centrosymmetric space group. The BF_4^- counterion is disordered in three positions that occupy a spherical site.

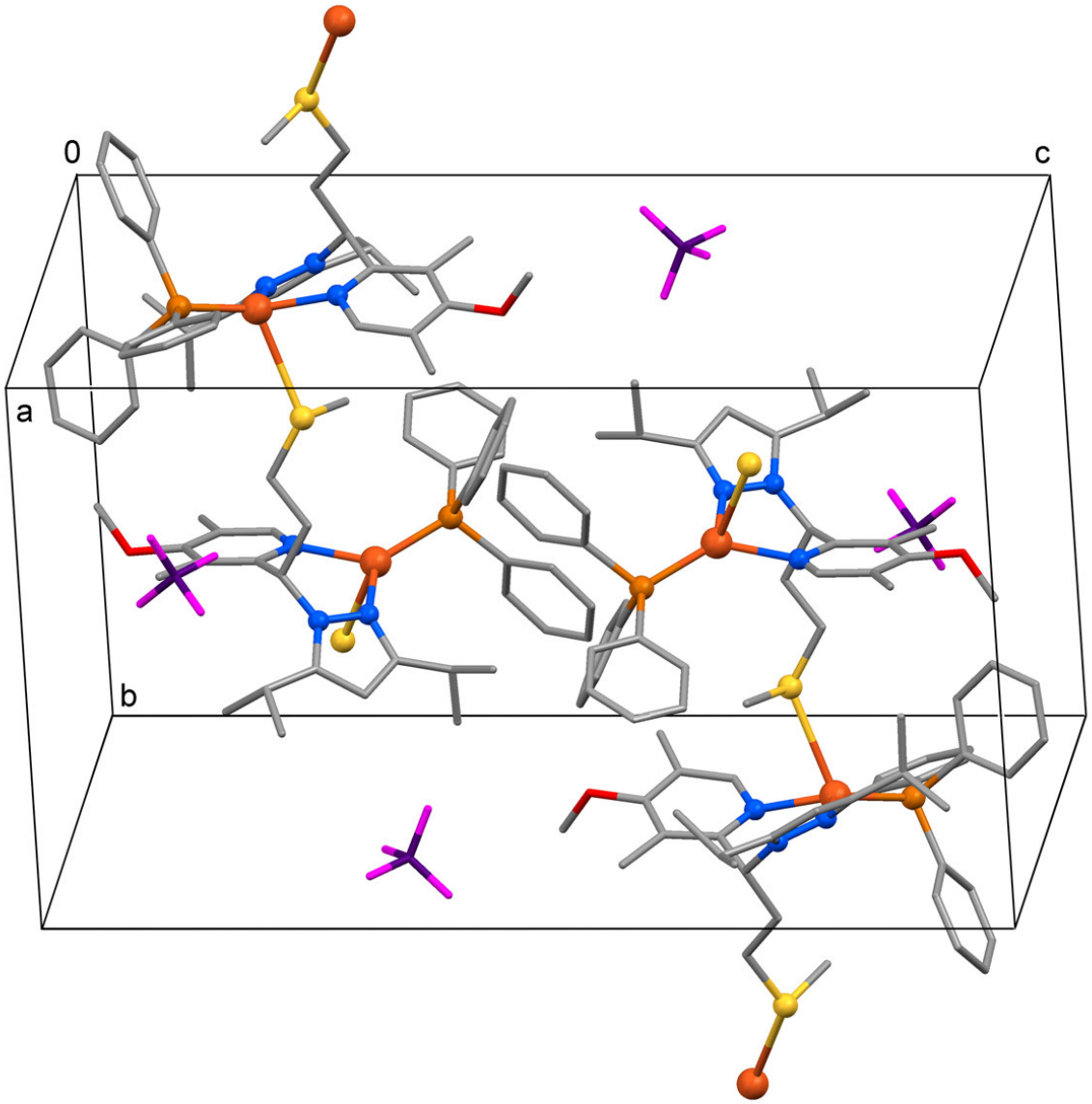

Figure 6.2 Crystal packing of $[Cu(L^*)(PPh_3)]BF_4$. The hydrogen atoms are omitted for clarity.

In order to investigate the nuclearity of the complex in solution, we performed ^{1}H-PGSE NMR experiments[271] in different deuterated solvents (acetonitrile, acetone and choloform; copper concentration = 10^{-2} M). The hydrodynamic volume (V_H) of the complex is as follow: 1070(30) Å^3 in acetonitrile, 1120(30) Å^3 in acetone and 1400(40) Å^3 in chloroform. The V_H values are slightly greater than the volume of an hypothetic mononuclear entity (V_0 ~950 Å^3) [289], so that the preservation of the polymeric framework in solution can be excluded. The discrepancy of the experimental V_H with V_0 could be the result of partial aggregation of the complex cations mediated by the BF_4^- anions (formation of ion pairs/ion quadruples).[257] The

V_H values diminish as increasing the dielectric constant of the solvent (acetonitrile > acetone > chloroform), pointing to a greater ion pair disruption in acetonitrile with respect to chloroform.

The emission properties of $[Cu(L^*)(PPh_3)]BF_4$ were investigated: the solid state fluorescence spectrum is reported in Figure 6.3.

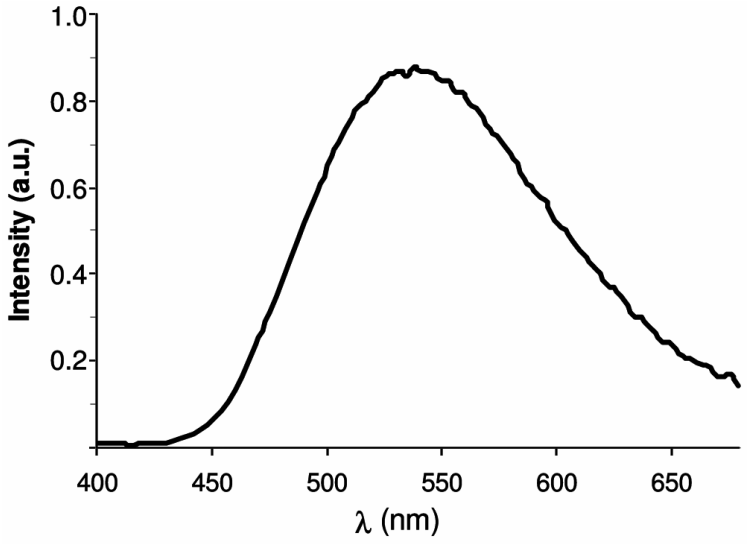

Figure 6.3 Solid state emission spectrum of $[Cu(L^*)(PPh_3)]BF_4$ recorded at room temperature(λ_{ex} = 370 nm).

The complex exhibits an emission band at 540 nm upon excitation at 370 nm. The excited state may be of metal-to-ligand charge transfer nature, in agreement with the presence of empty 3d phosphorous orbitals or empty antibonding P-C orbitals, and the d^{10} metal ion.[290,291] Another possibility resides in the copper to L* charge transfer due to the presence of heterocyclic aromatic systems.[292] On the opposite, there are no evidences of emitting properties in acetonitrile, acetone or chloroform solutions (10^{-4}-10^{-5} M). The fluorescence quenching in solution is probably due to the loss of structural rigidity, accountable with the fragmentation of the solid state polymer attested by PGSE NMR. In particular, in polar and coordinating solvents a contribution to the quenching could derive from a direct metal-solvent interaction, whereas the ion pair formation between the metal complex and the BF_4^- anions may be the prevalent relaxation pathway in non-polar solvents.[293]

6.1.1 *Experimenta*

Synthesis of L^2. A mixture of 2-Chloromethyl-4-methoxy-3,5-dimethylpyridine hydrochloride (1.45 g, 6.53 mmol), 3,5-Diisopropyl-1H-pyrazole (1.00 g, 6.57 mmol), NaOH (40% water, 15 ml), NBu_4OH (40% water, 10 drops) was heated at reflux for 3 h in 50 ml of toluene. The organic phase was separated, washed with brine (10 ml), dried with anhydrous Na_2SO_4 and filtered. The organic phase was then vacuum dried and the product collected (L^2, 1.37g, 4.55 mmol, 70%). IR (cm^{-1}): 2962s, 2927s, 2867m, 1588w, 1566m, 1540m, 1474m, 1436m, 1394m, 1381w. ^1H NMR (300 MHz, $CDCl_3$): δ 1.05 (d, 6H), 1.21 (d, 6H), 2.22 (d, 6H), 2.93 (m, 2H), 3.69 (s, 3H), 5.36 (s, 1H), 5.83 (s, 1H), 8.15 (s, 1H). Anal. calcd for $C_{18}H_{27}N_3O$ (301.21): C, 71.71; H, 9.03; N, 13.95; Found: C, 71.45; H, 9.49; N, 13.48.

Synthesis of L.* L^2 (1.37 g, 4.55 mmol) was dissolved in THF dry (80 ml) in a 250 ml Schlenk flask under nitrogen. The solution was cooled to -78°C and *n*-BuLi (1.6 M in hexanes, 3.13 ml, 5.00 mmol) was slowly added. The deep red solution was stirred for 40 min at -78°C. Ethylene sulfide (0.29 ml, 4.90 mmol) was then added and the solution was warmed to room temperature and stirred for 1.5 h. CH_3I (0.31 ml, 4.90 mmol) was then added and the solution was stirred for 1 h. The mixture was vacuum dried and then CH_2Cl_2 (30 ml) and water (20 ml) were added to the solid. The organic phase was separated, dried with anhydrous Na_2SO_4 and filtered. The organic phase was vacuum dried and the resulting red oil was purified by column cromatography (Silica gel, hexane/ethyl acetate 70:30) yielding a colorless oil (L*, 921 mg, 2.46 mmol, 54%). IR (cm^{-1}): 3128w, 3052w, 2958m, 2926m, 2865w, 1586m, 1579m, 1539m, 1480s, 1436s, 1258m, 1093s, 992m. ^1H NMR (300 MHz, $CDCl_3$): δ 0.89 (d, 3H), 1.05 (d, 3H), 1.23 (d, 6H), 2.11 (s, 3H), 2.14 (s, 3H), 2.26 (s, 3H), 2.72 (m, 3H), 2.95 (m, 2H), 3.71 (s, 3H), 5.76 (m, 1H), 5.84 (s, 1H), 8.26 (s, 1H). Anal. calcd for $C_{21}H_{33}N_3OS$ (375.23): C, 67.16; H, 8.86; N, 11.19; Found: C, 66.89; H, 8.58; N, 11.43.

Synthesis of [Cu(L)(PPh_3)]BF_4.* L* (0.667 g, 1.77 mmol) and PPh_3 (0.466 g, 1.77 mmol) were dissolved in acetonitrile (20 ml) under nitrogen. A solution of $[Cu(CH_3CN)_4]BF_4$ in 10 ml di acetonitrile was then added and the mixture was stirred for 1.5 h. The solution was vacuum dried and the solid was redissolved in diethyl ether. The mixture was filtered and vaccum dried yielding a pale yellow solid ($[Cu(L^*)(PPh_3)]BF_4$, 1.36 g, 1.73 mmol, 97%). ^1H NMR (300 MHz, $CDCl_3$): δ 0.75 (d, 3H), 1.01 (d, 3H), 1.24 (d, 3H), 1.41 (d, 3H), 1.97 (s, 3H), 2.03 (s, 3H), 2.53 (s, 3H), 2.85 (m, 1H), 3.27 (m, 1H), 2.75-2.47 (m, 4H), 3.89 (s, 3H),

5.97 (s, H), 6.17 (m, 1H), 7.47 (m, 15H), 7.60 (s, 1H). Anal. calcd for $C_{39}H_{48}BCuF_4N_3OPS$ (787.26): C, 59.43; H, 6.14; N, 5.33; Found: C, 59.78; H, 6.31; N, 5.02. Crystals suitable for X-ray analysis were obtained by stratification of pentane on a dichloromethane solution of the complex.

Data collection for the compound was performed on a Bruker Smart 1000 CCD diffractometer equipped with graphite-monochromated Mo-Ka radiation (λ = 0.71073 Å). Crystal data: $C_{39}H_{48}BCuF_4N_3OPS$, crystal dimensions: 0.25 x 0.15 x 0.10 mm^3, FW = 788.18, monoclinic, space group $P2_1/n$, a = 11.037(3) Å, b = 15.038(7) Å, c = 23.996(8) Å, β = 92.88(3), V = 3978(2) $Å^3$, Z = 4, Dc = 1.316 mg/m^3, μ = 0.694 mm^{-1}, F(000) = 1646, GOF = 1.002, $\rho_{max/min}$ = 0.541/-0.263 $eÅ^{-3}$. Data collection: 1.60 < θ < 26.10, 3036 observed reflections with I > 2σ(I) out of 7852 unique reflections (Rint = 0.1007). Final R_1 = 0.0595, wR_2 = 0.0631.

6.2 N_2S,S'-Heteroscorpionate Ligands Based on Bis(pyrazol-1-yl)methane and Complexation of Cu(I)

An alternative to the pyrazole-pyridine derivatives described in Chapter 5 as N_2S_2–tripodal ligands, consists in a bis(pyrazol-1-yl)methane platform (N_2-donor) functionalized with groups containing two S-thioether functions. This type of preorganized ligands could possibly encapsulate a copper(I) ion in way of yielding mononuclear tetrahedral complexes, wherein the ligand would control the topology of the metal. It is worth of note that, by using bis(pyrazolyl)methane derivatives, we overcome the complication of chirality, that was introduced in the case of pyrazole-pyridine scorpionates.

In this section we present the X-ray structures of binary complexes of Cu(I) with two new N_2S,S'-scorpionate ligands based on the bis(pyrazolyl)methane moiety, L^x and L^y. The synthetic route to the ligands is based on a reported method for the formation of dipyrazolylalkanes starting from bis(pyrazolyl) ketones and aliphatic or aromatic carbonyl compounds (Scheme 6.2).[196,294-296]

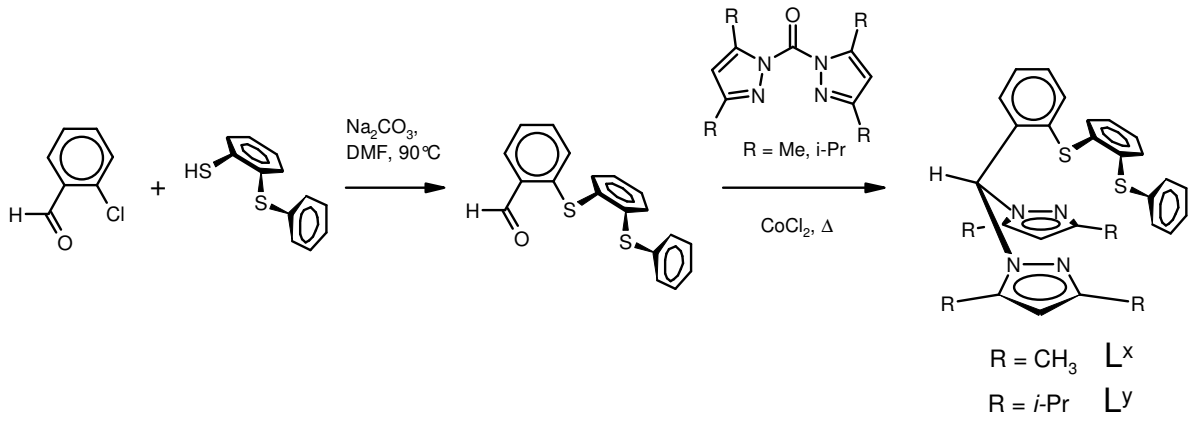

Scheme 6.2

The ligands L^x and L^y differ only for the nature of the substituents on the pyrazole rings, respectively methyl and more hindered isopropyl for L^x and L^y. The target would be to obtain κ^4-N_2S,S' coordination on Cu(I), but X-ray analysis disproves it. In fact, testing the coordination properties of L^x with Cu(I), the resulting complex crystallized from an acetonitrile:water mixture presents the structure reported in Figure 6.4. It is a dinuclear compound with stoichiometry $[Cu_2(L^x)_2(CH_3CN)](BF_4)_2$ (**1a**); thus, the ligand is not successful in imposing a tetrahedral geometry on the metal center to give a mononuclear compound. The lack of stereochemical control from L^x is attested by: (1) the dinuclear

structure of the complex, (2) the coordination of a solvent molecule (CH_3CN) to one of the copper ions, and (3) the absence in the coordination sphere of Cu(I) of a potentially chelating S,S' group (S(18), S(19)). The former Cu(I) ion, namely Cu(1), is located in a trigonal planar environment, bound by three nitrogen atoms, two from a ligand L^x and one from acetonitrile, the latter presenting the shortest Cu-N distance (1.834(6) Å). The other copper center is approximately tetrahedral, bound by two N-pyrazole atoms from a second ligand and by two S-thioether groups, belonging to the former bridging L^x.

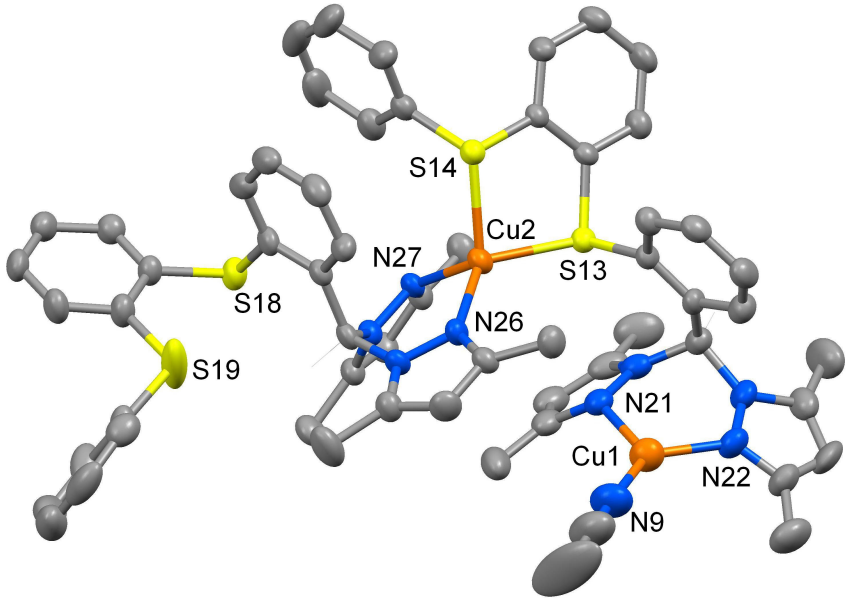

Figure 6.4 Molecular drawing of $[Cu_2(L^x)_2(CH_3CN)](BF_4)_2 \cdot 1.5CH_3OH$ (**1a**) at the 30% thermal ellipsoids probability level. The BF_4^- counterions and the hydrogen atoms (except for the methinic ones) are omitted for clarity. Selected bond distances (Å): Cu(1)-N(9) = 1.834(6), Cu(1)-N(21) = 2.010(5), Cu(1)-N(22) = 1.953(5), Cu(2)-N(26) = 2.024(4), Cu(2)-N(27) = 2.066(4), Cu(2)-S(13) = 2.321(2), Cu(2)-S(14) = 2.339(2).

Regarding the complexation of Cu(I) with L^y, it led to the crystallization of a coordination polymer,[285] corresponding to $[Cu(L^y)]_n(BF_4)_n$ (**2a**) (Figure 6.5). Two symmetrically non-equivalent Cu centers, Cu(1) and Cu(2), alternate in an infinite chain, which is hold together by strong Cu-S interactions (2.179(2)-2.186(2) Å distances). Both the Cu ions are trigonal planar, bound by two nitrogen atoms from pyrazolyl groups of a ligand and by a sulfur atom from an aryl-thioether group of an adiacent ligand. It is worth of note that only terminal S-thioethers, namely S(2) ans S(4), are bound to copper, whereas S(1) and S(2) are not coordinated.

In conclusion, the new heteroscorpionate ligands L^x and L^y here presented are unable to impose a κ^4-N_2S_2 coordination on Cu(I), thus giving mononuclear complexes; instead, the isolated compounds exhibit polynuclear structures. The reason for this may be the inability of the ligands to generate a proper tetrahedral coordination arrangement around Cu(I).

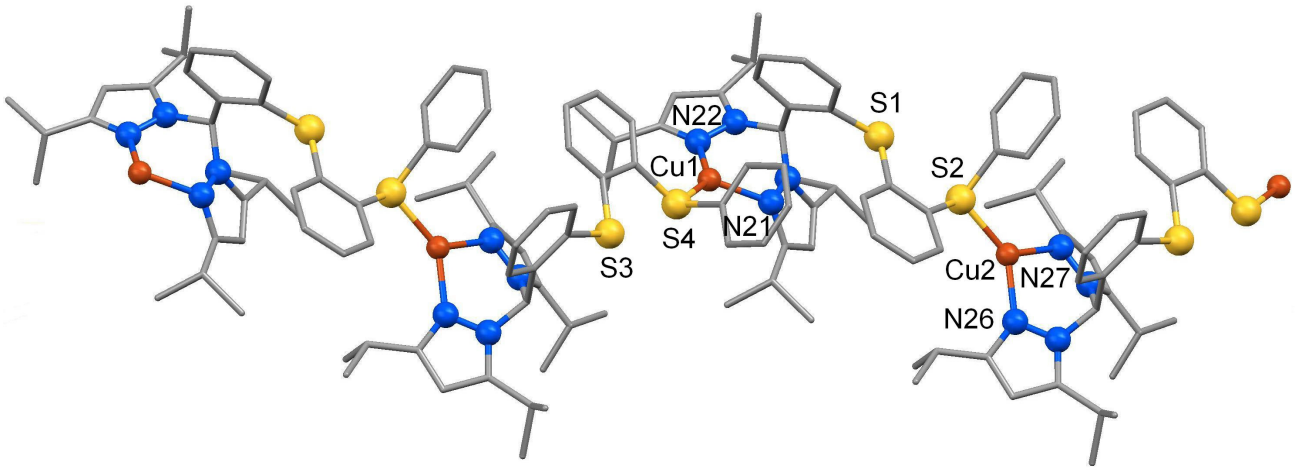

Figure 6.5 Molecular drawing of $[Cu(L^y)]_n(BF_4)_n$ (**2a**). The BF_4^- counterions and the hydrogen atoms are omitted for clarity. Selected bond distances (Å): Selected bond distances (Å): Cu(1)-N(21) = 2.028(5), Cu(1)-N(22) = 2.005(4), Cu(1)-S(4) = 2.179(2), Cu(2)-N(26) = 1.994(4), Cu(2)-N(27) = 2.014(4), Cu(2)-S(2) = 2.186(2).

6.2.1 Experimental

Synthesis of 2-(phenylthio)benzenethiol (modified from a reported procedure).[297] A solution of thiophenol (4 ml, 38.95 mmol) in cyclohexane (10 ml) was added to a solution of *n*-BuLi (1.6 M in hexane, 54 ml, 86.4 mmol) and N,N,N',N'-tetramethylethylenediamine (TMEDA, 13 ml, 86.70 mmol) in cyclohexane (60 ml) at 0 °C under nitrogen. The reaction was stirred for 30 min at 0 °C and for 6 h at room temperature. A solution of diphenyl disulfide (9.5 g, 43.57 mmol) in cyclohexane (90 ml) was added at 0 °C. After being stirred for 30 min at 0 °C, the mixture was stirred overnight at room temperature and quenched with 15% HCl(aq) (175 ml). The organic and water layers were separated and the latter was extracted with diethyl ether (3 x 50 ml).The organic phases were mixed and dried with anhydrous Na_2SO_4. Solvents were removed under vacuum. The solid was recrystallized from a CH_2Cl_2:EtOH mixture, yielding a colorless crystalline solid (4 g, 18.35 mmol, 47%). ^{1}H NMR (300 MHz, $CDCl_3$): δ 4.29 (s,

1H, SH), 7.1-7.6 (m, 9H, CH). Anal. calcd for $C_{12}H_{10}S_2$ (218.02): C, 66.01; H, 4.62. Found: C, 66.10; H, 4.44.

Synthesis of 2-(2-(phenylthio)phenylthio)benzaldehyde (analogous to a reported procedure for preparation of 2-(phenylthio)benzaldehyde).[298] To a stirred solution of 2-(phenylthio)benzenethiol (2 g, 9.17 mmol) and anhydrous Na_2CO_3 (1.3 g) in dry DMF (5 ml) under nitrogen at 90 °C, 2-chlorobenzaldehyde (0.9 ml, 7.99 mmol) was slowly added. The mixture was stirred at 90 °C overnight. After cooling, the reaction mixture was poured into water (50 ml) and extracted with diethyl ether (50 ml). The extract was washed with water (2 x 50 ml), dried with anhydrous Na_2SO_4, and concentrated under vacuum. The resulting oil was triturated with hexane in an ultrasoud bath for 20 min, filtered and dried under vacuum to afford a pale white solid (1.85 g, 5.74 mmol, 72%). ^{1}H NMR (300 MHz, $CDCl_3$): δ 7.11-7.51 (m, 12H, CH ph), 7.94 (d, J = 7.5 Hz, 1H, CH ph), 10.39 (s, 1H, CHO). Anal. calcd for $C_{19}H_{14}OS_2$ (322.05): C, 70.77; H, 4.38. Found: C, 70.53; H, 4.51.

Synthesis of 1,1'-((2-(2-(phenylthio)phenylthio)phenyl)methylene)bis(3,5-dimethyl-1H-pyrazole) (L^x). 2-(2-(phenylthio)phenylthio)benzaldehyde (900 mg, 2.79 mmol) and $CoCl_2 \cdot 6H_2O$ (5 mg, 0.021 mmol) were added to bis(3,5-dimethyl-1H-pyrazol-1-yl)chetone[299] (670 mg, 3.07 mmol) in a Schlenk flask under nitrogen. The mixture was heated at 90 °C and vigorously stirred until it set, during which time the mixture turned dark blue and evolution of CO_2 was observed. After 2 h the mixture was cooled to room temperature before $CHCl_3$ (50 ml) and water (50 ml) were added and the flask shaken until discoloration of the organic layer. The latter was separated and washed with water (2 x 50 ml), dried with anhydrous Na_2SO_4 and concentrated under vacuum to afford a pale oil, which was purified by purified by column cromatography (Silica gel, gradient of elution from hexane/ethyl acetate 18:1 to pure ethyl acetate). The resulting oil was triturated with hexane in an ultrasound bath, filtered and dried under vacuum, affording a white powder (L^x, 790 mg, 1.59 mmol, 57%). ^{1}H NMR (300 MHz, $CDCl_3$): δ 2.11 (s, 6H, CH_3), 2.20 (s, 6H, CH_3), 5.82 (s, 2H, CH pz), 6.99-7.14 (m, 5H, CH ph), 7.31 (m, 8H, CH ph), 7.86 (s, 1H, CH bridge). Anal. calcd for $C_{29}H_{28}N_4S_2$ (496.18): C, 70.13; H, 5.68; N, 11.28. Found: C, 69.96; H, 5.79; N, 11.36.

Synthesis of 1,1'-((2-(2-(phenylthio)phenylthio)phenyl)methylene)bis(3,5-diisopropyl-1H-pyrazole) (L^y). 2-(2-(phenylthio)phenylthio)benzaldehyde (770 mg, 2.39 mmol) and $CoCl_2 \cdot 6H_2O$ (4 mg, 0.017 mmol) were added to bis(3,5-diisopropyl-1H-pyrazol-1-

yl)chetone[299] (910 mg, 2.75 mmol) in a Schlenk flask under nitrogen. The mixture was heated at 150 °C and vigorously stirred until it set, during which time the mixture turned dark green. After 4 h the mixture was cooled to room temperature before $CHCl_3$ (50 ml) and water (50 ml) were added and the flask shaken until discoloration of the organic layer. The latter was separated and washed with water (2 x 50 ml), dried with anhydrous Na_2SO_4 and concentrated under vacuum to afford a dark oil, which was purified by purified by column cromatography (Silica gel, hexane:ethyl acetate 9:1). The resulting oil was recrystallized from hexane (2-3 ml) at room temperature, yielding a crystalline white solid (L^y, 640 mg, 1.05 mmol, 44%). ^{1}H NMR (300 MHz, $CDCl_3$): δ 0.92 (d, J = 6.9 Hz, 6H, CH_3), 0.99 (d, J = 6.9 Hz, 6H, CH_3), 1.20 (d, J = 6.9 Hz, 12H, CH_3), 2.91 (hept, J = 6.9 Hz, 2H, CH *i*-Pr), 3.15 (hept, J = 6.9 Hz, 2H, CH *i*-Pr), 5.91 (s, 2H, CH pz), 6.95 (m, 1H, CH ph), 7.08 (m, 4H, CH ph), 7.19-7.32 (m, 8H, CH ph), 8.00 (s, 1H, CH bridge). Anal. calcd for $C_{37}H_{44}N_4S_2$ (608.30): C, 72.98; H, 7.28; N, 9.20. Found: C, 73.07; H, 7.11; N, 9.12.

Synthesis of $[Cu_2(L^x)_2(CH_3CN)](BF_4)_2$ $1.5CH_3OH$ ***(1a)***. A mixture of L^x (100 mg, 0.20 mmol) and $[Cu(CH_3CN)_4]BF_4$ (65 mg, 0.21 mmol) were dissolved in CH_2Cl_2 (5 ml) under nitrogen. After stirring for 1 h, a white solid was precipitated with hexane (30 ml), filtered and dried under vacuum (**1**, 130 mg). ^{1}H NMR (300 MHz, CD_3CN): δ 2.18 (s, 6H, CH_3), 2.41 (s, 6H, CH_3), 6.03 (s, 2H, CH pz), 6.60 (d, 1H, J = 7.5 Hz, CH ph), 7.07 (m, 1H, CH ph), 7.18-7.31 (m, 11H, CH ph), 7.65 (s, 1H, CH bridge). Crystals suitable for X-ray analysis (**1a**) were obtained by stratification of pentane on a methanolic solution of **1** under nitrogen. Anal. calcd for $C_{61.50}H_{65}BCu_2F_4N_4S_2$ (1136.33): C, 64.95; H, 5.76; N, 4.93; Found: C, 64.78; H, 5.87; N, 5.00.

Synthesis of $[Cu(L^y)]_n(BF_4)_n$ ***(2a)***. A mixture of L^y (136 mg, 0.22 mmol) and $[Cu(CH_3CN)_4]BF_4$ (74 mg, 0.23 mmol) were dissolved in acetone (10 ml) under nitrogen. After stirring for 1/2 h, the solvent was removed under vacuum, affording a white solid (**2**, 145 mg, 0.19 mmol, 86%). ^{1}H NMR (300 MHz, CD_3CN): δ 1.16 (t, J = 6.3 Hz, 12H, CH_3), 1.25 (s br, 12H, CH_3), 3.08 (s br, 2H, CH *i*-Pr), 3.33 (m, CH *i*-Pr), 6.26 (s, 2H, CH pz), 6.48 (s br, 1H, CH ph), 7.12 (m, 2H, CH ph), 7.25-7.41 (m, 10H, CH ph), 7.85 (s, 1H, CH bridge). Crystals suitable for X-ray analysis (**2a**) were obtained by stratification of diethyl ether on a methanolic solution of **2** under nitrogen. Anal. calcd for $C_{37}H_{44}BF_4CuN_4S_2$ (758.23): C, 58.56; H, 5.85; N, 7.39; Found: C, 58.43; H, 5.89; N, 7.61.

Data collection for the compounds **1a** and **2a** was performed on a Bruker Smart 1000 CCD diffractometer equipped with graphite-monochromated Mo-Ka radiation (λ = 0.71073 Å). Crystal data for **1a**: $C_{61.50}H_{65}BCu_2F_4N_4S_2$, crystal dimensions: 0.15 x 0.10 x 0.05 mm^3, FW = 1383.17, monoclinic, space group $P2_1/n$, a = 12.017(8) Å, b = 14.253(7) Å, c = 38.495(9) Å, β = 90.45(3), V = 6593(6) $Å^3$, Z = 4, D_c = 1.393 mg/m^3, μ = 0.842 mm^{-1}, F(000) = 2852, GOF = 1.003, $\rho_{max/min}$ = 0.706/-0.510 $eÅ^{-3}$. Data collection: 1.06 < θ < 26.31, 13262 observed reflections with I > 2σ(I) out of 62809 unique reflections (Rint = 0.1140). Final R_1 = 0.0598, wR_2 = 0.1012.

Crystal data for **2a**: $C_{37}H_{44}BF_4CuN_4S_2$, crystal dimensions: 0.12 x 0.10 x 0.05 mm^3, triclinic, space group P-1, a = 17.791(5) Å, b = 18.127(7) Å, c = 25.875(9) Å, α = 94.87(3), β = 95.10(3), γ = 92.61(3), V = 8269.7(7) $Å^3$, Z = 2, D_c = 1.472 mg/m^3, μ = 0.74 mm^{-1}, F(000) = 3800. Final R_1 = 0.0915. Partial structure solution.

Appendix

Appendix 1

Least-square equation for the treatment of the slow exchange equilibrium: $[Cu(Tr^{Mes,Me})]_2 + 2py \rightleftharpoons 2[(py)Cu(Tr^{Mes,Me})]$

Molar fraction χ of $[Cu(L)]_2$ referred to total dimer concentration (C_D) can be calculated from integrals of $[Cu(L)]_2$ and [(py)Cu(L)] by the following equation (slow exchange condition):

$$\chi_{[Cu(L)]_2} = \frac{C_{[Cu(L)]_2}}{C_D} = \frac{I_{[Cu(L)]_2}}{I_{[Cu(L)]_2} + I_{[(py)Cu(L)]}}$$

thus

$$C_{[CuL]_2} = \frac{I_{[CuL]_2}}{I_{[CuL]_2} + I_{[(py)Cu(L)]}} C_D \qquad (A1)$$

where $C_{[Cu(L)]2}$ and C_D are the free and total dimer concentration, respectively, and $I_{[Cu(L)]2}$ and $I_{[(py)Cu(L)]}$ are the integrals of peaks corresponding to the same functional group in the two complexes. From the mass balance and the definition of *K* as equilibrium constant for the equilibrium $[Cu(L)]_2 + 2\ py \rightleftharpoons 2[(py)Cu(L)]$, Equation A2 is derived:

$$K_f = \frac{4\left(C_D - C_{[CuL]_2}\right)^2}{C_{[CuL]_2}\left(C_{Py} - 2\left(C_D - C_{[CuL]_2}\right)\right)^2} \qquad (A2)$$

By insertion of A1 in A2, Equation A3 is derived, representing the regression model for the experimental data:

$$\begin{aligned} &4K_f\left(\frac{I_{[CuL]_2}}{I_{[CuL]_2} + I_{[(py)Cu(L)]}} C_D\right)^3 - 4\left(K\left(2C_D - C_{py}\right) + 1\right)\left(\frac{I_{[CuL]_2}}{I_{[CuL]_2} + I_{[(py)Cu(L)]}} C_D\right)^2 + \\ &+ \left(K\left(4C_D{}^2 - 4C_D C_{py} + C_{py}{}^2\right) - 8C_D\right)\left(\frac{I_{[CuL]_2}}{I_{[CuL]_2} + I_{[(py)Cu(L)]}} C_D\right) + 4C_D{}^2 = 0 \end{aligned} \qquad (A3)$$

$I_{[Cu(L)]2}$ = sum of the integrals of the *z* and *v* mesityl protons (6), $I_{[(py)Cu(L)]}$ = sum of the integrals of the *z*' and *v*' mesityl protons (6).

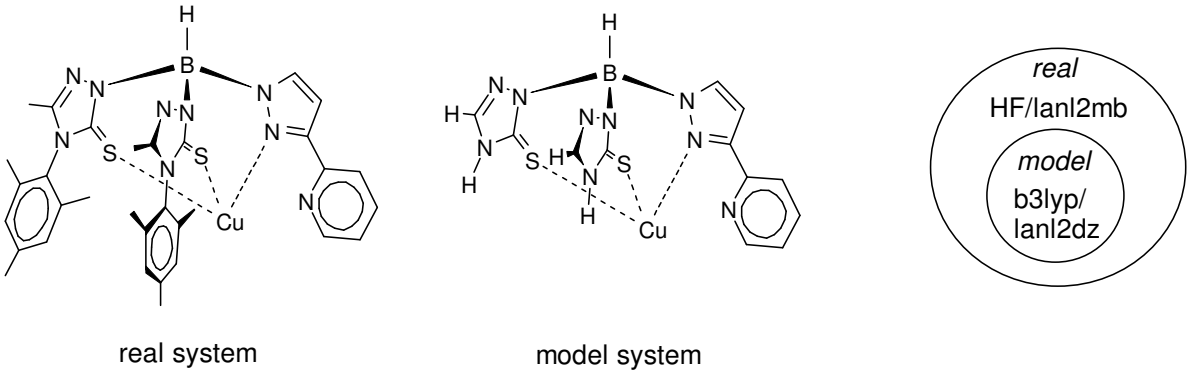

Figure A1. ONIOM partitioning scheme of the $CuBr^{Mes,Me}pz^{o\text{-}Py}$ fragment used for the geometry optimization of the isomers of **3**.

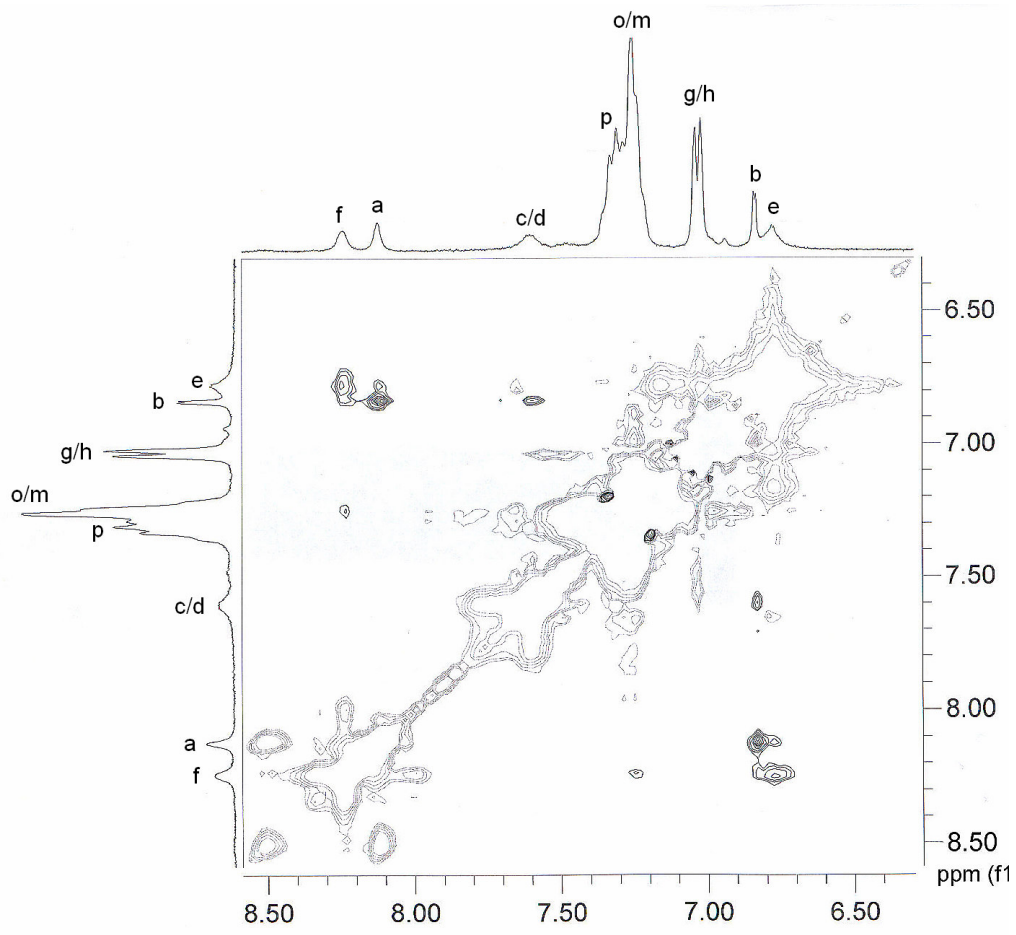

Figure A2. NOESY NMR spectrum of **3** at 300 K in $CDCl_3$. Solid lines denotes negative contours, dashed lines denotes positive cross-peaks.

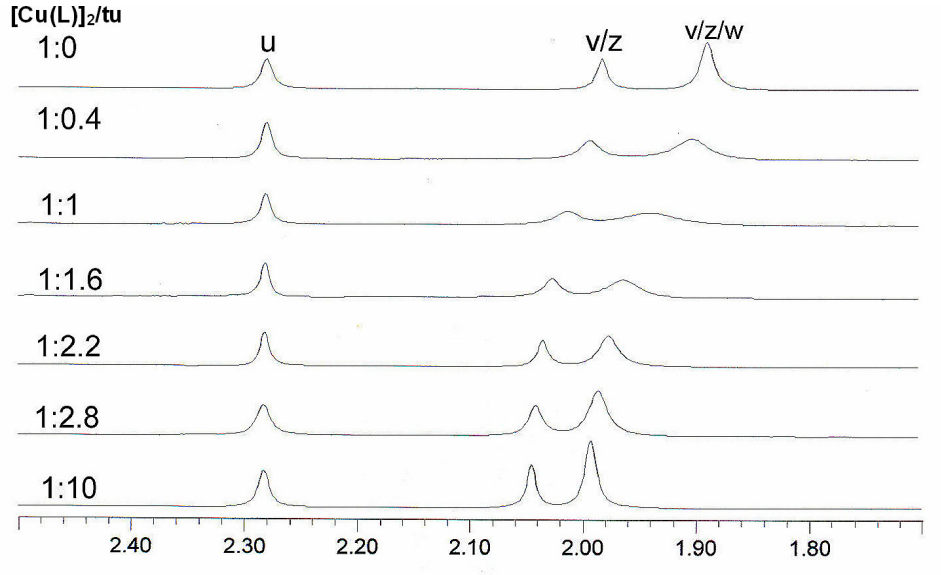

Figure A3. Stacking plot of the ^{1}H NMR spectra of [Cu(Tr^{Mes,Me})]$_2$ titrated with tu in $CD_3OD/CDCl_3$ 1:1 (u, v and z = *para* and *ortho* mesityl protons, w = methyl proton of triazoline).

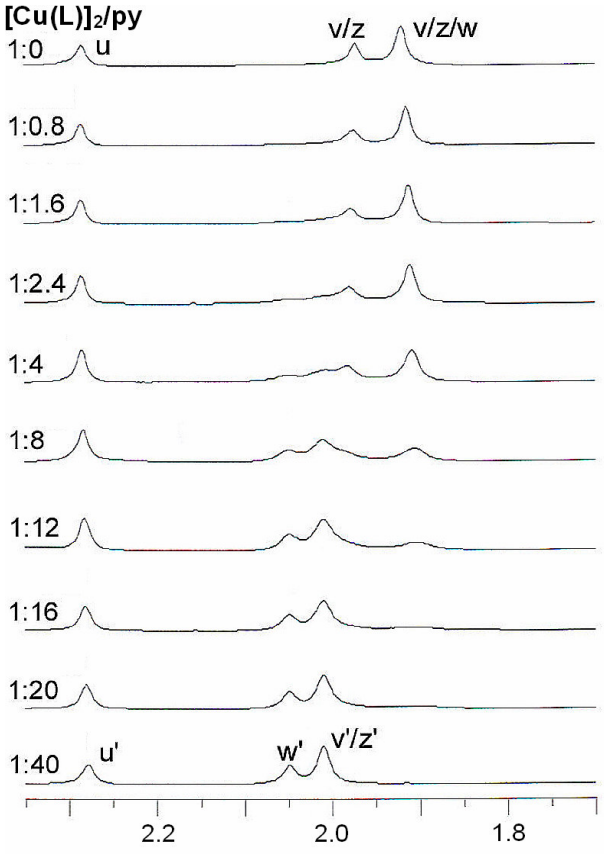

Figure A4. Stacking plot of the ^{1}H NMR spectra of [Cu(Tr^{Mes,Me})]$_2$ titrated with py in $CDCl_3$. (u, v and z = *para* and *ortho* mesityl protons, w = methyl proton of triazoline, ‘ indicates the adduct).

Table A1. Calculated bond lengths (Å) and angles (°) for **3a-b**.

		3a	
Cu-S(11)	2.425	B-H	1.204
Cu-S(12)	2.387	C(11)-S(11)	1.708
Cu-H	1.915	C(12)-S(12)	1.709
Cu-P	2.332		
S(11)-Cu-S(12)	114.70	S(12)-Cu-H	88.90
S(11)-Cu-H	90.22	S(11)-Cu-P	115.56
S(12)-Cu-P	126.06	H-Cu-P	109.07
		3b	
Cu-S(11)	2.446	B-H	1.194
Cu-S(12)	2.567	C(11)-S(11)	1.708
Cu-N(23)	2.079	C(12)-S(12)	1.701
Cu-P	2.356	Cu-N(33)	3.320
S(11)-Cu-S(12)	106.79	S(12)-Cu-N(23)	91.92
S(11)-Cu-N(23)	107.44	S(11)-Cu-P	107.88
S(12)-Cu-P	102.33	N(23)-Cu-P	135.85
		3c	
Cu-S(11)	2.505	B-H	1.193
Cu-S(12)	2.447	C(11)-S(11)	1.704
Cu-N(23)	2.092	C(12)-S(12)	1.706
Cu-P	2.363		
S(11)-Cu-S(12)	105.42	S(12)-Cu-N(23)	109.14
S(11)-Cu-N(23)	94.91	S(11)-Cu-P	104.54
S(12)-Cu-P	105.03	N(23)-Cu-P	134.15

Appendix 2

Semi-reaction rates r_{ij} and rate constants k_{ij} determination

For the equilibria (a) and (b) in Scheme 3.6, the following equations can be written:

(A4 a) $$\frac{\partial M_{y^{\#}(z^{\#})}}{\partial t} = k^{ex}_{yy^{\#}(zz^{\#})} M_{y(z)} \qquad \frac{\partial M_{y(z)}}{\partial t} = k^{ex}_{y^{\#}y(z^{\#}z)} M_{y^{\#}(z^{\#})}$$

(A4 b) $$\frac{\partial M_{y(z)}}{\partial t} = k^{ex}_{xy(xz)} M_{x} \qquad \frac{\partial M_{x}}{\partial t} = k^{ex}_{yx(zx)} M_{y(z)}$$

where M_x, M_y, M_z, $M_y^{\#}$ and $M_z^{\#}$ are the magnetizations of the corresponding exchanging species (X, $Y_{1\text{-}3}$ and $Z_{1\text{-}3}$). According to:

$$M_x = \eta[X]; \quad M_{y(z)} = 2\eta[Q]\chi; \quad M_{y^{\#}(z^{\#})} = 2\eta[Q]\chi^{\#}$$

where [*X*] is the equilibrium concentration of X, η is an unknown constant, χ and $\chi^{\#}$ are molar fractions of the different $[Zn(LOH)_2]^{2+}$ isomers and [Q] is the total equilibrium concentration of the $[Zn(LOH)_2]^{2+}$ isomers: $[Q] = \sum_{i=1}^{3}[Y_i] + \sum_{j=1}^{3}[Z_j]$ (the factor 2 in $M_{y(z)}$ formula is due to the presence of two ligands for each species), the semi-reaction rates r_{ij} can be determined (Table A2).

Table A2 Semi-reaction rates r_{ij} ($M \cdot s^{-1}$, i = column, j = row) calculated according to the mechanisms proposed in Scheme 3.6.

	X	**Y_1**	**Z_1**	**Z_2**	**Y_2**	**Z_3**	**Y_3**
X		0.00007(2)	0.00016(3)	0.00010(5)	0.00014(4)	0.00013(3)	0.00018(6)
Y_1	0.00007(2)				0.0012(1)		0.0003(2)
Z_1	0.00016(3)			0.0041(2)		0.0037(5)	
Z_2	0.00010(5)		0.0041(2)			0.0002(2)	
Y_2	0.00014(4)	0.0012(1)					0.006(1)
Z_3	0.00013(3)		0.0037(5)	0.0002(2)			
Y_3	0.00018(6)	0.0003(1)			0.006(1)		

(A5 a) $$r_{yy^{\#}(zz^{\#})} = \frac{\partial[Q]\chi^{\#}}{\partial t} = k^{ex}_{yy^{\#}(zz^{\#})}[Q]\chi \qquad r_{y^{\#}y(z^{\#}z)} = \frac{\partial[Q]\chi}{\partial t} = k^{ex}_{y^{\#}y(z^{\#}z)}[Q]\chi^{\#}$$

(A5 b) $$r_{xy(xz)} = \frac{\partial[Q]\chi}{\partial t} = \frac{1}{2}k^{ex}_{xy(xz)}[X] \qquad r_{yx(zx)} = \frac{1}{2}\frac{\partial[X]}{\partial t} = k^{ex}_{yx(zx)}[Q]\chi$$

Supposing a first-order mechanism for (a) and a second-order one for (b), the semi-reaction rates can be defined as follows:

(A6 a) $$r_{yy^{\#}(zz^{\#})} = k_{yy^{\#}(zz^{\#})}[Q]\chi \qquad r_{y^{\#}y(z^{\#}z)} = k_{y^{\#}y(z^{\#}z)}[Q]\chi^{\#}$$

(A6 b) $$r_{xy(xz)} = k_{xy(xz)}[X]^2 \qquad r_{yx(zx)} = k_{yx(zx)}[(ZnCl_4^{2-})][Q]\chi$$

By subtracting (A5 a) to the corresponding (A6 a), and (A5 b) to the corresponding (A6 b), the rate constants are thus obtained, Table A3:

(A7 a) $$k_{yy^{\#}(zz^{\#})} = k^{ex}_{yy^{\#}(zz^{\#})} \qquad k_{y^{\#}y(z^{\#}z)} = k^{ex}_{y^{\#}y(z^{\#}z)}$$

(A7 b) $$k_{xy(xz)} = \frac{k^{ex}_{xy(xz)}}{2[X]} \qquad k_{yx(zx)} = \frac{k^{ex}_{yx(zx)}}{[(ZnCl_4^{2-})]}$$

Table A3 Matrix of rate constants k_{ij} (i = column, j = row) between the different Zn^{2+}/LOH species in CD_3OD (1A, 2A-E, see Figure 3.7) calculated according to the mechanism proposed in Scheme 3.6. The corresponding X, Y_{1-3} and Z_{1-3} exchanging-sites (NMR signals) are reported in the same order of the EXSY spectrum (Figure 3.6).

	X	**Y_1**	**Z_1**	**Z_2**	**Y_2**	**Z_3**	**Y_3**	
X		1.7(5)	3.7(7)	3(1)	4(1)	4(1)	5(2)	← (M s^{-1})
Y_1	12(4)		-	-	0.48(4)	-	0.14(7)	
Z_1	29(6)	-		1.8(1)	-	1.7(2)	-	
Z_2	19(6)	-	1.4(1)		-	0.12(9)	-	
Y_2	25(7)	0.45(2)	-	-		-	2.7(3)	
Z_3	25(5)	-	1.3(2)	0.11(8)	-		-	
Y_3	32(10)	0.13(6)	-	-	2.6(3)	-		
	↑ (M s^{-1})							(s^{-1})

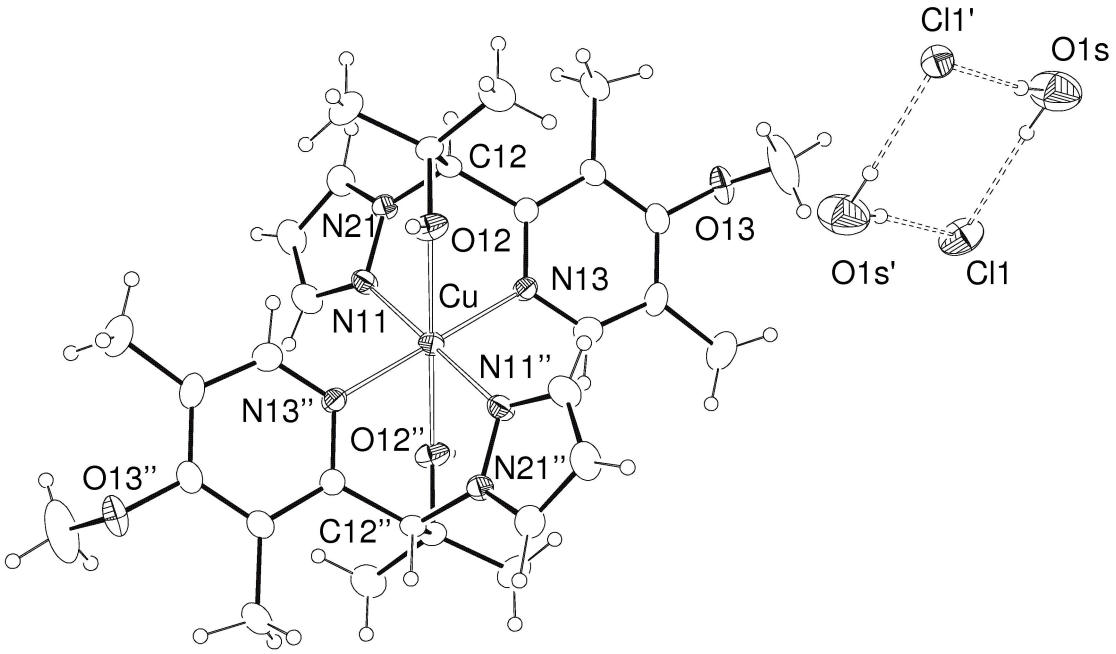

Figure A5 Ortep drawing of $[Cu(LOH)_2]Cl_2 \cdot 2H_2O$ (**4a**) at the 30% thermal ellipsoids probability level. ' = -x; 1-y; 1-z; '' = -x; -y; -z.

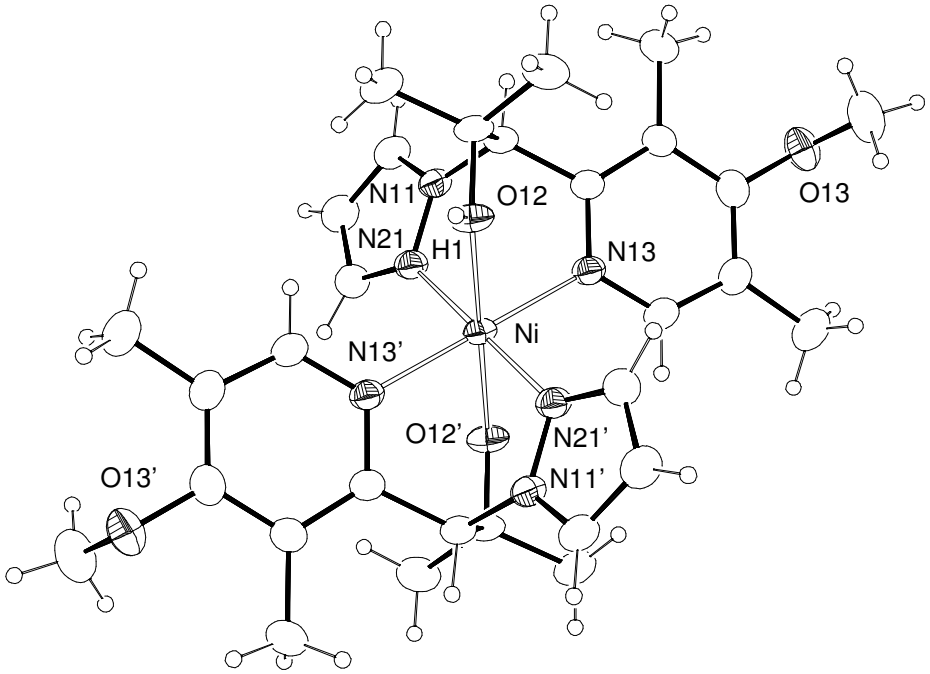

Figure A6 Ortep drawing of $[Ni(LOH)_2]Cl_2 \cdot 3MeOH$ (**2a**). The cation complex $[Ni(LOH)_2]^{2+}$ is reported. ' = -x, -y, -z.

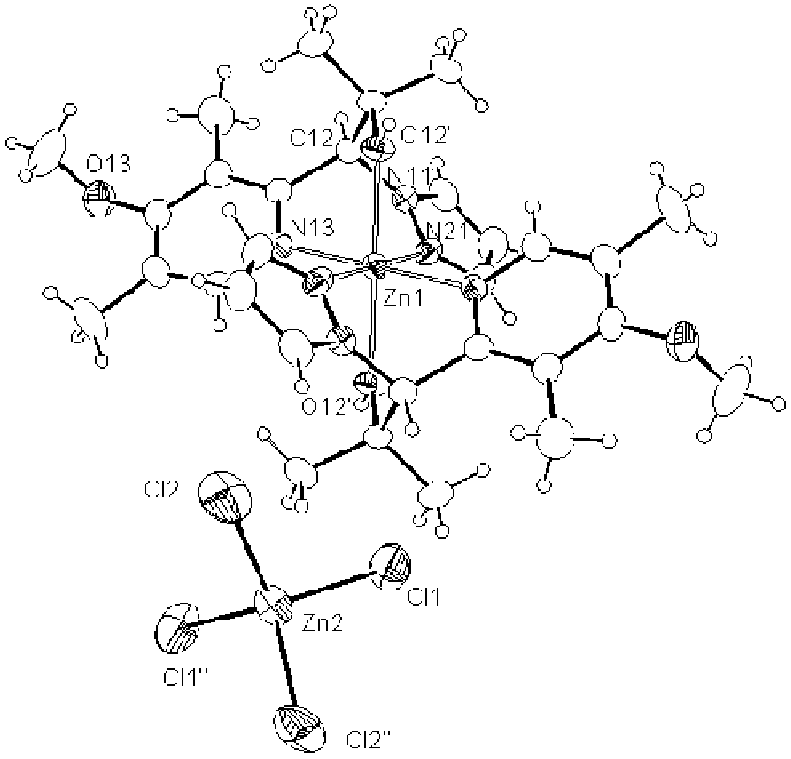

Figure A7 Ortep drawing of $[Zn(LOH)_2]ZnCl_4 \cdot 2(CH_3CN)$ (**5a**). Crystallization solvent molecules are removed for clarity. ‘ = ½-x; ½-y; -z, ‘’ = -x; y; ½-z.

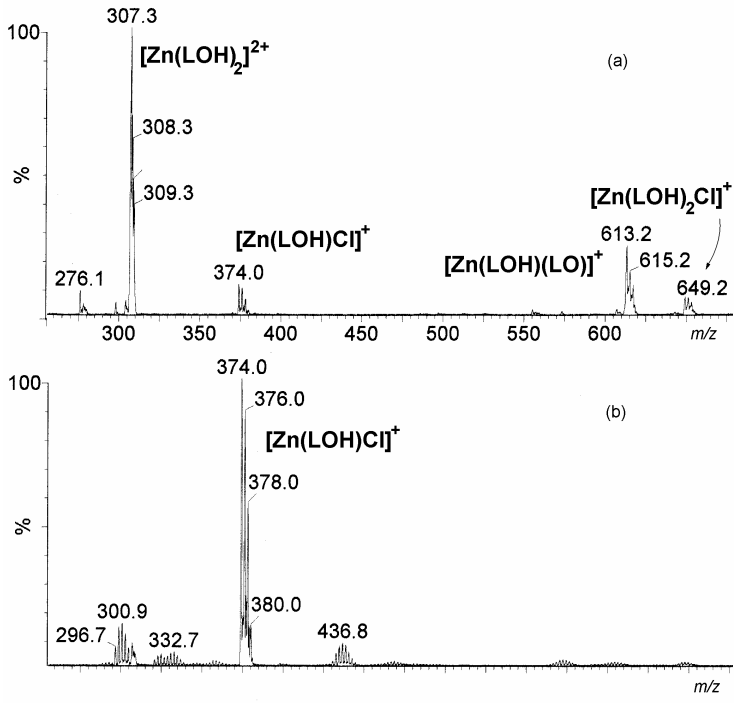

Figure A8 ESI-Mass spectra of the Zn^{2+}/LOH system in 1:1 ratio (a), and in 1:~10 ratio (b) in methanol.

Appendix 3

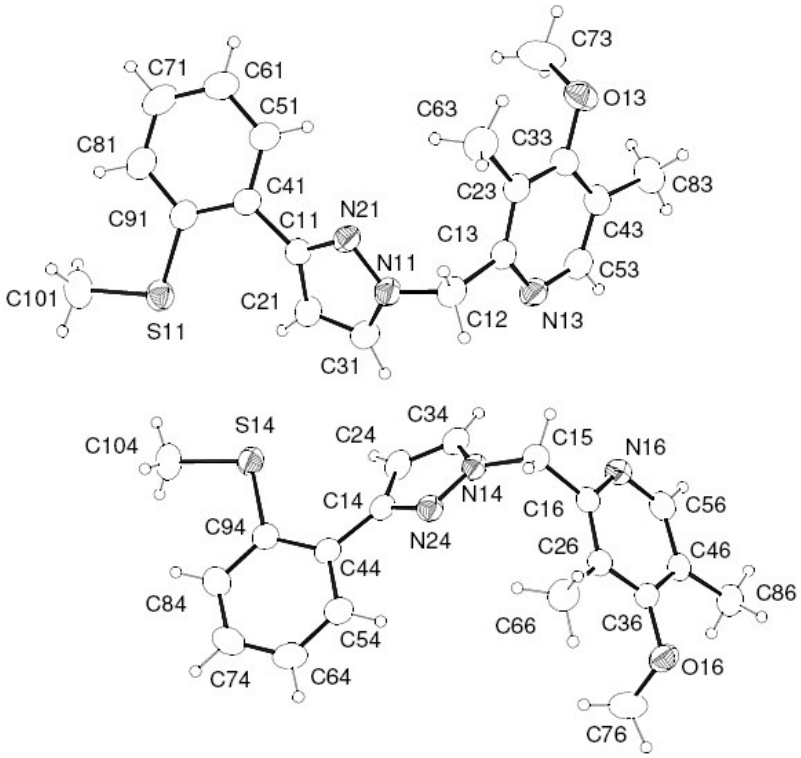

Figure A9 Ortep drawing of the ligand L^1 at the 30% thermal ellipsoids probability level. The asymmetric unit is represented by two independent molecules roughly related by a *pseudo* plane of symmetry. The molecules differs by the value of the torsion angle [N24-N14-C15-C16] = 95°, and [N21-N11-C12-C13] = -82°.

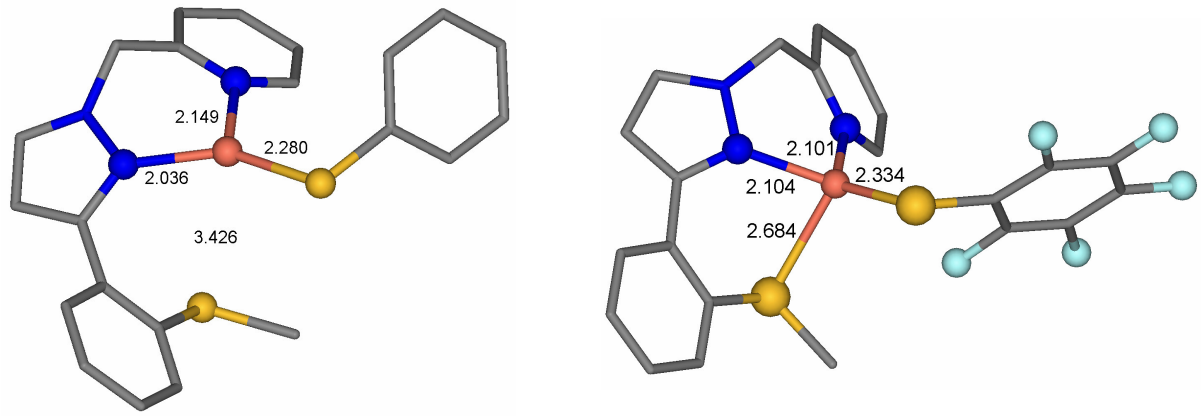

Figure A10 Comparison between the DFT optimized structures (B3LYP/lanl2dz) of [Cu(L')(C_6H_5S)] (left) and [Cu(L')(C_6F_5S)] (right).

Appendix 4

Determination of zero ionic strength equilibrium constants

By considering the mass balance ($C_{Cu} = C_M + 2C_D$) and the stoichiometric dimerization constant ($K = C_D/C_M^2$), the ionic strength (I) can be derived for each sample:

$$I = \frac{1}{2}\left(3C_{Cu} - \frac{\sqrt{8KC_{Cu}+1}-1}{4K}\right) \qquad \text{(A8)}$$

according to Davies empirical expression, the correction factors $f(I)$ can be determined for each sample:

$$f(I) = A\sum z_i^2\left(\frac{\sqrt{I}}{1+\sqrt{I}} - 0.3I\right) \qquad \text{(A9)}$$

$$K = K^0 10^{f(I)} \qquad \text{(A10)}$$

where K^0 = stability constant extrapolated at zero ionic strength, A = 0.509 (empirical factor), and $\Sigma z_i^2 = z_D^2 - 2z_M^2 = 2$ (z_D and z_M are the charges of the dimer and the monomer, respectively). Taking into account that:

$$\delta = \delta_M \frac{C_M}{C_{Cu}} + \delta_D \frac{2C_D}{C_{Cu}} \qquad (\delta = \text{observed chemical shifts}) \qquad \text{(A11)}$$

and introducing: the mass balance, the definition of K and the Davies correction, we can write the following expression:

$$\delta = \delta_M \frac{\sqrt{8K^0 10^{f(I)} C_{Cu}+1}-1}{4K^0 10^{f(I)} C_{Cu}} + \delta_D\left(1 - \frac{\sqrt{8K^0 10^{f(I)} C_{Cu}+1}-1}{4K^0 10^{f(I)} C_{Cu}}\right) \qquad \text{(A12)}$$

that was used as regression model on δ and C_{Cu} data for the refinement of K^0 values.

Determination of the non-linear regression equation for the hydrodynamic volumes

Equation 5.1 is derived by the following expression:

$$V_H = V_H^0(M)\frac{C_M}{C_M + C_D} + V_H^0(D)\frac{C_D}{C_M + C_D} \qquad \text{(A13)}$$

where V_H is the experimental hydrodynamic volume, $V^0_H(M)$ and $V^0_H(D)$ are the hydrodynamic volumes of the monomer and the dimer, respectively, and C_M and C_D are the corresponding equilibrium concentrations. Defining the dissociation grade α as:

$$\alpha = \frac{C_M}{C_{Cu}} = \frac{C_M}{C_M + 2C_D}$$

and remembering that for a dimerization process $K = C_D/C_M^2$ and $C_{Cu} = C_M + 2C_D$ (mass balance), α can be written as:

$$\alpha = \frac{\sqrt{8KC_{Cu} + 1} - 1}{4KC_{Cu}} \qquad \text{(A14)}$$

Introducing the definition of α into A13, A15 is obtained:

$$V_H = V_H^0(M)\frac{2\alpha}{\alpha + 1} + V_H^0(D)\frac{1 - \alpha}{\alpha + 1} \qquad \text{(A15)}$$

By substituting α with the second member of equation A14 into A15, we obtain Equation 5.1:

$$V_H = \frac{(V_H^0(D) - 2V_H^0(M))(\sqrt{8KC_{Cu} + 1} - 4KC_{Cu}V_H^0(D) - V_H^0(D) + 2V_H^0(M)}{\sqrt{8KC_{Cu} + 1} + 4KC_{Cu} - 1} \qquad \text{(5.1)}$$

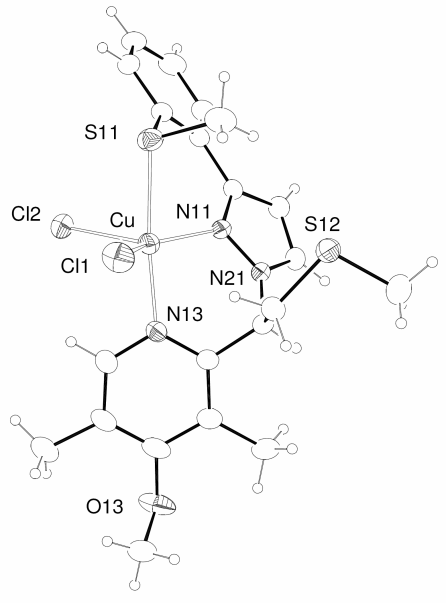

Figure A11 Ortep drawing of $[Cu(L^b)Cl_2]$ with thermal ellipsoids shown at 30% probability. Selected distances: Cu-N(11) = 2.017(2) Å, Cu-N(13) = 2.036(2) Å, Cu-S(11) = 2.361(1) Å, Cu-Cl(1) = 2.285(1) Å, Cu-Cl(2) = 2.424(1) Å.

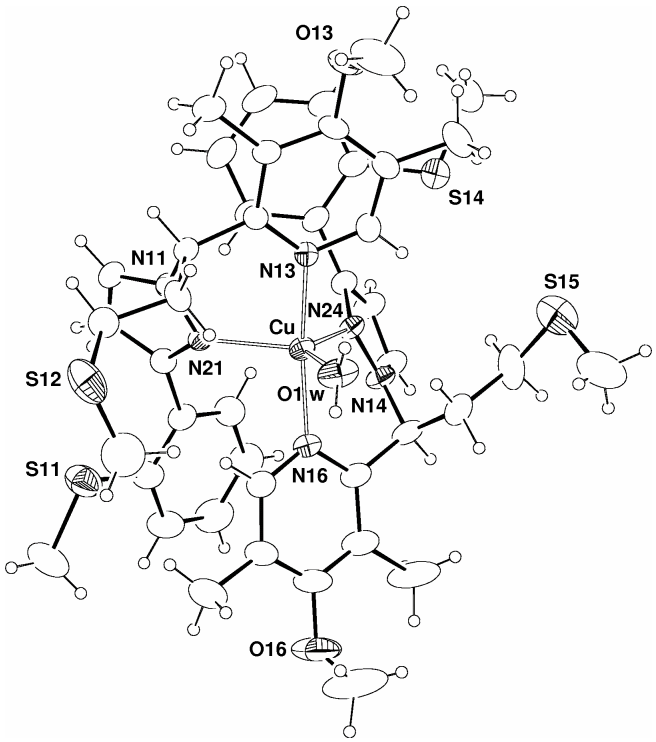

Figure A12 Ortep drawing of $[Cu(L^a)_2(H_2O)](OTf)_2 \cdot H_2O \cdot CH_3OH$ with thermal ellipsoids shown at 30% probability. The $^-$OTf counterions and the crystallization solvent (CH_3OH) are omitted for clarity. Selected distances: Cu-N(13) = 1.988(3) Å, Cu-N(16) = 1.997(3) Å, Cu-N(21) = 2.117(3) Å, Cu-N(24) = 2.105(3) Å, Cu-O = 2.040(3) Å.

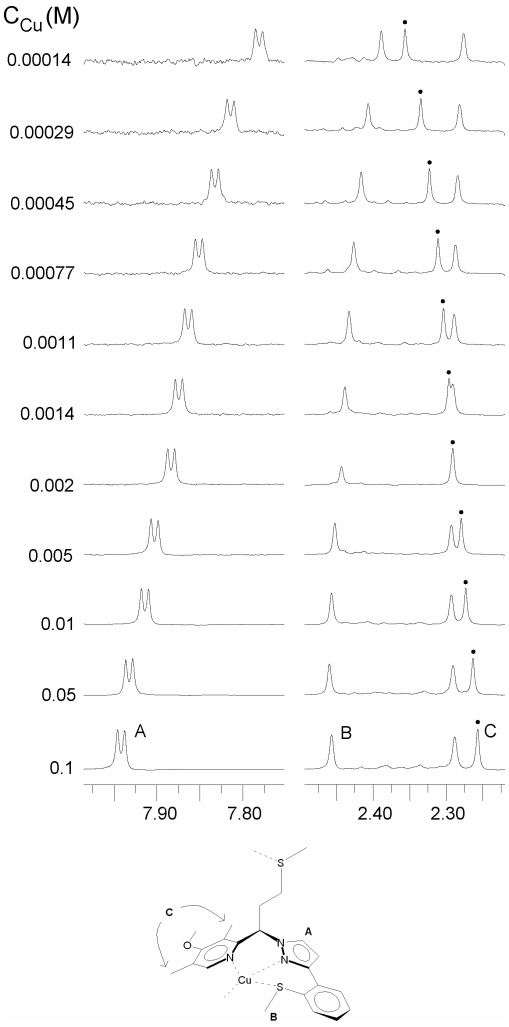

Figure A13 Stacking plot of ^{1}H NMR spectra of $\mathbf{a_2}(BF_4)_2$ in CD_3CN at different C_{Cu}. The drifts of the chemical shifts of the protons A, B and C were computed to derive the logK for $2\mathbf{a}^+ \rightleftharpoons \mathbf{a_2}^{2+}$.

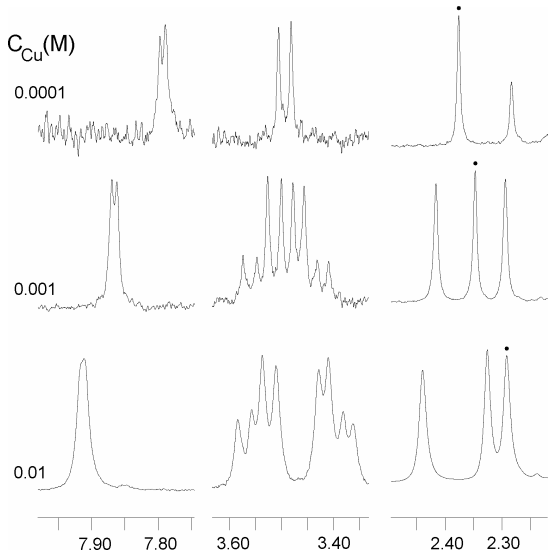

Figure A14 Stacking plot of ^{1}H NMR spectra of $\mathbf{b_2}(BPh_4)_2$ in CD_3CN at different C_{Cu}

References

1. Trofimenko, S. *J. Am. Chem. Soc.* **1966**, *88*, 1842-1844.
2. Trofimenko, S. *J. Am. Chem. Soc.* **1967**, *89*, 3170-3177.
3. Trofimenko, S. *Acc. Chem. Res.* **1971,** *4*, 17-22.
4. Trofimenko, S. *Chem. Rev.* **1993,** *93*, 943-980.
5. Trofimenko, S. *Scorpionates: The Coordination Chemistry of Polypyrazolylborate Ligands;* London, **1999**.
6. Trofimenko, S. *Polyhedron* **2004,** *23*, 197-203.
7. Pettinari, C.; Santini, C. *Compr. Coord. Chem. II* **2004**, *1*, 159-210.
8. Parkin, G. *Chem. Commun.* **2000,** 1971-1985.
9. Edelmann, F. T. *Angew. Chem. Int. Ed.* **2001,** *40*, 1656-1660.
10. Kitajima, N.; Koda, T.; Hashimoto, S.; Kitagawa, T.; Morooka, Y. *J. Am. Chem. Soc.* **1991,** *113*, 5664-5671.
11. Ball, R. G.; Ghosh, C. K.; Hoyano, J. K.; McMaster, A. D.; Graham, W. A. G. *J. Chem. Soc., Chem. Commun.* **1989,** *1989*, 341-342.
12. Bucher, U. E.; Currao, A.; Nesper, R.; Rueegger, H.; Venanzi, L. M.; Younger, E. *Inorg. Chem.* **1995,** *34*, 66-74.
13. Chauby, V.; LeBerre, C. S.; Kalck, P.; Daran, J. C.; Commenges, G. *Inorg. Chem.* **1996,** *35*, 6354-6355.
14. Malbosc, F.; Kalck, P.; Daran, J. C.; Etienne, M. *J. Chem. Soc., Dalton Trans.* **1999,** 271-272.
15. Dias, H. V. R.; Lu, H. L. *Inorg. Chem.* **2000,** *39*, 2246.
16. Herberhold, M.; Eibl, S.; Milius, W.; Wrackmeyer, B. *Zeit. Anorg. Allg. Chem.* **2000,** *626*, 552-555.
17. Gutierrez, E.; Hudson, S. A.; Monge, A.; Nicasio, M. C.; Paneque, M.; Carmona, E. *J. Chem. Soc., Dalton Trans.* **1992,** 2651-2652.
18. Paneque, M.; Sirol, S.; Trujillo, M.; Gutierrez-Puebla, E.; Monge, M. A.; Carmona, E. *Angew. Chem. Int. Ed.* **2000,** *39*, 218.
19. Amoroso, A. J.; Thompson, A. M. C.; Jeffery, J. C.; Jones, P. L.; McCleverty, J. A.; Ward, M. D. *J. Chem. Soc., Chem. Commun.* **1994,** 2751-2752.
20. Amoroso, A. J.; Jeffery, J. C.; Jones, P. L.; McCleverty, J. A.; Rees, L.; Rheingold, A. L.; Sun, Y. M.; Takats, J.; Trofimenko, S.; Ward, M. D.; Yap, G. P. A. *J. Chem. Soc., Chem. Commun.* **1995,** 1881-1882.
21. Kitajima, N.; Tolman, W. B. *Progr. Inorg. Chem.* **1995,** *43*, 419-531.

22. Calabrese, J. C.; Domaille, P. J.; Trofimenko, S.; Long, G. J. *Inorg. Chem.* **1991,** *30*, 2795-2801.
23. Rheingold, A. L.; Haggerty, B. S.; Trofimenko, S. *J. Chem. Soc., Chem. Commun.* **1994,** 1973-1974.
24. Rheingold, A. L.; Ostrander, R. L.; Haggerty, B. S.; Trofimenko, S. *Inorg. Chem.* **1994,** *33*, 3666-3676.
25. Alsfasser, R.; Powell, A. K.; Vahrenkamp, H. *Angew. Chem. Int. Ed.* **1990,** *29*, 898-899.
26. Pullen, E. E.; Rheingold, A. L.; Rabinovich, D. *Inorg. Chem. Commun.* **1999,** *2*, 194-196.
27. Blackwell III, W. C.; Bunich, D.; Concolino, T. E.; Rheingold, A. L.; Rabinovich, D. *Inorg. Chem.Commun.* **2000,** *3*, 325-327.
28. Steiner, A.; Stalke, D. *Inorg. Chem.* **1995,** *34*, 4846-4853.
29. Breakell, K. R.; Patmore, D. J.; Storr, A. *J. Chem. Soc., Dalton Trans.* **1975,** 749-754.
30. Sorrell, T. N.; Allen, W. E.; White, P. S. *Inorg. Chem.* **1995,** *34*, 952-960.
31. Psillakis, E.; Jeffery, J. C.; McCleverty, J. A.; Ward, M. D. *J. Chem. Soc., Dalton Trans.* **1997,** 1645-1651.
32. Joshi, V. S.; Kale, V. K.; Sathe, K. M.; Sarkar, A.; Tavale, S. S.; Suresh, C. G. *Organometallics* **1991,** *10*, 2898-2902.
33. Abufarag, A.; Vahrenkamp, H. *Inorg. Chem.* **1995,** *34*, 2207-2216.
34. Szczepura, L. F.; Witham, L. M.; Takeuchi, K. J. *Coord. Chem. Rev.* **1998,** *174*, 5-32.
35. Trofimenko, S. *J. Am. Chem. Soc.* **1970,** *92*, 5118-5126.
36. Reger, D. L. *Comm. Inorg. Chem.* **1999,** *21*, 1-28.
37. Bigmore, H. R.; Lawrence, S. C.; Mountford, P.; Tredget, C. S. *Dalton Trans.* **2005,** 635-651.
38. Pettinari, C.; Pettinari, R. *Coord. Chem. Rev.* **2005,** *249*, 525-543.
39. Pettinari, C.; Pettinari, R. *Coord. Chem. Rev.* **2005,** *249*, 663-691.
40. Otero, A.; Fernandez-Baeza, J.; Antinolo, A.; Tejeda, J.; Lara-Sanchez, A. *Dalton Trans.* **2004,** 1499-1510.
41. Parkin, G. *Adv. Inorg. Chem.* **1995,** *42*, 291-393.
42. Byers, P. K.; Canty, A. J.; Honeyman, R. T. *Adv. Organomet. Chem.* **1992,** *34*, 1-65.
43. Reger, D. L. *Coord. Chem. Rev.* **1996,** *147*, 571-595.
44. Etienne, M. *Coord. Chem. Rev.* **1996,** *156*, 201-236.
45. Marques, N.; Sella, A.; Takats, J. *Chem. Rev.* **2002,** *102*, 2137-2159.

46. Ruman, T.; Ciunik, Z.; Trzeciak, A. M.; Wolowiec, S.; Ziolkowski, J. J. *Organometallics* **2003,** *22*, 1072-1080.
47. Garner, M.; Reglinski, J.; Cassidy, I.; Spicer, M. D.; Kennedy, A. R. *Chem. Commun.* **1996,** 1975-1976.
48. Reglinski, J.; Garner, M.; Cassidy, I. D.; Slavin, P. A.; Spicer, M. D.; Armstrong, D. R. *J. Chem. Soc., Dalton Trans.* **1999,** 2119-2126.
49. Mason, M. R.; Ogrin, D.; Fneich, B.; Barnard, T. S.; Kirschbaum, K. *J. Organomet. Chem.* **2005,** *690*, 157-162.
50. Carella, A.; Vives, G.; Cox, T.; Jaud, J.; Rapenne, G.; Launay, J. P. *Eur. J. Inorg. Chem.* **2006,** 980.
51. Janiak, C.; Scharmann, T. G.; Green, J. C.; Parkin, R. P. G.; Kolm, M.; Riedel, E.; Mickler, W.; Elguero, J.; Claramunt, R. M.; Sanz, D. *Chem. Eur. J.* **1996,** *2*, 992.
52. Sargent, A. L.; Titus, E. P.; Riordan, C. G.; Rheingold, A. L.; Ge, P. *Inorg. Chem.* **1996,** *35*, 7095-7101.
53. Shapiro, I. R.; Jenkins, D. M.; Thomas, J. C.; Day, M. W.; Peters, J. C. *Chem. Commun.* **2001,** 2152-2153.
54. Betley, T. A.; Peters, J. C. *Inorg. Chem.* **2002,** *41*, 6541-6543.
55. Bailey, P. J.; Lanfranchi, M.; Marchiò, L.; Parsons, S. *Inorg. Chem.* **2001,** *40*, 5030-5035.
56. Humphrey, E. R.; Mann, K. L. V.; Reeves, Z. R.; Behrendt, A.; Jeffery, J. C.; Maher, J. P.; McCleverty, J. A.; Ward, M. D. *New J. Chem.* **1999,** *23*, 417-423.
57. Fujisawa, K.; Ono, T.; Aoki, H.; Ishikawa, Y.; Miyashita, Y.; Okamoto, K.; Nakazawa, H.; Higashimura, H. *Inorg. Chem. Commun.* **2004,** *7*, 330-332.
58. Reger, D. L.; Grattan, T. C.; Brown, K. J.; Little, C. A.; Lamba, J. J. S.; Rheingold, A. L.; Sommer, R. D. *J. Organomet. Chem.* **2000,** *607*, 120-128.
59. Julia, S.; Del Mazo, J. M.; Avila, L.; Elguero, J. *Org. Prep. Proced. Int* **1984,** *16*, 299-307.
60. Reger, D. L.; Grattan, T. C. *Synthesis* **2003,** 232-238.
61. Goodman, M. S.; Bateman, M. A. *Tetr. Lett.* **2001,** *42*, 5-7.
62. Huckel, W.; Bretschneider, H. *Ber. Chem.* **1937**, 2024-2026.
63. Huynh, M. H. V.; Smyth, J.; Wetzler, M.; Mort, B.; Gong, P. K.; Witham, L. M.; Jameson, D. L.; Geiger, D. K.; Lasker, J. M.; Charepoo, M.; Gornikiewicz, M.; Cintron, J. M.; Imahori, G.; Sanchez, R. R.; Marschilok, A. C.; Krajkowski, L. M.;

Churchill, D. G.; Churchill, M. R.; Takeuchi, K. J. *Angew. Chem. Int. Ed.* **2001,** *40*, 4469.

64. Hikichi, S.; Tanaka, M.; Moro-oka, Y.; Kitajima, N. *J. Chem. Soc., Chem. Commun.* **1992,** 814-815.
65. Brand, U.; Rombach, M.; Vahrenkamp, H. *Chem. Commun.* **1998,** 2717-2718.
66. Hammes, B. S.; Carrano, C. J. *Inorg. Chem.* **1999,** *38*, 4593-4600.
67. Parkin, G. *Chem. Rev.* **2004,** *104*, 699-767.
68. Morlok, M. M.; Janak, K. E.; Zhu, G.; Quarless, D. A.; Parkin, G. *J. Am. Chem. Soc.* **2005,** *127*, 14039-14050.
69. Thompson, J. S.; Marks, T. J.; Ibers, J. A. *Proc. Natl. Acad. Sci. U.S.A* **1977,** *74*, 3114-3118.
70. Thompson, J. S.; Harlow, R. L.; Whitney, J. F. *J. Am. Chem. Soc.* **1983,** *105*, 3522-3527.
71. Kitajima, N. *Adv. Inorg. Chem.* **1992,** *39*, 1-77.
72. Kitajima, N.; Morooka, Y. *Chem. Rev.* **1994,** *94*, 737-757.
73. Ruf, M.; Pierpont, C. G. *Angew. Chem. Int. Ed.* **1998,** *37*, 1736-1739.
74. Armstrong, W. H.; Lippard, S. J. *J. Am. Chem. Soc.* **1984,** *106*, 4632-4633.
75. Czernuszewicz, R. S.; Sheats, J. E.; Spiro, T. G. *Inorg. Chem.* **1987,** *26*, 2063-2067.
76. Beck, A.; Barth, A.; Hubner, E.; Burzlaff, N. *Inorg. Chem.* **2003,** *42*, 7182-7188.
77. Holmes, S.; Carrano, C. J. *Inorg. Chem.* **1991,** *30*, 1231-1235.
78. Eagle, A. A.; Laughlin, L. J.; Young, C. G.; Tiekink, E. R. T. *J. Am. Chem. Soc.* **1992,** *114*, 9195-9197.
79. Young, C. G.; Wedd, A. G. *Chem. Commun.* **1997,** *1997*, 1251-1257.
80. Hammes, B. S.; Chohan, B. S.; Hoffman, J. T.; Einwachter, S.; Carrano, C. J. *Inorg. Chem.* **2004,** *43*, 7800-7806.
81. Eagle, A. A.; Tiekink, E. R. T.; Young, C. G. *J. Chem. Soc., Chem. Commun.* **1991,** 1746-1748.
82. Eagle, A. A.; Harben, S. M.; Tiekink, E. R. T.; Young, C. G. *J. Am. Chem. Soc.* **1994,** *116*, 9749-9750.
83. Kitajima, N.; Osawa, M.; Tanaka, M.; Moro-oka, Y. *J. Am. Chem. Soc.* **1991,** *113*, 8952-8953.
84. Kitajima, N.; Osawa, M.; Tamura, N.; Morooka, Y.; Hirano, T.; Hirobe, M.; Nagano, T. *Inorg. Chem.* **1993,** *32*, 1879-1880.

85. Alsfasser, R.; Trofimenko, S.; Looney, A.; Parkin, G.; Vahrenkamp, H. *Inorg. Chem.* **1991,** *30*, 4098-4100.
86. Looney, A.; Parkin, G.; Alsfasser, R.; Ruf, M.; Vahrenkamp, H. *Angew. Chem. Int. Ed.* **1992,** *31*, 92-93.
87. Looney, A.; Han, R.; McNeill, K.; Parkin, G. *J. Am. Chem. Soc.* **1993,** *115*, 4690-4697.
88. Ruf, M.; Vahrenkamp, H. *Inorg. Chem.* **1996,** *35*, 6571-6578.
89. Kitajima, N.; Fujisawa, K.; Morooka, Y. *J. Am. Chem. Soc.* **1990,** *112*, 3210-3212.
90. Kitajima, N.; Fujisawa, K.; Tanaka, M.; Morooka, Y. *J. Am. Chem. Soc.* **1992,** *114*, 9232-9233.
91. Carrier, S. M.; Ruggiero, C. E.; Houser, R. P.; Tolman, W. B. *Inorg. Chem.* **1993,** *32*, 4889-4899.
92. Randall, D. W.; George, S. D.; Holland, P. L.; Hedman, B.; Hodgson, K. O.; Tolman, W. B.; Solomon, E. I. *J. Am. Chem. Soc.* **2000,** *122*, 11632-11648.
93. Solomon, E. I.; Baldwin, M. J.; Lowery, M. D. *Chem. Rev.* **1992,** *92*, 521-542.
94. Gray, H. B.; Malmström, B. G.; Williams, R. J. P. *J. Biol. Inorg. Chem.* **2000,** *5*, 551-559.
95. Marcus, R. A.; Sutin, N. *Biochim. Biophys. Acta* **1985,** *811*, 265-322.
96. Hoffmann, R. *Angew. Chem. Int. Ed.* **2008,** *21*, 711.
97. Slugovc, C.; Schmid, R.; Kirchner, K. *Coord. Chem. Rev.* **1999,** *185*, 109-126.
98. Slugovc, C.; Padilla-Martinez, I.; Sirol, S.; Carmona, E. *Coord. Chem. Rev.* **2001,** *213* (1), 129-157.
99. Thomas, J. C.; Peters, J. C. *J. Am. Chem. Soc.* **2001,** *123*, 5100-5101.
100. Dias, H. V. R.; Browning, R. G.; Richey, S. A.; Lovely, C. J. *Organometallics* **2004,** *23*, 1200-1202.
101. Braga, A. A. C.; Maseras, F.; Urbano, J.; Caballero, A.; Diaz-Requejo, M. M.; Perez, P. J. *Organometallics* **2006,** *25*, 5292-5300.
102. Foley, N. A.; Lail, M.; Lee, J. P.; Gunnoe, T. B.; Cundari, T. R.; Petersen, J. L. *J. Am. Chem. Soc.* **2007,** *129*, 6765-6781.
103. Cundari, T. R.; Grimes, T. V.; Gunnoe, T. B. *J. Am. Chem. Soc.* **2007,** *129*, 13172-13182.
104. Diaz-Requejo, M. M.; Belderrain, T. R.; Trofimenko, S.; Perez, P. J. *J. Am. Chem. Soc.* **2001,** *123*, 3167-3168.

105. Dıaz-Requejo, M. M.; Belderrain, T. R.; Perez, P. J. *Chem. Commun.* **2000,** 1853-1854.
106. Morilla, M. E.; Diaz-Requejo, M. M.; Belderrain, T. R.; Nicasio, M. C.; Trofimenko, S.; Perez, P. J. *Chem. Commun.* **2002,** 2998-2999.
107. Dias, H. V. R.; Lu, H. L.; Kim, H. J.; Polach, S. A.; Goh, T. K. H. H.; Browning, R. G.; Lovely, C. J. *Organometallics* **2002,** *21*, 1466-1473.
108. Shay, D. T.; Yap, G. P. A.; Zakharov, L. N.; Rheingold, A. L.; Theopold, K. H. *Angew. Chem. Int. Ed* **2005,** 1508-1510.
109. Milione, S.; Montefusco, C.; Cuenca, T.; Grassi, A. *Chem. Commun.* **2003,** 1176-1177.
110. Milione, S.; Bertolasi, V.; Cuenca, T.; Grassi, A. *Organometallics* **2005,** *24*, 4915-4925.
111. Milione, S.; Cuomo, C.; Grassi, A. *Topics in Catalysis* **2006,** *40*, 163-172.
112. Milione, S.; Grisi, F.; Centore, R.; Tuzi, A. *Organometallics* **2006,** *25*, 266-274.
113. Otero, A.; Fernandez-Baeza, J.; Antiñolo, A.; Carrillo-Hermosilla, F.; Tejeda, J.; Diez-Barra, E.; Lara-Sanchez, A.; Sanchez-Barba, L.; Lopez-Solera, I.; Ribeiro, M. R. *Organometallics* **2001,** *20*, 2428-2430.
114. Howe, R. G.; Tredget, C. S.; Lawrence, S. C.; Subongkoj, S.; Cowley, A. R.; Mountford, P. *Chem. Commun.* **2006,** 223-225.
115. Dias, H. V. R.; Wu, J. *Angew. Chem. Int. Ed.* **2007,** *46*, 7814-7816.
116. Camerano, J. A.; Casado, M. A.; Ciriano, M. A.; Oro, L. A. *Dalton Trans.* **2006,** 5287-5293.
117. Keyes, M. C.; Young, V. G.; Tolman, W. B. *Organometallics* **1996,** *15*, 4133-4140.
118. Janiak, C. *Dalton Trans.* **2003,** 2781-2804.
119. Silva, R. M.; Gwengo, C.; Lindeman, S. V.; Smith, M. D.; Gardinier, J. R. *Inorg. Chem.* **2006,** *4*6, 10998-11007.
120. Zhai, B.; Shen, W. Z.; Chen, X. Y.; Song, H. B.; Shi, W.; Cheng, P. *Inorg. Chem. Commun.* **2006,** *9*, 1293-1296.
121. McCleverty, J. A.; Ward, M. D. *Acc. Chem. Res.* **1998,** *31*, 842-851.
122. Janiak, C.; Scharmann, T. G.; Albrecht, P.; Marlow, F.; MacDonald, R. *J. Am. Chem. Soc.* **1996,** *118*, 6307-6308.
123. Hamilton, B. H.; Kelly, K. A.; Wagler, T. A.; Espe, M. P.; Ziegler, C. J. *Inorg. Chem.* **2002,** *41*, 4984-4986.

124. Hamilton, B. H.; Cardon, T. B.; Lorigan, G. A.; Ziegler, C. J. *Dalton Trans.* **2005,** 2941-2944.
125. Reger, D. L.; Semeniuc, R. F.; Smith, M. D. *Inorg. Chem.* **2003,** *42*, 8137-8139.
126. Reger, D. L.; Gardinier, J. R.; Semeniuc, R. F.; Smith, M. D. *Dalton Trans.* **2003,** 1712-1718.
127. Reger, D. L.; Semeniuc, R. F.; Rassolov, V.; Smith, M. D. *Inorg. Chem.* **2004,** *43*, 537-554.
128. Reger, D. L.; Elgin, J. D.; Semeniuc, R. F.; Pellechia, P. J.; Smith, M. D. *Chem. Commun.* **2005,** 4068-4070.
129. Reger, D. L.; Semeniuc, R. F.; Gardinier, J. R.; O'Neal, J.; Reinecke, B.; Smith, M. D. *Inorg. Chem.* **2006,** *45*, 4337-4339.
130. Schibli, R.; Schubiger, A. P. *Eur. J. Nucl. Med. Mol. Imag.* **2002,** *29*, 1529-1542.
131. Garcia, R.; Paulo, A.; Domingos, A.; Santos, I.; Ortner, K.; Alberto, R. *J. Am. Chem. Soc.* **2000,** *122*, 11240-11241.
132. Garcia, R.; Paulo, A.; Domingos; Santos, I. *J. Organomet. Chem.* **2001,** *632*, 41-48.
133. Garcia, R.; Paulo, A.; Domingos; Santos, I. *Dalton Trans.* **2003,** 2757-2760.
134. Porchia, M.; Papini, G.; Santini, C.; Lobbia, G. G.; Pellei, M.; Tisato, F.; Bandoli, G.; Dolmella, A. *Inorg. Chem.* **2005,** *44*, 4045-4054.
135. Porchia, M.; Papini, G.; Santini, C.; Lobbia, G. G.; Pellei, M.; Tisato, F.; Bandoli, G.; Dolmella, A. *Inorg. Chim. Acta* **2006,** *359*, 2501-2508.
136. Herrick, R. S.; Brunker, T. J.; Maus, C.; Crandall, K.; Cetin, A.; Ziegler, C. J. *Chem. Commun.* **2006,** 4330-4331.
137. Maria, L.; Paulo, A.; Santos, I. C.; Santos, I.; Kurz, P.; Spingler, B.; Alberto, R. Very *J. Am. Chem. Soc.* **2006,** *128*, 14590-14598.
138. Garcia, R.; Gano, L.; Maria, L.; Paulo, A.; Santos, I.; Spies, H. *J.Biol. Inorg. Chem.* **2006,** *11*, 769-782.
139. Williams, R. J. P. *Eur. J. Biochem.* **1995,** *234*, 363-381.
140. Vallee, B. L.; Williams, R. J. P. *Proc. Natl. Acad. Sci. U.S.A* **1968,** *59*, 498-505.
141. Solomon, E. I.; LaCroix, L. B.; Randall, D. W. *Pur. Appl. Chem.* **1998,** *70*, 799-808.
142. Randall, D. W.; Gamelin, D. R.; LaCroix, L. B.; Solomon, E. I. *J. Biol. Inorg. Chem.* **2000,** *5*, 16-29.
143. Solomon, E. I.; Szilagyi, R. K.; George, S. D.; Basumallick, L. *Chem. Rev.* **2004,** *104*, 419-458.

144. Ryde, U.; Olsson, M. H. M.; Pierloot, K.; Roos, B. O. *J. Mol. Biol.* **1996,** *261*, 586-596.

145. Ryde, U.; Olsson, M. H. M.; Roos, B. O.; De Kerpel, J. O. A.; Pierloot, K. *J. Biol. Inorg. Chem.* **2000,** *5*, 565-574.

146. Ryde, U.; Olsson, M. H. M.; Roos, B. O.; Borin, A. C. *Theor. Chem. Acc.* **2001,** *105*, 452-462.

147. Cammi, R.; Gennari, M.; Giannetto, M.; Lanfranchi, M.; Marchio, L.; Mori, G.; Paiola, C.; Pellinghelli, M. A. *Inorg. Chem.* **2005,** *44*, 4333-4345.

148. Gennari, M.; Lanfranchi, M.; Marcho, L.; Pellinghelli, M. A.; Tegoni, M.; Cammi, R. *Inorg. Chem.* **2006,** *45*, 3456-3466.

149. Melnik, M.; Macaskova, L.; Holloway, C. E. *Coord. Chem. Rev.* **1993,** *126*, 71-92.

150. Smith, D. R. *Coord. Chem. Rev.* **1998,** *172*, 457-573.

151. Keim, W. *J. Mol. Catal.* **1989,** *52*, 19-25.

152. Fielding, L. *Tetrahedron* **2000,** *56*, 6151-6170.

153. *Area-Detector Absorption Correction,* Siemens Industrial Automation Inc., Madison, WI, **1996.**

154. Walker, N.; Stuart, D. *Acta Cryst.* **1983,** *39*, 158-166.

155. Altomare, A.; Burla, M. C.; Camalli, M.; Cascarano, G. L.; Giacovazzo, C.; Guagliardi, A.; Moliterni, A. G. G.; Polidori, G.; Spagna, R. *J. Appl. Crystallogr.* **1999,** *32*, 115-119.

156. *SHELX97, Programs for Crystal Structure Analysis,* version Release 97-2; University of Göttingen, Germany, **1997**

157. Farrugia, L. J. *J. Appl. Crystallogr.* **1999**, *32*, 837-838.

158. Sluis P.; Spek, A. L. *Acta Cryst.* **1990,** *A46*, 194.

159. *Mercury,* version 1.4.2; CCDC, **2001**

160. *Gaussian 03,* Revision C.02, Frisch, M. J.; Trucks, G. W.; Schlegel, H. B.; Scuseria, G. E.; Robb, M. A.; Cheeseman, J. R.; Montgomery, Jr., J. A.; Vreven, T.; Kudin, K. N.; Burant, J. C.; Millam, J. M.; Iyengar, S. S.; Tomasi, J.; Barone, V.; Mennucci, B.; Cossi, M.; Scalmani, G.; Rega, N.; Petersson, G. A.; Nakatsuji, H.; Hada, M.; Ehara, M.; Toyota, K.; Fukuda, R.; Hasegawa, J.; Ishida, M.; Nakajima, T.; Honda, Y.; Kitao, O.; Nakai, H.; Klene, M.; Li, X.; Knox, J. E.; Hratchian, H. P.; Cross, J. B.; Bakken, V.; Adamo, C.; Jaramillo, J.; Gomperts, R.; Stratmann, R. E.; Yazyev, O.; Austin, A. J.; Cammi, R.; Pomelli, C.; Ochterski, J. W.; Ayala, P. Y.; Morokuma, K.; Voth, G. A.; Salvador, P.; Dannenberg, J. J.; Zakrzewski, V. G.; Dapprich, S.; Daniels, A. D.;

Strain, M. C.; Farkas, O.; Malick, D. K.; Rabuck, A. D.; Raghavachari, K.; Foresman, J. B.; Ortiz, J. V.; Cui, Q.; Baboul, A. G.; Clifford, S.; Cioslowski, J.; Stefanov, B. B.; Liu, G.; Liashenko, A.; Piskorz, P.; Komaromi, I.; Martin, R. L.; Fox, D. J.; Keith, T.; Al-Laham, M. A.; Peng, C. Y.; Nanayakkara, A.; Challacombe, M.; Gill, P. M. W.; Johnson, B.; Chen, W.; Wong, M. W.; Gonzalez, C.; and Pople, J. A.; Gaussian, Inc., Wallingford CT, **2004**

161. Svensson, M.; Humbel, S.; Froese, R. D. J.; Matsubara, T.; Sieber, S.; Morokuma, K. *J. Phys. Chem.* **1996,** *100*, 19357-19363.
162. Humbel, S.; Sieber, S.; Morokuma, K. *J. Chem. Phys.* **1996,** *105*, 1959-1967.
163. Dapprich, S.; Komaromi, L.; Byun, K. S.; Morokuma, K.; Frisch M. J. *J. Mol. Struct. (Theochem.)* **1999,** 461-462.
164. Becke, A. D. *Phys. Rev. A.* **1988,** *38*, 3098-3100.
165. Becke, A. D. *J. Chem. Phys.* **1993,** *98*, 5648-5652.
166. Hay, P. J.; Wadt, W. R. *J.Chem. Phys.* **1985,** *82*, 299-310.
167. Wadt, W. R.; Hay, P. J. *J. Chem. Phys.* **1985,** *82*, 284-298.
168. Frassineti, C.; Ghelli, S.; Gans, P.; Sabatini, A.; Moruzzi, M. S.; Vacca, A. *Anal. Biochem.* **1995,** *231*, 374-382.
169. Alderighi, L.; Gans, P.; Ienco, A.; Peters, D.; Sabatini, A.; Vacca, A. *Coord. Chem. Rev.* **1999,** *184*, 311-318.
170. Leftin, J. H. *Chem. Abstr.* **1967,** *66*, 46487e.
171. Lobbia, G. G.; Pettinari, C.; Santini, C.; Somers, N.; Skelton, B. W.; White, A. H. *Inorg. Chim. Acta* **2001,** *319*, 15-22.
172. Crabtree, R. *The Organomet. Chem.of the Transition Metals,* **2005**.
173. Careri, M.; Elviri, L.; Lanfranchi, M.; Marchio, L.; Mora, C.; Pellinghelli, M. A. *Inorg. Chem.* **2003,** *42*, 2109-2114.
174. Kimblin, C.; Bridgewater, B. M.; Churchill, D. G.; Hascall, T.; Parkin, G. *Inorg. Chem.* **2000,** *39*, 4240-4243.
175. Kimblin, C.; Churchill, D. G.; Bridgewater, B. M.; Girard, J. N.; Quarless, D. A.; Parkin, G. *Polyhedron* **2001,** *20*, 1891-1896.
176. Foreman, M. R. S. J.; Hill, A. F.; Owen, G. R.; White, A. J. P.; Williams, D. J. *Organometallics* **2003,** *22*, 4446-4450.
177. Alvarez, H. M.; Tanski, J. M.; Rabinovich, D. *Polyhedron* **2004,** *23*, 395-403.
178. Gennari, M.; Tegoni, M.; Lanfranchi, M.; Pellinghelli, M. A.; Marchio, L. *Inorg. Chem.* **2007,** *46*, 3367-3377.

179. Dowling, C.; Parkin, G. *Polyhedron* **1996,** *15*, 2463-2465.
180. Ghosh, P.; Parkin, G. *J. Chem. Soc., Dalton Trans.* **1998,** 2281-2284.
181. Kail, B.; Nemykin, V. N.; Davie, S. R.; Carrano, C. J.; Hammes, B.; Basu, P. *Inorg. Chem.* **2002,** *41*, 1281-1291.
182. Hammes, B. S.; Kieber-Emmons, M. T.; Letizia, J. A.; Shirin, Z.; Carrano, C. J.; Zakharov, L. N.; Rheingold, A. L. *Inorg. Chim. Acta* **2003,** *346*, 227-238.
183. Beck, A.; Weibert, B.; Burzlaff, N. *Eur. J. Inorg. Chem.* **2001,** 521.
184. Hegelmann, I.; Beck, A.; Eichhorn, C.; Weibert, B.; Burzlaff, N. *Eur. J. Inorg. Chem.* **2003,** 339-347.
185. Mueller, R.; Hubner, E.; Burzlaff, N. *Eur. J. Inorg. Chem.* **2004,** 2151-2159.
186. Bruijnincx, P. C. A.; Lutz, M.; Spek, A. L.; van Faassen, E. E.; Weckhuysen, B. M.; van Koten, G.; Gebbink, R. J. M. K. *Eur. J. Inorg. Chem.* **2005,** 779-787.
187. Kopf, H.; Pietraszuk, C.; Hubner, E.; Burzlaff, N. *Organometallics* **2006,** *25*, 2533-2546.
188. Hoffman, J. T.; Tran, B. L.; Carrano, C. J. *Dalton Trans.* **2006,** 3822-3830.
189. Otero, A.; Fernandez-Baeza, J.; Tejeda, J.; Antiñolo, A.; Carrillo-Hermosilla, F.; Dιez-Barra, E.; Lara-Sanchez, A.; Fernandez-Lopez, M.; Lanfranchi, M.; Pellinghelli, M. A. *J. Chem. Soc., Dalton Trans.* **1999,** 3537-3539.
190. Otero, A.; Fernandez-Baeza, J.; Antiñolo, A.; Tejeda, J.; Lara-Sanchez, A.; Sanchez-Barba, L.; Rodriguez, A. M. *Dalton Trans.* **2004,** 3963-3969.
191. Otero, A.; Fernandez-Baeza, J.; Antiñolo, A.; Tejeda, J.; Lara-Sanchez, A.; Sanchez-Barba, L.; Martinez-Caballero, E.; Rodriguez, A. M.; Lopez-Solera, I. *Inorg. Chem.* **2005,** *44*, 5336-5344.
192. Burzlaff, N.; Hegelmann, I.; Weibert, B. *J. Organomet. Chem.* **2001,** *626*, 16-23.
193. Otero, A.; Fernandez-Baeza, J.; Tejeda, J.; Antiñolo, A.; Carrillo-Hermosilla, F.; Diez-Barra, E.; Lara-Sanchez, A.; Fernandez-L≤pez, M. *J. Chem. Soc., Dalton Trans.* **2000,** 2367-2374.
194. Otero, A.; Fernandez-Baeza, J.; Antiñolo, A.; Tejeda, J.; Lara-Sanchez, A.; Sanchez-Barba, L.; Rodriguez, A. M. *Eur. J. Inorg. Chem.* **2004,** 260-266.
195. Higgs, T. C.; Carrano, C. J. *Inorg. Chem.* **1997,** *36*, 298-306.
196. Higgs, T. C.; Carrano, C. J. *Inorg. Chem.* **1997,** *36*, 291-297.
197. Higgs, T. C.; Spartalian, K.; O'Connor, C. J.; Matzanke, B. F.; Carrano, C. J. *Inorg. Chem.* **1998,** *37*, 2263-2272.
198. Hammes, B. S.; Carrano, C. J. *Inorg. Chem.* **1999,** *38*, 3562-3568.

199. Kläui, W.; Berghahn, M.; Rheinwald, G.; Lang, H. *Angew. Chem. Int. Ed.* **2000,** *39*, 2464-2466.
200. Kläui, W.; Schramm, D.; Peters, W.; Rheinwald, G.; Lang, H. *Eur. J. Inorg. Chem.* **2001,** 1415.
201. Kläui, W.; Berghahn, M.; Frank, W.; Reiss, G. J.; Schoenherr, T.; Rheinwald, G.; Lang, H. *Eur. J. Inorg. Chem.* **2003,** 2059-2070.
202. Papish, E. T.; Taylor, M. T.; Jernigan III, F. E.; Rodig, M. J.; Shawhan, R. R.; Yap, G. P. A.; Jovθ, F. A. *Inorg. Chem.* **2006,** *45*, 2242-2250.
203. Gross, F.; Vahrenkamp, H. *Inorg. Chem.* **2005,** *44*, 3321-3329.
204. Otero, A.; Fernandez-Baeza, J.; Antiñolo, A.; Tejeda, J.; Lara-Sanchez, A.; Sanchez-Barba, L.; Exposito, M. T.; Rodriguez, A. M. *Dalton Trans.* **2003,** 1614-1619.
205. Hegelmann, I.; Burzlaff, N. *Eur. J. Inorg. Chem.* **2003,** 409-411.
206. Peters, L.; Burzlaff, N. *Polyhedron* **2004,** *23*, 245-251.
207. Taking as reference $\delta(CHD_2OD) = 3.34$ ppm.
208. *SMART (control) and SAINT (integration) software for CCD systems,* Bruker AXS, Madison, WI, USA, **1994**
209. Gampp, H.; Maeder, M.; Meyer, C. J.; Zuberbuhler, A. D. *Talanta* **1985,** *32*, 257-264.
210. *Specfit32,* version 3.0; Spectrum Software Associates, Marlborough, MA, USA, **2008**
211. Perrin, C. L.; Dwyer, T. J. *Chem. Rev.* **1990,** *90*, 935-967.
212. *EXSY Calculator,* version 1.0, MestreLab Research, www.mestrec.com, **2004.**
213. House, D. A.; Steel, P. J.; Watson, A. A. *Aust. J. Chem.* **1986,** *39*, 1525-1536.
214. Katritzky, A. R.; Bdelurahman, A. E.; Leahy, D. E.; Schwarz, O. A. *Tetrahedron* **1983,** *39*, 4133-4142.
215. Antiñolo, A.; Carrillo-Hermosilla, F.; Diez-Barra, E.; Fernandez-Baeza, J.; Fernandez-Lopez, M.; Lara-Sanchez, A.; Moreno, A.; Otero, A.; Rodriguez, A. M.; Tejeda, J. *J. Chem. Soc., Dalton Trans.* **1998,** 3737-3743.
216. Farrugia, L. J. *J.Appl. Crystallogr.* **1997,** *30*, 568.
217. Irving, H.; Williams, R. J. P. *J. Chem. Soc* **1953,** 3192.
218. Sigel, H.; McCormick, D. B. *Acc. Chem. Res.* **1970,** *3*, 201-208.
219. Curtiss, L. A.; Raghavachari, K.; Redfern, P. C.; Pople, J. A. *Chem. Phys. Lett.* **1997,** *270*, 419-426.
220. Curtiss, L. A.; Raghavachari, K.; Redfern, P. C.; Rassolov, V.; Pople, J. A. *J. Chem. Phys.* **1998,** *109*, 7764.

221. Gennari, M.; Lanfranchi, M.; Cammi, R.; Pellinghelli, M. A.; Marchio, L. *Inorg. Chem.* **2007,** *46*, 10143-10152.
222. Malmstrom, B. G.; Leckner, J. *Curr. Opin. Chem. Biol.* **1998,** *2*, 286-292.
223. Solomon, E. I.; Sundaram, U. M.; Machonkin, T. E. *Chem. Rev.* **1996,** *96* , 2563-2605.
224. Solomon, E. I.; Chen, P.; Metz, M.; Lee, S. K.; Palmer, A. E. *Angew. Chem. Int. Ed.* **2001**, *40*, 4570-4590.
225. Solomon, E. I.; Tuczek, F.; Root, D. E.; Brown, C. A. *Chem. Rev.* **1994,** *94*, 827-856.
226. Colman, P. M.; Freeman, H. C.; Guss, J. M.; Murata, M.; Norris, V. A.; Ramshaw, J. A. M.; Venkatappa, M. P. *Nature* **1978**, *272*, 319-324.
227. Durley, R.; Chen, L. Y.; Mathews, F. S.; Davidson, V. L. *Prot. Sci.* **1993,** *2,* 739-752.
228. Hart, P. J.; Nersissian, A. M.; Herrmann, R. G.; Nalbandyan, R. M.; Valentine, J. S.; Eisenberg, D. *Prot. Sci.* **1996,** *5*, 2175-2183.
229. Shibata, N.; Inoue, T.; Nagano, C.; Nishio, N.; Kohzuma, T.; Onodera, K.; Yoshizaki, F.; Sugimura, Y.; Kai, Y. *J. Biol. Chem.* **1999,** *274*, 4225-4230.
230. Chan, J. N.; Huang, Z. Y.; Merrifield, M. E.; Salgado, M. T.; Stillman, M. J. *Coord. Chem. Rev.* **2002,** *233*, 319-339.
231. Holm, R. H.; Kennepohl, P.; Solomon, E. I. *Chem. Rev.* **1996,** *96*, 2239-2314.
232. Belle, C.; Rammal, W.; Pierre, J. L. *Biochemistry* **2005,** *99*, 1929-1936.
233. Coucouvanis, D.; Murphy, C. N.; Kanodia, S. K. *Inorg. Chem.* **1980,** *19*, 2993-2998.
234. Dance, I. G. *Polyhedron* **1986**, *5*, 1037-1104.
235. Fujisawa, K.; Imai, S.; Kitajima, N.; Moro-oka, Y. *Inorg. Chem.* **1998,** *37*, 168-169.
236. Henkel, G.; Krebs, B. *Chem. Rev.* **2004,** *104*, 801-824.
237. Presta, A.; Fowle, D. A.; Stillman, M. J. *J. Chem. Soc., Dalton Trans.* **1997,** 977-984.
238. Calderone, V.; Dolderer, B.; Hartmann, H. J.; Echner, H.; Luchinat, C.; Del Bianco, C.; Mangani, S.; Weser, U. *Proc. Natl. Acad. Sci. U.S.A* **2005,** *102*, 51-56.
239. Zuccaccia, D.; Macchioni, A. *Organometallics* **2005,** *24*, 3476-3486.
240. Pregosin, P. S. *Progr. Nucl. Magn. Reson. Spectr.* **2006,** *49*, 261-288.
241. Connolly, M. L. *J. Am. Chem. Soc.* **1985,** *107*, 1118-1124.
242. *DS Viewer Pro,* version 5.0, Accelrys Inc., **2002.**
243. Parkin, S.; Moezzi, B.; Hope, H. *J. Appl. Crystallogr.* **1995,** *28*, 53-56.
244. Flack, H. D. *Acta Crystallogr. A* **1983,** *39*, 876.
245. Cances, E.; Mennucci, B.; Tomasi, J. *J. Chem. Phys.* **1997,** *107*, 3032-3041.
246. Mennucci, B.; Cances, E.; Tomasi, J. *J. Phys. Chem. B* **1997,** *101*, 10506-10517.

247. Mennucci, B.; Tomasi, J. *J. Chem. Phys.* **1997,** *106*, 5151-5158.
248. Tomasi, J.; Mennucci, B.; Cances, E. *J. Mol. Struct.-Theochem.* **1999,** *464*, 211-226.
249. Tomasi, J.; Mennucci, B.; Cammi, R. *Chem. Rev.* **2005,** *105*, 2999-3093.
250. Cossi, M.; Barone, V.; Cammi, R.; Tomasi, J. *Chem. Phys. Lett.* **1996,** *255*, 327-335.
251. *WINDNMR software: NMR Spectrum Calculations,* version 7.1.11; **2008.**
252. Sandstrom, J. *Dynamic NMR spectroscopy,* Academic Press, London, **1982**.
253. Tejel, C.; Villoro, J. M.; Ciriano, M. A.; Lopez, J. A.; Eguizabal, E.; Lahoz, F. J.; Bakhmutov, V. I.; Oro, L. A. *Organometallics* **1996,** *15*, 2967-2978.
254. Janssen, M. D.; Grove, D. M.; vanKoten, G. *Progr. Inorg. Chem.,* **1997,** *46*, 97-149.
255. Ford, P. C.; Cariati, E.; Bourassa, J. *Chem. Rev.* **1999,** *99*, 3625-3647.
256. Geary, W. J. *Coord. Chem. Rev.* **1971,** 7, 81-122.
257. Zuccaccia, D.; Bellachioma, G.; Cardaci, G.; Ciancaleoni, G.; Zuccaccia, C.; Clot, E.; *Organometallics* **2007,** *26*, 3930-3946.
258. Howell, J. A. S. *Polyhedron* **2006,** *25*, 2993-3005.
259. Fujisawa, K.; Fujita, K.; Takahashi, T.; Kitajima, N.; Moro-oka, Y.; Matsunaga, Y.; Miyashita, Y.; Okamoto, K. *Inorg. Chem. Commun.* **2004,** *7*, 1188-1190.
260. Gennari, M.; Lanfranchi, M.; Marcho, L.; Pellinghelli, M. A.; Giannetto, M.; Tegoni, M. *Inorg. Chem.*, accepted for publication.
261. Chaka, G.; Kandegedara, A.; Heeg, M. J.; Rorabacher, D. B. *Dalton Trans.* **2007,** 449-458.
262. Corfield, P. W. R.; Ceccarelli, C.; Glick, M. D.; Moy, I. W. Y.; Ochrymowycz, L. A.; Rorabacher, D. B. *J. Am. Chem. Soc.* **1985,** *107*, 2399-2404.
263. Gorelsky, S. I.; Basumallick, L.; Vura-Weis, J.; Sarangi, R.; Hodgson, K. O.; Hedman, B.; Fujisawa, K.; Solomon, E. I. *Inorg. Chem.* **2005,** *44*, 4947-4960.
264. Holland, P. L.; Tolman, W. B. *J. Am. Chem. Soc.* **1999,** *121*, 7270-7271.
265. Matsunaga, Y.; Fujisawa, K.; Ibi, N.; Miyashita, Y.; Okamoto, K. *Inorg. Chem.* **2005,** *44*, 325-335.
266. Vande Linde, A. M. Q.; Westerby, B. C.; Ochrymowycz, L. A.; Rorabacher, D. B. *Inorg. Chem.* **1993,** *32*, 251-257.
267. Hattori, S.; Wada, Y.; Yanagida, S.; Fukuzumi, S. *J. Am. Chem. Soc.* **2005,** *127*, 9648-9654.
268. Gratzel, M. *Inorg. Chem.* **2005,** *44*, 6841-6851.
269. Davies, C. W. *Ion Association,* **1962**.
270. *SPSS Inc., a*ll rights reserved, **1989-2006.**

271. Macchioni, A.; Ciancaleoni, G.; Zuccaccia, C.; Zuccaccia, D. *Chem. Soc. Rev.,* **2008**.
272. Dinnebier, R. E.; Dollase, W. A.; Helluy, X.; Kummerlen, J.; Sebald, A.; Schmidt, M. U.; Pagola, S.; Stephens, P. W.; Van Smaalen, S. *Acta Cryst. B* **1999**, *55*, 1014-1029.
273. Chen, H. C.; Chen, S. H. *J. Phys. Chem.* **1984,** *88*, 5118-5121.
274. Bondi, A. *J. Phys. Chem*. **1964,** *68*, 441-451.
275. Macchioni, A. *Chem. Rev.* **2005,** *105*, 2039-2073.
276. To a white suspension of $\mathbf{b_2}(BF_4)_2$ in THF, $KBPh_4$ was added in equimolar ratio with stirring. The solid was filtered off, and the resulting clear yellow solution was concentrated. A creamy white powder was precipitated with hexane and dried under vacuum, corresponding to $\mathbf{b_2}(BPh_4)_2$.
277. Deng, H. T.; Kebarle, P. *J. Am. Chem. Soc.* **1998,** *120*, 2925-2931.
278. Berger, M.; Schmidtchen, F. P. *Angew. Chem. Int. Ed.* **1998,** *37*, 2694-2696.
279. Linton, B. R.; Goodman, M. S.; Fan, E.; van Arman, S. A.; Hamilton, A. D. *J. Org. Chem.* **2001,** *66*, 7313-7319.
280. Fiammengo, R.; Timmerman, P.; de Jong, F.; Reinhoudt, D. N. *Chem. Commun.* **2000,** 2313-2314.
281. Corbellini, F.; Fiammengo, R.; Timmerman, P.; Crego-Calama, M.; Versluis, K.; Heck, A. J. R.; Luyten, I.; Reinhoudt, D. N. *J. Am. Chem. Soc.* **2002,** *124*, 6569-6575.
282. Zanello, P. *Inorganic Electrochemistry: Theory, Practice and Application,* Royal Society of Chemistry, Cambridge, **2003**.
283. Zanello, P. *Comm. Inorg. Chem.* **1988,** *8*, 45-78.
284. Ciancaleoni, G.; Zuccaccia, C.; Zuccaccia, D.; Macchioni, A. *Organometallics* **2007,** *26*, 3624-3626.
285. Swiegers, G. F.; Malefetse, T. J. *Chem. Rev.* **2000,** *100*, 3483-3538.
286. Evans, O. R.; Lin, W. *Acc. Chem. Res.* **2002,** *35*, 511-522.
287. Marin, V.; Holder, E.; Hoogenboom, R.; Schubert, U. S. *Chem. Soc. Rev.* **2007,** *36*, 618-635.
288. Wong, W. Y. *Dalton Trans.* **2007,** 4495-4510.
289. This approximate volume can be derived by dividing the unit cell volume by the number of $[Cu(L^*)(PPh_3)]$ assemblies contained (4). This neglects the volume of BF_4^- and assumes that the thioether arm of the ligand is not involved in any metal interaction.
290. Vogler, A.; Kunkely, H. *Coord. Chem. Rev.* **2002,** *230*, 243-251.
291. Henary, M.; Wootton, J. L.; Khan, S. I.; Zink, J. I. *Inorg. Chem.* **1997,** *36*, 796-801.

292. McMillin, D. R.; Kirchhoff, J. R.; Goodwin, K. V. *Coord. Chem. Rev.* **1985,** *64*, 83-92.

293. Ruthkosky, M.; Kelly, C. A.; Castellano, F. N.; Meyer, G. J. *Coord. Chem. Rev.* **1998,** *171*, 309-322.

294. The, K. I.; Peterson, L. K. *Can. J. Chem.* **1973,** *51*, 422-426.

295. The, K. I.; Peterson, L. K.; Kiehlmann, E. *Can. J. Chem.* **1973,** *51*, 2448-2451.

296. Peterson, L. K.; Kiehlmann, E.; Sanger, A. R.; The, K. I. *Can. J. Chem.* **1974,** *52*, 2367-2374.

297. Figuly, G. D.; Loop, C. K.; Martin, J. C. *J. Am. Chem. Soc.* **1989,** *111*, 654-658.

298. Heynderickx, A.; Samat, A. *J. Heter. Chem.* **2001,** *38*, 737-742.

299. Prepared in analogy to bis(pyrazol-1-yl)chetone: Byers, P. K.; Canty, A. J.; Honeyman, R. T. *J. Organomet. Chem.* **1990,** *385*, 417-427.